Winter 2017

# Influence of moisture content distribution in soil on pavement and geothermal energy

Md Adnan Khan

# INFLUENCE OF MOISTURE CONTENT DISTRIBUTION IN SOIL ON PAVEMENT AND GEOTHERMAL ENERGY

by

Md Adnan Khan, B.S., M.S.

A Dissertation Presented in Partial Fulfillment
of the Requirements for the Degree
Doctor of Philosophy

COLLEGE OF ENGINEERING AND SCIENCE
LOUISIANA TECH UNIVERSITY

February 2017

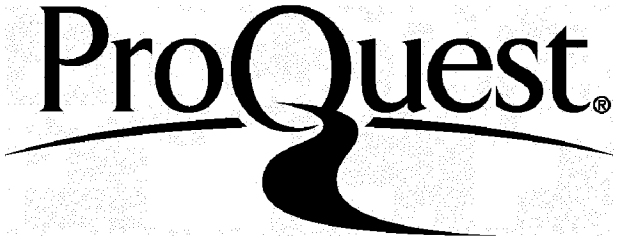

LOUISIANA TECH UNIVERSITY

**THE GRADUATE SCHOOL**

12/13/2016

Date

We hereby recommend that the dissertation prepared under our supervision by MD ADNAN KHAN

entitled INFLUENCE OF MOISTURE CONTENT DISTRIBUTION IN SOIL ON PAVEMENT AND GEOTHERMAL ENERGY

be accepted in partial fulfillment of the requirements for the Degree of Doctor of Philosophy

Supervisor of Dissertation Research

Head of Department

ENGINEERING

Department

Recommendation concurred in:

Advisory Committee

**Approved:**

Director of Graduate Studies

**Approved:**

Dean of the Graduate School

Dean of the College

GS Form 13a
(6/07)

## ABSTRACT

Moisture content in soil has a great implication in engineering design, and it has been heavily investigated by soil engineers and scientists. If moisture content in expansive soil changes drastically, it will create significant volume change in the soil. If expansive soil is present in building foundation or pavement subgrade, it may result in structural failure. On the other hand, if sufficient moisture content is present in soil, it will increase the production of geothermal energy from the ground soil. This dissertation is an effort to understand the effects of moisture content on both expansive soils and geothermal energy that is extracted from ground soils.

Louisiana has been affected by its expansive soil. In north Louisiana especially, pavements often get longitudinal cracks due to the expansive subgrade soil. In this dissertation, one of the major types of expansive soils, which is called Moreland clay, is investigated to understand the swell-shrink properties. The dissertation research started with the characterization of Moreland clay by performing a series of laboratory tests. As a by-product, a GIS-based swelling potential map of expansive soil in Louisiana was developed. It is concluded from the characterization that Moreland clay is one of the most expansive soils in the world.

In the dissertation research, an easily implementable model is developed based on the theory of beam on elastic foundation, in which the mechanism of soil strength is

mathematically considered. The predicted heave or shrinkage of expansive soils below the pavement is integrated in the model as the beam deflection. In the proposed method, pavement is simplified as a beam with a virtual load as a form of Fourier series applied on top of the beam to mimic the heave/settlement caused by the volume change of expansive soils. The virtual load is determined by making the predicted subgrade soil heave/settlement equal to the beam deflection. Finally, a closed-form solution of the beam's deflection, rotation, bending moment and shear force are developed, which is caused by the heave/shrinkage of the expansive soil below the pavement. Compared with the traditional finite element models, the proposed analytical model is significantly more simple and more easily implemented. The closed-form solutions make pavement stress analyses and soil heave predictions separate. All the equations and calculations are incorporated in the Excel spreadsheet. The Excel-based software package will be the only required tool for design calculations. As a part of the expansive soil research, using different soil stabilizers (e.g., geopolymer concrete (GPC) and cement) to stabilize the expansive soil is also investigated.

Finally, the moisture content of soil on geothermal energy is investigated. At the beginning, a three-story building in New Orleans is designed with an energy-pile foundation as an example to see the prospect of geothermal energy in Louisiana. The research shows, if geothermal energy is used for the building's heating and cooling energy source, less carbon dioxide would be emitted compared to its traditional heating and cooling energy source (i.e., electricity, natural gas, etc.). As a part of the research, a simple graph method is proposed to design a borehole heat exchanger for small apartments and offices. A small apartment in Ruston, Louisiana, is designed as an

example using the graph method and later again designed with the two very popular commercial software GLD 2012 and GLHEPRO. The result from the graph method shows a great convergence with both commercial software programs. At the end, a sensitivity analysis of different design parameters of energy pile is performed to have a better understanding of the geothermal energy system.

## APPROVAL FOR SCHOLARLY DISSEMINATION

The author grants to the Prescott Memorial Library of Louisiana Tech University the right to reproduce, by appropriate methods, upon request, any or all portions of this Thesis (or Dissertation). It is understood that "proper request" consists of the agreement, on the part of the requesting party, that said reproduction is for his personal use and that subsequent reproduction will not occur without written approval of the author of this Thesis (or Dissertation). Further, any portions of the Thesis (or Dissertation) used in books, papers, and other works must be appropriately referenced to this Thesis (or Dissertation).

Finally, the author of this Thesis (or Dissertation) reserves the right to publish freely, in the literature, at any time, any or all portions of this Thesis (or Dissertation).

Author 

Date 02.06.2017

# DEDICATION

To my parents, my loving sister Trisha, my wonderful friend, Saleh Mahbub, and my beautiful wife, Rafia Qandeel Baloch, for their great support and encouragement.

TABLE OF CONTENTS

LIST OF TABLES

LIST OF FIGURES

ACKNOWLEDGEMENTS

First and foremost, I wish to thank God Almighty for the life he gave me. I owe all that I am to him. It is my immense pleasure in thanking the persons and organizations that helped me over the years to bring my Ph.D. dissertation to the final form.

I would like to express my deep gratitude and sincere appreciation to Professor Dr. Jay Wang for his technical guidance, continuous support and constructive suggestions throughout the course of this research. Without his dedication, effort, and active involvement, this work would not have been possible.

I would also like to thank Dr. Nazimuddin Wasiuddin, Dr. William B. Patterson, Dr. Carlos Montes and Dr. Arun Jaganathan for serving as my committee members. Thank you for allowing my defense to be an enjoyable experience and for your valuable comments and suggestions.

I want to thank Dr. Readul Islam and Shams Arafat for their help with the laboratory work and Saleh Mahbub for always listening to me, offering me advice and supporting me through this entire process.

Thanks go especially to my beloved parents for all their love and sacrifices. Thank you for teaching me to work hard and being supportive of my dream to obtain my Ph.D.

Finally, and most importantly, I would like to thank my wife Qandeel. Her support, encouragement, quiet patience, countless sacrifices and unwavering love were undeniably the bedrock upon which the past two years of my life have been built. You have been a constant source of strength and inspiration for my work.

# CHAPTER 1

# INTRODUCTION

Moisture content in expansive soil has been the cause of distress for engineers for many years. For geotechnical engineers, this distress manifests as constant worry about the uplift of expansive soil by increased/decreased moisture content in foundation soil, whereas for pavement engineers, it manifests as great concern about the longitudinal cracks on pavements if the subgrade soil is expansive with a high degree of moisture change throughout the year. In Louisiana, especially in the southern part, the soil moisture content is high due to its elevated ground water table (GWT). Recently, using the soil's high degree of moisture content, another research field has flourished, which is harvesting geothermal energy from the soil. In geothermal energy system design, moisture content in ground soil has been identified as the key parameter; therefore, an increase in soil's moisture content indicates that more energy can be found from the soil. In this research, the contradiction of moisture content in Louisiana's soil was investigated.

## 1.1 Relationship between Expansive Soil with Moisture Content

In the mechanism of expansive soil, an increase in moisture content causes the soil to swell. Increased soil volume will cause the structure to fail. On the other hand, during summer time when soil moisture content decreases, it causes the soil to shrink,

which can result once again in a structural failure. Expansive soil is truly unique as compared to regular soil for its presence of minerals like kaolinite, illite and montmorillonite. Although most of the clay soil show some form of volume change with moisture, for expansive soil, the volume change happens abnormally. Louisiana has been well known for its expansive soil related structural damages. In this research, Louisiana's Moreland clay, which is expansive in nature, has been extensively investigated. A complete understanding of the Moreland Clay will help engineers to design future structures in Louisiana safer than before.

### 1.2 Relationship between Geothermal Energy and Moisture Content

In the mechanism of harvesting geothermal energy from the ground soil, the difference between atmospheric and soil temperature is used to heat/cool buildings or produce electricity directly. For moist soil, the heat capacity depends mostly on the moisture content of the soil. In Louisiana, especially in the southern part (i.e., New Orleans) where the GWT is high, the soil has higher moisture content, and piles/boreholes can be used to draw energy from the moist soil. Increased moisture content not only means more energy in the soil; it also means a greater effective zone for each energy pile/borehole. This will also help to harvest a more efficient geothermal energy system from the relatively smaller area.

### 1.3 Hypothesis and Objective

As seen from before, moisture content-induced damage is one of the most commonly observed distresses in the structures on expansive soils, but moisture content in ground soil is also the key design parameter of renewable geothermal energy. The main hypothesis of this study is as follows:

"Using the Winkler foundation model, a closed-form analytical solution can be developed to calculate the effects of expansive soil on pavements."

The objective of this study is to characterize and find the swell-shrink properties of Louisiana's Moreland clay, develop an analytical model to find the stress in pavement due to the presence of expansive soil in the subgrade, and investigate geothermal energy potential for Louisiana's soil. In the geothermal energy research, the utilization cases of the geothermal energy system for both North and South Louisiana are evaluated, and finally, a simplified graphical model is developed to design a small-scale geothermal energy system for Louisiana.

## 1.4 Outline of the Dissertation

This dissertation is focused on explaining the volume change behavior of expansive soil with the newly developed analytical model of pavement stress using Winkler foundation. The dissertation also includes findings from two case studies of geothermal energy systems, and a simplified method of designing a geothermal system in Louisiana. The literature review and findings of the soil study are presented in six chapters. Chapter 2 is the literature review, Chapters 3 through 6 contain the expansive soil study. Chapter 7 presents the geothermal energy study, and finally, Chapter 8 gives the overall conclusions and recommendations for future studies.

Chapter 2 introduces a state-of-the-art literature review on expansive soil and geothermal energy. This chapter also includes mineralogy, swelling mechanism, heave prediction methodologies, important factors of geothermal energy and types of geothermal energy.

Chapter 3 describes the process of producing expansive Moreland clay distribution map, soil sampling and disseminating details of all the soil experiments to find the swell-shrink properties of the Moreland clay. The one-meter Moreland clay heave prediction using the material properties from the experiment results led to the production of the Louisiana soil's swelling potential map.

Chapter 4 describes using six boundary conditions to determine the three-dimensional constitutive surfaces for a soil. In the chapter, for the first time, the Moreland clay constitutive surface is plotted.

Chapter 5 presents in detail the development of an analytical method to analyze pavement stress caused by soil expansion or shrinkage. On the beam theory, a virtual load-based model is developed to find the soil heave/settlement induced stresses.

Chapter 6 describes the research on expansive soil stabilization with geopolymer cement (GPC) and cement. Four groups (5% GPC, 10% GPC, 20% GPC and 10% cement) of stabilized Moreland soil samples are prepared, and each group is studied with three samples produced and stabilized for seven, fourteen and thirty days, respectively. At the end of each curing time, consolidation tests are conducted to find the samples' stabilization effectiveness that is dependent on curing time and GPC percentage.

Chapter 7 presents two case studies of the application of geothermal energy for small buildings in both North and South Louisiana. A graphical method is also developed to design a geothermal energy system for small buildings in Louisiana.

Chapter 8 summarizes important conclusions from the previous chapters. Recommendations for future studies are included.

# CHAPTER 2

# LITERATURE REVIEW

## 2.1 Introduction

In nature, moisture content plays a key role in our living conditions. During the rainy season when soil moisture content increases so does the soil volume, which might cause structural failure. On the other hand, an increase in moisture content implies a potential increase in geothermal energy extraction from the soil. The structure can also incur damage due to soil volume reduction in a dry season. In this chapter, a comprehensive summary of expansive soil mineralogy, its swelling mechanism, different heave predicting methodologies, and soil stabilization using geopolymer material are included. Finally, a state-of-the-art complete review of geothermal energy, including types of geothermal energy and important design parameters of geothermal energy, is explained in detail.

## 2.2 Expansive Soil

Expansive soil refers to any soil that has significant changes in its volume that correspond with changes in its moisture content. Generally, when expansive soil gets wet, its volume increases, and when it dries, it shrinks. Because of its seasonal volume change, it might create structural failure, if the volume change is not carefully considered during the design of the structure. Many researchers have tried to find the consequences of

expansive soil on structures. In 1973, Jones and Holtz reported that, in the US alone, "each year, shrinking and swelling soil inflicts at least $2 billion in damages to houses, buildings, roads, and pipelines more than twice the damage from floods, hurricanes, tornadoes, and earthquakes!" [1]. They also concluded that 60% of the new houses built in the US will experience minor damage during their useful life cycle, and 10% will experience significant damage beyond any form of repair. Krohn and Slosson in 1980 estimated that $7 billion is spent each year in the US because of damage to all types of structures built on expansive soil [2]. In 1986, Snethen stated, "While few people have ever heard of expansive soil and even fewer realize the magnitude of the damage they cause, more than one-fifth of American families live on such soil, and no state is immune from the problem they cause. Expansive soil has been called the 'hidden disaster': while they do not cause loss of life, economically these soils have become one of the US' costliest natural hazards" [3]. In 1979, Fredlund explained there are two main reasons behind the lack of significant development for unsaturated soil mechanics: (1) insufficient science with theoretical background because the stress condition and mechanics involved in an unsaturated expansive soil are not properly understood and (2) insufficient financial recovery for engineers because the possible liability to the engineer is often large relative to the financial remuneration, especially with regard to expansive soil. Consultants might find other areas of geotechnical engineering more profitable. More structural soundness and more economical design is possible if volume change behavior of expansive soil can be reliably estimated [4].

## 2.3 Origin of Expansive Soil

In 1969, Donaldson divided the parent materials associated with expansive soil into two groups [5]. They are (1) igneous rocks in which the feldspar and pyroxene minerals configure montmorillonite and other secondary minerals through decomposing and (2) sedimentary rocks that contain montmorillonite, one of the constituents that breaks down physically to form expansive soil. In 1973, the paleogeographic condition in the Rocky Mountain and Great Plains regions of the US was investigated by Tourtelot [6]. Montmorillonite was believed to be formed from two separate origins: (1) the products of weathering and erosion of the rocks and (2) the ash generated by the volcanic eruptions. The origin and distribution of expansive materials are generally a combination of the geological history, sedimentation and present local climatic conditions. Expansive materials result from the following sources, working individually or in combination: (a) weathering, (b) diagenetic alteration of pre-existing minerals, and (c) hydrothermal alteration [7]. Eberl [8] explained that the weathering is the most important source of clay formation, which is a combination of three different mechanisms: (a) inheritance, (b) neo-formation, and (c) transformation. Mitchell and Soga [9] explained these reactions are typically characterized by ion exchange with the surrounding environment and/or layer transformation in which the structure of octahedral, tetrahedral, or fixed interlayer cations is modified.

## 2.4 Clay Mineralogy

As Grim [10] defined, clay minerals are chemically composed of a combination of silicates of aluminum and/or iron and magnesium. Clay minerals are mostly sheet-like in structure and can have various shapes. A typical clay particle or expansive soil is made

of microscopic platelets with negative electrical charges on their flat surfaces and positive electrical charges on their edges [11]. The structure of expansive soil can be visualized as building blocks. Mitchell and Soga [9] gave a detailed description of these building blocks, which include two basic elements: silicon tetrahedron and alumino-magnesium octahedron, as shown in Fig. 2.1 and 2.2. The blue balls in the tetrahedral sheet and the green balls in the octahedral sheet represent oxygen. Red triangles/balls in the tetrahedral sheet represent silicon, and dark blue triangles/ balls in the octahedral sheet represent aluminum.

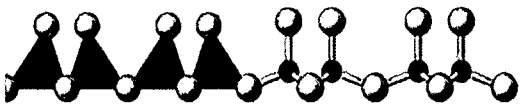

**Fig. 2.1 Silicon Tetrahedron Sheet-like Structure [12]**

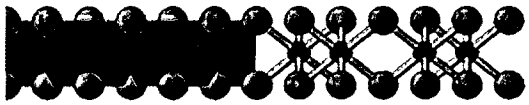

**Fig. 2.2 Alumino-Magnesium Octahedral Sheet-like Structure [12]**

Silicon tetrahedron is made up of silicon and oxygen atoms where alumino-magnesium octahedron consists of aluminum or magnesium atoms surrounded by hydroxyls. In the silicon tetrahedron, oxygen atoms have an unsatisfied chemical bond and the oxygen atoms at the base are shared with the adjacent tetrahedron. This silicon tetrahedron formation satisfies the oxygen atoms at the base, creating a sheet-like structure. However, the oxygen atoms at the apex will still have unsatisfied bonds, as shown in Fig. 2.1 [11-13]. Octahedral units share their hydroxyls creating a sheet-like

structure as illustrated in Fig. 2.2. In this arrangement, there are no unsatisfied chemical bonds [11-13].

From the different arrangements of these two building blocks mentioned above, a variety of clay minerals can be created. Mitchell and Soga [9] depicted several different minerals. Natural clay soil is most of the time a combination of three basic minerals. The minerals are 1) kaolinite, 2) illite and 3) montmorillonite [11]. They are tiny crystalline structures with sizes varying between 10-6 mm to 1 μm. These crystalline structures are generally named colloids. Unlike sands and silts, the grain size distribution of clays has almost no influence on the engineering behavior; whereas colloidal properties, such as adsorption of water due to the large specific surface area of the particles, dominate the performance of the clay soil [13-16].

Kaolinite consists of alternating layers of silica and alumina sheet (1:1 or two-layer type). The layers are held together by hydrogen bonding between hydroxyls from the alumina sheet and oxygens from the silica sheet, as shown in Fig. 2.3. Such bonding is very strong, preventing water from entering the basic layers and allowing many layers to build up to make a rather large crystal. A typical kaolinite crystal may be 70 to 100 layers thick. Due to the relatively large particle size and low specific surface area, i.e., total surface area of particles per unit mass, kaolinite shows less plasticity and swelling than most other clay minerals [11-13].

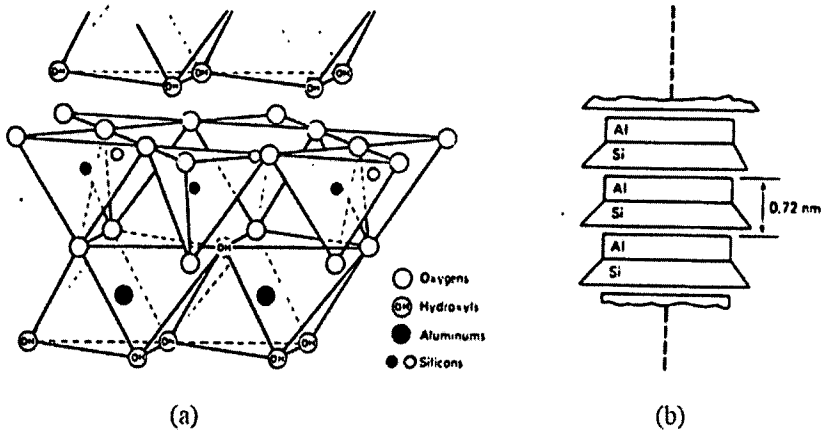


**Fig. 2.3 (a) Atomic Structure of Kaolinite and (b) Symbolic Structure of Kaolinite [10, 13, 17]**

Montmorillonite is made of repeating layers of an alumina sheet (gibbsite) sandwiched by two silica sheets (2:1 or three-layer type). Since the bonding between the silica sheets is weak and isomorphous, substitution of aluminum with magnesium or iron in the octahedral sheet occurs, and water and exchangeable ions enter easily between layers as illustrated in Fig. 2.4, pushing the layers farther apart. As a result, the specific surface increases several times. Because of the extremely small particle sizes and unbalanced charge in the octahedral sheet, montmorillonite shows a distinctive swelling/ shrinking behavior. Upon wetting, montmorillonite clays may swell several times their dry volume, and when dried, they tend to shrink and crack. Usually, such dry soil is very hard [11-13].

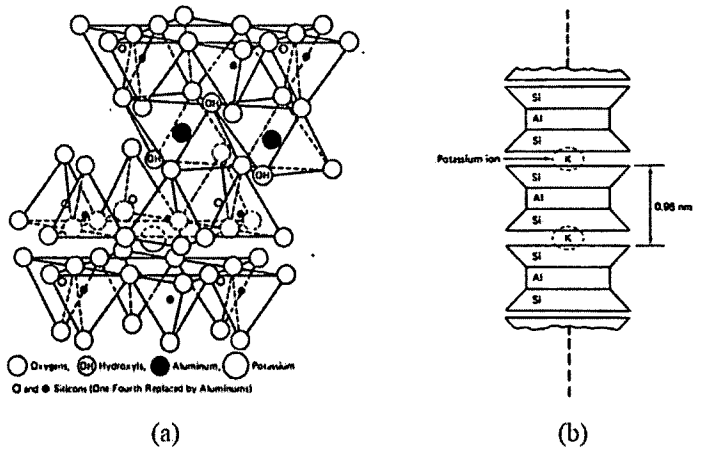


(a) (b)

**Fig. 2.4 (a) Atomic Structure of Montmorillonite and (b) Symbolic Structure of Montmorillonite [10, 13, 17]**

Illite is also a 2:1 type (three-layer) mineral with repeating layers of an alumina sheet in the middle and silica sheet at both top and bottom. It is very similar to montmorillonite, but the layers are bonded together with potassium cations, as shown in Fig. 2.5. The potassium cations are almost exactly fitted into the hexagonal hole (formed by the silica tetrahedral sheets) due to the relatively high-density negative charges induced from the isomorphous substitution of aluminum ions for silicon ions in the tetrahedral sheets. Such a tight bonding between layers prevents the expansion of the entire lattice and makes illite much less expansive in nature than montmorillonite. The engineering behavior of illite is between kaolinite and montmorillonite [11-13].

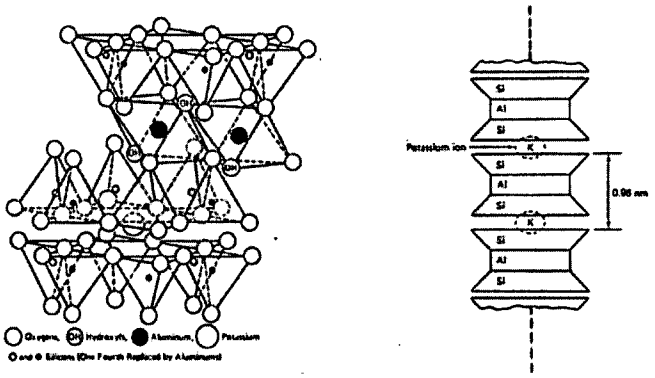

(a) (b)

**Fig. 2.5 (a) Atomic Structure of Illite and (b) Symbolic Structure of Illite [10, 13, 17]**

In most cases, natural clay soils consist of more than one mineral type. They are often the complex mixture of several different minerals. Furthermore, the internal structure is different from previously described idealized minerals. Mixed or interstratified internal structures are very common. Therefore, clay minerals are often composite minerals such as illite-montmorillonite, chloride-illite, etc. Sometimes these minerals are loosely termed bravaisite [13]. Identification of different clay minerals usually involves using X-ray diffraction, differential thermal analysis (DTA), or electron microscopy transmission and scanning. These methods are rather sophisticated, and quantitative analysis is not possible. In 1948, Casagrande suggested using Atterberg Limits to identify clay minerals [18]. A plasticity chart for clay mineral identification was developed by Holtz and Kovacs, as shown in Fig. 2.6 [19]. From an engineering point of view, this method gives about the same information as the most sophisticated analyses [19]. Different zones in such plasticity charts indicate the behavior of a soil within a particular zone is controlled by the corresponding mineral type. It does not necessarily mean the soil is 100% of the labeled mineral. Table 2.1 shows free swell for common clay minerals.

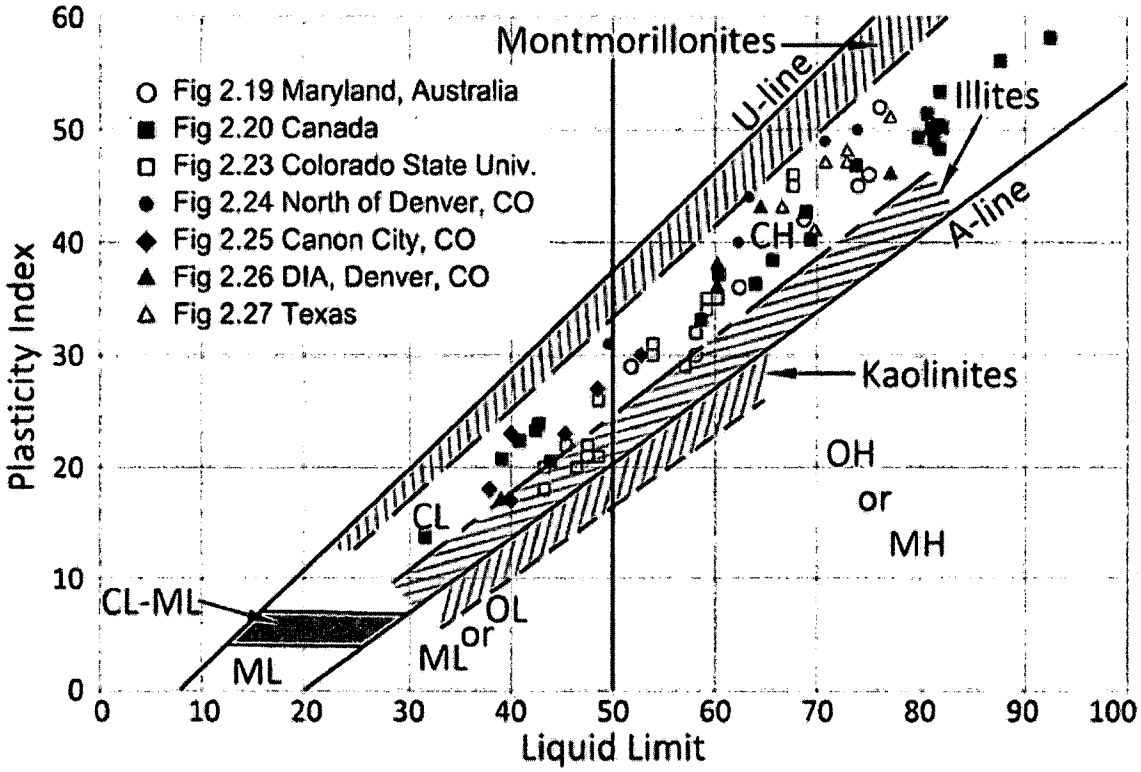


**Fig. 2.6 Location of Common Clay Minerals on Casagrande's Plasticity Chart [19]**

**Table 2.1 Typical Values of Free Swell for Common Clay Minerals [7]**

| Clay Minerals | Free swell % | |
|---|---|---|
| | Grim [20] | Shamburger *et al.* [21] |
| Na-montmorillonite | 1400-2000 | 1400-1600 |
| Ca-montmorillonite | 45-145 | 65-145 |
| Illite | 60-120 | 60-120 |
| Kaolinite | 5-60 | 5-60 |

## 2.5 Interaction Between Clay and Water

To understand the interaction between clay and water, it is important to understand the three components of this interaction – the associated water, the cations and the mineral. Clays tend to have either small plate or tubular-like shapes. Shapes like these make the electrical charge unbalanced and form a crystalline structure. Table 2.2

shows some properties of clay minerals. Another unique property of clays is they have a high affinity to water, actively reacting to it. Because of their high attraction to water, clays found in nature are most likely to be hydrated. The hydration process is done by electrically attracting water molecules to the surface areas of the clay particles, forming multiple water envelope layers around the clay soil. The final envelope is called as double-layer water or osmotic water, which is actually a factor of the shrink-swell potential, plasticity and cohesion between particles [11, 19, 22]. Within the several layers of this envelope, the innermost layer is referred to as absorbed water because it has the strongest bond with the particle [23]. The ions distribution on the clay particle surface is shown in Fig. 2.7. The effective thickness of the envelope layer can be measured using the Gouy-Chapman theory, as shown in Eq. 2.1:

$$z = \frac{1}{ev}\sqrt{\frac{\varepsilon kT}{8\pi n_0}} \tag{2.1}$$

where

z = the characteristic length or thickness;

e = unit charge of an electron, $4.77 \times 10^{-10}$ esu;

e = dielectric constant;

k = Boltzmann constant, $1.38 \times 10^{-6}$ erg/K;

v = valency of the ions;

$n_0$ = concentration of the ions in the bulk solution in ions/cm$^3$; and

T = temperature, K.

**Table 2.2 Relative Dimensions of Common Clay Minerals (Reproduced after Huang [13])**

| Typical Thickness (nm) | Typical Diameter (nm) | Specific Surface ($km^2/kg$) |
|---|---|---|
| 3 | 100*1000 | 0.8 |
| 30 | 10000 | 0.08 |
| 30 | 10000 | 0.08 |
| 50-2000 | 300-4000 | 0.015 |

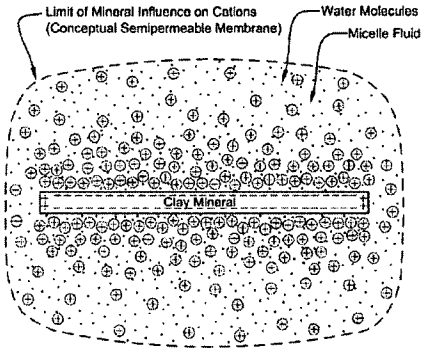


**Fig. 2.7 Distribution of Ions Near Particle Surface [11]**

Clay particles are surrounded by cations in two layers, as shown in Fig. 2.7. These two layers are called the Stern layer and the diffuse layer, where the cations within the Stern layer are those that adhere to the clay particle surface. It is believed water present in the Stern layer is significantly different in terms of structure and physiochemical properties than the water outside the Stern layer (free water) [13]. This negatively charged inner mineral surrounded by positively charged cations to balance each other can be visualized as a unit called clay micelle [11]. The attraction force between these two charges results in the change in the structure of the adsorbed water. Because of highly-oriented ionic packing, density and viscosity of adsorbed water can be much higher than free water. Figure 2.8 illustrates such a phenomenon. Adsorbed osmotic water is usually considered part of the clay mineral. As the distance from the clay particle increases,

cations within the diffuse layer gradually decrease in concentration, and the water eventually becomes "free." This results in a gradient in the cation concentration that is highest near the surface and decreases with distance away from the surface.

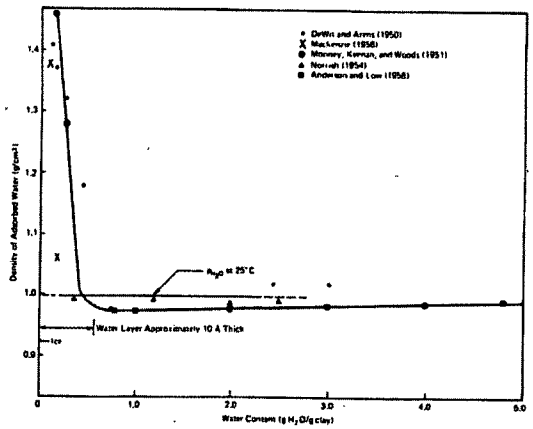

**Fig. 2.8 Density of Adsorbed Water [24]**

Hillel [15] explained the balance of ionic distribution between the Stern layer and diffuse layer is due to the twofold tendencies: 1) electrostatic attraction between positively charged clay particles and the surrounding cations keep the minimum energy, and 2) the kinetic motion of the water molecules pushes the adsorbed cations outward to seek the same concentration within the whole solution phase. This makes all clays show some degree of volume increase once they are in contact with water. Expansive soil is a special case where they continue swelling due to high moisture contents. Atomic structure, large surface area and ion exchangeability are important parameters of the degree of swelling. For example, Montmorillonite soil has larger surface area than kaolinite and illite clays, resulting in the thicker double-layer water around the particle and between the layer spaces. Again, when hydrated, the ions increase in size, resulting in clay swelling. The smaller the ion is, the greater the amount of hydration the ion

undergoes. The most common ions in a clay-water system, in order of increasing ionic radii, are sodium (Na), magnesium (Mg) and potassium (K). Therefore, the Na-montmorillonite clay soil experience higher expansivity than K-montmorillonite clay soil. Also, montmorillonite clays showing high volume change because of repulsion resulting from diffuse ion layer interpenetration, which depends on the distance between clay particles. Clay with a uniform distribution of ions has a net attraction force between particles. As water is introduced into soil, water molecules adsorbed on the clay surface will force adjacent particles apart. When the distance of two particles reaches about $15A^0$, two diffuse ion layers are formed, one associated with each surface. In this case, there is a net repulsion. Soil with kaolinite and/or illite minerals exhibit much less volume change since the interpenetration of ions is not available. Microscale mechanisms of shrink/swell expansive soil, such as clay mineral type, clay-water interaction, etc., are only useful for qualitative analysis since the influence of the different components of volume change is difficult to separate. Also, exact measurements for the type and amount of different clay minerals are impossible to obtain. Because of all these factors, the physical and/or mechanical properties of soil that reflect the microscale mechanisms of expansive soil are used for engineering purposes [13, 19, 22, 25].

## 2.6 Swelling Mechanism

Researchers and soil scientists have been trying to understand the swelling mechanism for quite some time. Different researchers have tried to describe the process in different kinds of literature [14, 20, 22, 26-32]. Bolt [26] subdivided swelling processes into 1) mechanical swelling, which happens in the presence of elastic and time-dependent stress unloading (i.e., digging excavations, tectonic uplift, or erosion) and 2)

physicochemical swelling, which is classified into hydration energy driven crystalline swelling and electrical double-layer effect generated osmotic swelling [7, 29].

### 2.6.1 Crystalline Swelling

Likos [33] explained the mechanism of crystalline swelling as swelling resulting from a short-range hydration and intercalation of multiple discrete layers of water between the clay mineral interlayers. This process is referred to as "Type I" swelling [34, 35] after which "Type II" swelling or osmotic swelling starts. Osmotic swelling is done by longer-range electrical doublelayer effects. Likos [33] explained crystalline swelling is driven primarily by the energy associated with the initial hydration of exchangeable interlayer cations and hydrogen bonding or charged surface-dipole attraction effects associated with solid-liquid interactions occurring in the immediate vicinity of the clay particle surfaces. Figure 2.9 shows the sequential crystalline swelling process for montmorillonite. Once the clay sheet interlayer distance exceeds about $10A^0$ (a distance of four water molecules), hydration force becomes minimal compared to electrostatic repulsion force between adjacent plates. According to Newman [34], in this situation, the distance between plates might increase until the plates become completely dissociated, and the swelling that happens is called "osmotic swelling."

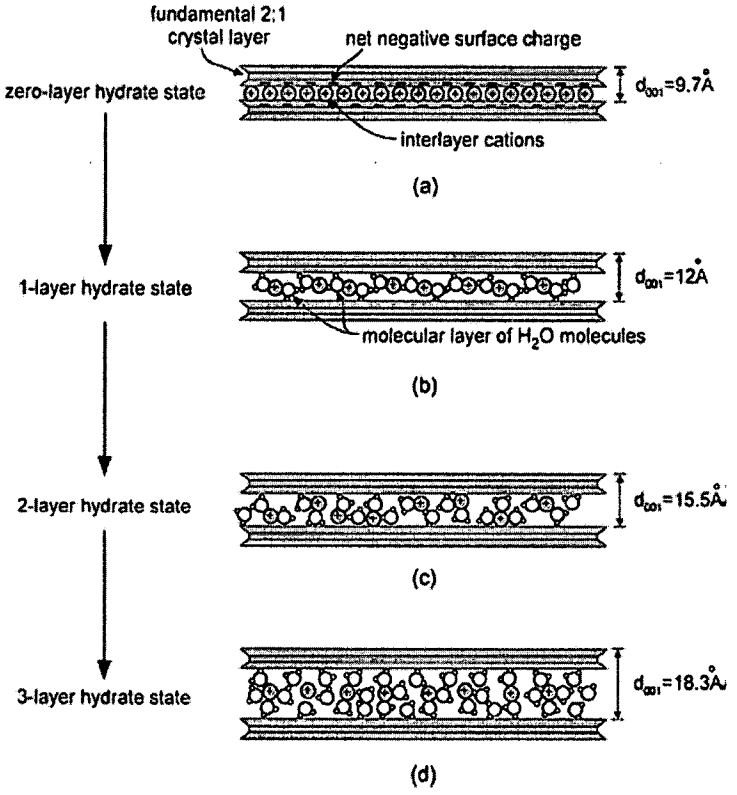


**Fig. 2.9 Theoretical Model of the Montmorillonite Mineral's Sequential Crystalline Swelling Process [33]**

2.6.2 Osmotic Swelling

Greathouse *et al.* [36] explained that the clay mineral montmorillonite lattice has a chemical composition that consists of aluminum oxide and silicon oxide, where on its surface a net negative charge is developed when any divalent metals (i.e., magnesium or calcium) substitute for the aluminum or silicon. When an aqueous electrolyte solution is present, a double-layer system is formed through the attraction force between negatively charged mineral surfaces with cations and polar water as illustrated in Fig. 2.10. The overlap of both layers results in a repulsive force, pushing the clay platelets apart and causing an excess cation concentration between the platelets. Therefore, free water must be drawn into the system to restore equilibrium. Different researchers have worked on understanding double-layer repulsion induced soil expansion [36-42]. Montmorillonite

shows the highest degree of double-layer response, whereas illite has an intermediary response, and finally, the kaolinite changes volume exclusively by mechanical unloading phenomenon [29].

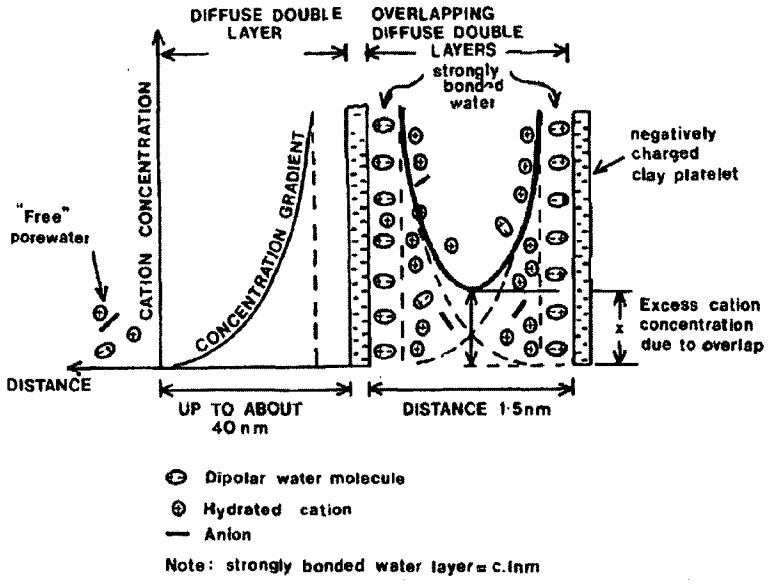


**Fig. 2.10 Theoretical Model of Osmotic Swelling (Double-layer) of Two Clay Mineral Platelets [29]**

## 2.7 Factors Influencing Swelling and Shrinking of Soil

Expansive clays have a complex swelling process influenced by different factors as summarized in Table 2.3 and 2.4. A clay particle, with its platelet shape, has a negative electrical charge on its surface and positively charged edges (Fig. 2.7). These negative charges get balanced by the cations in the Stern layer. This overall force field is a function of the Van der Waals force and the adsorptive force of the charged clay particle and cation filled double-layer water. This internal electrochemical force system must be balanced with the application of externally applied stresses and capillary tension (matric suction) in the soil water. If for some reason this internal force equilibrium gets disturbed, clay shows swell-shrink behavior. This unbalanced force field may occur due to change

of water in the double-layer or change of chemical composition. Factors influencing this swell-shrink behavior of soil can be divided into three different groups: soil characteristics, environmental factors and stress state. Table 2.3 and 2.4 only show the soil and environmental factors of the swell-shrink behavior of the clay soil.

**Table 2.3 Soil Properties that Influence Shrink-swell Potential [31]**

| Factor | Description | References |
|---|---|---|
| Clay mineralogy | Clay minerals that typically cause soil volume changes are montmorillonites, vermiculites and some mixed-layer minerals. Illites and kaolinites are infrequently expansive but can cause volume changes when particle sizes are extremely fine (less than a few tenths of a micron). | [14, 43-45] |
| Soil water chemistry | Swelling is repressed by increased cation concentration and increased cation valence. For example, $Mg^{2+}$ cations in the soil water would result in less swelling than Na+ cations. | [45] |
| Soil Suction | Soil suction is an independent effective stress variable, represented by the negative pore pressure in unsaturated soil. Soil suction is related to saturation, gravity, pore size and shape, surface tension, and electrical and chemical characteristics of the soil particles and water. | [46-50] |
| Plasticity | In general, soil that exhibit plastic behavior over wide ranges of moisture content and that have high liquid limits have greater potential for swelling and shrinking. Plasticity is an indicator of swell potential. | -- |
| Soil structure and fabric | Flocculated clays tend to be more expansive than dispersed clays. Cemented particles reduce swell. Fabric and structure are altered by compaction at higher moisture content or remolding. Kneading compaction has been shown to create dispersed structures with lower swell potential than soil statically compacted at lower moisture contents. | [51, 52] |
| Dry density | Higher densities usually indicate closer particle spacing, which may mean greater repulsive forces between particles and larger swelling potential. | [53] |

**Table 2.4 Environmental Conditions that Influence Shrink-swell Potential [31]**

| Factor | Description | References |
|---|---|---|
| 1. Initial moisture condition | A desiccated expansive soil will have a higher affinity for water, or higher suction, than the same soil at higher moisture content and lower suction. Conversely, a wet soil profile will lose water more readily on exposure to drying influences and shrink more than a relatively dry initial profile. The initial soil suction must be considered in conjunction with the expected range of final suction conditions. | -- |
| 2. Moisture variations | Changes in moisture content in the active zone near the upper part of the profile primarily define heave. It is in those layers that the widest variation in moisture content and volume change will occur. | [54] |
| 2.1 Climate | Amount and variation of precipitation and evapotranspiration greatly influence the moisture content availability and depth of seasonal moisture content fluctuation. Greatest seasonal heave occurs in semiarid climates that have pronounced, short wet periods. | [55] |
| 2.2 Groundwater | Shallow water tables provide a source of moisture content, and fluctuating water tables contribute to moisture content. | |
| 2.3 Drainage and manmade water sources | Surface drainage features, such as ponding around a poorly graded house foundation, provide sources of water at the surface; leaky plumbing can give the soil access to water in greater depth. | [56, 57] |
| 2.4 Vegetation | Trees, shrubs and grasses deplete moisture content from the soil through transpiration and cause the soil to be differentially wetted in areas of varying vegetation. | [58] |
| 2.5 Permeability | Soil with higher permeability, particularly due to fissures and cracks in the field soil mass, allow faster migration of water and promote faster rates of swell. | [59, 60] |
| 2.6 Temperature | Increasing temperatures cause moisture content to diffuse to cooler areas beneath pavements and buildings. | [61, 62] |

| Factor | Description | References |
|---|---|---|
| 3. Stress conditions | | |
| 3.1 Stress history | An overconsolidated soil is more expansive than the same soil at the same void ratio but normally consolidated. Swell pressures can increase on the aging of compacted clays, but the amount of swell under light loading has been shown to be unaffected by aging. Repeated wetting and drying tend to reduce swell in laboratory samples, but after a certain number of wetting-drying cycles, swell is unaffected. | [45, 63] |
| 3.2 In situ conditions | The initial stress state in a soil must be estimated to evaluate the probable consequences of loading the soil mass and/or altering the moisture content environment therein. The initial effective stresses can be roughly determined through sampling and testing in a laboratory, or by making in situ measurements and observations. | -- |
| 3.3 Loading | The magnitude of surcharge load determines the amount of volume change that will occur for a given moisture content and density. An externally applied load acts to balance interparticle repulsive forces and reduces swell. | [64] |
| 3.4 Soil profile | The thickness and location of potentially expansive layers in the profile considerably influence potential movement. The greatest movement will occur in profiles that have expansive clays extending from the surface to depths below the active zone. Less movement will occur if expansive soil is overlain by non-expansive material or overlies bedrock at a shallow depth. | [55] |

## 2.8 Soil Suction

State of water is described by the concept of energy term soil suction, which was originally developed in the soil physics of the 1900's [65-67]. The general terminology of soil suction is the free energy state of soil water [68]. Thus, soil suction describes the state of water in the soil [7]. Everything in nature contains two kinds of energy: kinetic and potential. For water inside the soil, kinetic energy is negligible as water moves very slowly through the pores, making the potential energy the key factor. Hillel [15] explained that, in determining the internal condition with regard to change in the mode of a soil water system, potential energy of water is the most important factor. From the quantitative definition, soil suction represents the interaction between soil particles and water as a negative gage pressure. There is a distinctive difference between soil suction and the pore-water pressure because pore-water pressure is usually related to water density, distance from the ground water table (GWT) and the force associated with surface tension [69].

The total suction ($\psi$), which is used to characterize the effect of moisture content on the volume and strength properties of soil, indicates the potential of absorbing pore liquid to satisfy the water deficit of the soil and volumetric swell tendency [7, 46, 48, 49]. This total suction represents the free energy present in the soil water compared with the pure water outside the soil at the same elevation. Alternatively, total suction can be defined as the energy difference between the water inside the soil and the pure water outside the soil, which can draw the pure water into the soil by compensating the friction force, resistance force of water and the expansion force of the clay lattice. This free energy is a function of soil composition and the cation environment [70]. Total energy is

calculated using the following Kelvin equation (Eq. 2.2) based on thermodynamic principles [71]:

$$\psi = -\frac{RT}{\upsilon_{w0}\omega_{\upsilon}} \ln\left(\frac{\bar{u}_{\upsilon}}{\bar{u}_{\upsilon 0}}\right) \tag{2.2}$$

Where,

$\psi$ = soil suction or total suction;

R = universal (molar) gas constant (i.e., 8.31432 J/mol/K);

T = absolute temperature [i.e., T = (273.16 + t°) (K)], $t^0$ = temperature (°C);

$\upsilon_{w0}$ = specific volume of water or the inverse of the density [i.e., $1/\rho_w$ ($m^3$/kg)];

$\rho_w$ = density of water (i.e., 998 kg/$m^3$ at $t^0 = 20^0$C);

$\omega_{\upsilon}$ = molecular mass of water vapor (i.e., 18.016 kg/kmol);

$\bar{u}_{\upsilon}$ = partial pressure of pore-water vapor (kPa); and

$\bar{u}_{\upsilon 0}$ = saturation pressure of water vapor over a flat surface of pure water at the same temperature (kPa); the term $\bar{u}_{\upsilon}/\bar{u}_{\upsilon 0}$ is called relative humidity ($R_h$).

The total suction has two components: matric suction and osmotic suction (Eq. 2.3). Matric suction is also called as capillary potential. Matric suction is also referred to as matrix potential, soil-water suction and soil-moisture retention force. While matric suction is associated with the capillary phenomenon on the air-water interface, osmotic suction $\pi$ is associated with the agent dissolved in the soil water [7]:

$$\psi = (u_a - u_w) + \psi_0 \tag{2.3}$$

Where,

$u_a - u_w$ = matric suction;

$u_a$ = pore air pressure;

$u_w$ = pore-water pressure; and

$\psi_0$ = osmotic suction.

2.8.1 Matric Suction

The most complete definition of matric suction is given by Aitchison and quoted by the International Society of Soil Science as "the equivalent suction derived from the measurement of the partial pressure of the water vapor in equilibrium with the soil water, relative to the partial pressure of the water vapor in equilibrium with a solution identical in composition with the soil water" [50, 72].

Matric suction (or capillary pressure) is the function of moisture content and external load along the slight effect of air pressure while osmotic suction represents the effect of solutes, soluble salts. The difference in the type and concentration of the solutes between pore water and free water (from outside sources) leads to an osmotic imbalance such that physical changes in soil structure may occur through water moving in or out of the pore spaces. Moisture content and external load do not affect the osmotic suction. The matric suction component of total suction is associated with the capillary phenomenon on the air-water interface [7, 13, 15, 46]. Figure 2.11 illustrates the physical model and phenomenon related to capillarity, and Fig 2.12 shows the matric suction mechanism inside the soil.

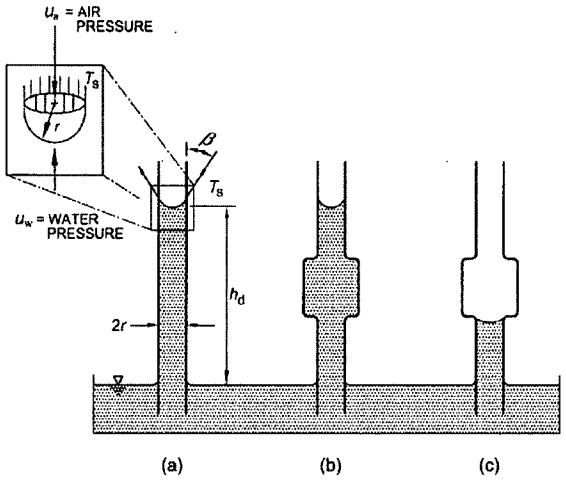


**Fig. 2.11 Physical Model and Phenomenon Related to Capillarity [11]**

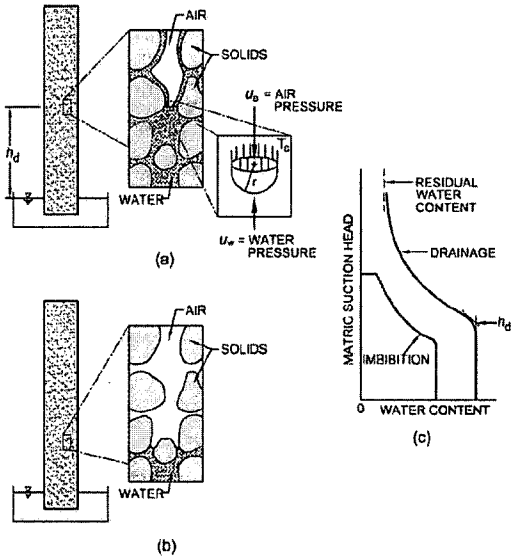


**Fig. 2.12 Matric Suction in Soil: (a) Drainage Condition, (b) Imbibition Condition, and (c) Soil Water Characteristic Curve [11, 31]**

Figure 2.11 shows the surface tension of water arising from the unbalanced molecular interactions on the air-water interface through the capillary phenomenon. The Young-Laplace equation (Eq. 2.4) presents the relationship between the pressure difference ($u_a - u_w$) across the air-water interface, and the surface tension $T_s$ acting on the air-water interface. Figure 2.13 shows the contractile skin of principal radii of Eq. 2.4.

$$(u_a - u_w) = \Delta P = T_s\left(\frac{1}{R_1} + \frac{1}{R_2}\right) = T_s\frac{1}{R_m} \qquad (2.4)$$

where

$R_1$ and $R_2$ = the principal radii of curvature of the interface (Fig. 2.13), and

$(R_1^{-1} + R_2^{-1})^{-1}$ = the first or mean radius of curvature $R_m$.

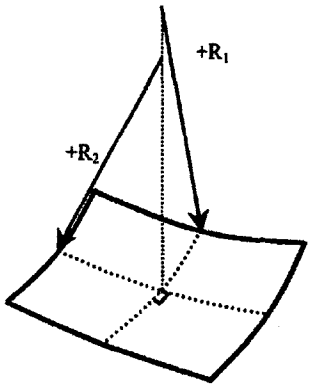


**Fig. 2.13 Schematic Diagram of Principal Radii of the Contractile Skin [73]**

The terms used for radii in Eq. 2.4 are dependent on the geometries for the air-water interface. If the interface is a sphere and the influence of gravity is ignored, the $R_m$ value is equal to R/2 (where R = radius of the sphere); while in the case of a saddle-type meniscus, $R_1$ is equal to $-R_2$ (Fig. 2.14d). Figure 2.14 illustrates some simplified geometries for the air-water interface that might form in an unsaturated soil.

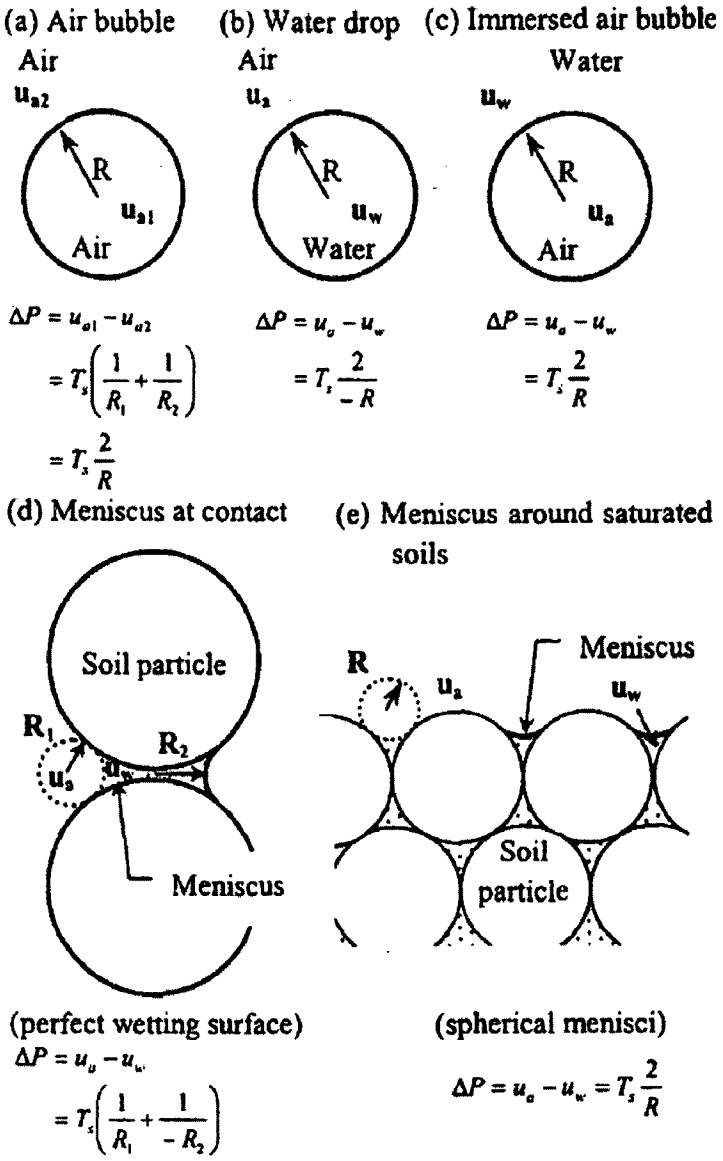


**Fig. 2.14 Simplified Geometry of the Air-water Interface and Associated Pressure Difference ΔP across the Interface Based on the Young-Laplace Equation [73]**

2.8.2 Osmotic Suction

Aitchison [50] defined osmotic suction as "the equivalent suction derived from the measurement of the partial pressure of the water vapor in equilibrium with a solution identical in composition with the soil water, relative to the partial pressure of water vapor in equilibrium with free pure water." Osmotic suction is basically caused by the

difference in salt concentration at a different location in the soil water. The mechanism of osmotic suction is as follows: salt is dissolved in the pore water, creating a pressure difference between water vapor pressure over the solvent surface and the surface of the pure water. As the solution concentration increases so does the reduction of the vapor pressure, leading to a decrease in the relative humidity. This process will result in the increment of total suction where the part of the total suction related to the dissolved salts is referred to as osmotic suction ($\psi_0$). From Fig 2.15, the process can be explained more easily, where two clay particles are in close proximity. As both clay particles are trying to attract the cations, a high concentration of salt is found in the space between and around the particles. Therefore, a "pseudo-semipermeable" membrane is created where the increased concentration of salt pushes the water molecules outside of their influence. This pressure is the osmotic pressure [7, 11].

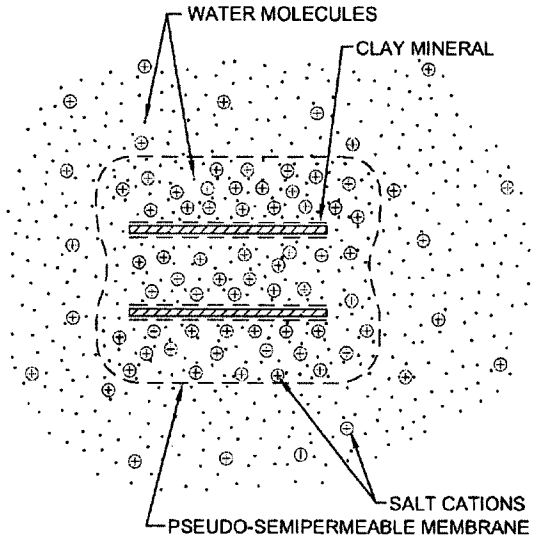


**Fig. 2.15 Pseudo-semipermeable Membrane Effect Causing Osmotic Suction in Clay [11]**

Van't Hoff's law explains that substances in a dilute solution obey ideal gas laws [7]. The magnitude of the osmotic pressure (suction) can be computed using Eq. 2.5.

$$\psi_0 = \frac{n}{V}RT = C_iRT = \rho_s g h_0 \quad (2.5)$$

where

R = the gas constant;

T = the absolute temperature;

n = the number of moles of solute dissolved in volume V of the solution;

$C_i$ (= n/V) = the molar concentration of solute i in the dilute solution;

$\rho_s$ = solute mass density;

g = gravitational acceleration; and

$h_0$ = osmotic pressure head.

Although the experimental research showed in NaCl-amended specimens the major part of total suction is osmotic, it has been described by many researchers that compared to matric suction, osmotic suction has a lesser influence on the mechanical behavior of soil [74-80]. When comparing different soils, different osmotic suctions of the soils (depending on the salt concentration of each soil) create a problem, and it is advisable to assume osmotic suction as a constant value and subtract it from the total suction to find the matric suction [72, 74]. Table 2.5 shows some common laboratory suction measuring methods.

**Table 2.5 Common Laboratory Suction Measurement Methods [13]**

| Test method | Suction components | Range (kPa) | Advantages | Disadvantages |
|---|---|---|---|---|
| Thermocouple Psychrometers (TCPs) | Total | 300 to $10^6$<br>(±10) Lab<br>(±50) Field | 1. Field and laboratory applications<br>2. Convenient range for most soil<br>3. Fairly inexpensive equipment<br>4. Commercially available | 1. Temperature calibration required<br>2. Not applicable in moist soil<br>3. Requires 2- to 7-day equilibration time |
| Filter Paper Sensors | Total | 0 to $10^6$<br>(±10) | 1. Measures full range of suction<br>2. Very inexpensive<br>3. No specialized equipment required<br>4. Simple procedure | 1. Requires 7-day equilibration time<br>2. Care required for moist soil to prevent saturation of sensors |
| Pressure membranes (Axis Translation Technique) | Matric | 0 to 155,500 | 1. Can develop continuous moisture/suction relationship for a single sample<br>2. Measures matrix suction stress state variable directly<br>3. Commercially available | 1. Conceptual and measurement problems of axis-translation technique<br>2. Wetting-drying hysteresis<br>3. Requires 2- to 10-day equilibration time for each moisture-section measurement<br>4. More appropriate for coarse-grained soil |
| Membrane Oedometers | Total<br>Matric<br>Osmotic | 0 to 4000<br>10 to 1000<br>0 to40000 | 1. Can control stress state variable simultaneously<br>2. Australian model measures suction components separately | 1. Requires specialized equipment<br>2. Not available commercially |
| Tensiometers and Pressure Plates | Matric | 0 to 100 | 1. Measures matric suction stress state variable directly<br>2. Commercially available | 1. Low suction range applicable in moist soil only |

2.8.3 Soil-water Characteristic Curve (SWCC)

The SWCC defines the relationship between the moisture content and the soil suction (Fig. 2.16). The SWCC shows the changes in matric suction with the changes of moisture content variation. Because matric suction is a function of soil pore size, it may be concluded that the SWCC reflects the pore size distribution in clay soil. The moisture content is generally quantified in terms of gravimetric water content, volumetric water content or degree of saturation. The SWCC has an important role in terms of understanding the water in the soil pores. It can be visualized as an interpretive model of an elementary capillary model. The effects of soil texture, gradation and void ratio have also become part of the interpretation of measured laboratory SWCC data. The SWCC is also referred to as the water retention curve, soil moisture curve, soil water retention curve, soil water characteristic etc. Different graphical representations are possible for the SWCC by taking the amount of water in the soil in terms of gravimetric moisture content (w)/volumetric moisture content ($\theta$)/degree of saturation (S) or by making the soil suction-axis either a logarithmic or arithmetic scale [7, 11, 13, 81, 82].

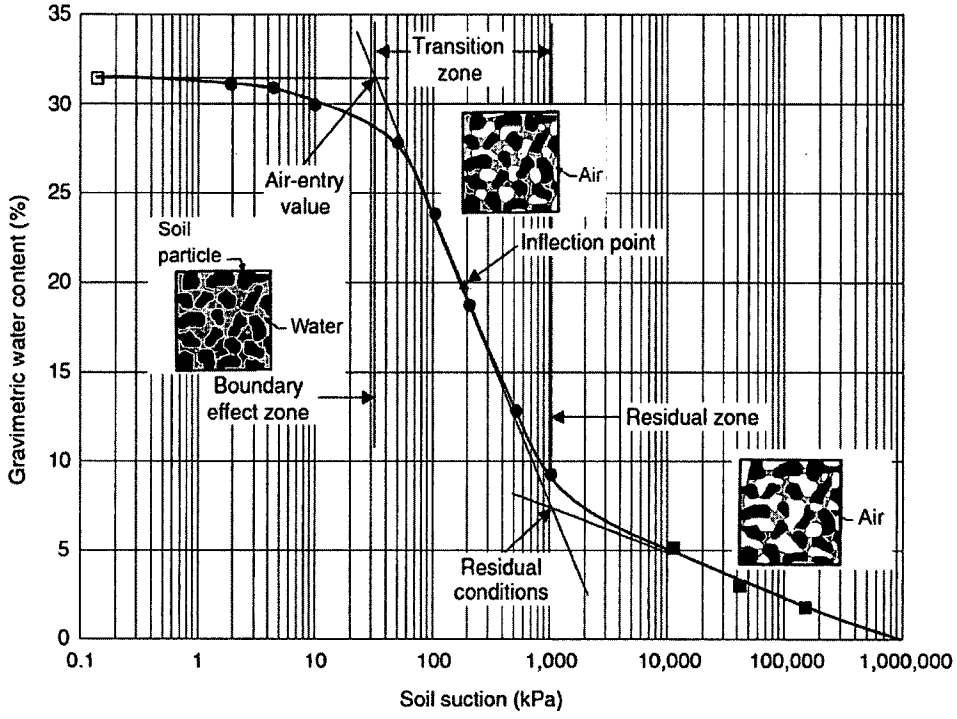


**Fig. 2.16 Typical Unimodal SWCC Curve Showing Desaturation Zone (Modified after [82, 83])**

2.8.4 Important Terminology of SWCC

*Air-entry value* (AEV), also ($\psi_a$), refers to the matric suction value that must be exceeded before air recedes into the soil pores. AEV is also referred to as "displacement pressure" in petroleum engineering and as "bubbling pressure" in ceramics engineering. The AEV of the soil is obtained by extending the constant slope portion of the SWCC to intersect the suction axis at 100% saturation (Fig. 2.17) [84-87].

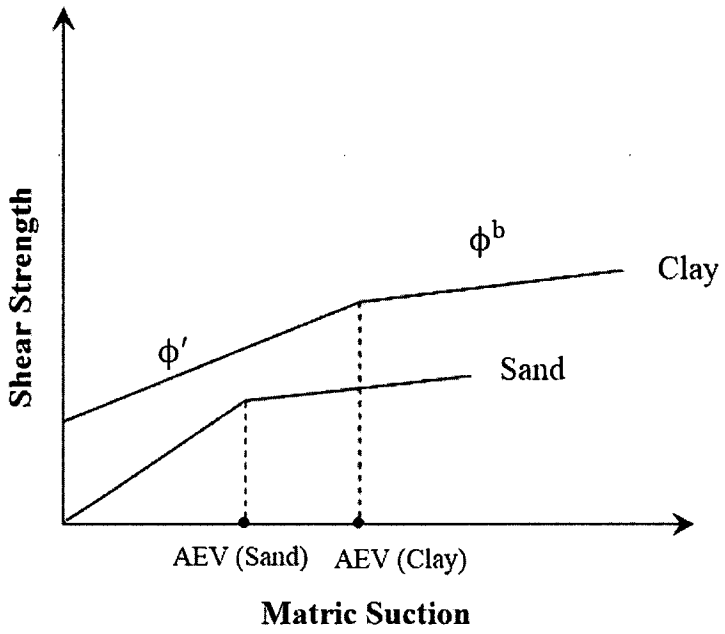


**Fig. 2.17 Effect of Air-Entry Value (AEV) on Unsaturated Shear Strength Envelopes**

*Residual moisture content* ($w_r$) refers to a characteristic of soil indicated by the shrinkage curve, which also indicates the air-entry value of the soil. To remove additional water from the soil, a large suction change, i.e., residual suction ($\psi_r$), is required. The moisture content corresponding to the residual suction is referred to as residual moisture content ($w_r$) [82, 85-87].

*Boundary effect zone* refers to the zone located from zero suction to residual suction. The soil is essentially saturated within this zone. [77].

*Transition zone* refers to the desaturation zone located within the suction range of $\psi_a$ to $\psi_r$. As the suction continues after the residual suction, soil starts to lose water [77].

*Residual zone* refers to the desaturation zone in between $\psi_r$ and $10^6$ kPa. In this zone, large increases in suction lead to a relatively small change in moisture content [77].

2.8.5 Hysteresis Effect of SWCC

The SWCC can be found either by desorption process (drying curve) or by adsorption process (wetting curve). There is a hysteresis effect during these processes, and generally, the drying curve is typically located over the wetting curve (Fig. 2.18). Bear [88] explained that the contact angle at an advancing interface during the wetting process is different from that at a drying interface during the drying process, thereby causing the hysteresis effect. Fredlund and Rahardjo [84] also concluded the entrapped air in the soil influences hysteresis.

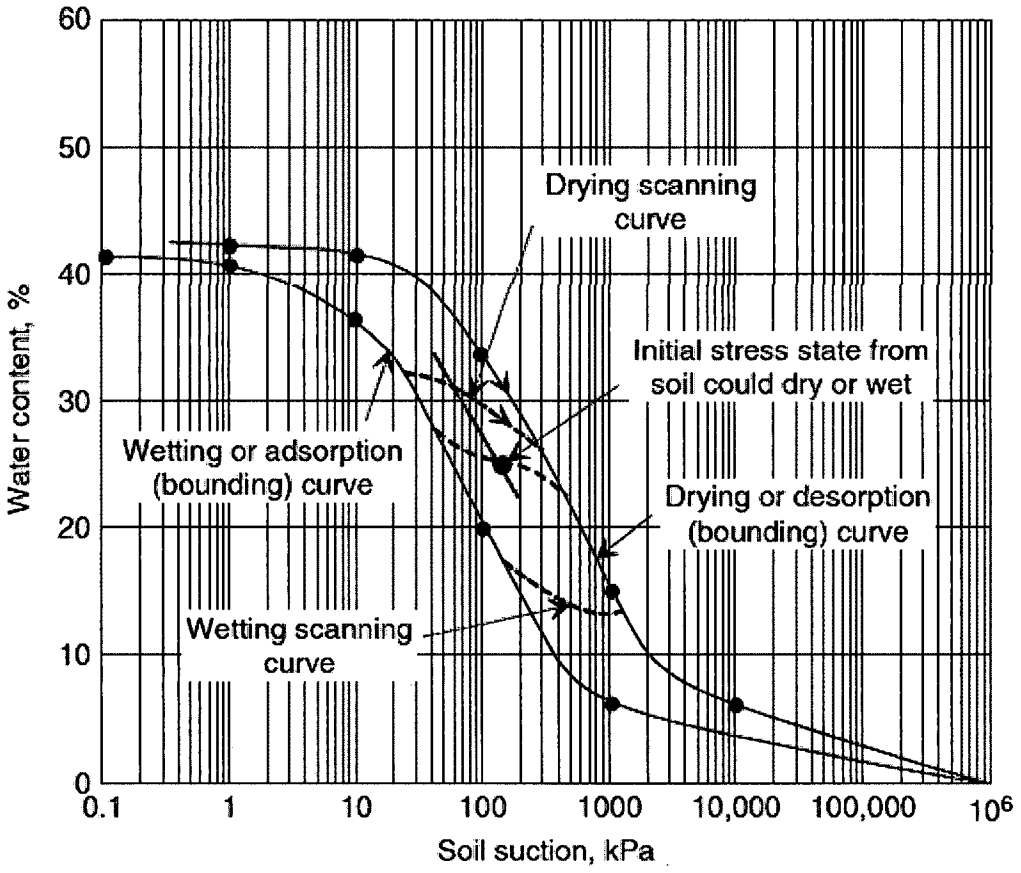


**Fig. 2.18 Hysteresis Loops of SWCC [82]**

2.8.6 Equations for SWCC

Researchers and soil scientists have proposed many closed-form, empirical equations to either best fit the experimentally found SWCC data or to use empirical methods to predict the SWCC curve based on the pore size distribution [75, 87, 89-95]. These methods are only applicable in unimodal SWCC (i.e., with two bending curves only); they fail when the SWCC of the soil is either bimodal (Fig. 2.19) or multimodal [96]. Bimodal SWCC is generally found in aggregate loam or soil with cracks [97-102]. A typical shape of bimodal SWCC is shown in Fig. 2.19. Numerous SWCC fitting equations are proposed by different researchers. Table 2.6 provides a comprehensive summary of these equations (Eq. 2.6 to 2.22) from the literature.

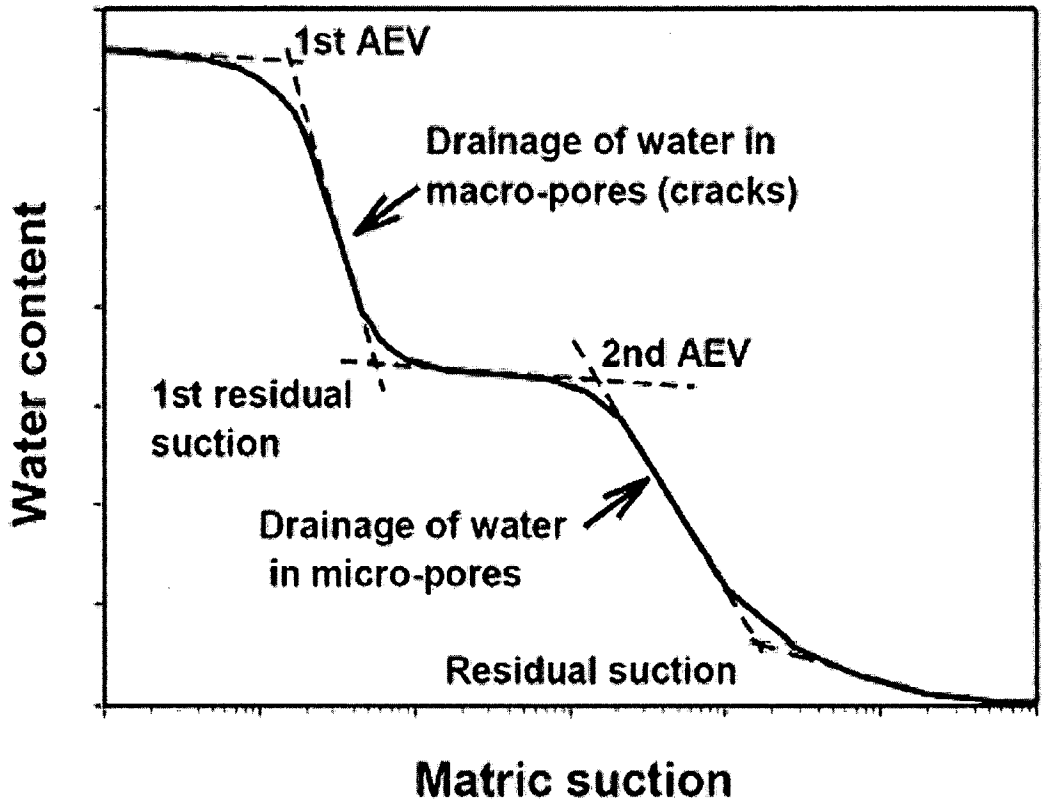


**Fig. 2.19 Typical Bimodal SWCC [103]**

**Table 2.6 Equations Used to Best Fit SWCC Data [7, 82]**

| Reference | Equation | Description | Nature of SWCC | Eq. |
|---|---|---|---|---|
| Gardner [89] | $\Theta_d = \frac{1}{1 + a_g \psi^{n_g}}$ where $\Theta_d = \frac{w(\psi)}{w_s}$ | $a_g$ = fitting parameter that is a function of the AEV of the soil; $n_g$ = fitting parameter that is a function of the rate of water extraction from soil once AEV of soil has been exceeded. | Unimodal | (2.6) |
| Brooks and Corey [90] | $w(\psi) = w_s$ or $\Theta_n = 1$ for $\psi \leq \psi_{aev}$ $\Theta_n = \left[\frac{\psi}{\psi_{aev}}\right]^{-\lambda_{bc}}$ $\psi > \psi_{aev}$ where $\Theta_n = \frac{w(\psi)-w_r}{w_s-w_r}$ | $\psi_{aev}$ = AEV of soil; $\lambda_{bc}$ = pore size distribution index; $w_r$ = residual moisture content located through a trial-and-error process that yields straight line on semi-log plot of degree of saturation versus suction. | Unimodal | (2.7) |
| Brutsaert [104] | $\Theta_n = \frac{1}{1 + \left[\frac{\psi}{a_b}\right]^{n_b}}$ where $\Theta_n = \frac{w(\psi)-w_r}{w_s-w_r}$ | $a_b$ = fitting parameter that is a function of the AEV of soil; $n_b$ = fitting parameter that is a function of the rate of water extraction from soil once an AEV has been exceeded. | Unimodal | (2.8) |
| Laliberte [105] | $\Theta_n = \frac{1}{2}\text{erfc}\left[a_1 - \frac{b_1}{c_1 + \left(\frac{\psi}{\psi_{aev}}\right)}\right]$ where $\Theta_n = \frac{w(\psi)-w_r}{w_s-w_r}$ | $a_l$, $b_l$, $c_l$ = parameters assumed to be unique functions of pore-size distribution index $\lambda$. | Unimodal | (2.9) |

| Reference | Equation | Description | Nature of SWCC | Eq. |
|---|---|---|---|---|
| Campbell [106] | $w = w_s, \psi < \psi_{aev}$<br>$w = w_s \left[\frac{\psi}{\psi_{aev}}\right]^{-\frac{1}{b_c}}, \psi \geq \psi_{aev}$ | $\psi_{aev}$ = AEV of soil;<br>$b_c$ = fitting parameter. | Unimodal | (2.10) |
| Van Genuchten [75] | $\Theta_n = \frac{1}{[1 + (a_{vg}\psi)^{n_{vg}}]^{m_{vg}}}$<br>where<br>$\Theta_n = \frac{w(\psi) - w_r}{w_s - w_r}$ | $a_{vg}$, $a_{vm}$, $a_{vb}$ = fitting parameters primarily related to the inverse of AEV (units equal to 1/kPa);<br>$n_{vg}$, $n_{vm}$, $n_{vb}$ = fitting parameters primarily related to rate of water extraction from soil once AEV has been exceeded;<br>$m_{vg}$, $m_{vm}$, $m_{vb}$ = fitting parameters that are primarily related to residual moisture content conditions. | Unimodal | (2.11) |
| van Genuchten [75] – Mualem [91] | $\Theta_n = \frac{1}{[1 + (a_{vm}\psi)^{n_{vm}}]^{m_{vm}}}$<br>where<br>$m_{vm} = 1 - \frac{1}{n_{vm}}$ | | Unimodal | (2.12) |
| van Genuchten [75] – Burdine [107] | $\Theta_n = \frac{1}{[1 + (a_{vb}\psi)^{n_{vb}}]^{m_{vb}}}$<br>where<br>$m_{vb} = 1 - \frac{2}{n_{vb}}$ | | Unimodal | (2.13) |
| McKee and Bumb [108] (Boltzmann distribution) | $\Theta_n = \exp\left[\frac{a_{m1} - \psi}{n_{m1}}\right]$<br>where<br>$\Theta_n = \frac{w(\psi) - w_r}{w_s - w_r}$ | $a_{m1}$ = curve-fitting parameter;<br>$n_{m1}$ = curve-fitting parameter. | Unimodal | (2.14) |

| Reference | Equation | Description | Nature of SWCC | Eq. |
|---|---|---|---|---|
| McKee and Bumb [108] (Fermi distribution) | $\Theta_n = \frac{1}{1+\exp\left[\frac{(\psi - a_{m2})}{n_{m2}}\right]}$ where $\Theta_n = \frac{w(\psi) - w_r}{w_s - w_r}$ | $a_{m2}$ = curve-fitting parameter; $n_{m2}$ = curve-fitting parameter. | Unimodal | (2.15) |
| Fredlund and Xing [87] | $w(\psi) = C(\psi)\frac{w_s}{\left\{\ln\left(e + \left(\frac{\psi}{a_f}\right)^{n_f}\right)\right\}^{m_f}}$ where $\Theta_n = \frac{w(\psi)}{w_s}$ $C(\psi) = 1 - \frac{\ln\left(1+\frac{\psi}{\psi_r}\right)}{\ln\left[1+\left(\frac{10^6}{\psi_r}\right)\right]}$ | $a_f$ = fitting parameter that is primarily a function of the AEV of soil; $n_f$ = fitting parameter that is primarily a function of the rate of water extraction from soil once an AEV has been exceeded; $m_f$ = fitting parameter that is primarily a function of residual moisture content; $C(\psi)$ = correction factor that is primarily a function of suction corresponding to residual moisture content | Unimodal | (2.16) |
| Pereira and Fredlund [109] | $w(\psi) = w_r + \frac{w_s - w_r}{\left[1+\left(\frac{\psi}{a_p}\right)^{n_p}\right]^{m_p}}$ | $a_p$ = fitting parameter that is primarily a function of the AEV of soil; $n_p$ = fitting parameter that is primarily a function of the rate of water extraction from soil, once an AEV has been exceeded; $m_p$ = fitting parameter that is primarily a function of residual moisture content. | Unimodal | (2.17) |

| Reference | Equation | Description | Nature of SWCC | Eq. |
|---|---|---|---|---|
| Burger and Shackelford [110] | $\theta = \begin{cases} C(\psi) = \dfrac{\theta_j}{\left\{\ln\left[e+\left(\frac{\psi}{a'}\right)^{n'}\right]\right\}^{m'}}; \psi_j < \psi \\ C(\psi) = \dfrac{\theta_s}{\left\{\ln\left[e+\left(\frac{\psi}{a}\right)^{n}\right]\right\}^{m}}; \psi_j \geq \psi \end{cases}$ where $C(\psi) = \begin{cases} 1 - \dfrac{\ln\left(1+\frac{\psi}{\psi_r}\right)}{\ln\left[1+\left(\frac{10^6}{\psi_r}\right)\right]}; \psi_j < \psi \\ 1 - \dfrac{\ln\left(1+\frac{\psi}{\psi_r}\right)}{\ln\left[1+\left(\frac{10^6}{\psi_r}\right)\right]}; \psi_j \geq \psi \end{cases}$ | $\theta$ = volumetric moisture content; $\theta j$ = junction volumetric moisture content; $\theta r$ = residual volumetric moisture content; $\theta s$ = saturated volumetric moisture content; $\psi$ = soil suction; $\psi j$ = soil suction at the junction point; $\psi r$ and $\psi' r$ = residual soil suctions for macroscopic and microscopic portions of data; e = base of the natural logarithm; a, m, n = fitting parameters for a macroscopic portion of data; a′, m′, n′ = fitting parameters for a microscopic portion of data | Bimodal | (2.18) |
| De F. N. Gitirana Jr. and Fredlund [111] | $S = \dfrac{S_1 - S_2}{1 + \left(\psi/\sqrt{\psi_{b1}\psi_{res1}}\right)^{d1}} + \dfrac{S_2 - S_3}{1 + \left(\psi/\sqrt{\psi_{b2}\psi_{res1}}\right)^{d2}} + \dfrac{S_3 - S_4}{1 + \left(\psi/\sqrt{\psi_{b2}\psi_{res2}}\right)^{d2}} + S_4$ $S_i = \dfrac{(1+\tan^2\theta_i)}{(1 - r_i^2\tan^2\theta_i)} \sqrt{r_i^2 \ln^2(\psi/\psi_i^a) + \dfrac{a^2(1+\tan^2\theta_i)}{(1 - r_i^2\tan^2\theta_i)}} + S_i^a$ | i = 1, 2, 3, 4; $\theta i = -(\lambda i\text{-}1 + \lambda i)/2$, hyperbolas rotation angles; $ri = \tan[(\lambda i\text{-}1 + \lambda i)/2]$, aperture angles tangents; $\lambda 0 = 0$; $\lambda i$ = arctan = desaturation slopes Sa1 = 1, Sa2= Sres1, Sa3= Sb, Sa4= Sres2, Sa5= 0, $\psi a1 = \psi b$, $\psi a2 = \psi res1$, $\psi a3 = \psi b2$, $\psi a4 = \psi res2$, $\psi a5 = 106$, $dj = 2\exp^*[1/\ln(\psi aj + 1/\psi aj)]$ = weighting factors, j = 1, 2, 3. | Bimodal | (2.19) |

| Reference | Equation | Description | Nature of SWCC | Eq. |
|---|---|---|---|---|
| Pham and Fredlund [112] | $\begin{cases} w_1(\psi) = w_u - S_1 \log(\psi) & 1 \le \psi < \psi_{aev} \\ w_2(\psi) = w_{aev} - S_2 \log\left(\frac{\psi}{\psi_{aev}}\right) & \psi_{aev} \le \psi < \psi_r \\ w_3(\psi) = S_3 \log\left(\frac{10^6}{\psi}\right) & \psi_r \le \psi < 10^6 \text{kPa} \end{cases}$ | $S_1$, $S_2$, $S_3$ = slope of straight line portions of SWCC within each of three zones; $w_u$ = moisture content at one kPa; $w_{aev}$ = moisture content at AEV; $w_1$, $w_2$, $w_3$ = moisture content in line segments 1, 2, and 3, respectively. | Unimodal | (2.20) |
| Zhang and Chen [96] | $\theta(\psi) = P_l n_{pl} \left[1 - \frac{\ln\left(1+\frac{\psi}{\psi_{rl}}\right)}{\ln\left(1+\frac{10^6}{\psi_{rl}}\right)}\right] \left\{\frac{1}{\ln\left[e+\left(\frac{\psi}{a_l}\right)\right]^{nl}}\right\}^{ml} + P_s n_{ps} \left[1 - \frac{\ln\left(1+\frac{\psi}{\psi_{rs}}\right)}{\ln\left(1+\frac{10^6}{\psi_{rs}}\right)}\right] \left\{\frac{1}{\ln\left[e+\left(\frac{\psi}{a_s}\right)\right]^{ns}}\right\}^{ms}$ $\theta_S = \theta_{Sl} + \theta_{SS}$; $\theta_{Sl} = P_l n_{pl}$ $\theta_{SS} = P_s n_{ps}$ | e = base of the natural logarithm; $\psi_r$ = soil suction in the residual condition; a, m, n = three parameters of the SWCC; function subscripts l and s represent the large-pore series component and the small-pore series component, respectively. | Bimodal | (2.21) |

| Reference | Equation | Description | Nature of SWCC | Eq. |
|---|---|---|---|---|
| Satyanaga *et al.* [113] | $\theta_w = \left[1 - \frac{\ln\left(1+\frac{\psi}{\psi_r}\right)}{\ln\left(1+\frac{10^6}{\psi_r}\right)}\right]\left[\theta_r + (\theta_{s1}-\theta_{s2})\left(1 - \operatorname{erfc}\frac{\ln\left(\frac{\psi_{a1}-\psi}{\psi_{a1}-\psi_{m1}}\right)}{S_1}\right) + (\theta_{s2}-\theta_r)\left(1 - \operatorname{erfc}\frac{\ln\left(\frac{\psi_{a1}-\psi}{\psi_{a1}-\psi_{m1}}\right)}{S_1}\right)\right]$<br>$S = (\theta_{s2})\exp\sqrt{\frac{\sum_{i=1}^{n}\left(\ln\frac{\psi_i}{\mu}\right)}{n}}$<br>$\mu = \sqrt[n]{\psi_1\psi_2 \dots \dots \psi_n}$<br>$\operatorname{erfc} = \int_{-\infty}^{x}\frac{1}{\sqrt{2\pi}}\exp\left(-\frac{x^2}{2}\right)dx$ | $\theta_w$ = calculated volumetric moisture content;<br>$\theta_s$ = saturated volumetric moisture content;<br>(measured in the laboratory);<br>$\psi$ = the matric suction under consideration;<br>$\psi_a$ = AEV of soil;<br>$\psi_m$ = matric suction at the inflection point of SWCC;<br>$\theta_r$ = residual volumetric moisture content;<br>$\psi_r$ = matric suction corresponding to residual volumetric moisture content;<br>s = geometric standard deviation of SWCC;<br>$\mu$ = geometric mean of matric suction;<br>erfc = complimentary error function. | Bimodal | (2.22) |

## 2.9 Expansive Soil Identification

Identification of expansive soil is important, and the tasks and methods used to identify can be divided into two categories. The first category of the methods mostly uses soil physical properties (i.e., Atterberg limits, free swell and potential volume change), whereas the second category uses the soil's mineralogical and chemical properties (i.e., clay content, cation exchange capacity and specific surface area).

### 2.9.1 Methods Based on Physical Properties

*Methods Based on Plasticity* – Atterberg limits (i.e., plasticity index and liquid limit) are used in many methods to identify expansive soil. Peck *et al.* [115] described a relationship between the plasticity index and expansion potential of the soil, as shown in Table 2.7.

**Table 2.7 Expansion Potential of Soil Based on the Plasticity Index [115]**

| Plasticity Index, PI (%) | Expansion Potential |
|---|---|
| 0 - 15 | Low |
| 0 - 35 | Medium |
| 20 - 55 | High |
| > 35 | Very High |

To define expansive soil, Skempton [116] combined the plasticity index and the clay content, thereby introducing a new term called the activity ($A_C$), which is the ratio between the PI and percent of weight finer than 2μm, as shown in Table 2.8.

**Table 2.8 Skempton Classification of Expansive Soil [116]**

| Activity (Ac) | Soil Type |
|---|---|
| < 0.75 | Inactive |
| 0.75 – 1.25 | Normal |
| > 1.25 | Active |

Zapata *et al.* [117] showed that the swelling index of expansive soil has a poor relationship with the PI ($R^2 = 0.41$) and the sieve analysis ($R^2 = 0.27$), respectively. However, a significant correlation came up when both were combined ($R^2 = 0.61$). Thus, the Skempton [116] method is considered superior to the method described by Peck *et al.* [115]. The expansion index (EI) test was developed in California and later adopted in many agencies of California and the Uniform Building Code [118]. The standardized test for the EI is given in ASTM D4829 [119]. In the uniform building code, the EI is also used to identify expansive soil, as shown in Table 2.9.

**Table 2.9 Expansion Potential Based on the Expansion Index [118]**

| Expansion Index (EI) | Expansion Potential |
|---|---|
| 0-20 | Very Low |
| 21-50 | Low |
| 51-90 | Medium |
| 91-130 | High |
| Above 130 | Very High |
| **Note: Table 29-C from Uniform Building Code and Standards (1991) | |

Other notable methods based on physical properties include the free swell test, the potential volume change test, the expansion index (EI) test, the coefficient of linear extensibility (COLE) test and the standard absorption moisture content (SAMC) test.

*Mineralogical Methods* – The most common mineralogical methods of identification include X-ray diffraction (XRD), differential thermal analysis (DTA) and electron microscopy.

*Chemical Methods* – Popular chemical methods that are used to identify clay minerals include measurement of cation exchange capacity (CEC), specific surface area (SSA) and total potassium (TP).

## 2.10 Important Terminology of Soil Heave

*Active zone* is a term often confused because different researchers have used different definitions to determine the "active zone." To clarify these confusions, Nelson *et al.* [120] used four definitions as follows.

*Active zone* ($Z_A$) refers to the zone of soil that is contributing to heave due to soil expansion at any particular time. Therefore, the depth of the active zone can vary with time.

*Zone of seasonal moisture content fluctuation* ($Z_s$) refers to the zone of soil in which water content changes due to climatic changes at the ground surface. This does not include water coming from external sources (i.e., pipe leakage, irrigation).

*Depth of wetting* ($Z_w$) refers to the depth to which water contents have increased due to the introduction of water from external sources or due to capillary after the elimination of evapotranspiration.

*Depth of potential heave* ($Z_p$) refers to the depth to which the overburden vertical stress equals or exceeds the swelling pressure of the soil.

*Design active zone ($Z_{AD}$)* refers to the zone of soil that is expected to become wet by the end of the design life. This is the active zone for which the foundation is to be designed [11].

*Free-field heave* refers to the soil heave without the application of any surcharge load. Generally, the load coming from the slabs and pavements on the ground is very minimal, and heave underneath them can be considered free-field heave. This is a very common term used by researchers around the world and sometimes [121-128] also referred to as free-field movement [129-133].

*Current heave* refers to the heave produced by the current degree of wetting in the active zone. In the measurement of current heave, it is assumed that the soil has been fully or partially saturated.

*Ultimate heave* refers to the maximum amount of heave in the potential zone if wetted 100%.

*Future maximum heave* refers to the expected future heave in the active zone of the soil if wetted fully at the time of the investigation.

*Design heave* refers to the amount of heave that will be experienced during the design life of the foundation. Design heave is calculated based on the change in the subsurface moisture content profile in the design active zone. Water migration modeling can be used to predict the final moisture content profile at the end of the design life of the foundation. Calculations of the design free-field heave should also consider the degree of wetting in the design active zone. It is also the amount of heave that the foundation must be designed to tolerate within its design life [11].

*Oedometer test* refers to a soil test in which 100% saturated soil is laterally confined but under one-dimensional vertical load.

*Consolidation-swell (CS) test* refers to a soil test in which the sample is wetted under a prescribed 1 kPa token pressure and allowed to swell.

*Constant volume (CV) test* refers to a soil test in which the sample is restrained from swelling while it is being wetted.

*Consolidation-swell swelling pressure* ($\sigma''_{CS}$) refers to the load required to compress the soil to its original thickness after it has been inundated and allowed to swell in a consolidation-swell (CS) test [11]. It can be found from the e-logP graph.

*Constant volume swelling pressure* ($\sigma''_{CV}$) refers to the load required to prevent swell and thus maintain a constant volume of the soil after it has been inundated in a constant volume (CV) test [11].

*Swelling potential (SP%)* refers to the swelling capacity of an expansive soil while it is absorbing moisture. It either can be quantified from the results of oedometer tests (i.e., percent swell, swelling pressure) or can be empirically qualified based on soil index properties.

*Percent swell (S%)* refers to a characteristic commonly determined from an oedometer swell test following free-swell procedures that allow a laterally confined sample to soak to swell under a certain amount of token load (i.e., 1kPa or 7kPa) [52, 134, 135].

*Swelling index* ($C_s$) refers to the slope of the rebound curve of the e-logP graph obtained from oedometer tests.

## 2.11 Heave Prediction Methodologies

By late 1950, the heave prediction methodologies were first introduced. At the beginning, the research was constrained to volume change due to the settlement of saturated soil using oedometer tests [136]. Later, more refined methods were developed. Taylor [137] showed how layered saturated expansive soil heave can be mathematically computed. Jennings and Knights [138] for the first time extended the settlement theories to heave prediction while Salas and Serratosa [139] introduced swelling pressure concept. Palit [140] completely defined swelling pressure for the first time. One of earliest investigators Aitchison [141], for the first time, developed a model of soil heave considering the change in pore-pressure, but it was probably Fredlund *et al.* [142] who properly developed the theoretical framework of the suction induced heave. All the heave estimating methods can be divided into three main categories based on (i) empirical methods, (ii) oedometer test methods and (iii) soil suction methods [143, 144].

### 2.11.1 Empirical Methods

In the empirical methods, geotechnical index parameters of the soil (i.e., atteberg limits, plasticity index, clay fraction, activity, dry density and initial moisture content) are used to predict the soil heave. Empirical methods are often developed based on limited data and some of them may not be applicable for all types of soil. For this reason, it is advisable to use multiple methods to predict the heave of soil. A summary of empirical methods (Eq. 2.23 to 2.49) is given in Table 2.10.

**Table 2.10 Summary of the Empirical Methods [7, 31, 143-147]**

| References | Description | Eq. |
|---|---|---|
| Seed *et al.* [148] | $SP = 0.00216 \times PI^{2.44}$; SP = swelling potential, %; PI = plasticity index. | (2.23) |
| Van der Merwe [149] | $\Delta H = Fe^{-0.377D}\left(e^{-0.377H} - 1\right)$; H = volume change; ΔH = total heave; F = correction factor for degree of expansiveness; D = the thickness of non-expansive layer. | (2.24) |
| Ranganatham & Satyanarayana [150] | $SP = 0.000413I_S^{2.67}$; $I_S$: shrinkage index, (LL-SL). | (2.25) |
| Nayak & Christensen [151] | $SP = \frac{0.00229I_P(1.45c)}{w_i} + 6.38$; $P_S(psi) = \left[\frac{(3.58 \times 10^{-2})PI^{1.22}c^2}{w_i^2}\right] + 3.79$; $w_i$ = initial moisture content; $P_s$ = is the swelling pressure; c = clay content. | (2.26) |
| Vijayavergiva & Ghazzaly [152] | $SP = \frac{1}{12 \times (0.4LL - w_i + 5.55)}$; $\log SP = 0.0526\gamma_d + 0.033LL - 6.8$; LL= liquid limit. | (2.27) |
| Schneider & Poor [153] | $\log SP = 0.9 \times \left(\frac{PI}{w_i}\right) - 1.19$ | (2.28) |
| Chen [28] | $SP = 0.2558e^{0.8381I_P}$ | (2.29) |
| Weston [154] | $SP = 0.00411LL_w^{4.17}\sigma_V^{-3.86}w_i^{-2.33}$; $LL_w$ = weighted liquid limit. | (2.30) |
| Picornell & Lytton [155] | $\Delta H = \sum_1^n f_i\left(\frac{\Delta V}{V}\right)_i H$; H: the stratum thickness; ΔV/Vi = volume change with respect to initial volume; $f_i$ = a factor to include the effects of the lateral confinement. | (2.31) |
| Dhowian [156] | $\Delta H = (SP\%)\frac{H}{100}$ | (2.32) |
| McCormack & Wilding [157] | $SP = 7.5 - 0.8 \times w_i + 0.203c$ | (2.33) |
| Brackley [158] | $SP = \left\{5.3 - \left(\frac{147e}{PI}\right) - \log P\right\} \times (0.525PI + 4.1 - 0.85w_i)$; P = surcharge. | (2.34) |
| O'Neil & Ghazzaly [159] | $SP = 2.77 + 0.131w_i - 0.27w_n$; $w_n$ = natural moisture content. | (2.35) |
| Johnson [160] | $S\% = 23.82+0.7346\times PI-0.1458\times H-1.7\times w_0+(0.0025\times PI)w_0-(0.00884\times PI)\times H$; $S\% = -9.18+1.5546\times PI+0.08424\times H+0.1\times w_0-(0.0432\times PI)\times w_0-(0.01215\times PI)\times H$. | (2.36) |

| References | Description | Eq. |
|---|---|---|
| Bandyopadhyay [161] | $SP = 0.00114A^{2.559}C^{3.44}$ | (2.37) |
| Basma [162] | $SP = 0.00064PI^{1.37}c^{1.37}$ | (2.38) |
| Çokça [163] | $SP = -121.807 + 12.1696MBV + 27.6579 \log \psi_i$ | (2.39) |
| Erguler & Ulusay [164] | $P_s = -227.27 + 2.14w_i + 1.54w_l + 72.49\gamma_d.$ | (2.40) |
| Rao *et al.* [145] | $SP = 4.24\gamma_{di} - 0.47w_i - 0.14q_i - 0.06FSI - 55;$<br>$\gamma_{di}$ = dry unit weight; $q_i$ = initial surcharge;<br>FSI = free swell index. | (2.41) |
| Erzin & Erol [165] | $\log P_s = -4.812 + 0.01450I_p + 2.39\gamma_d - 0.0163w_i;$<br>$\log P_s = -5.020 + .01383PI + 2.356\gamma_d.$ | (2.42) |
| Sabtan [166] | $SP = 1.0 + 0.06(c + PI - w_i);$<br>$P_s = 135.0 + 2.0(c + PI - w_i).$ | (2.43) |
| Azam [167] | $SP = 0.6PI^{1.188}$ | (2.44) |
| Yilmaz [168] | $SP = 2.0981e^{-1.7169IL};$<br>IL= Liquidity index = [($w_l$-w)-PI]. | (2.45) |
| Türköz and Tosun [169] | $SP = -57.865 + 37.076\rho_d + 0.524MBV + \varepsilon;$<br>$\varepsilon$ = mean-zero Gaussian random error term. | (2.46) |
| Çimen *et al.* [146] | $(SP)_1 = \left(0.3139\gamma_d^{0.3552} - 0.1177w_i^{0.4470}\right)PI^{0.9626};$<br>$(\log P_s)_1 = 0.0276PI - 365.211\gamma_d^{-2.4616} - 0.0213w_i + 2.2292;$<br>$(SP)_2 = \left(0.4768\gamma_d^{0.3888} - 0.0033w_i^{1.6045}\right)PI^{0.7224};$<br>$(\log P_s)_2 = 0.0239PI - 1285.3723\gamma_d^{-3.2768} - 0.039w_i + 2.3238;$<br>$SP = \text{mean}\,(SP_1, SP_2);$<br>$\log P_s = \text{mean}\,[(\log P_s)_1, (\log P_s)_2]$ | (2.47) |
| Zumrawi [170] | $SP = 24.5(q)^{-0.26}(I_Pc)^{1.26}[F_i - 7.1(q)^{0.22}(PIc)^{1.26}];$<br>q = surcharge;<br>$F_i$ = initial state factor. | (2.48) |
| Vanapalli *et al.* [171] | $\Delta H = C_s \frac{H}{1+e_0} \log\left\{\frac{KP_f}{10^{\left(\frac{C_s \Delta w}{C_w}\right)}}\right\};$<br>H = thickness of the soil layer;<br>$P_f (= \sigma_y + \Delta\sigma_y - u_{wf})$ = final stress state;<br>$P'_s$ = corrected swelling pressure;<br>K = correction parameter;<br>$C_s$ = swelling index;<br>$\sigma_y$ = total overburden pressure;<br>$\Delta\sigma_y$ = change in total stress;<br>$u_{wf}$ = final pore-water pressure;<br>$e_0$ = initial void ratio;<br>$C_w$ = suction modulus ratio;<br>$\Delta w$ = change in moisture content. | (2.49) |

2.11.2 Oedometer Test Methods

Oedometer-based methods are widely used because of their simplicity compared with the other two methods. The oedometer test can be used to find void ratio (initial and final), SP%, swelling index and swelling pressure. Because this test is done in fully saturated condition, oedometer-based methods predict maximum possible heave. Tables 2.11 and 2.12 (Eq. 2.50 to 2.54) summarize these methods. Current refined oedometer-based methods are largely functions of index parameter. The most common ones are swelling index ($C_s$) and heave index ($C_H$). Burland [172] first proposed using the slope of the rebound curve from the consolidation swell test, and later Fredlund [173] showed the rebound curve slope found from the constant swell test is approximately same as the slope found from the rebound curve of the constant volume test. The Fredlund [173] method and the Nelson & Miller [31] method use test results found from both the constant volume test and consolidation-swell test. Nelson *et al.* [174] and Bonner [175] later presented a method of estimating the index properties only found from the consolidation-swell tests. Later, Nelson *et al.* [176] proposed a method to determine SP% as a function of inundation pressure.

**Table 2.11 Heave Prediction Tests Using Oedometer [7, 31, 143]**

| Name of the Method | Location | Description |
|---|---|---|
| Double oedometer method [138] | South Africa | Two tests performed on adjacent samples: a consolidation-swell test under a small surcharge pressure and a consolidation test performed in a conventional manner but at natural moisture content. The analysis accounts for sample disturbance and allows simulation of various loading conditions and final pore-water pressures. |
| Volumenometer method [177] | South Africa | Uses specialized apparatus; air-dried samples were inundated slowly under overburden pressure. |
| Sampson, Schuster & Budge method [178] | Colorado, USA | Two tests performed on adjacent samples to simulate highway cut conditions: a consolidation-swell test under overburden surcharge and a constant volume-rebound upon load removal test. |
| Noble method [179] | Canada | Consolidation-swell tests of remolded and undisturbed samples at various surcharge loads to develop empirical relationships for Canadian prairie clays. |
| Sullian and McClelland method [180] | USA | Constant volume test samples initially under overburden pressure on inundation. |
| Komornik, Wiseman & Ben-Yacob Method [181] | Israel | Constant volume tests at various depths and swell-consolidation tests at various initial surcharge pressures representing overburden plus equilibrium pore-water suction used to develop swell versus depth curves. |
| Navy method [182] | USA | Swell versus depth curves determined by consolidation-swell tests at various surcharge pressures representing overburden plus structural loads. |
| Wong & Yong method [183] | England | Swell versus depth is determined as in the Komornik, Wiseman & Ben-Yacob method and Navy method, but surcharge loads of overburden plus hydrostatic pore-water pressures are used. |
| USBR method [184] | USA | Double sample test: a consolidation-swell under light load and a constant volume test. |
| Direct model Method [185] | Texas, USA | Consolidation-swell tests on samples inundated at overburden or end-of-construction surcharge loads. |
| Simple Oedometer [186] | South Africa | Improved from double oedometer test. The single sample is loaded to overburden, then unloaded to constant. |
| Mississippi State Highway Dept. method [187-189] | Mississippi USA | Consolidation-swell tests on remolded or undisturbed samples inundated at overburden surcharge loads. |

| Name of the Method | Location | Description |
|---|---|---|
| Controlled strain test [190] | Colorado, USA | Constant volume swells pressure obtained on inundation followed by incremental, strain-controlled pressure reduction. |
| University of Saskatchewan [142] | Canada | Constant volume test with the procedure including sample disturbance and apparatus deflection. |
| Sridharan, Rao & Sivapullaiah method [191] | India | Tested results from three methods: a) conventional consolidation tests, b) equilibrium void ratios for different consolidation loads and c) constant volume method are combined to study the swelling pressure of expansive soil. Results show that method a) gives an upper bound value, method b) gives the least value, and method c) gives the intermediate value. |
| Erol, Dhowian & Youssef method [192] | Saudi Arabia | Assessment of the various oedometer test methods of ISO (improved swell oedometer test), CVS (constant volume swell test) and SO (swell overburden test) is used for heave prediction. |
| Shanker, Ratnam & Rao method [193] | India | Studied the multi-dimensional swell behavior by testing cubic soil samples in oedometers; swelling of samples is allowed to occur in 1, 2 or 3 dimensions under a token surcharge. |
| Al-Shamrani & Al-Mhaidib method [194] | Saudi Arabia | The stress path triaxial cell and oedometer are used to evaluate the vertical swell of expansive soil under multi-dimensional loading conditions; several series & triaxial swell tests were conducted in which the influence of confinement on the predicted vertical swell was evaluated. |
| Basma, Al-Homoud & Malkawi method [195] | Jordan | Two commonly used methods, the zero-swell test and the swell-consolidation test; and two relatively new techniques, "restrained swell test" and "double oedometer swell test" are used to study the swell pressure of the expansive soil. The restrained swell test is believed to give more reasonable results for swell pressure determination and thus is considered to resemble field conditions more closely. |
| Subba Rao & Tripathy method [196] | India | One-dimensional oedometer is used to study the swell-shrinkage behavior of the compacted expansive soil. The compression-rebound tests were conducted on aged and un-aged compacted specimens by incrementally loading them up to a certain surcharge and then unloading, and the cyclic swell-shrinkage tests were carried out in fixed-ring oedometers with the facility for shrinking the specimens at fixed temperature under constant surcharge pressure. |

**Table 2.12 Summary of the Oedometer-Based Methods**

| Author | Description | Eq. |
|---|---|---|
| Department of the Army [197] | $\Delta H = H\frac{C_{DA}}{1+e_0}\log\left\{\frac{\sigma''_{CS}}{\sigma''_f}\right\}$; CDA = Department of Army heave parameter or DA heave index; $e_0$ = initial void ratio of the soil layer; $\sigma''_{CS}$ = swelling pressure from CS test; and $\sigma''_f$= final vertical effective pressure. | (2.50) |
| Fredlund [173] | $\Delta H = H\frac{C_s}{1+e_0}\log\left\{\frac{P_f}{P'_s}\right\}$; $H_i$ = thickness of the $i_{th}$ layer; Pf (= σy + Δσy – uwf) = final stress state; $P'_s$ = corrected swelling pressure; Cs = swelling index; $\sigma_y$ = total overburden pressure; $\Delta\sigma_y$ = change in total stress; $u_{wf}$ = final pore-water pressure; $e_0$ = initial void ratio. | (2.51) |
| Dhowian [156] | $\Delta H = H\frac{C_s}{1+e_0}\log\left\{\frac{P_s}{P_0}\right\}$; $C_s$ = swell index; $P_s$ = swelling pressure; $P_0$ = effective overburden pressure. | (2.52) |
| Nelson & Miller [31] | $\Delta H = H\frac{C_\rho}{1+e_0}\log\left\{\frac{\sigma'_f}{\sigma'_{CV}}\right\}$; $C_\rho$ = heave index; $\sigma'_{CV}$= swelling pressure from constant volume swell test; $\sigma'_f$ = vertical stress at the midpoint of the soil layer for the conditions under which heave is being computed. | (2.53) |
| Nelson *et al.* [198] | $\Delta H = HC_H\log\left\{\frac{\sigma''_{CV}}{\sigma''_i}\right\}$; $C_H = \frac{\%S}{\log\left\{\frac{\sigma''_{CV}}{(\sigma''_i)_A}\right\}}$; CH = heave index; $\sigma''_{CV}$ = swelling pressure from constant volume swell test; $\sigma''_i$= vertical stress at the midpoint of the soil layer for the conditions under which heave is being computed. | (2.54) |

2.11.2.1 Department of the Army (1983) The first approach was proposed by the US Department of the Army (Fig. 2.20) [197], where two approaches are described to find the soil heave using the consolidation swell (CS) test. $C_{DA}$ and $C_H$ expressed in Eq. 2.55 and 2.56 are basically similar where the first one is found from the loading curve of the constant swell consolidation test and the second one is found from the loading curve of the constant volume consolidation test.

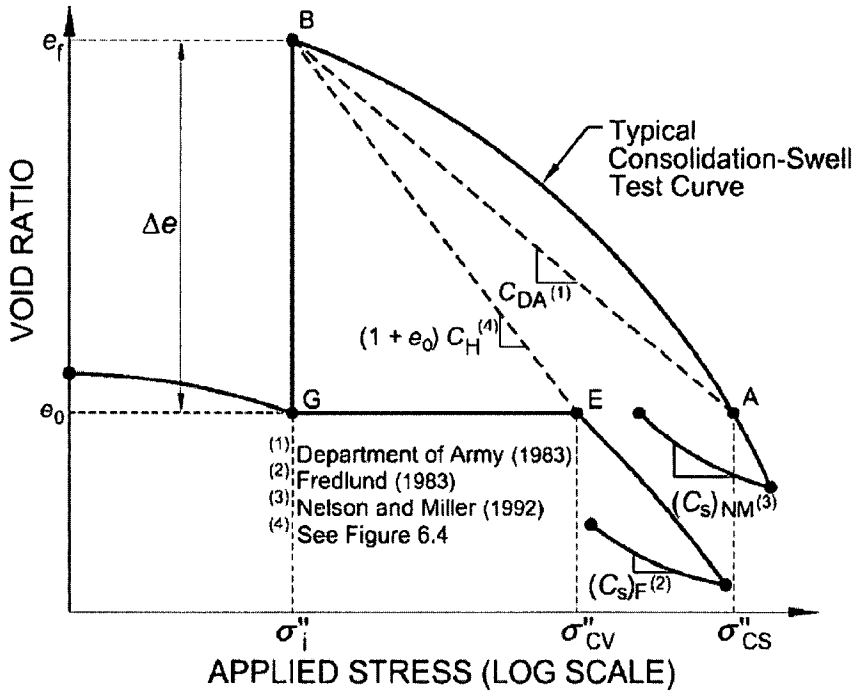


**Fig. 2.20 Comparison of Different Heave Parameters [11]**

$$C_{DA} = \frac{\Delta e}{\log \sigma''_{CS} - \log \sigma''_i} = \frac{\Delta e}{\log\left[\frac{\sigma''_{CS}}{\sigma''_i}\right]} \tag{2.55}$$

$$C_H = \frac{\Delta e}{\log \sigma''_{CV} - \log \sigma''_i} = \frac{\Delta e}{\log\left[\frac{\sigma''_{CV}}{\sigma''_i}\right]} \tag{2.56}$$

2.11.2.2 Fredlund Method (1983) Fredlund [173] proposed a method to predict soil heave using its constant volume consolidation test data. In this process, the soil sample was put in a water bath with a token pressure (7 kPa). An equation that can be used to calculate the 1-D heave in expansive soil using the constant volume swell (CVS) oedometer test resulted. The main two parts of Eq. 2.51 are swelling pressure and swelling index. In this process, matric suction was brought to zero by making the soil sample inundated. Once the soil swelling was started, the total stress on the soil sample was increased to make the volume change zero. This process was continued until the soil did not show any more tendency to swell. The applied load at that point was referred to as "uncorrected swelling pressure." This "uncorrected swelling pressure" was believed to be the result of sample disturbance. Figure 2.21 shows the ideal stress path of the test and sampling disturbance. The swelling pressure needed to be corrected to get the corrected swelling pressure. Casagrande [199] proposed an empirical construction that can be applied to the laboratory-measured compression curve for the determination of pre-consolidation pressure. Fredlund *et al.* [82] explained the procedure of the correction (Fig. 2.22). First, the point with maximum curvature is located, and two lines are drawn from that one. One line is parallel to the horizontal axis, and the second one is the tangent of the curve going through that point. Then a bisector is drawn in the angle formed between these two lines, and finally, a line tangential to the recompression curve is drawn. The intersecting point between the bisector line and the recompression curve tangential line is the corrected swelling pressure.

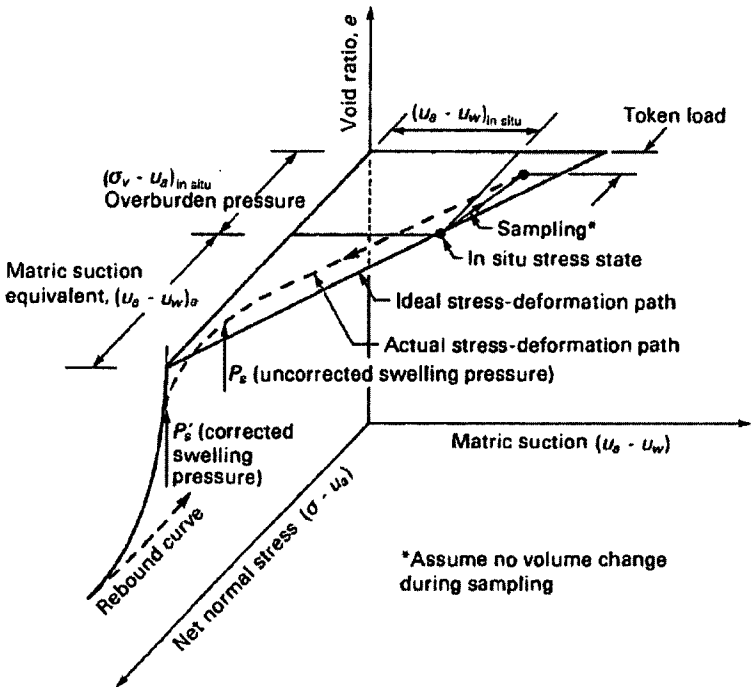


**Fig. 2.21 Ideal and Actual Stress Paths Showing Effect of Sampling Disturbance [82]**

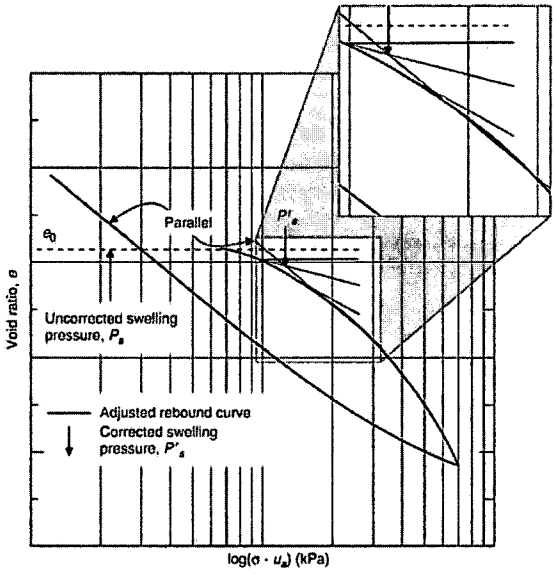


**Fig. 2.22 Procedure to Find Corrected Swelling Pressure [82]**

2.11.2.3 Nelson and Miller (1992) Nelson and Miller [31] proposed a method based on the method given by Fredlund [173], where they described how, from the slope of the constant swelling consolidation test, rebound curve swelling index ($C_s$) can be found. This method employs an unrestrained shrinkage test on an undisturbed soil sample, using a resin coating technique. Irregular lumps of soil can be used. The volume of the sample is determined as a function of its moisture content as it dries, providing a volume change index. The method has been found capable of providing reliable ground movement predictions [31] but is limited to situations where ground movements occur under relatively constant net stress conditions [200].

2.11.2.4 Relationship Between CS and CVS Swelling Pressures (the M Method) Swelling pressure found from the CS test is significantly higher than the swelling pressure found from the CVS test due to crystalline and osmotic swell [11, 31]. Most of geotechnical engineering labs are equipped only to perform constant swelling consolidation tests. But some of the oedometer-based methods use $C_H$ value, which can only be found once the $\sigma''_{CV}$ is known. Using the m-method, a relation can be found between $\sigma''_{CV}$ and $\sigma''_{CS}$ as shown in Eq. 2.57.

$$\log \sigma''_{CV} = \frac{\log\sigma''_{CS} + m \times \log\sigma'_i}{1+m} \tag{2.57}$$

The parameter, m, depends on the particular soil, its expansive nature and other properties of the soil. Figure 2.23 shows the graph to find the m value for a particular soil.

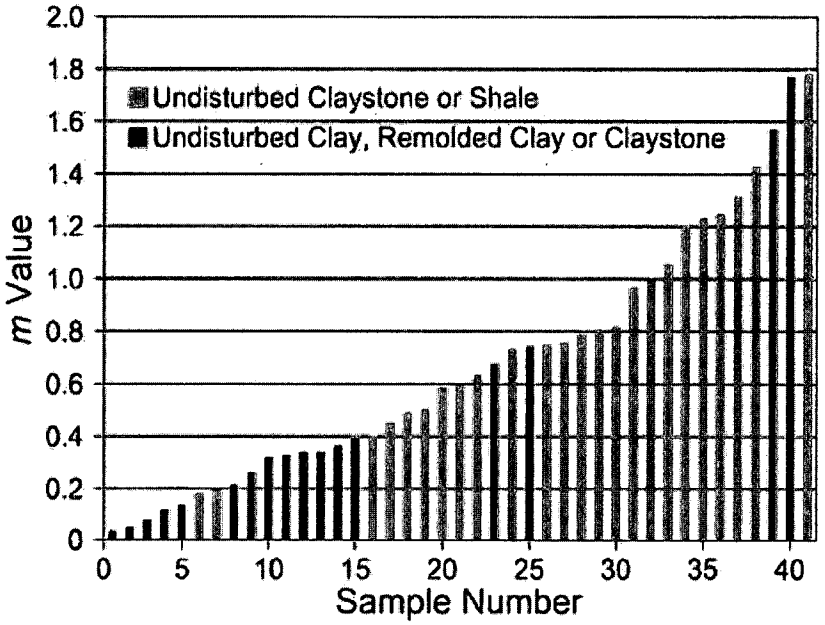


**Fig. 2.23 Calculated Values of m Sorted by Value [11]**

2.11.3 Soil Suction Methods

The suction method, which is based on suction stress state, gives a more reliable measure of one-dimensional heave. Table 2.13 summarizes different suctions based on methods (Eq. 2.58 to 2.74).

The swelling pressure and the 1-D heave in expansive soil can be more reliably measured or calculated using soil suction methods because they are based on the information of the stress state (i.e., suction). In these methods, the influence of suction is considered using different parameters. Several heave prediction formulations based on soil suction methods proposed by various researchers are summarized in this section.

**Table 2.13 Summary of Soil Suction Methods [7, 11, 13, 143, 144]**

| References | Description | Eq. |
|---|---|---|
| Richards [205] | $\Delta H = \frac{H}{3}\frac{(w_f - w_i)G_S}{(100 + w_i G_S)}$;<br>$\Delta H$ = soil heave;<br>H = soil layer thickness;<br>$w_i$ = initial moisture content (measured);<br>$w_f$ = final moisture content (estimated in terms of the equilibrium matric suction);<br>$G_s$ = specific gravity. | (2.58) |
| Aitchison [141] | $\Delta H = \int_0^{H_S} I_{Pt}\Delta u \Delta h$;<br>$\Delta H$ = surface movement;<br>$I_{Pt}$ = instability index of the soil;<br>$\Delta u$ = change in suction, in pF units, at depth z;<br>$\Delta h$ = thickness of the soil layer under consideration;<br>$H_s$ = depth of the design suction change. | (2.59) |
| Lytton [206] | $\Delta H = \gamma_h \log_{10}(h_f/h_i) - \gamma_\sigma \log_{10}(\sigma_f/\sigma_i)$;<br>$h_f$, $h_i$ = final and initial water potentials;<br>$\sigma_f$ = applied octahedral normal stress;<br>$\sigma_i$ = the octahedral normal stress above which overburden pressure restricts volumetric expansion;<br>$\gamma_h$, $\gamma_\sigma$ = two constants characteristic of the soil. | (2.60) |
| Johnson & Snethen [51] | $\Delta H = H\frac{C_\tau}{1+e_0}\log\frac{h_0}{h_f + \alpha\sigma_f}$;<br>$C_\tau = \frac{\alpha G_S}{100B}$;<br>$\log h_0 = A - Bw_0$;<br>H = the stratum thickness;<br>$C\tau$ = suction index;<br>$\alpha$ = compressibility index;<br>$e_0$ = initial void ratio;<br>$h_f$ = final matric suction, kPa;<br>$\sigma_f$ = final applied pressure, (overburden + external load), kPa;<br>$h_0$ = matric suction without surcharge pressure, kPa. | (2.61) |
| Fredlund [4] | $\Delta H = \frac{H_i}{1+e_0}[C_t\Delta\log(\sigma - u_a) + C_m\Delta\log(u_a - u_w)]$;<br>$\Delta H$ = soil heave;<br>$H_i$ = thickness of the $i_{th}$ soil layer;<br>n = total number of soil layers considered;<br>$e_i$ = void ratio of the $i_{th}$ soil layer;<br>$C_t$ = compressive index with respect to total stress;<br>Cm = compressive index with respect to matric suction;<br>$(\sigma - u_a)$ = total stress;<br>$(u_a - u_w)$ = matric suction. | (2.62) |

| References | Description | Eq. |
|---|---|---|
| Snethen [46] | $\Delta H = H\frac{C_\tau}{1+e_0}(A - Bw_0) - \log(\tau_{mf} + \alpha\sigma_f)$; $C_\tau = \frac{\alpha G_S}{100B}$; $\log\tau_m = A - Bw_0$; Cτ = suction index; $\tau_{mf}$ = final matric suction; $\sigma_f$ = final applied pressure (overburden + external load); α = compressibility factor; A, B = constants (y-intercept and slope of soil suction versus moisture content curve, respectively). | (2.63) |
| McKeen [207] | $\Delta H = -\gamma_h H \log\frac{h_f}{h_i}$; $\gamma_h = -\frac{\Delta v/v_i}{\log\frac{h_f}{h_i}}$; $H = C_h \log\Delta\tau f_s$; $C_h = (-0.02673)\left(\frac{d_h}{d_w}\right) - 0.38704$; $f = \frac{1+k_0}{3}$; $s = 1 - 0.01(\%SP)$; $\gamma_h$ = suction compression index; $h_f$, $h_i$ = final and initial weighted suction, respectively; $\Delta v/v_i$ = volume change with respect to initial volume; $C_h$ = suction compression index; Δτ = suction change in pF; f = lateral restraint factor; $K_0$ = coefficient of earth pressure at rest, equal to 1; s = coefficient for load effect on heave; SP = percent of swell pressure applied. | (2.64) |
| Mitchell & Avalle [208] | $\Delta H = I_{Pt}\Delta u H$; $I_{pt} = \frac{\Delta L/L}{\Delta w} * \frac{\Delta w}{\Delta u}$; $I_{Pt}$ = instability index; Δu = soil suction change. | (2.65) |
| Hamberg & Nelson [209] | $\Delta H = H\frac{C_w}{1+e_0}\Delta w$; $C_w = \frac{\Delta e}{\Delta w}$; $\Delta H = H\frac{C_w}{1+e_0}\log(h)_i$; $C_h = C_w D_h$; $C_w$ = suction modulus ratio; Δw = change in moisture content; $C_h$ = suction index with respect to void ratio; $D_h$ = suction index with respect to moisture content. | (2.66) |
| Wray [210] | $\Delta H = H\gamma_h(\Delta pF - \Delta pP)$; ΔH = shrinkage or swell over vertical increment; H = vertical increment over which shrink or swell is occurring; $\gamma_h$ = suction compression index; ΔpF = change in soil suction over vertical increment; ΔpP = change in soil overburden over vertical increment. | (2.67) |
| Hamberg [25] | $\Delta H = \frac{H_i}{1+e_0}(C_h\Delta\log h)_i$; ΔH = soil heave; $H_i$ = thickness of the $i_{th}$ soil layer; $e_0$ = initial void ratio; $C_h$ = suction index with respect to void ratio; h = soil suction; n = number of layers to a depth of the active zone. | (2.68) |

| References | Description | Eq. |
|---|---|---|
| Dhowian [156] | $\Delta H = H\frac{C_\psi}{1+e_0}\log\frac{\psi_i}{\psi_f}$; $C_\psi = \frac{\alpha G_S}{100B}$; $\Delta H = H\frac{\alpha G_S}{1+e_0}(w_f - w_i)$; $\Delta H = HC_w(w_f - w_i)$; $C_w = \frac{\alpha G_S}{1+e_0}$; $C_\psi$ = suction index; $\psi_i$ = initial suction; $\psi_f$ = final suction; $\alpha$ = volume compressibility factor; B = slope of suction versus moisture content relationship; $G_s$ = specific gravity of solid particles. | (2.69) |
| Lytton [211] | $\frac{\Delta V}{V} = -\gamma_{\psi m}\log\left[\frac{\psi_{mf}}{\psi_{mi}}\right] - \gamma_\sigma \log\left[\frac{\sigma_f''}{\sigma_i''}\right] - \gamma_{\psi_o}\log\left[\frac{\psi_{of}}{\psi_{oi}}\right]$; $\Delta V/V$ = volumetric strain; $\psi$mi, $\psi$mf = initial and final matric suction; $\sigma_i''$ , $\sigma_f''$ = initial and final mean principal stress; $\psi$oi, $\psi$of = initial and final osmotic suction; $\gamma\psi$m = matric suction volumetric compression index; $\gamma\sigma$ = mean principal stress volumetric compression index; $\gamma\psi$o = osmotic suction volumetric compression index. | (2.70) |
| Fityus & Smith [212] | $\Delta H = HI_V\alpha(w_{0i} - w_{0f})$; $\Delta H = HC_w(w_f - w_i)$; $I_v$ = volume index; $\alpha$ = empirical factor accounting for confining stress differences in lab and field; $w_{0i}$ = average initial moisture content; $w_{0f}$ = average final moisture content, respectively; $\sigma_v$ = vertical stress at the midpoint of the layer. | (2.71) |
| Cover & Lytton [213] | $S_f = f_i\left(\frac{\Delta V}{V}\right)_i \Delta Z_i$; $\left(\frac{\Delta V}{V}\right)_i = -\gamma_h\log\frac{h_f}{h_i} - \gamma_\sigma\log\frac{\sigma_f}{\sigma_i}$; $\gamma_h = \frac{\gamma(\text{swelling case}) + \gamma(\text{Shrinkage case})}{2}$; $\gamma(\text{swelling case}) = \left(\frac{COLE}{100}+1\right)^3 - 1$; $\gamma(\text{Shrinkage case}) = 1 - \frac{1}{\left(\frac{COLE}{100}+1\right)^3}$; Sf = surface displacement; fi = lateral confine factor; $\left(\frac{\Delta V}{V}\right)_i$ = average volume strain; $\Delta z_i$ = thickness of $i_{th}$ soil layer; n = total number of soil layers considered; $h_i$, $h_f$ = initial and final water potentials; $\sigma_f$ = applied octahedral normal stress; $\sigma_i$ = octahedral normal stress above which overburden pressure restricts volumetric expansion; $\gamma_h$ = matric suction compression index; $\gamma_\sigma$ = mean principal stress compression index; COLE = coefficient of linear extensibility. | (2.72) |

| References | Description | Eq. |
|---|---|---|
| Briaud *et al.* [214] | $\Delta H = Hf(\Delta w - E_w)$;<br>$E_w = \Delta w(\Delta V/V_0)$;<br>$f = (\Delta H/H_0)(\Delta V/V_0)$;<br>$E_w$ = shrink–swell modulus, slope of the moisture content versus the volumetric strain line;<br>f = shrinkage ratio, the ratio of the vertical strain to the volumetric strain. | (2.73) |
| Lytton *et al.* [215] | $S_f = f\left(\frac{\Delta V}{V}\right)_i \Delta Z_i$;<br>$\left(\frac{\Delta V}{V}\right)_{i,swelling} = -\gamma_h \log\left(\frac{h_f}{h_i}\right) - \gamma_\sigma \log\left(\frac{\sigma_f}{\sigma_i}\right)$;<br>$\left(\frac{\Delta V}{V}\right)_{i,shrinkage} = -\gamma_h \log\left(\frac{h_f}{h_i}\right) - \gamma_\sigma \log\left(\frac{\sigma_f}{\sigma_i}\right)$;<br>$\Delta H$ = surface displacement;<br>f = crack fabric factor = 0.67 – 0.44 $\Delta$pF, $1/3 \leq f \leq 1.0$;<br>$\left(\frac{\Delta V}{V}\right)_i$ = volume strain;<br>$\Delta z_i$ = the $i_{th}$ depth increment;<br>n = number of depth increment;<br>$h_i$, $h_f$ = initial and final values of matric suction;<br>$\sigma_i$, $\sigma_f$ = initial and final values of mean principal stress;<br>$\gamma_h$ = matric suction compression index;<br>$\gamma_\sigma$ = mean principal stress compression index = $C_c / (1 + e_0)$;<br>$\Delta$pF = change of suction;<br>$C_c$ = compression index;<br>$e_0$ = void ration. | (2.74) |

2.11.3.1 Aitchison (1973) Method One of the earliest suction-based models, this model was initially proposed for investigating foundation on expansive soil [201]. Equation 2.59 shows the Aitchison proposed equation. Instability index ($I_{pt}$) came from the experimentally observed ratio of vertical strain to suction change [202, 203]. Instability index is similar to suction index ($C_\tau$) or compression index ($\gamma_h$) [143]. Three methods were specified by the Australian Standard for the design and construction of residential slabs and footing in the AS 2870-1996 [204] to estimate instability index.

1) Laboratory tests: Using suggested tests, including 1) shrink-swell test, AS 1289.7.1.1 - 1992; 2) loaded shrinkage test, AS 1289.7.1.2 - 1992; and 3) core shrinkage test, AS 1289.7.1.3 - 1992
2) Data Correlation: Finding correlations between the shrinkage index and other clay index tests
3) Visual-tactile identification: Using an experienced engineer or engineering geologist to identify soil.

The mentioned above methods were widely practiced in geotechnical engineering, especially the third method, which was named the visual-manual method [201, 212, 216]. This method includes a visual inspection of the soil and manually molding and kneading the soil to estimate its plasticity index, which makes this method highly classifier-dependent, time-consuming, expensive and difficult [201].

2.11.3.2 Hamberg & Nelson (1984) Methods Hamberg and Nelson [209] proposed a simplified method to predict heave using the CLOD test. The CLOD test provides the relationship between the changes in moisture content and the change in volume. Equation 2.66 shows the method, and the details of the method are described in

Nelson and Miller [31]. The CLOD is a special form of COLE test [217]. The COLE test was introduced to predict the heave underneath airfield pavements [69, 218]. Figure 2.24 shows the procedure of the CLOD test. The slope pf the curve in Fig. 2.24 is the suction modulus.

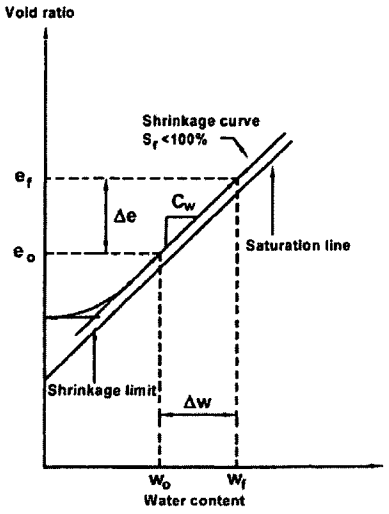


**Fig. 2.24 Measuring Cw from Moisture Content versus Void Ratio Relationship (Modified after [25]).**

Equation 2.66 has a major limitation, which is that it only considers suction change induced heave without considering effective stress on the soil. It was observed that generally the initial water content near the surface did not fall much below the shrinkage limit when the maximum water content under the simulated floor slab did not significantly exceed the plastic limit [25]. In Fig. 2.25, these values represent the minimum and maximum water contents at the surface for the initial and final water content profiles.

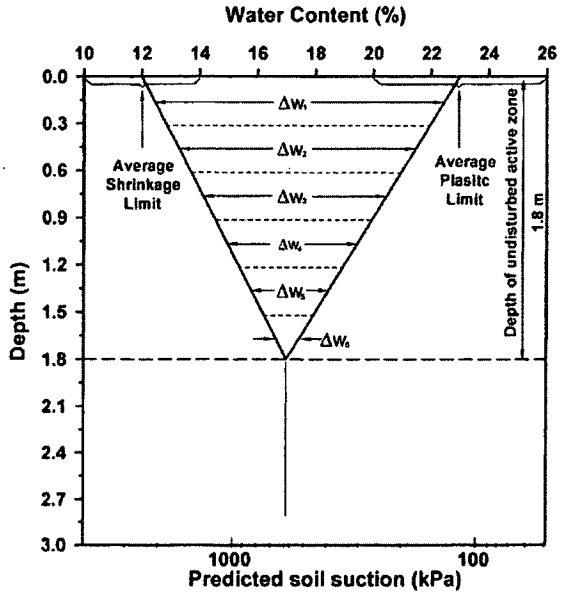


**Fig. 2.25 Idealized Moisture Boundary Profile [25]**

2.11.3.3 Lytton (1977, 1994) Method In 1977, Lytton [206] proposed a method to predict heave based on a simple laboratory test and some field observations of the shrinkage crack network. Equation 2.75 gives the volumetric strain.

$$\frac{\Delta V}{V_0} = \gamma_h \log_{10}(h_f/h_i) - \gamma_\sigma \log_{10}(\sigma_f - \sigma_i) \qquad (2.75)$$

Here, the first term is the volumetric strain due to suction change. The second term, which has a negative sign, is only considered with increasing depth until the strains become zero [155].

In 1994, Lytton [211] proposed Eq. 2.70, consisting of three stress state variables to predict soil heave. Three stress states include matric suction, osmotic suction and mean principal stress. Among these three, the major heave causing factor is the matric suction since osmotic suction rarely changes significantly, and mean principal stress change is nominal unless the soil is under significant surcharge. Lytton [211] also explained that

heave expressed as vertical strain can be estimated from the volumetric strain by using a crack fabric factor (f) using Eq. 2.76.

$$\frac{\Delta H}{H} = f * \left[\frac{\Delta V}{V}\right] \tag{2.76}$$

2.11.3.4 Johnson & Snethen (1978) Method Suction change in the active zone causes the major part of the soil heave. Johnson and Snethen [51] proposed Eq. 2.61 based on the theory, as the soil got wet, the suction decreased, and the volume increased. Compressibility factor can be found from Table 2.14, and the matric suction can be measured by thermocouple psychrometer or filter paper method. The value of parameters A and B can be found from the suction vs. moisture content semi-log graph. Parameter A is the soil suction value at zero moisture content; B is the slope of soil suction vs. moisture content curve.

**Table 2.14 Compressibility Factor [51]**

| Compressibility Factor (α) | Condition |
|---|---|
| $\alpha = 0$ | PI < 5 |
| $\alpha = 0.0275*IP-0.125$ | $5 \leq PI \leq 40$ |
| $\alpha = 1$ | PI > 40 |

Snethen [46] suggested to consider four cases about the final (1) zero suction throughout the depth of active zone; (2) suction increasing linearly increasing with depth through the active zone; (3) saturated moisture content profile; (4) constant suction at some equilibrium value.

2.11.3.5 Snethen (1980) Method Snethen [46] proposed this method using soil suction data to predict soil heave. Figure 2.26 shows a typical SWCC graph where the

suction in logarithmic scale. Soil suction without the external load and swelling pressure can be found using Eq. 2.77 and Eq. 2.78, respectively.

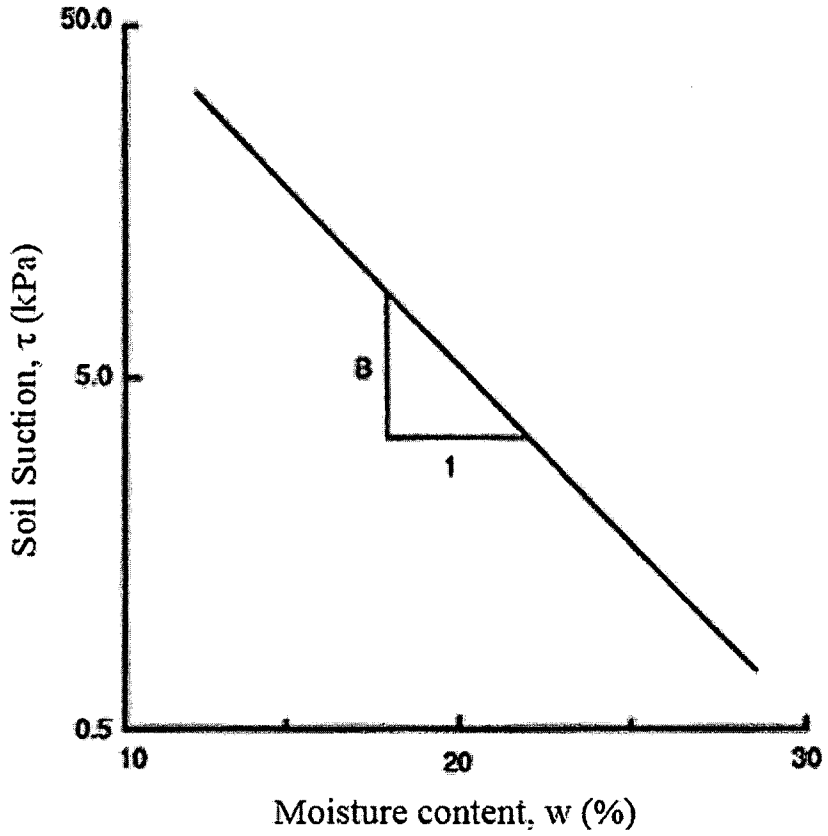


**Fig. 2.26 Soil Suction versus Moisture Content Relationships (Modified after Huang [13])**

$$\log \tau_m = A - Bw_0 \tag{2.77}$$

$$\log P_s = A - (100Be_0/G_S) \tag{2.78}$$

The equation provides predictions of in-situ heave of a soil with respect to soil composition, structure, initial and equilibrium moisture profiles, and confining pressures [144].

2.11.3.6 McKeen (1980, 1992) Methods Lytton [206] first introduced the suction compression index ($\gamma_h$) parameter, which was later used in a proposed method by

McKeen [207, 219] in Eq. 2.64. The required data are drying soil samples' volume change and suction change measurements [219]. Data can be collected in one-dimensional (oedometer test) or three-dimensional (COLE test) soil configuration. Suction compression index ($\gamma_h$) can be measured using the empirical relationship found from the statistical analysis [218]. Equation 2.79 is used when clay content (C) is between 40% and 70%; however, if the clay content is between 25% and 70%, Eq. 2.80 must be used.

$$\gamma_h = 0.00179C - 0.041 \tag{2.79}$$

$$\gamma_h = 0.00057C - 0.00057 \tag{2.80}$$

where C = percent < 2 μm.

Using a Texas soil database, a correlation between suction potential index (dh/dw) and suction compression index ($C_h$) was attempted to classify soil, as shown in Eq. 2.81 [218, 220, 221]. The relation was found to be linear as illustrated in Fig. 2.27. Olsen [222] explained that 85% of the $C_h$ values are larger than would be predicted by the relationship. Table 2.15 shows McKeen's soil classification.

$$C_h = (-0.02673)\left(\frac{d_h}{d_w}\right) - 0.38704 \tag{2.81}$$

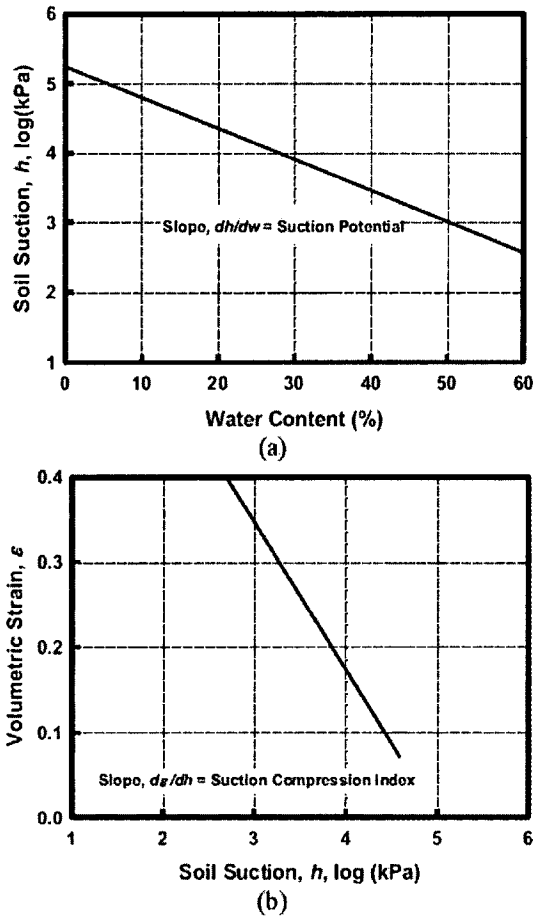


**Fig. 2.27 Determination of the Suction Compression Index [144]**

**Table 2.15 McKeen's Swelling Potential Categories [222]**

| Category | Swell Potential | Suction Potential dh/dw | Suction Compression Index, $C_h$ |
|---|---|---|---|
| I | Very High (McKeen calls this category "Special Case") | >-6 | <-0.227 |
| II | High | -6 to -10 | -0.227 to -0.120 |
| III | Moderate | -10 to -13 | -0.120 to -0.040 |
| IV | Low | -13 to -20 | -0.030 to non-expansive |

Suction potential index (dh/dw) and suction compression index ($C_h$) are functions of type, structure, amount of clay content in the soil, pore-fluid chemistry of the soil, and finally, the geologic origin and history [144, 222].

2.11.3.7 Mitchell & Avalle (1984) Method Mitchell & Avella [208] proposed a simple method to predict soil heave, as shown in Eq. 2.65. The assumption behind this method was based on an experimental observation, which was that vertical strain is linearly proportional to soil suction for expansive soil [202, 203]. Shrinkage testing was performed to measure the instability index ($I_{Pt}$). The test procedure for measuring $I_{Pt}$ is given as follows: 1) two soil samples are needed; 1) one soil specimen is air dried for two days; 2) the length and mass of the sample are measured intermittently during these two days; 3) at the end of the test, the sample is oven dried to get the final moisture content; 4) the second soil sample is used to find the SWCC. Equation 2.82 shows the expression for the $I_{Pt,}$ which can be measured using the linear strain versus moisture content and moisture content versus suction graphs (Fig. 2.28). Mitchell & Avella [208] tried to find a simple relationship between $I_{Pt}$ and $I_P$. Unfortunately, after testing as many as 83 soil samples from Australia, they concluded there was no simple relationship between them.

$$I_{Pt} = \frac{\Delta L/L}{\Delta w} * \frac{\Delta w}{\Delta u} \tag{2.82}$$

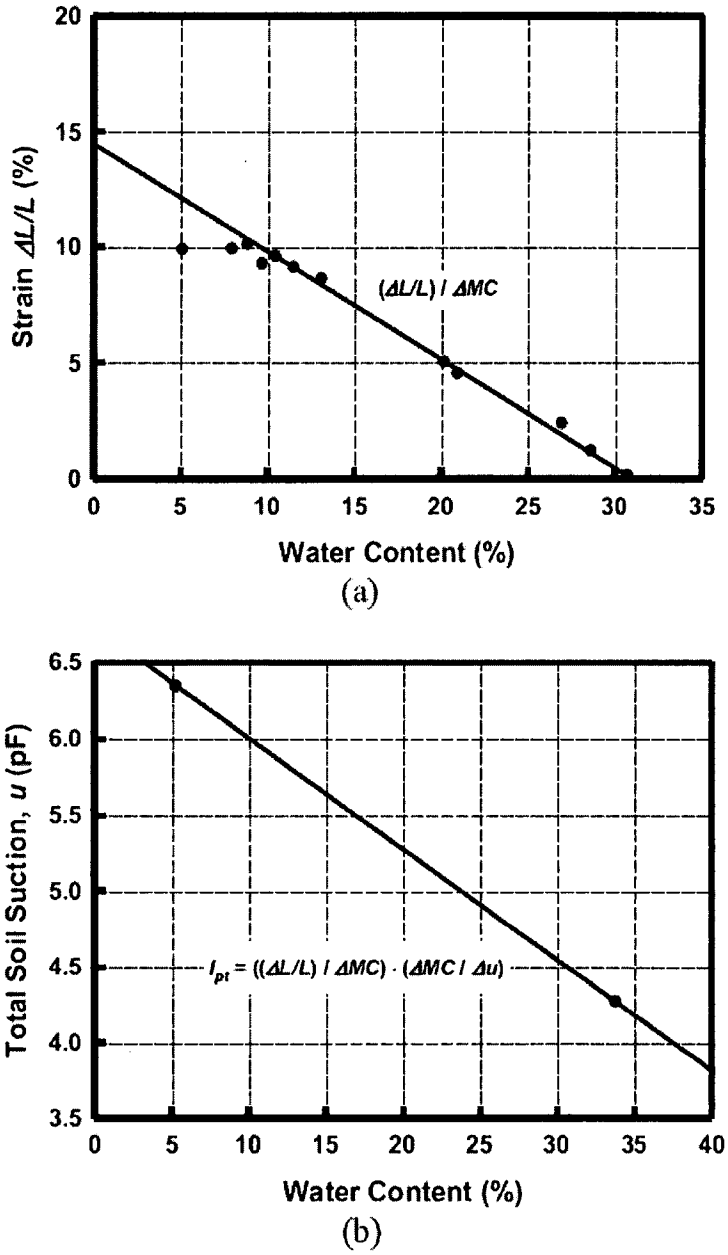


**Fig. 2.28 Determination of Instability Index [144]**

2.11.3.8 Dhowian (1990) Method In 1990, Dhowian [156] proposed a method to measure heave in expansive soil. The method was determined from the extensively instrumented field stations. The investigation was taken on a site located in the town of Al-Ghatt, Saudi Arabia. Interestingly, no montmorillonite mineral was found in the clay fraction of the shale (Fig. 2.29).

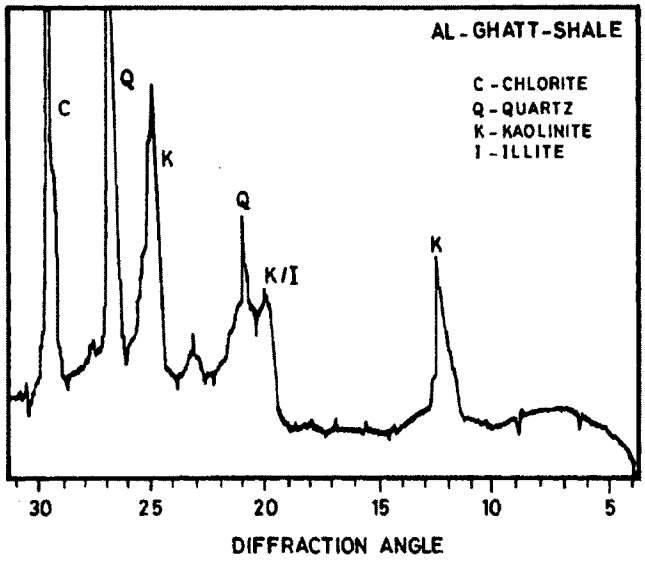


**Fig. 2.29 X-ray Diffraction Patterns of Al-Ghatt Shale [156]**

Heave was predicted using both oedometer and suction-based methods, and both were checked with the actual heave. Undisturbed shale samples were tested using the improved oedometer tests (ISO), constant volume tests (CVS) and swell overburden tests (OSO). Figures 2.30 and 2.31 show the results.

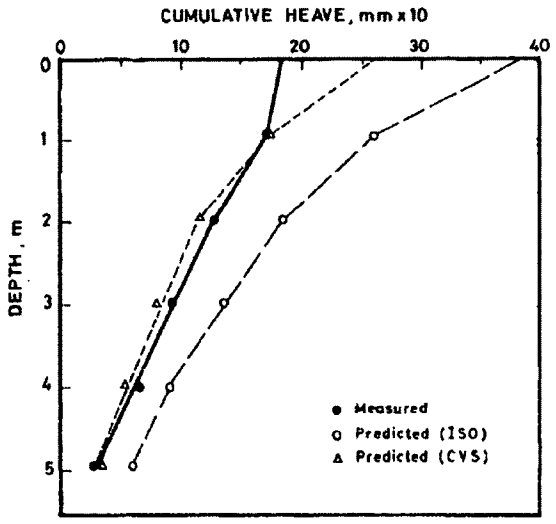


**Fig. 2.30 Predicted and Measured Heave Based on Oedometer Technique [156]**

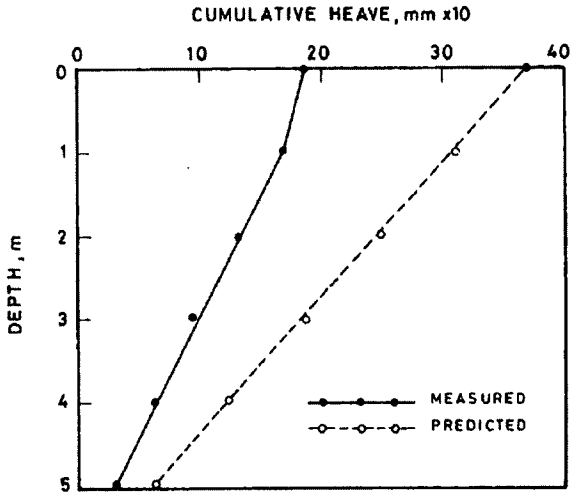


**Fig. 2.31 Predicted and Measured Heave Based on Suction Method [156]**

Dhowian [156] concluded that the discrepancy between the experimentally and field-determined parameters was because of 1) the tested samples were carefully selected from the specified location and depth, and due to their small size, they tended to be more homogeneous and less contaminated by non-expandable materials; and 2) the samples in the oedometer chamber wee laterally restrained; thus, the volume increase took place in the vertical direction only, whereas the field vertical movement constituted a fraction of the volume change.

2.11.3.9 Fityus & Smith (1998) Method In 1998, Fityus and Smith [212] presented Eq. 2.71, which can predict soil heave within the active zone. This method has some assumptions, including (1) the change in moisture content will always correspond with the same change in strain, (2) volume index ($I_v$) is applicable to predict both swelling and shrinking behavior, and (3) use of factor $\alpha$ of 0.33 will accommodate between one and three-dimensional volume changes. One of the main parameters of this method is the volume index ($I_v$), which can be found from a series of one-dimensional

swell tests in which a soil sample is allowed to swell under a token pressure that is equal to the calculated vertical stress experienced under field conditions. Figure 2.32 shows the process of finding volume index of Maryland clay.

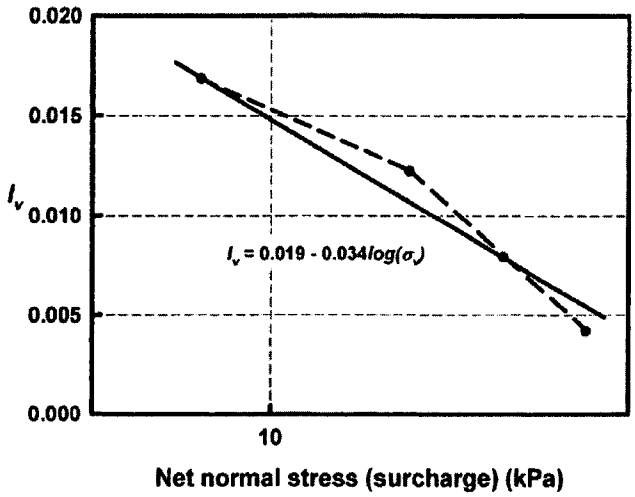


**Fig. 2.32 Estimation of the Volume Change Index (Iv) for Maryland Clay [144]**

2.11.3.10 Briaud *et al.* (2003) Method In 2003, Briaud *et al.* [214] proposed a method based on moisture content to estimate the soil heave. The step-by-step procedure of the Briaud method is as follows: 1) first determine the depth $Z_{max}$ of moisture content fluctuation, and break the depth $Z_{max}$ into an appropriate number of n layers, $h_i$ being the thickness of layer i; 2) collect samples at the site within $Z_{max}$ depth; 3) perform shrink tests and find shrink–swell modulus ($E_w$) and shrinkage ratio (f); 4) determine the change in moisture content, $\Delta w$, as a function of depth within $Z_{max}$; 5) for each layer i, calculate the shrink or swell movement $\Delta h_i$ of that layer by using Eq. 2.73.

Two important parameters of the method shrink–swell modulus ($E_w$) and shrinkage ratio (f) come from the shrinkage test. The test procedure is given as follows: 1) the soil sample needed to be trimmed to the recommended 75-mm diam×150-mm

high; 2) at time t = 0, weight $W_0$, height $H_0$ and diameter $D_0$ of the sample needed to be recorded with a minimum of three heights and three diameter measurements for each height at $120^0$ intervals being recommended; 3) after that soil sample is air dried, weight W, height H and diameter D needed to be recorded at different time intervals, and Briaud [214] suggested recording readings every hour for the first 8h, recording a minimum of three height and three diameter measurements for each height at $120^0$ intervals during each reading for two days to obtain sufficient data; 4) once the last reading was taken, the soil sample needed to be oven dried and weighed; 5) the whole time temperature and the relative humidity needed to be monitored; 6) finally, the $\Delta H/H_0$ versus $\Delta V/V_0$ and w versus $\Delta V/V_0$ graph f and $E_w$ were plotted and measured.

## 2.12 Soil Stabilization

The volume change behavior of expansive soil can be minimized by adding cementitious materials to it. The common cementitious materials are cement and lime. Nowadays geopolymer cement is also used as an alternative to cement and lime. Other ways include cut and fill method or placing geotextile inside the subgrade. The advantage of geopolymer material over Portland cement is still not widely known. Portland cement, if used in construction, will have a design life of about 50 years and maybe 100 years for bridge engineering, which is not found in real life due to the original design and construction errors, potential damages caused by mechanical actions and environmental effects, and changes in functionality, etc. [223]. Davidovits [224] described in the book titled *Why the pharaohs built the pyramids with fake stones?* that the Egyptians already knew how to build huge concrete blocks that can last for thousands of years, and they used geopolymers as construction materials. The key ingredient of geopolymer is Fly ash (FA) which is one of the

coal combustion products. The American Coal Ash Association (ACAA) in its coal combustion products (CCP) production & use survey for 2014 [225] reported an annual fly ash production of approximately 51 million tons in the USA. Among them only 23 million were put to a productive use, leaving 28 million to be placed in storage lagoons at a significant cost. Fly ash disposal costs are expected to increase due to pending government regulations aimed at regulating fly ash disposal. Storage lagoons, commonly used as long-term storage facilities, also pose a potential environmental hazard in case of a spill, such as the one that took place in Kingston, Tennessee, on December 22, 2008, when an ash storage lagoon failed to release 2.6 million cubic yards of ash into Emory river near a residential area [226]. In recent years, the new application of geopolymers as a soil stabilizer has emerged.

In industry, most commonly used stabilizers are either cement or lime. Using geopolymer as an alternative to expensive cement or lime has been seriously evaluated recently. Using activated fly-ash-based geopolymers for soil stabilization has limited application due to its corrosive activators (i.e., sodium hydroxide and sodium silicate). In this research, for this reason, more practical add-water geopolymer was used.

The department of transportation (DOT) in various states established its own criteria for modification and stabilization. In the following paragraphs, soil stabilization standards and specifications for Louisiana and its neighboring states will be discussed in brief.

Louisiana - From Tables 2.16 and 2.17, LADOTD 2016 specifications required cement or lime far less than their 2006 specifications. According to Tables 2.16 and 2.17, it can be concluded that 1) cement percentage has significantly reduced, 2) there is no specification for GPC-based soil stabilization, and 3) there is no stabilization standard for soils with a PI value higher than 35 (i.e., Moreland clay).

**Table 2.16 LADOTD 2016 Specification [227]**

| Plasticity Index (PI) | Lime/Cement (% Volume) |
|---|---|
| 0 - 15 | 6% Cement |
| 16 - 25 | 6% Lime + 6% Cement |
| 26 - 35 | 9% Lime + 6% Cement |

**Table 2.17 LADOTD 2006 Specification [228]**

| Plasticity Index (PI) | Lime/Cement (% Volume) |
|---|---|
| 0 - 15 | 9% Cement |
| 16 - 25 | 6% Lime + 9% Cement |
| 26 - 35 | 9% Lime + 9% Cement |

Texas – According to 2005 TxDOT, there is a standard and specification for subgrade and base stabilization by either cement, lime or fly ash. Figure 2.33 shows the subgrade stabilization specification and Fig. 2.34 shows base stabilization specification. [229, 230]

Oklahoma – According to the Oklahoma DOT, stabilization additive shall be determined by the AASHTO group classification. Figure 2.35 shows the stabilization table.

New Mexico – According to NMDOT published manual, "Standard Specifications for Highway and Bridge Construction," the subgrade must be in accordance with the State Materials Bureau's mix design [231]. Unfortunately, no detailed information was found about the percentage of cement or lime that must be used.

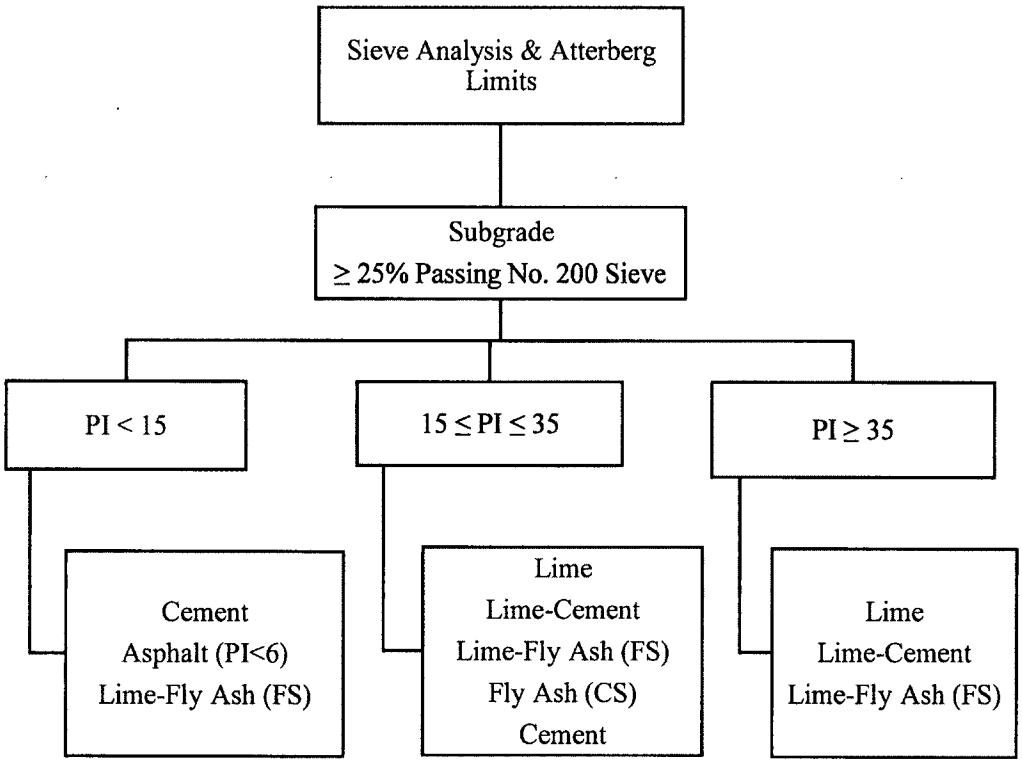


**Fig. 2.33 TxDOT Subgrade Stabilization Specification [229]**

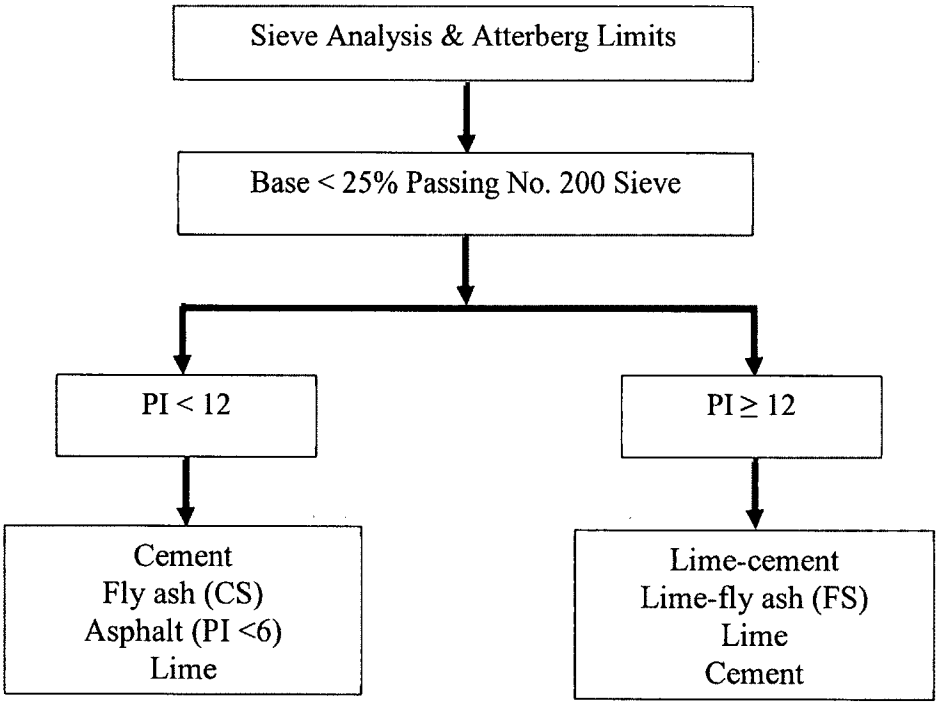


**Fig. 2.34 TxDOT Base Stabilization Specification [230]**

| SOIL STABILIZATION TABLE | | | | | | | | | | | | |
|---|---|---|---|---|---|---|---|---|---|---|---|---|
| ADDITIVE (Expressed as a percentage added on oven dry basis) | SOIL GROUP CLASSIFICATION - AASHTO M145 | | | | | | | | | | | |
| | A-1 | | A-2 | | | | A-3 | A-4 | A-5 | A-6 | A-7 | |
| | A-1-a | A-1-b | A-2-4 | A-2-5 | A-2-6 | A-2-7 | | | | | A-7-5 | A-7-6 |
| PORTLAND CEMENT | 4 | 4 | 4 | 4 | 4 | 4 | 5 | √ | √ | √ | | |
| FLY ASH | | | | | 12 | 12 | 13 | 14 | 14 | 14 | | |
| CEMENT KILN DUST (Pre-Calciner Plants) | 5 | 5 | 5 | 5 | 5 | 5 | 6 | √ | √ | | | |
| CEMENT KILN DUST (Other Type Plants) | 10 | 10 | 10 | 11 | 11 | 11 | 12 | 12 | 12 | | | |
| HYDRATED LIME* | | | | | | | | | | 4 | 5** | 5** |

**Fig. 2.35 Oklahoma DOT Soil Stabilization Specification [232]**

Arkansas – According to Arkansas State Highway and Transportation Department, if lime is used to stabilize subgrade soil, then the mixture shall not contain more than 8% lime by weight. For base course treatment done by cement, the mixture shall not contain more than 4% cement by weight. Fly ash may be used as a partial replacement for cement but not more than 25% [233].

Indiana – According to Indiana DOT cement, lime or fly ash can be used to stabilize the subgrade soil, as shown in Table 2.18 [234].

**Table 2.18 INDOT Soil Stabilization Specification [234]**

| Treatment | Soil property | Additive type | Suggested amount |
|---|---|---|---|
| Stabilization | PI>10 and clay content (2μ) >10% | Lime (quick lime) | If lime or lime byproduct is used: 4% to 7%<br>If cement is used: 4% to 6%<br>If fly ash C class is used: 10% to 16% |
| | PI < 10 and < 20% passing #200 sieve | Cement | |
| Modification | PI ≥ 5 and > 35% passing #200 sieve | Lime | |
| | 5<PI<20 and >35% passing #200 sieve | Lime-fly ash blends | |
| | PI < 5 and ≤ 35% passing #200 sieve | Cement and/or fly ash (C class) | |

## 2.13 Mechanism of Stabilization

The soil stabilization mechanism can be portrayed as coating and/or binding of soil particle to form another output soil with improved characteristics [235]. The efficiency and effectiveness of the stabilizer depend on the type of soil to be stabilized, the type and properties of stabilizer, the associated moisture content during compaction, as well as the long-term moisture content. Furthermore, the effectiveness of the stabilizer can be measured by its ability to provide enough calcium to chemical reaction. Lime, Portland cement and fly ash materials are the most frequently used chemical stabilizers. Fly ash that possesses self-cementing property that can stabilize/treat soil without cement or lime is called class C fly ash, whereas the type often used either with lime or cement to make it more reactive is called class F or non-cementing fly ash. The mechanism of stabilization for these stabilizers is similar regardless of a few different processes. The overall stabilization process can be summarized into four different processes [236, 237]. All four processes (Cation exchange, Flocculation and agglomeration, Cementitious hydration, Pozzolanic reaction) will occur in cement treated subgrade soil, whereas in the case of lime treated soil cementitious hydration will be absent due to the lack of calcium aluminate hydrate (C-A-H) after hydration of the stabilizer [238].

## 2.14 Geothermal Energy

Geothermal energy is one of the most promising renewable energy sources available in the world. The power source for geothermal energy is through using heat energy from the center of the earth to produce electricity, and it also uses the temperature difference between the soil and atmosphere to heat and cool buildings in different seasons. The earth's core temperature can reach up to 7000 to 12000 degrees Fahrenheit,

which is caused by the slow radioactive decay of heavy elements at the earth's core [239]. Through thermal conduction, the heat energy is then available at the earth's surface. Worldwide there were a total number of 82 countries using geothermal energy in 2015, which was an increase of about 5.27 times over the last 10 years [240]. Among them, the US has become the world leader in usage of geothermal energy, generating over 3.5 GW in 2015, as illustrated in Fig. 2.36.

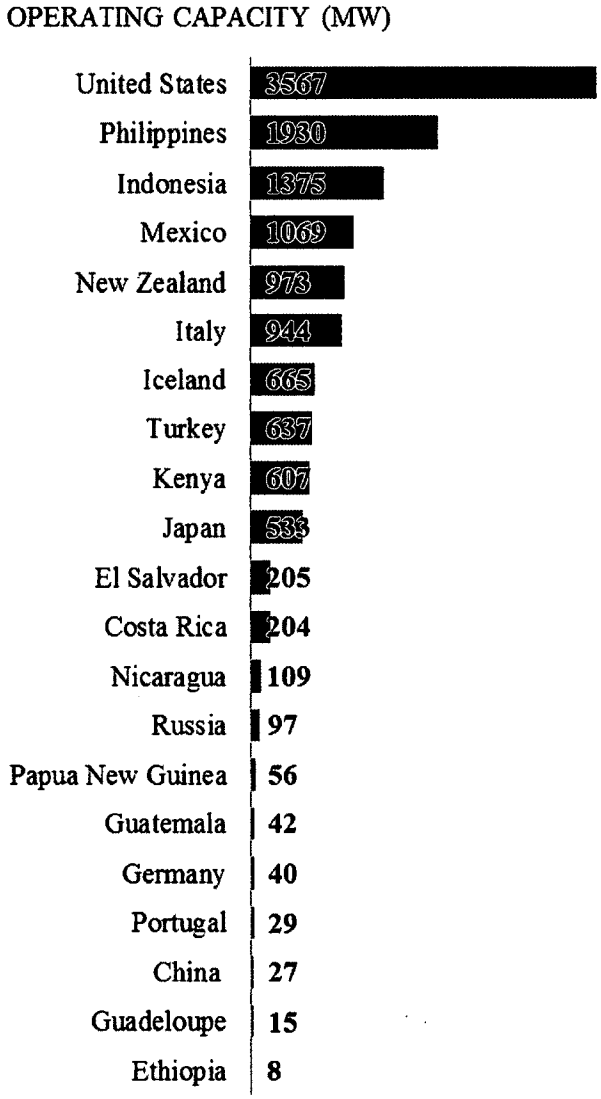


**Fig. 2.36 Geothermal Power Operating Capacity by Country [241]**

## 2.15 Major Advantages of Geothermal Energy

Compared with other sources of energy, geothermal energy has advantages, including the following:

1. Reduced environmental impact – It produces less $CO_2$ emissions in the atmosphere and does not cause significant amounts of pollution.
2. Significantly reduced cost – It does not need any fuels and maintenance cost is low as well.
3. Less land use – A small footprint on land is required, and the equipment is built partially underground; thus, it is a type of energy that can be developed in the backyard of a small household.
4. Ease of access – It is accessible everywhere, although only some resources can be profitably exploitable. It must be noted that technological advancement is moving quickly, and enhanced geothermal systems have made more resources available with lowered costs.
5. Independence of weather – As compared with many other types of renewable energy, such as solar energy, geothermal energy is not dependent on weather.
6. Security – It is excellent for meeting the base load energy demand, as opposed to other renewables, such as wind or solar energy.

## 2.16 Important Facts about Geothermal Energy

Lund and Boyd [240] explained in 2015 that worldwide consumption of only direct-use geothermal energy was 592,638 TJ. Geothermal energy was produced at the cost of very few harmful byproducts such as carbon, $CO_2$, $SO_X$ and $NO_X$, compared to traditional energy sources. It is estimated that a barrel (bbl) of oil equals 6.06×109J of

energy, which means that 592,638 TJ of energy is equivalent to 282 million barrels or 42.3 million tons of oil. According to Lund and Boyd, that amount of oil is about equivalent to a three-day consumption of oil worldwide. They also summarized the research done by Lawrence Livermore Laboratory and private consultant Goddard and Goddard, which showed that if 592,638 TJ of energy as a form of electricity was produced from natural gas, oil or coal, a huge amount of carbon, $CO_2$, $SO_X$ and $NO_X$ would be produced, as shown in Table 2.19. Table 2.19 shows that if 592,638 TJ of energy as a form of heat was produced, the numbers would be halved. In the USA, there are many tax rebates available for renewable energy users, including those who are using geothermal energy. There is a complete database available, which was created and kept updated by the North Carolina Clean Energy Technology Center [242]. The work is funded by the US Department of Energy. The database includes in-depth information about how many different types of tax rebates or financial incentives are available for using geothermal energy. The rebates and financial incentives are provided by the federal government and are for each state government, including Louisiana. From the database, a total of 18 financial incentives is available for using geothermal energy in Louisiana for either residential or commercial purposes.

**Table 2.19 Worldwide Direct-Use Savings in Energy of 2015, Carbon and Greenhouse Gases using Geothermal Energy Including Geothermal Heat Pump in the Cooling Mode (Figures in Millions) in Terms of Fuel Oil (TOE = tons of oil equivalent, bbl = barrel of oil) [240]**

| | Fuel Oil | | Carbon | $CO_2$ | $SO_X$ | $NO_X$ |
|---|---|---|---|---|---|---|
| | bbl | TOE | TOE | TOE | TOE | TOE |
| As electricity | 352 | 52.8 | 46.1 | 149.1 | 1.03 | 0.031 |
| As direct use | 176 | 26.2 | 22.9 | 74.4 | 0.51 | 0.015 |

## 2.17 Different Types of Geothermal Energy Systems and Their Potential Use in the State of Louisiana

There are mainly three types of geothermal systems available in the world: the hydrothermal system, the direct-use system, and the heat-pump system. Figure 2.37 is the geothermal resource map of the conterminous US, which shows that the western region of the US has higher heat flow than the eastern region, making it ideal for the development of the hydrothermal system. In reality, that's why most of the installed hydrothermal power plants are in the western region of the US, especially in California and Nevada, as shown in Fig. 2.38. Based on Figs. 2.37 and 2.38, the most appropriate system might be the heat-pump system in Louisiana because the ground temperature is not as high as in the western region of the US. More explanation will be found in the following paragraphs.

Unfortunately, unlike other states, Louisiana does not provide any incentive towards geothermal energy compared to the generous tax breaks offered for wind and solar energy. For example, according to Louisiana Administrative Code (LAC): 61:1907, the incentive for using wind and solar energy is a Louisiana tax credit of 50% for the first $25,000 of spending, but there is no mention of incentives for using geothermal energy. The most notable incentive, which can be used in geothermal energy installation in Louisiana includes a federal government-provided 30% tax credit if certain efficiency criteria are met [243].

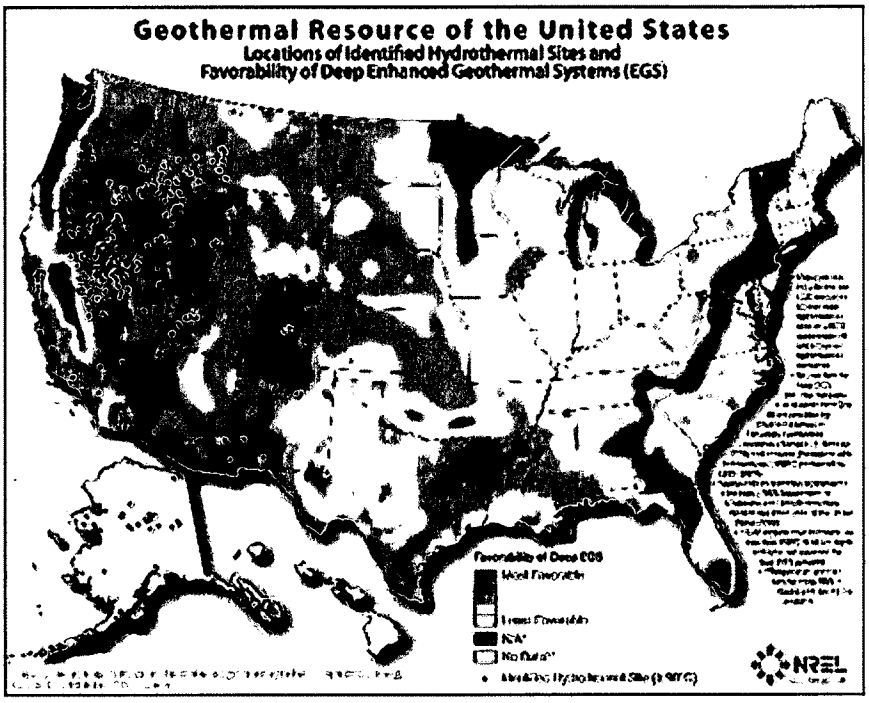


**Fig. 2.37 Suitable Hydrothermal System Locations in the US [244]**

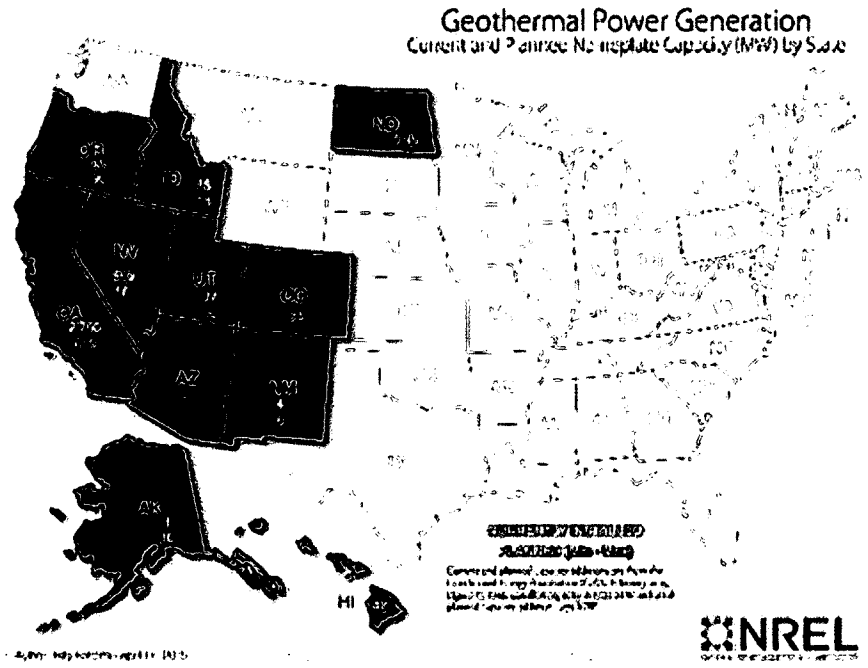


**Fig. 2.38 Geothermal Power Generation Map in the US [245]**

## 2.18 Types of Geothermal System

A summary of all the three geothermal energy systems are given below (Fig. 2.39) and were taken from the US Energy Information Administration website and Missouri Department of Economic Development's Division of Energy website [239, 246]:

*Hydrothermal System:* In this type of system, ground water heated by geothermal energy is used to produce electricity, as shown in Fig. 2.39. This category of systems is further subdivided into three subtypes.

*Dry Steam Plant:* In this type of system, high pressure (geo-pressure) steam coming directly from the deep geothermal reservoir is used to produce electricity with the help of a turbine.

*Flash Steam Plant:* In this type of system, geo-pressured, high-temperature water is collected and then converted into steam. The steam is then used to turn the generator turbine. When the steam is condensed to water, it is injected back into the earth. Most of the hydrothermal plants follow this principal.

*Binary Steam Plant:* In this type of system, sometimes it is more convenient to make another liquid turn into steam compared to water. In this process, heat energy from the geothermal hot water is transferred to the second liquid, and using the steam of the second liquid, power is generated.

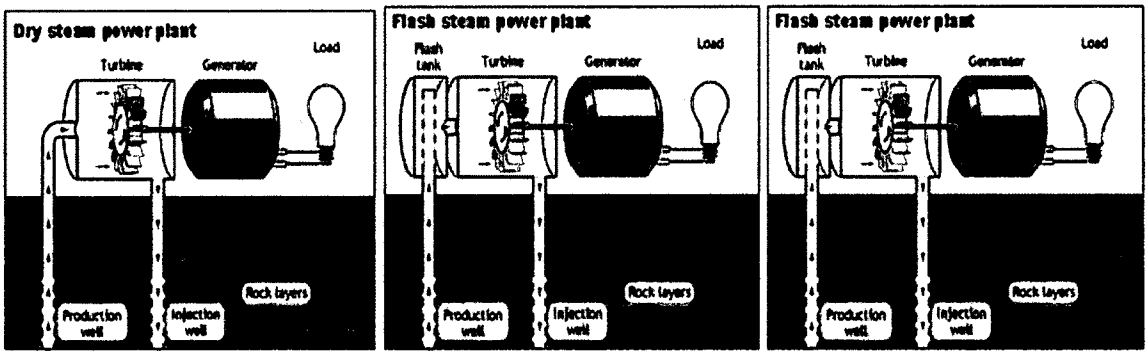


**Fig. 2.39 The Hydrothermal System [246]**

Some preliminary studies of this hydrothermal system, which is also called an Enhanced Geothermal System (EGS), have been done in Louisiana. A part of the research was completed in 1981 near Cameron Parish where a 4825-m deep test well was used. The system kept running until it was shut down in October 1987. Over the four years, the test well produced more than 67 million barrels of brine and 676 MMscf (Million Standard cubic feet, the unit used in the oil industry) of associated gas. Eleven potential zones were selected where significant geo-pressure was found. However, a conclusion was made later that there was a major uncertainty about the overall reservoir size and longevity of the production [247]. In 2009, a massive study was undertaken by Louisiana Tank, Inc. and Jordan Oil Company, Inc. The project had a grant of $5 million, which was funded by the Department of Energy in the same parish to make a definitive conclusion about the prospect of EGS in Cameron. In the final project report, some drawbacks were mentioned about the utilization of the hydrothermal reservoir, including the absence of Renewable Portfolio Standard (RPS) in Louisiana. Concerns expressed in the report included that the policy did not require utility supply companies to produce a specified fraction of their electricity from renewable energy sources. Because Louisiana's policy makers are heavily dependent on the use of fossil fuel, it's hard for any startup

geothermal company to secure a power purchase agreement (PPA) with a utility company that might be interested in paying a premium price for the "green" energy. After a total spending of $867,850.84 out of $5 million, the project was closed [248, 249].

*Direct Use System:* In many locations in the US, hot water is available near the ground surface but not heated enough to be used in a hydrothermal system. The direct use of geothermal energy is a good option in these locations. The direct use system has been a popular option for many countries and some states in the US, such as Utah, Oregon and California. Its uses include heating domestic water, pool water, and water at fish farms, etc., raising plants in greenhouses, drying of fish and fruits, heating sidewalks and several industrial processes, etc. There is no evidence of the direct use of geothermal energy in Louisiana, possibly because there is no presence of heated water near the ground surface in Louisiana [239].

*Heat-Pump System:* In this system, no energy electricity is produced directly. However, this system significantly reduces requirements for heating, ventilating and air conditioning (HVAC) of residential and commercial buildings. This geothermal system takes advantage of the constant temperatures found just ten to fifteen feet underground. The difference between the atmosphere and soil temperatures is used to heat and cool buildings in winter and summer, respectively. The most common type is the open- or closed-loop system. In the open-loop system, fluid is not circulated in the high-density polyethylene (HDPE) pipe. Fluid comes into the system from the inlet and gets out from the outlet. A good example of the open-loop system is the surface water heat exchanger, as shown in Fig. 2.40. In a closed-loop system, the fluid constantly circulates in the HDPE pipe. The closed-loop system can be mainly divided into the horizontal and

vertical heat exchanger systems. In the horizontal closed-loop system, an HDPE pipe is generally laid in shallow-depth trenches. In the vertical closed-loop, system heat is exchanged with the soil using either a borehole or energy pile. In the borehole type, a heat exchanger HDPE pipe is laid vertically into the soil and then filled up with grout. This is mostly applicable for a residential building where space is limited around the building, and the building does not need any pile foundation for structural reasons. If the soil has less bearing capacity and pile foundation is a necessity, the HDPE pipe can be installed within the concrete piles, which are called energy piles. Figures 2.41 and 2.42 show a borehole geothermal heat exchanger (GHX), and Fig 2.43 shows an energy-pile GHX. The heat-pump system has a huge potential in Louisiana as one of the world's largest geothermal, heat-pump systems has been installed at Fort Polk Army base, Louisiana. Privately funded for about $18.9 million, the system provided heating and cooling energy for 4003 homes, saving annually $345,000 for 20 years during the contract period [250, 251]. Even after the contract expired, it was believed that the financial savings were about $2.2 million per year. This installation reduced electricity consumption by 26 million kWh (33%) and $CO_2$ emission by 22,400 tons/year. The heat-pump, borehole heat exchanger system in Fort Polk is shown in Fig. 2.42. In north Louisiana, where a regular pile foundation is not necessary, the horizontal/vertical, borehole, closed-loop heat exchanger system can be an excellent solution. In south Louisiana, where pile foundation is utilized more frequently, the energy pile is more appropriate.

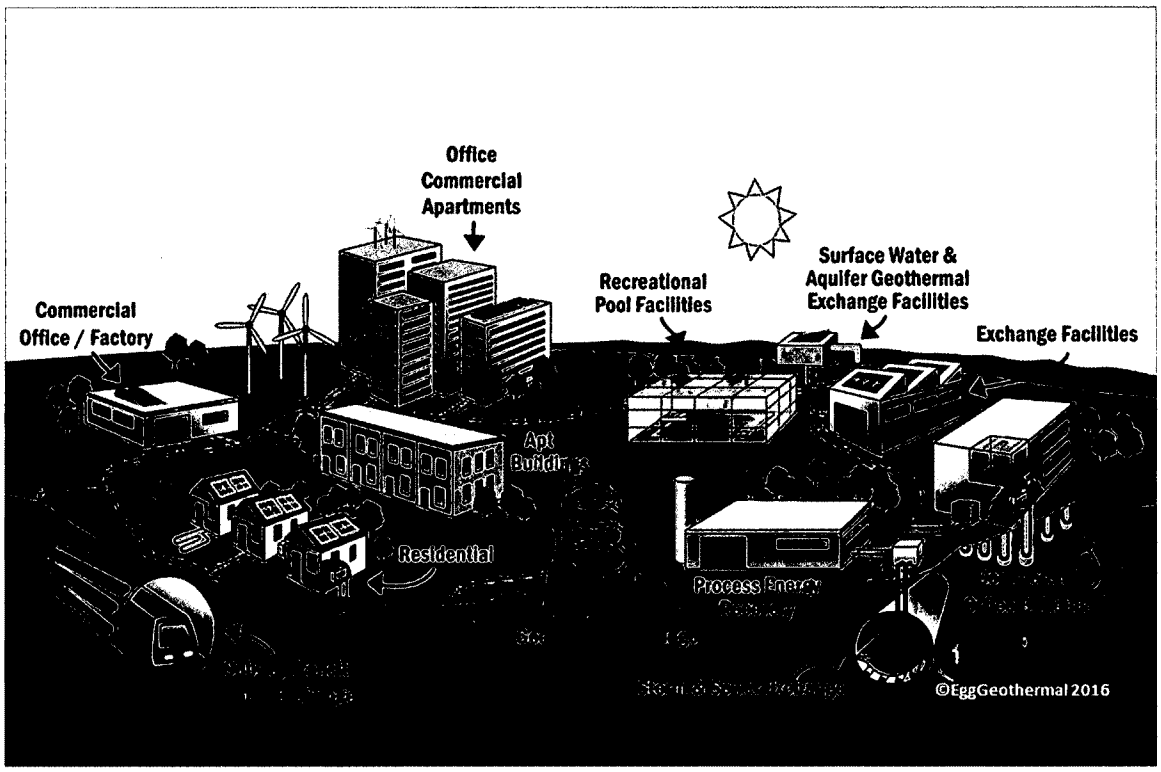


**Fig. 2.40 Different Types of Geothermal Systems, Illustration by Sarah Cheney [252]**

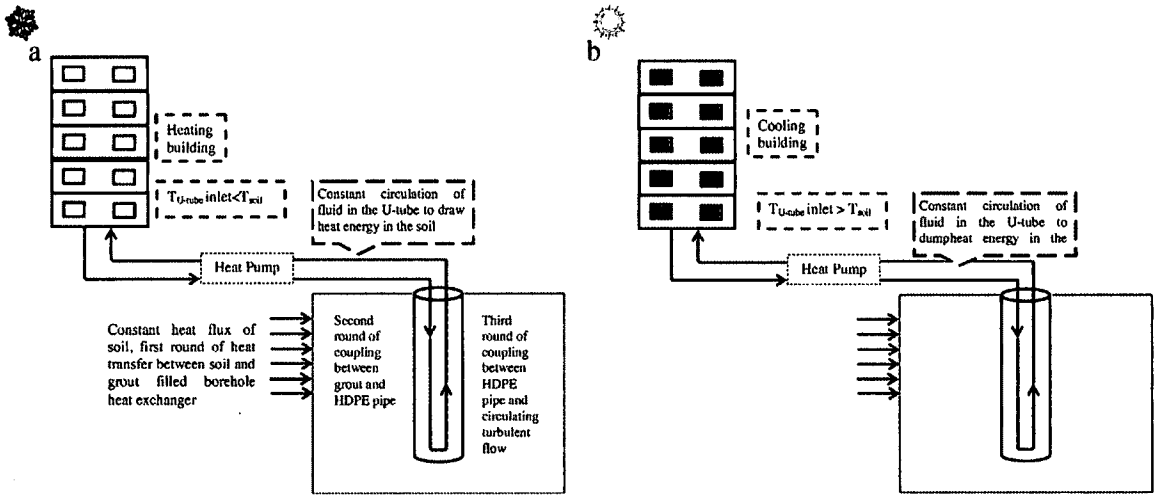


**Fig. 2.41 Heat Transfer in a Borehole GHX [253]**

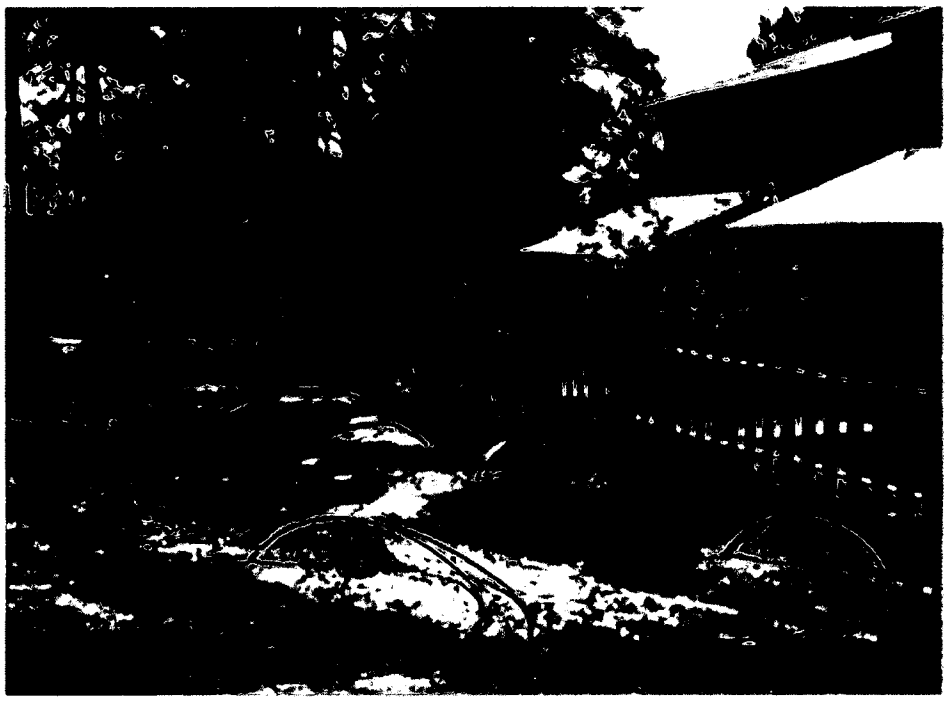

**Fig. 2.42 Borehole Installation in Fort Polk, Louisiana [251]**

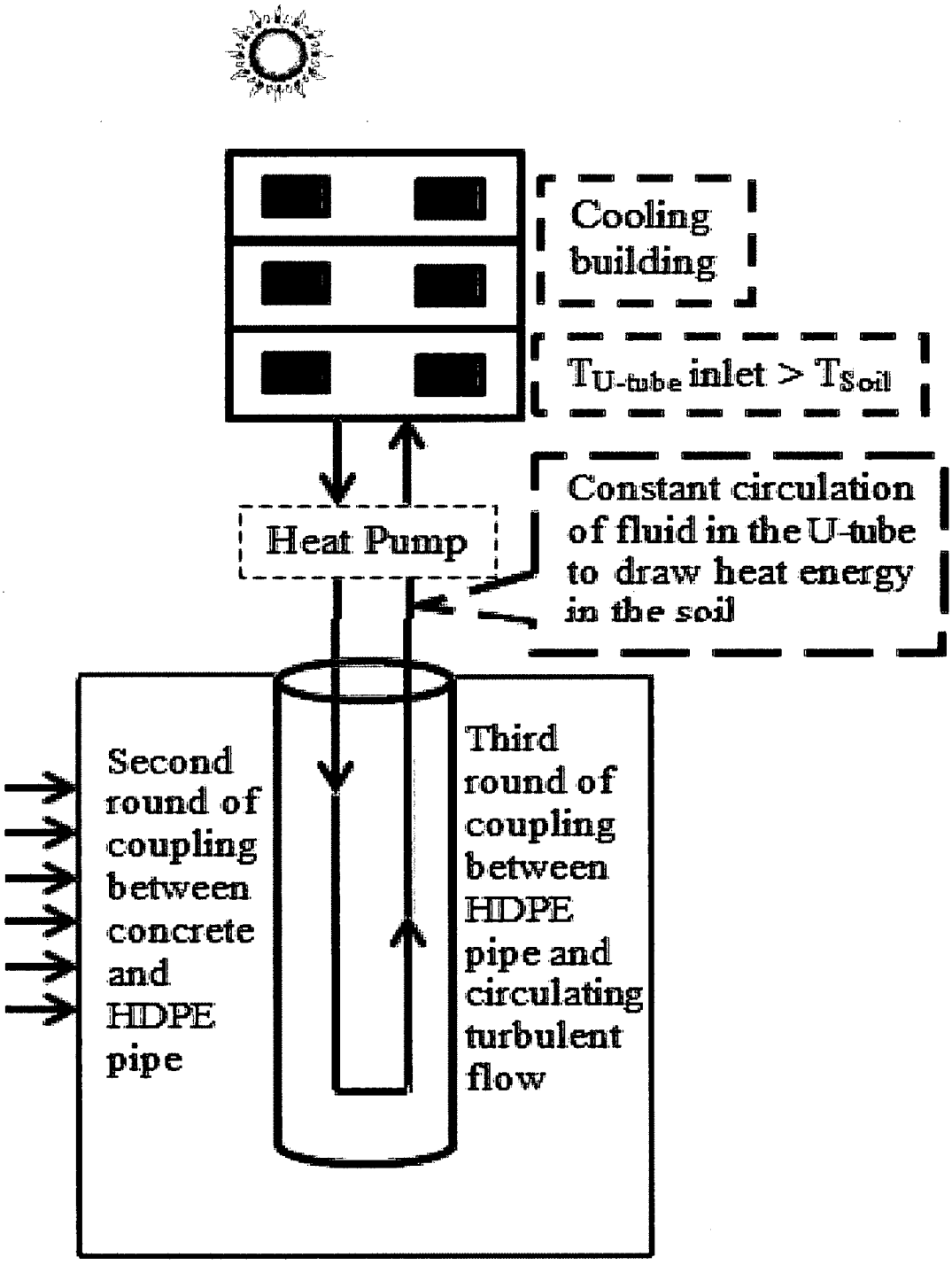
Cooling building
$T_{U\text{-}tube\ inlet} > T_{Soil}$
Heat Pump
Constant circulation of fluid in the U-tube to draw heat energy in the soil
Second round of coupling between concrete and HDPE pipe
Third round of coupling between HDPE pipe and circulating turbulent flow

(a)

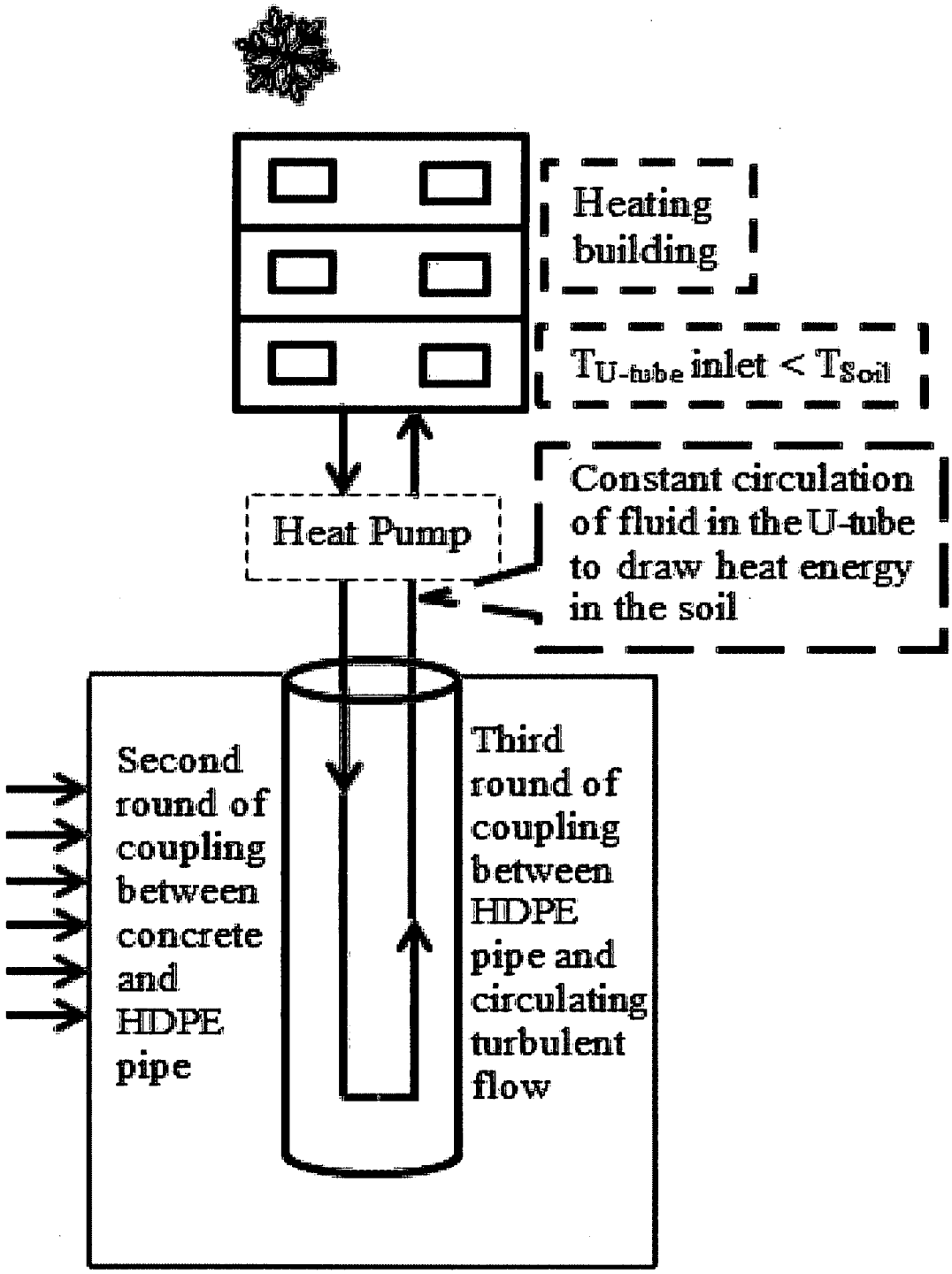


(b)

**Fig. 2.43 Energy Pile in (a) Summer and (b) Winter [254]**

# CHAPTER 3

# SOIL SAMPLING, LABORATORY EXPERIMENTS AND DATA ANALYSES

## 3.1 Introduction

To investigate the structural damage by expansive soil, its expansive nature must be investigated first. For the soil properties, the regular soil tests and tests done exclusively for expansive soil are performed. To get soil samples from Bossier parish in northern Louisiana, a permitted site is selected near Interstate 220 (I-220), next to The Pentecostals of Bossier City church, as illustrated in Fig. 3.1. The church already shows some structural damage due to the presence of expansive soil underneath its existing buildings. In the church location, there are visible cracks in multiple slab-column joints. These cracks are then recorded through a series of pictures. Figure 3.2 shows the foundation damage of the church. Another location is also chosen to investigate the intensity of expansive soil in northern Louisiana. Figure 3.3 is taken from Tacoma Blvd. in Caddo Parish. The location of the road is very close to the church. Interestingly, the road was constructed with geogrid, but the expansive nature of the subgrade soil is so severe that even with the presence of the geogrid the roads experienced numerous longitudinal cracks.

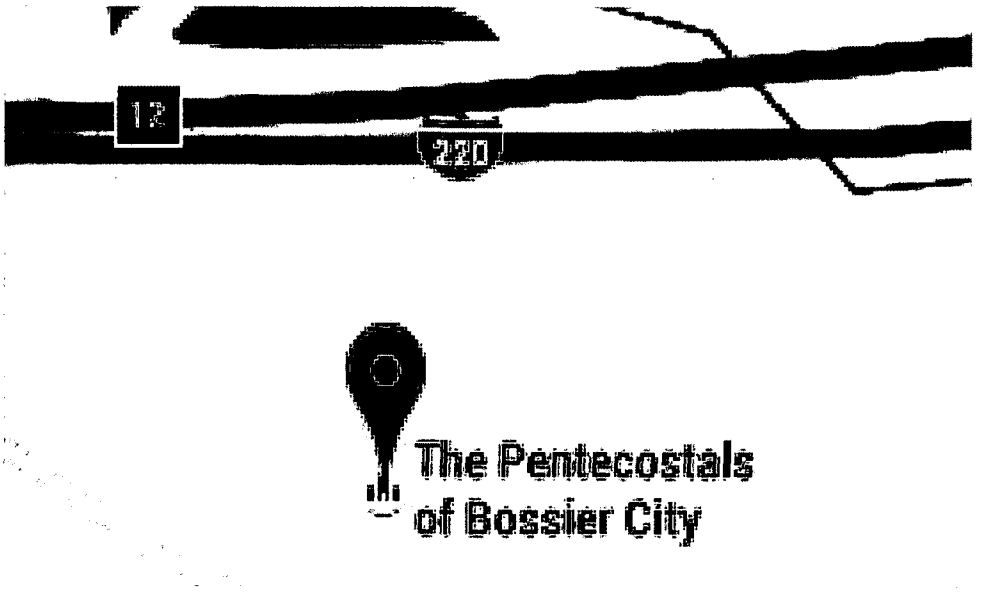


(a)

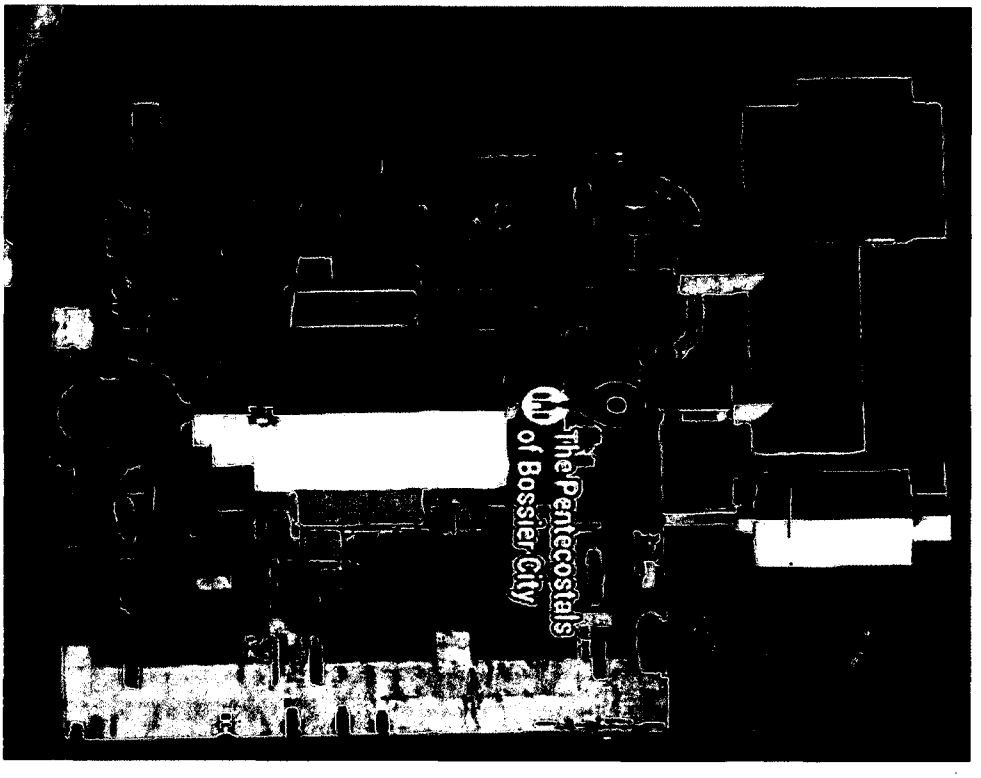


(b)

**Fig. 3.1 Location of the Soil Sampling Site (a) Near I-220 (b) Top View of the Church**

**Fig. 3.2 Structural Damage in the Slab-column Joint Due to Expansive Soil**

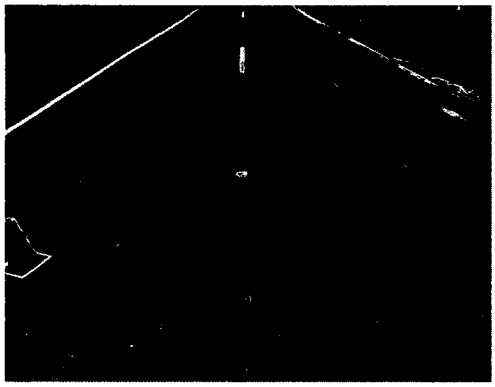

**Fig. 3.3 Longitudinal Cracks in Roads in Caddo Parish, LA**

## 3.2 Laboratory Experiments

The objectives of the lab tests are to understand the severity of the expansive soil and to find enough information to predict volume change behaviors of the soil. All the lab tests can be divided into two categories. The first category refers to the regular soil tests, and the second category includes the tests for expansive soil only.

## 3.3 Soil Sampling

Expansive clay is obtained from a local test pit in Bossier City, Louisiana, in accordance with ASTM D1452-09 [255] for disturbed soil samples and ASTM D1587/D1587M-15 [256] for undisturbed soil samples. The samples are retrieved in

sealed containers and transported to the Geotechnical Testing Laboratory at Louisiana Tech University.

## 3.4 Regular Soil Tests

Regular soil tests are used to determine soil geotechnical index properties according to the following standard procedures.

### 3.4.1 General Soil Properties

The activity of soil is 1.37, average field void ratio is 1.27, and bulk density is 1.24 gm/cm$^3$. Liquid limit (79), plastic limit (28), shrinkage limit (9), plasticity index (51), field moisture content (32%) and saturated moisture content (52%) are also measured [257].

Figure 3.4 shows identification of soil using a USDA-provided "web soil survey" tool. In Fig 3.4, the soil collection site is selected as an area of interest in the interactive websoil survey tool and found marked as "MoA," which means Moreland clay. According to United States Department of Agriculture (USDA) soil taxonomy classification, it is Moreland clay, which is very fine, smectitic, thermic Oxyaquic Hapluderts. It is also very poor as a construction and road fill material and is expansive in nature [258]. Using the "soil series extent mapping tool," Moreland clay presence in the US is plotted (Fig 3.5). From Fig 3.5, it can be concluded that even though 4872710 acres of Moreland clay spreads over Louisiana, Arkansas and Oklahoma, most of it is present in Louisiana. After breaking the total acres down by individual county/parish, it is found that Caddo Parish (43580 acres) and Bossier Parish (31781 acres) have the fourth and fifth highest acres of Moreland clay, whereas Avoyelles parish (116293 acres) has the most acres of Moreland clay [258].


(a)

Search

Map Unit Legend

Bossier Parish, Louisiana (LA015)

| Map Unit Symbol | Map Unit Name | Acres in AOI | Percent of AOI |
|---|---|---|---|
| MoA | Moreland clay, 0 to 1 percent slopes, rarely flooded | 0.5 | 100.0% |
| Totals for Area of Interest | | 0.5 | 100.0% |

(b)

**Fig. 3.4 USDA Web Soil Survey Soil Classification (a) Selected Area Labeled as MoA and (b) Description on Map Symbol [258]**

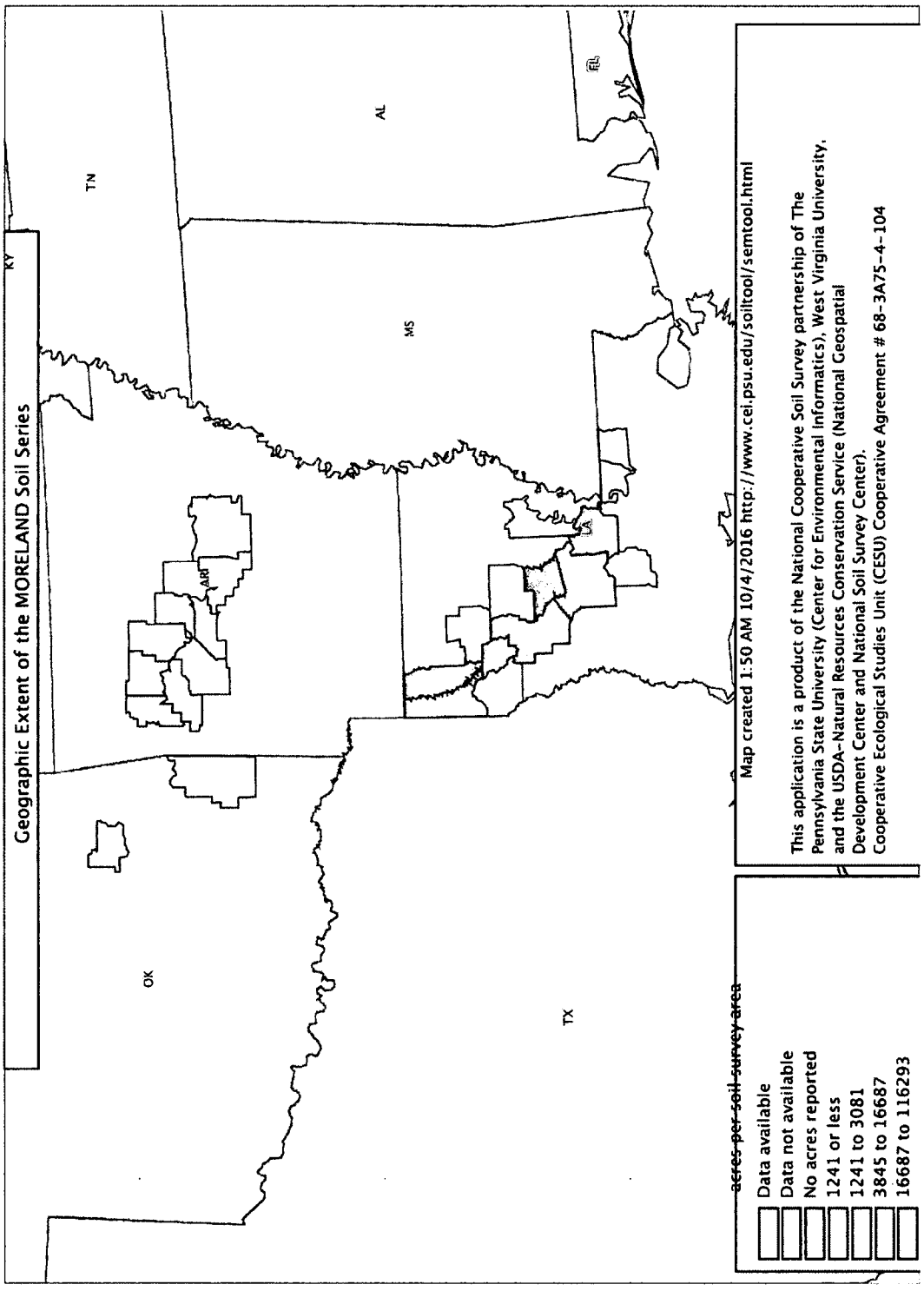


**Fig. 3.5 Moreland Clay Map of US [259]**

### 3.4.2 Specific Gravity ($G_s$)

The specific gravity is measured following ASTM D854-10 [260], and it is 2.75.

### 3.4.3 Sieve Analysis

Using ASTM D422-63 [261], the grain-size distribution curve is plotted. The soil is found extremely fine, with 99% passing through the 0.075mm sieve.

### 3.4.4 Soil Classification

Soil classification is completed using the Unified Soil Classification System (ASTM D2487-11 [262]), and the soil is classified as Fat Clay (CH).

### 3.4.5 Standard Proctor Test

The soil compaction tests are conducted according to ASTM D698-12 (Method A) [263], using the standard compactive effort. The Moreland clay is air dried, pulverized, and sieved to obtain material finer than 0.075 mm. A known quantity of water is added to a known amount of clay, and the mix is covered using plastic wrap. The mix is compacted in three layers using 25 blows per layer in a 943 $cm^3$ mold after an equilibration time of about 24 h. The gravimetric water content (w) is determined by ASTM D2216-10 [264] and used in conjunction with the measured sample weight and volume to determine the dry density ($\rho_d$) using basic phase relationships. From Fig. 3.6, it is found that the maximum dry density is 14.52 $kN/m^3$ (1.48 $gm/cm^3$), and optimum moisture content is 27%. According to Marinho and Oliveira [265], the optimum water content is within ±5% of the plastic limit for cohesive soil. In the lab test, a similar relation is found.

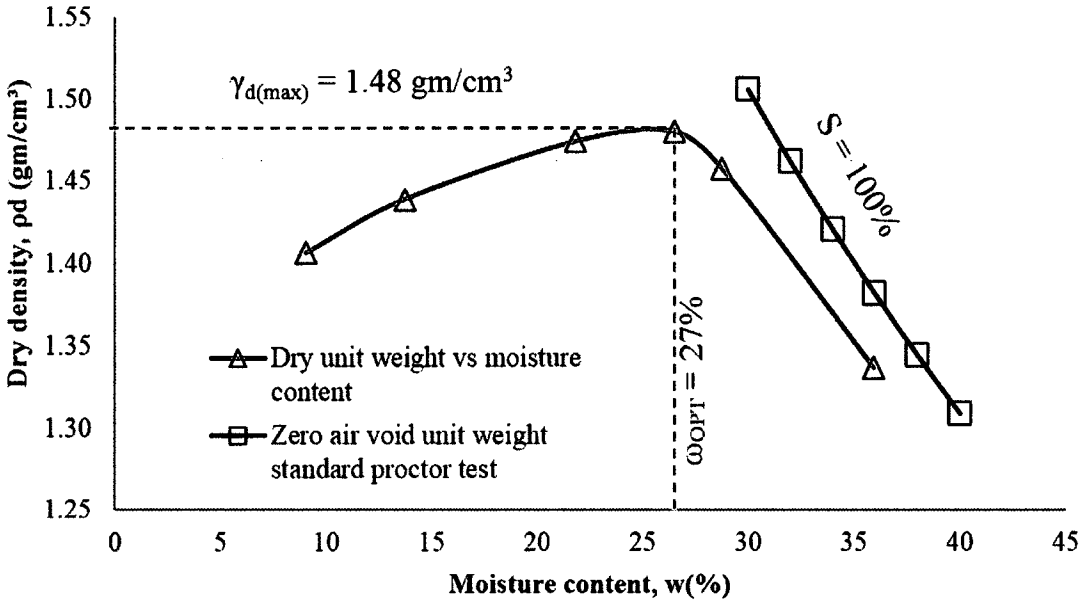


**Fig. 3.6 The Modified Proctor Test of Moreland Clay**

3.4.6 Consolidation Test (Loading and Unloading Behaviors of Expansive Soil)

A consolidation test is performed to measure the compression index, swelling index and swelling pressure of the Moreland clay. Three undisturbed soil samples have been tested to find the initial void ratio, and the average value was found to be 1.27. From Fig. 3.7, the swelling pressure for initial void ratio is found to be 120 kPa. Disturbance in soil structure during collecting from the field may result in a reduction of the swelling pressure [11]. Percentage error in the swelling pressure can be in excess of 100%, and the swelling index up to 50% [266]. A graphical procedure, which was proposed by Fredlund *et al.* [82], has been adopted for the swelling pressure correction. The corrected swelling pressure is found to be 180 kPa. The compression index ($C_c$ = 0.36) and the swelling index ($C_s$ = 0.11) are determined from the slope of the loading curve and the rebound curve in Fig. 3.7. The $C_s$ fell within the range typical of inorganic silty clays, which is in between 1/4 or 1/5 of $C_c$ [267]. The relatively high $C_s/C_c$ ratio indicates the samples collected from the field are stiff in nature. Consolidation test results can be used to

predict soil heave using oedometer-based heave equations, for example, the Fredlund *et al.* [82] formula.

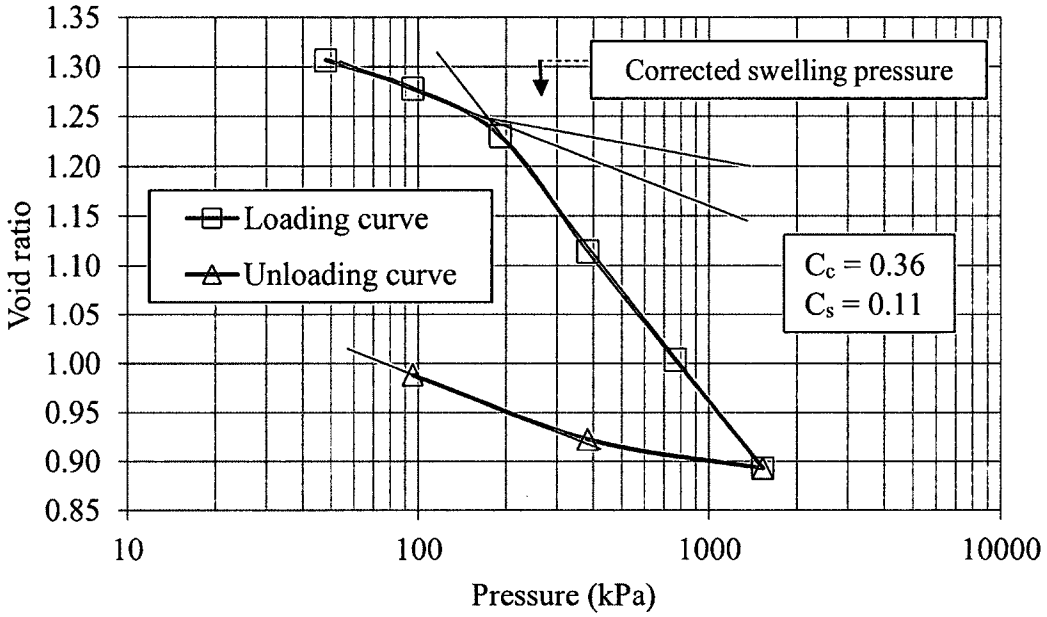


**Fig. 3.7 Consolidation Test of Moreland Clay**

## 3.5 Soil Test for Expansive Soil

Apart from the regular soil tests, some expansive soil exclusive tests are done to understand the volume change behavior of soil with the change in moisture content.

### 3.5.1 Soil Water Characteristic Curve (SWCC)

The SWCC defines the relationship between soil water retention and soil suction. Classical soil mechanics was mainly focused on saturated soil, ignoring the situations where negative pore pressure is present. In the 1960s and 1970s, unsaturated soil mechanics emerged. In-depth soil tests have shown a strong correlation between unsaturated soil properties with the SWCC. It has been a very common practice to predict any unsaturated soil property empirically using the SWCC and the same soil property in a

saturated condition. The SWCC is created for the sampled Moreland clay using two methods. An impact corer is used to collect three cores from the sample site at a depth of 10 m. The aluminum cylinder inside the corer is 5 cm in length and 4.8 cm in inner diameter. Soil cores in the cylinders are trimmed in the field exactly to the cylinder length, and the cylinders are immediately capped at both ends and transported to the laboratory. Uncapped cylinders are placed on a 1 bar ceramic pressure plate, which is inundated for 48 h. Water is placed on the ceramic plate, and the cylinders are saturated from the bottom for 72 h. The cylinders are removed from the saturated ceramic plate and weighed, followed by placing them back on the plate for an additional 48 h. As illustrated in Fig. 3.8a, the saturated ceramic plate and cylinders are placed in a pressure plate apparatus (5 Bar Pressure Plate Extractor, Cat. No. 1600, Soil Moisture Equipment Corp., Santa Barbara, CA, USA) and pressure is increased to 33 kPa and maintained for 48 h [268]. The cylinders and their soil are then weighed and placed in an oven at 110°C for 48 h. After that, they are moved in a desiccator and then weighed again. These measurements of gravimetric soil water content at 0 kPa (saturation) and -33 kPa (field capacity) represent the wetter points on the SWCC. The bulk density of the cores are calculated based on the cylinder volumes and the oven-dried soil weights, and they are used to calculate the volumetric moisture content of the soil cores [269].

The second method used to create the SWCC is the chilled mirror dew point technique, using the WP4-T Dewpoint Potentiameter by Decagon Devices on disturbed soil samples, as shown in Fig. 3.8b [270]. Approximately 15 g of the crushed soil, which has been passed through a 2-mm diameter sieve, is placed into stainless steel sample cups. Thirteen Moreland soil samples are prepared by varying moisture contents. Sample

cups are placed on the upper surface of the WP4-T to allow temperature equilibration. Each sample cup is placed into the WP4-T for the water potential measurement. Drier samples have one measurement each, but the wetter six samples have three or four measurements of water potential. After the water potential measurement, samples are placed in an oven and maintained at $110^0$C for 24 h, and then are placed in a desiccator for one hour before being weighed to the nearest 0.0001 g. The bulk density of the undisturbed soil samples is measured by placing crushed, sieved (<0.002mm diameter) soil into the stainless-steel cups, which have an inner height of 1.0 cm, and an inner diameter of 3.75 cm. Various moisture levels are dropped into 19 sample cups, and the samples are left to equilibrate for 48 h. If a sample swells beyond the sample cup's volume, the soil is trimmed to the cup's height. The samples are then placed in an oven at 110°C for 48 h, followed by cooling in a desiccator for one hour, and then weighing to the nearest 0.01g. Bulk density is calculated as the soil volume ($cm^3$) divided by the oven-dried soil weight (g). Finally, a complete SWCC curve is plotted as illustrated in Fig. 3.9. As it clearly shows from Fig. 3.9, dry soil has a higher degree of suction compared to wet soil.

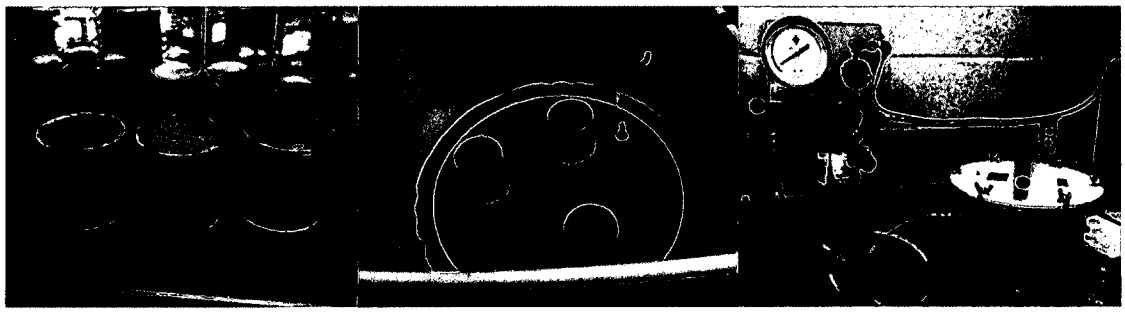

(a)

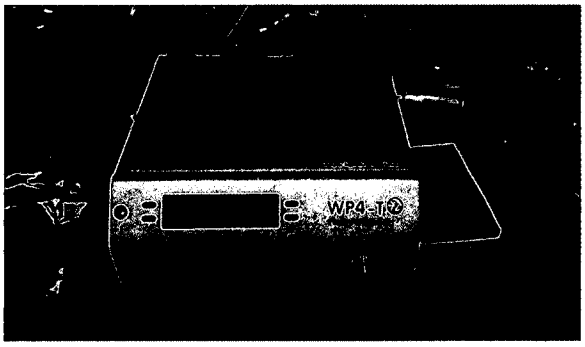


(b)

**Fig. 3.8 a) Pressure Plate Test and (b) WP4-T Test to Construct the Moreland Clay SWCC Curve**

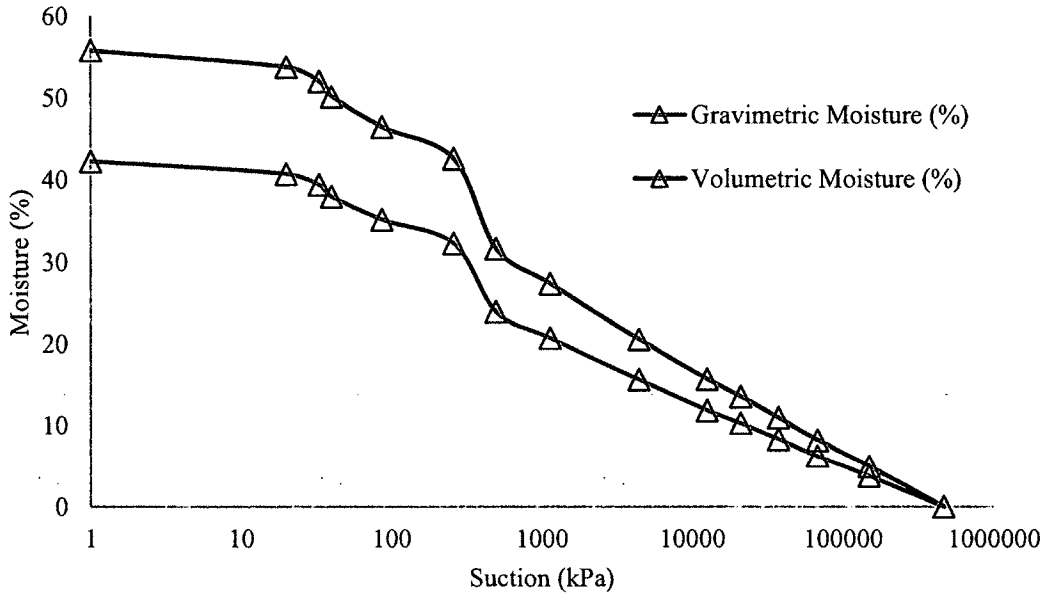


**Fig. 3.9 SWCC Curve for Moreland Clay**

3.5.2 Shrinkage Test

The significance of the shrinkage curve is that it shows the direct relation between changes of void ratio and changes of moisture content. Briaud *et al.* [214] described a simple method to obtain this shrinkage curve. A Moreland soil sample with a recommended dimension of 75 mm in diameter × 150 mm in height is used in the test. After measuring the initial height, diameter and weight with a minimum of three measurements of the diameter and height at an interval of $120^0$, the soil sample is allowed to air dry. Readings are taken at the one-hour interval for the first eight hours. After that, the time interval can be increased. It's recommended to take continuous measurements for two days. Once the last reading is taken, the sample is oven dried, and the weight is measured once again. Finally, a shrinkage curve of Moreland clay, as presented in Fig. 3.10, is produced.

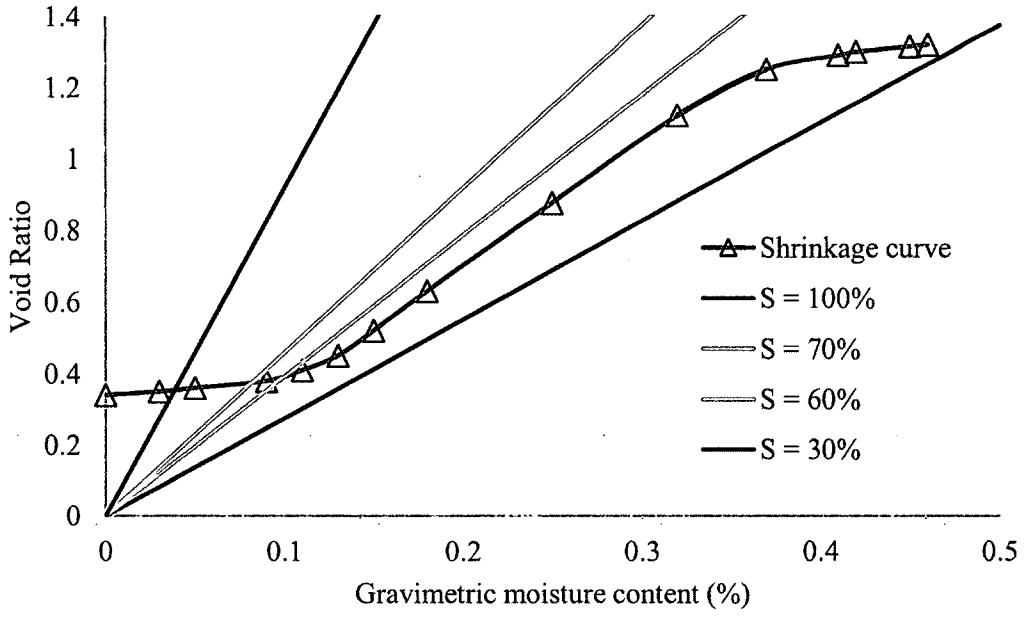


**Fig. 3.10 Shrinkage Test of Moreland Clay**

There are some limitations of producing the shrinkage graph following the method described above. One of most difficult stages is determining the void ratio when the moisture content goes below the shrinkage limit. This is because once the moisture content goes below the shrinkage limit, the soil started to experience cracks and fissures, making it almost impossible to make an accurate measurement of diameter and height of the soil core. Zhang [271] proposed a simple method to eliminate this problem by taking a constant void ratio below the shrinkage limit. Using the method, a modified shrinkage curve was produced, as presented in Fig. 3.11.

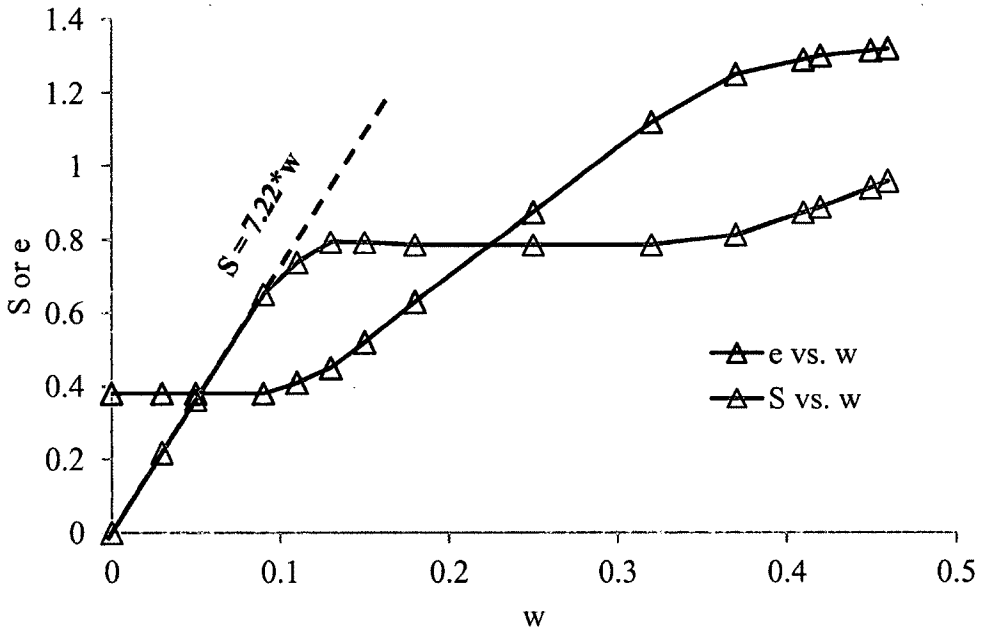


**Fig. 3.11 Modified Shrinkage Curve of Moreland Clay**

3.5.3 The Direct Shear Tests (for Characterizing Shear Strength of the Unsaturated Expansive Soil)

At the first step, the saturated Moreland soil is tested. Three undisturbed soil samples are taken from the field, and direct shear tests are conducted. After placing the soil sample in the shear box, it is kept in the water bath to make the soil sample fully

saturated. It took four days to get the job done. Three different normal stresses (75 kPa, 150 kPa and 250 kPa) are applied to the soil samples with a very slow strain rate, respectively. ASTM D3080-98 is followed, and the strain rate is kept below $5\times10^{-3}$ mm/min to avoid the generation of excess pore-water pressure in the soil samples. Figure 3.12 shows the soil sample preparation and soil after shear failure. Figure 3.13 presents a curve showing the relationship between shear stress and normal stress from the tested soil samples.

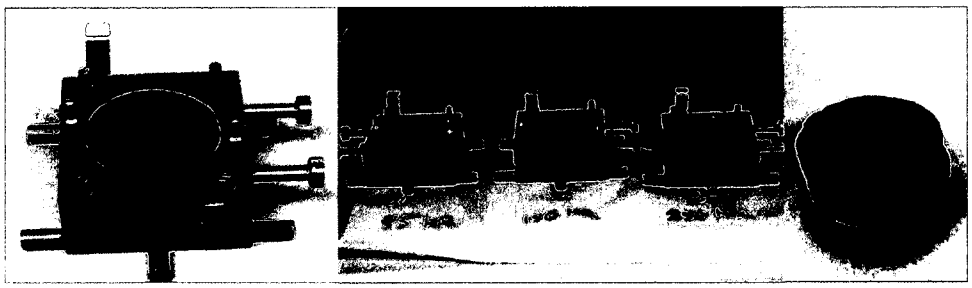

**Fig. 3.12 Direct Shear Test for Saturated Moreland Soil Sample**

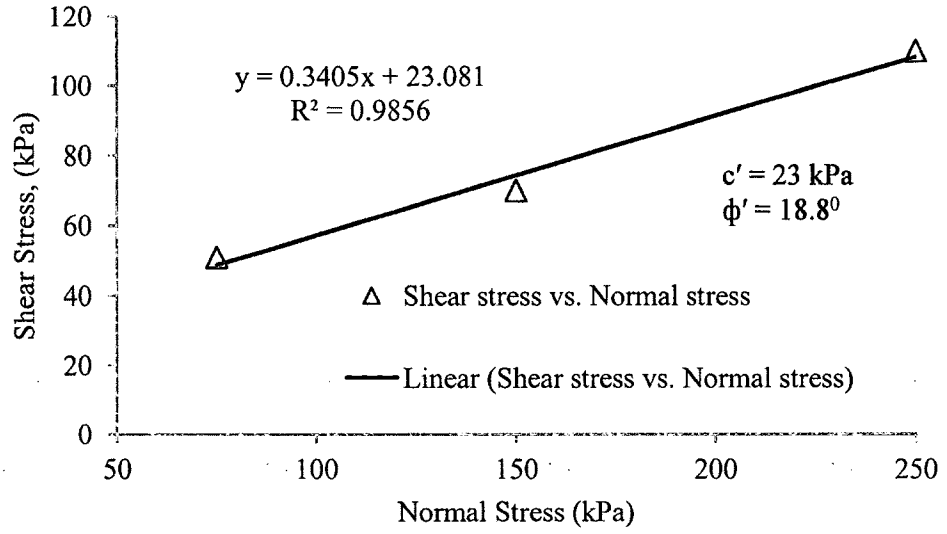


**Fig. 3.13 Shear Stress vs. Normal Stress for the Undisturbed Saturated Moreland Clay**

Measuring of shear strength of unsaturated soil can be directly completed using the triaxial tests or the modified direct shear tests. Both tests are time-consuming. For this reason, empirical equations are proposed to predict the shear strength of unsaturated soil. Equation 3.1 [272], which follows the well-known Mohr-Coulomb criterion, is used to evaluate the shear strength of saturated soil, whereas Eq. 3.2 [273] and Eq. 3.3 [77] are used for unsaturated soil. Using Eq. 3.2 needs the value of $\phi^b$, which is the slope of shear stress vs. matric suction line. Most of the regular geotechnical labs are not equipped with a direct shear test machine that can control the soil suction during the direct shear test. The use of Eq. 3.3 eliminates the need, and $\phi^b$ can be predicted using the SWCC and the fitting parameter k, which can be estimated from the plasticity index using graphs.

$$\tau = c' + (\sigma - u_a) \tan\phi' \tag{3.1}$$

$$\tau = c' + (\sigma - u_a) \tan\phi' + (u_a - u_w) \tan\phi^b \tag{3.2}$$

$$\tan\phi^b = (\theta_w/\theta_s)^\kappa \tan\phi' \tag{3.3}$$

Here,

$\tau$ = Shear stress at failure;

$c'$ = Cohesion determined from the direct shear testing on saturated samples;

$\sigma - u_a$ = Effective normal stress at failure;

$\phi'$ = Friction angle determined from the direct shear testing on saturated samples;

$u_a - u_w$ = Suction at failure measured from suction measurement device;

$\phi^b$ = Friction angle due to suction determination from the slope of shear stress ($\tau$) versus matric suction ($u_a - u_w$) plot;

$\theta_w$ = Volumetric water content obtained from compaction curve;

$\theta_s$ = Saturated volumetric water content obtained from the soil water characteristic curve;

$\kappa$ = Fitting parameter PI versus $\kappa$ plot.

3.5.4 Procedure of Measuring Fitting Parameter ($\kappa$)

Garven and Vanapalli [274] gave an empirical equation (Eq. 3.4) relating fitting parameter and plasticity index using nine different soil samples. Although the relation has been modified a couple of times, the latest is given in Fig. 3.14. Chowdhury [275] provided a different equation (Eq. 3.5) from five other soil samples, as shown in Fig. 3.15.

$$\kappa = -0.0016*PI^2 + 0.0975*PI + 1 \quad (3.4)$$

$$\kappa = -0.001*PI^2 + 0.0874*PI + 0.98 \quad (3.5)$$

Equation 3.4 gives fitting parameter ($\kappa$) value 1.81 for Louisiana soil (PI = 51), where using Eq. 3.5 the k value is found to be 2.84. Either one of them or the average of the values, which is 2.33, can be used. So, the shear strength of unsaturated Moreland clay can be found using Eq. 3.6, while volumetric water content can be found using Eq. 3.7.

$$\tau = 23 + (\sigma - u_a) *0.34 + (u_a - u_w) (\theta_w/\theta_s)^{2.33} *0.34 \quad (3.6)$$

$$\theta_w = w*(\gamma_d/\gamma_w) \quad (3.7)$$

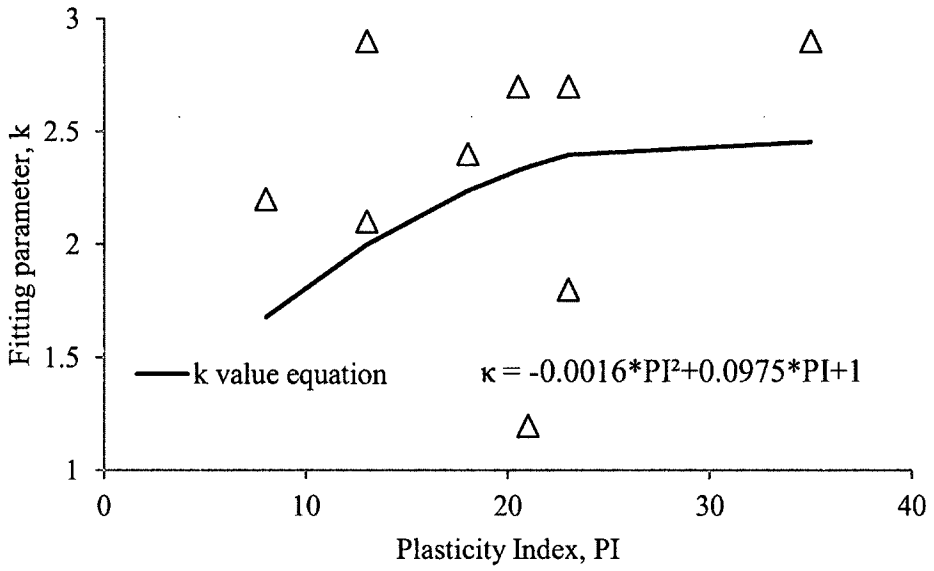


**Fig. 3.14 Relationship Between Parameter k and Plasticity Index (Modified after Fredlund et al. [82])**

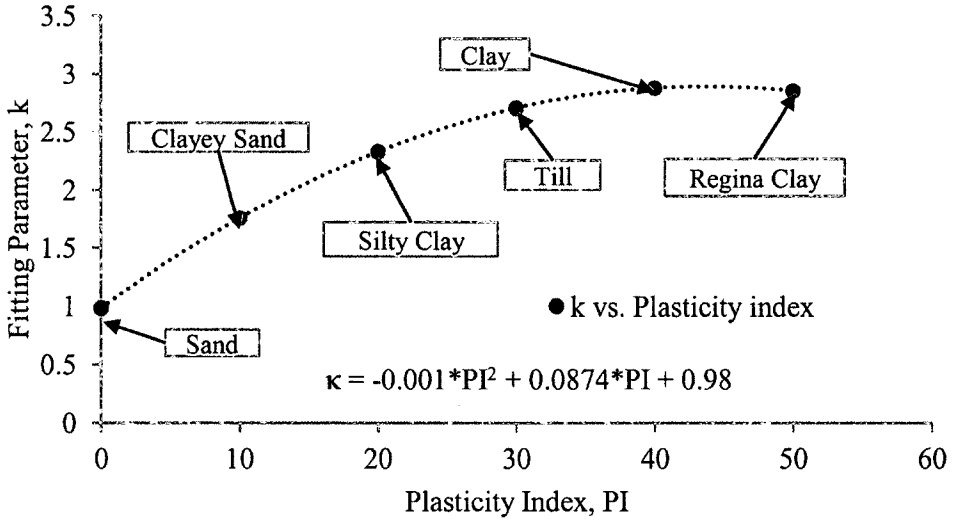


**Fig. 3.15 Relationship Between Parameter k and Plasticity Index (Modified after Chowdhury [275])**

3.5.5 Expansion Index (EI)

Following ASTM D-4829 [119], expansion index is measured. The procedure includes placing the undisturbed soil sample in the oedometer mold with the porous disk

on top and bottom of the soil. After that, a total pressure 6.9 kPa (1 lb-f/in$^2$) including the upper porous disk is placed on the soil. Once the soil consolidates for ten min this way, a soil sample is inundated, and the data should be recorded until the expansion becomes less than 0.0002 in/hr. For the Moreland clay, the test is run for three days. EI is measured from Eq. 3.8 and found to be 101, while the free swell is found to be 0.101 in.

$$EI = \frac{\Delta H}{H} * 1000 \tag{3.8}$$

## 3.6 Methods to Obtain the Boundary Condition of Constitutive Surfaces

The constitutive surface of the soil will help to understand in-depth about the volume change behavior of expansive soil. Experimentally, it can be developed from the tri-axial or consolidation test with an option to change the suction. Most of regular soil testing laboratories do not have this kind of sophisticated equipment setup, even with the presence of test setup, this is a very time-consuming test. A simplified method was suggested by Zhang [271] that uses six boundary curves (Eq. 3.9 to 3.14) to interpolate the whole surface. In Chapter 4, the process of constructing the unsaturated expansive soil constitutive surface is described, whereas in this chapter, the process of finding the six boundary curves is described. The boundary curves are given below:

$$e = f(\sigma - u_a, u_a - u_w = 0); \tag{3.9}$$

$$w = f(\sigma - u_a, u_a - u_w = 0); \tag{3.10}$$

$$S = f(\sigma - u_a, u_a - u_w = 0); \tag{3.11}$$

$$w = f(u_a - u_w, \sigma - u_a = 0); \tag{3.12}$$

$$e = f(u_a - u_w, \sigma - u_a = 0); \tag{3.13}$$

$$S = f(u_a - u_w, \sigma - u_a = 0). \tag{3.14}$$

Equations 3.9 to 3.11 can be found from the consolidation test, showing how the void ratio (e), moisture content (w) and degree of saturation (s) are changing exclusive to the change of net normal stress ($\sigma - u_a$). On the other hand, Eq. 3.12 to Eq. 3.14 can be found from the SWCC test, giving the information about how the soil volume changes only when the matric suction ($u_a - u_w$) changes. Equation 3.9 is the void ratio versus net normal stress curve when the matric suction is zero, and it can be found from the consolidation test. In consolidation test, the Moreland clay soil sample is submerged into the water the whole time, making the suction zero. Equation 3.10 is the water content versus net normal stress curve when the matric suction is zero, and it can be found from the formula $Se = wG_s$. As in the consolidation test, the degree of saturation is one and specific gravity ($G_s$) is a known value for any specific soil. A relation can be easily found between moisture content and net normal stress. Equation 3.11 is the degree of saturation versus mechanical stress curve when the matric suction is zero, and it is a constant value (=1) during the change of $\sigma - u_a$. Equation 3.12 is the moisture content versus suction curve when the net normal stress is zero, and it can be found from the SWCC test. In the SWCC test, no mechanical stress is applied. Equation 3.13 is the void ratio versus suction curve when the net normal stress is zero, and it can be found from the modified shrinkage test. Equation 3.14 is the degree of saturation versus matric suction curve when net normal stress is zero, and it can be found from the formula $Se = wG_s$.

To construct the constitutive surface of unsaturated expansive soil, the minimum test is needed as follows: 1) consolidation test, 2) SWCC and 3) free shrink test. All the tests were performed and described in the previous section of this chapter.

### 3.6.1 The Void Ratio versus the Net Mechanical Stress Curve When the Matric Suction is Equal to Zero

Using the consolidation test, e-log (σ) relation was found. Using commercial software Sigmaplot [276], regression analysis is done, and a mathematical expression for the curve is found. The expression is given in Eq. 3.15, and regression curve is shown in Fig. 3.16.

$$e = 0.80761 + \frac{0.50737}{1+\exp\left(\frac{\log_{10}(\sigma)-2.73049}{0.29184}\right)} \tag{3.15}$$

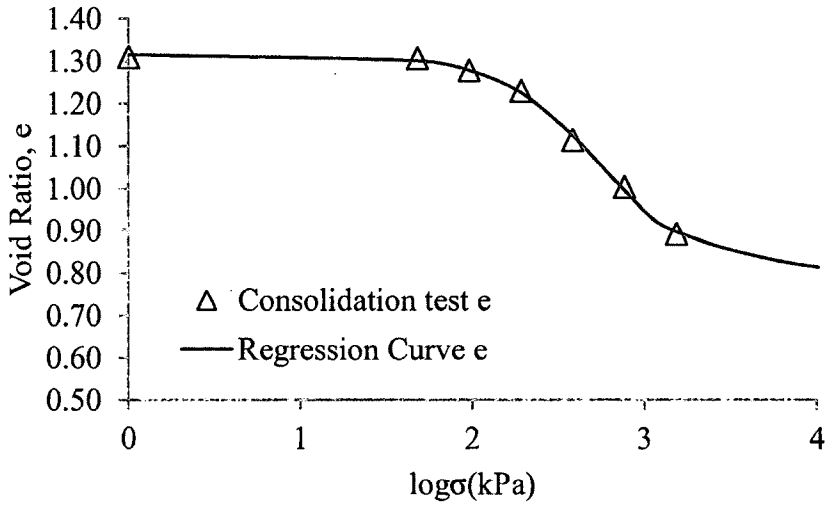


**Fig. 3.16 e-log ($\sigma_v$) Expression from the Consolidation Test**

### 3.6.2 The Moisture Content versus the Net Mechanical Stress Curve When the Matric Suction is Equal to Zero

Using the expression $Se = wG_s$, a relation between moisture content and net mechanical stress can be found. For the Moreland clay, $G_s$ value is found to be 2.75. A mathematical expression is given in Eq. 3.16, and the regression curve is shown in Fig. 3.17.

$$w = 0.80761 + \frac{0.50737}{1+\exp\left(\frac{\log_{10}(\sigma)-2.12377}{0.22699}\right)} \quad (3.16)$$

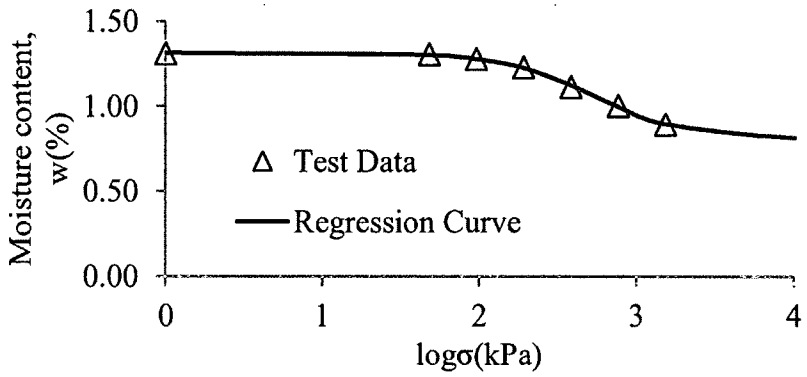


**Fig. 3.17 w-log (σ) Expression from the Consolidation Test**

3.6.3 The Degree of Saturation versus the Net Mechanical Stress Curve When the Matric Suction is Equal to Zero

In the consolidation test, the degree of saturation is always one with the change of mechanical stress. The expression is given in Eq. 3.17 and illustrated in Fig. 3.18.

$$S = 1 \quad (3.17)$$

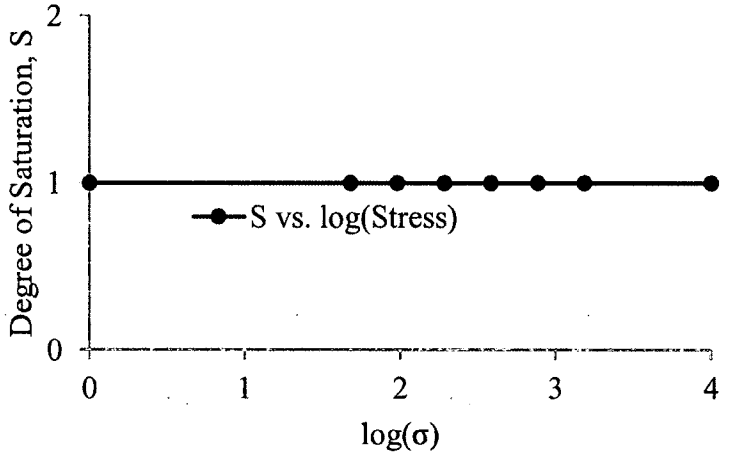


**Fig. 3.18 S-log (σ) Expression from the Consolidation Test**

### 3.6.4 The Water Content versus Matric Suction Curve When the Mechanical Stress is Equal to Zero

This boundary curve is found from the SWCC curve. The SWCC curve is used to understand the relationship between volumetric water content and the matric suction. Zhang [271] suggested using gravimetric water content instead. The reason behind the suggestion is that the slope of the gravimetric water content versus the matric suction is referred to as specific water capacity. The SWCC test is performed in between 1 kPa and 1000000 kPa, as shown in section 3.5.1. In SWCC test, two assumptions are made. First, when the soil is fully saturated, the suction is zero. The reason behind this is that, although theoretically at saturation point the suction is zero, log(0) is not a real number. Because the objective is to find the relation between water content (%) and suction in a logarithmic scale, the suction at fully saturated condition is taken as zero. The logic behind taking the logarithmic suction is to finally plot a 3-D graph between the void ratio, logarithmic net normal stress, and logarithmic suction, so all the boundary conditions should have either logarithmic mechanical stress or logarithmic suction. Secondly, in SWCC test at the oven-dried condition, the soil suction is assumed to be 1000000, as recommended by Zhang [271].

In Eq. 3.18, the mathematical expression is given, and in Fig. 3.19, the regression curve is shown. In Fig. 3.19, the two boundary conditions are marked in blue.

$$w(\%) = -1.68865 + \frac{52.50339}{1+\exp\left(\frac{\log_{10}(u_a - u_w) + 1.91858}{20.18804}\right)} \tag{3.18}$$

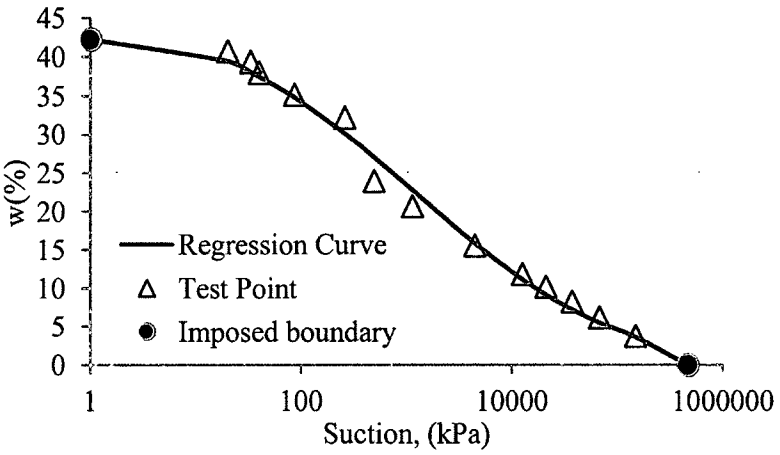


**Fig. 3.19 w-log ($u_a$-$u_w$) Expression from the SWCC Test**

3.6.5 The Degree of Saturation versus Matric Suction Curve When the Mechanical Stress is Equal to Zero

A free shrinkage curve and later modified shrinkage curve were plotted previously in section 3.5.2 [214, 271]. Moreland clay has a shrinkage limit of 9, so when the water content went below 0.9, it was assumed the void ratio was the same after that, as shown in modified shrinkage curve. As the void ratio is constant below the shrinkage limit, a linear relation can be found between S and w. When water content w is less than 0.9, the linear relation becomes S = 7.22*w. After considering this phenomenon, an expression between w and e can be found and is shown in Eq. 3.19, and the expression between S and w is given by Eq. 3.20 and Eq. 3.21.

$$e = 0.22218 + \frac{1.14759}{1+\exp\left(\frac{-w+0.22661}{0.07171}\right)} \tag{3.19}$$

$$S = -2.85551 + \frac{10.49865}{1+\exp\left(\frac{-w+3.51076}{5.24136}\right)} \text{ (when } w \geq 0.9) \tag{3.20}$$

$$1+\exp($$

$$S = 7.22 * w \text{ (when } w < 0.9) \tag{3.21}$$

### 3.6.6 The Void Ratio versus Matric Suction Curve When the Mechanical Stress is Equal to Zero

Equation 3.17 gives the relation between w (%) and log ($u_a$-$u_w$), and Eq. 3.17 gives the relation between e and w. Combining these two equations, an expression between e and log($u_a$-$u_w$) can be found and is given in Eq. 3.22, and the curve is shown in Fig. 3.20.

$$e = 0.347128 + \frac{0.992809}{1+\exp\left(\frac{\log_{10}(u_a-u_w)-2.766902}{0.682210}\right)} \qquad (3.22)$$

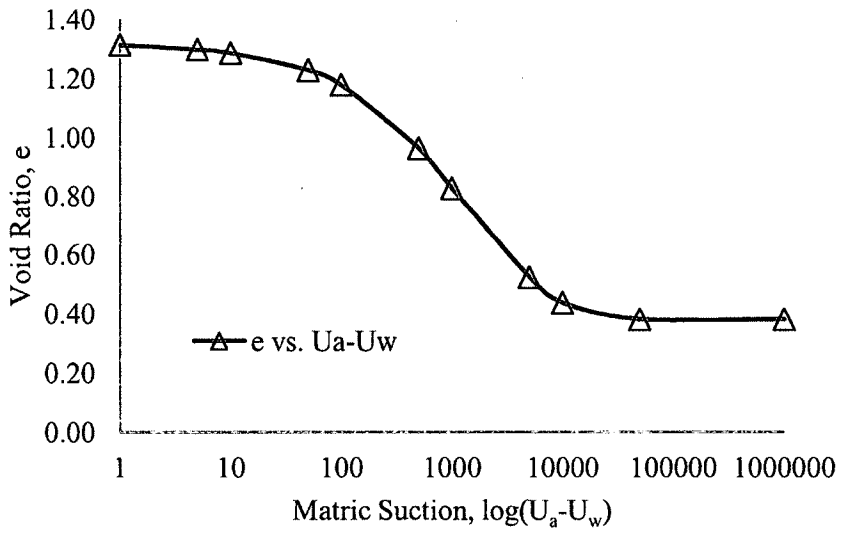


**Fig. 3.20 e-log ($U_a$-$U_w$) Expression from the SWCC Test**

## 3.7 Summary of the Moreland Clay Properties

Summary of the soil properties are given in Table 3.1. In Chapter 4, these properties will be used to predict the free heave using different methods.

**Table 3.1 Summary of the Laboratory Tests**

| Soil Properties | Value |
|---|---|
| USDA soil taxonomy classification | Very-fine, smectitic, thermic Oxyaquic Hapluderts |
| USCS soil classification | Fat clay |
| USCS soil symbol | CH |
| Specific gravity, $G_s$ | 2.75 |
| # 200 passing (%) | 99 |
| Liquid limit, LL | 79 |
| Plastic limit, PL | 28 |
| Shrinkage limit, SL | 9 |
| Plasticity index, PI | 51 |
| Opt moisture content | 27% |
| Max dry unit weight ($kN/m^3$) | 14.52 |
| Average field void ratio,e0 | 1.27 |
| Bulk density, $gm/cm^3$ | 1.24 |
| Bulk volume moisture content | 41.04 |
| Free soil swelling, in | 0.101 |
| Expansion index, EI | 101 |
| Activity of clay, $A_c$ | 1.37 |
| Compression index, $C_c$ | 0.36 |
| Swell index, $C_s$ | 0.11 |
| Corrected swelling pressure, KPa | 180 |
| Avg. field moisture content (%) | 32 |
| Avg. saturated moisture content (%) | 52 |
| Saturated unit weight ($kN/m^3$) | 19.70 |
| Field unit weight ($kN/m^3$) | 17.11 |

## 3.8 An Example Problem for Predicting Heave for one-m Active Zone in Northern Louisiana

A total of five different methods from Eq. 3.23 to Eq. 3.27 are selected from the three categories mentioned in section 2.11, and the range of the vertical heave is found to

be between 67 mm and 80 mm [46, 82, 144, 156, 214]. Table 5 shows that the average heave is 72.2 mm in the one-meter depth soil, which gives a swelling potential (SP) of 7.22%. In Table 3.3, the swelling potential of Moreland clay is compared to those of the expansive soil found in other places, and it showed that the expansive Moreland clay is one of the most expansive soils in the US and around the world [7, 136, 277, 278].

**Table 3.2 Heave Predictions of the One-Meter Depth Expansive Clay Using Different Equations**

| Methods | Parameters | Heave (mm) | Comment | Eq. |
|---|---|---|---|---|
| $\Delta H = C_s \frac{H}{1+e_0} \log(\frac{P_f}{P_s'})$ | Swelling index, $C_s$= 0.11; initial void ratio, $e_0$= 1.27; final stress state, $P_f$ = iteratively calculated for each layer; moist unit weight, $\gamma$ = 17.11 kN/m$^3$; corrected swelling pressure, corrected $P_s'$= 180 kPa. | 69 | Oedometer-based method | 3.23 |
| $\Delta H = C_s \frac{H}{1+e_0} \log\left(\frac{kP_f}{10^{(\frac{C_s}{C_w}\Delta w)}}\right)$ $k = 0.0039 * e^{0.64PI}$ $C_w = 0.019 * e^{0.64(\Delta w)}$ | Correction parameter, k = 0.004; suction modulus ratio, $C_w$ = 0.019; change in water content, $\Delta w$ = 0.2; plasticity index, PI = 51%. | 75 | Empirical Method | 3.24 |
| $\Delta H = HC_w (w_f - w_i)$ $C_w = \frac{\alpha G_s}{1+e_0}$ | Volumetric compressibility factor, $\alpha$ = 0.33; specific gravity, $G_s$ = 2.75; initial void ratio, $e_0$= 1.27; water content change ($w_f$ - $w_i$) = 0.2; suction index, $C_w$ = 0.4. | 80 | Suction Method | 3.25 |

| Methods | Parameters | Heave (mm) | Comment | Eq. |
|---|---|---|---|---|
| $\Delta H = \sum_{i=1}^{n} (h_i f_i \Delta w_i / E_{wi})$ | Water content change $\Delta w$ = 0.2; shrink swell modulus, $E_w$ = 0.45; shrinkage ratio, f = 0.13. | 67 | Empirical Method | 3.26 |
| $\Delta H = H \frac{C_\tau}{1+e_0} \log\left(\frac{\tau_{m_i^0}}{\tau_{m_f^0}}\right)$ $\log \tau_{m_i^0} = A - Bw$ $\tau_{m_f^0} = \alpha_0 \sigma_f - u_{wf}$ $C_\tau = \frac{\alpha G_s}{100B}$ | Compressibility factor $\alpha$ = 1 as PI>40; suction index, $C_\tau$ = 0.25; Y intercept of gravimetric SWCC A= 5.1; slope of gravimetric SWCC B= 0.11; final matric suction, $\tau_{m_f^0}$ = 0 kPa; final applied pressure, $\sigma_f$ = 17.11 kPa; $G_s$ = 2.75; $w_0$ = 0.32. | 70 | Suction-based method | 3.27 |

**Table 3.3 A Comparison of Expansive Soil in Different Places Based on the Swell Percent**

| Predominant Soil Type | % Swell | Results/Location |
|---|---|---|
| Moreland clay (CH) | 7.22 | Predicted value/Bossier City, Louisiana |
| Regina clay (CH) | 7.78 | Predicted value/Regina, Canada |
| Grayson | 9.8 | Lab test |
| Colorado | 8.2 | |
| San Antonio | 7.3 | |
| Oklahoma | 3.8 | |
| San Diego | 3.4 | |
| Denver | 6.5-7.4 | Lab test |
| Pierre Shale | 3.1-5.7 | |
| London clay (CH) | 2.12 | Predicted value/Chattenden, Kent, UK |
| Maryland clay (CH) | 3.56 | Predicted value/Newcastle, Australia |
| Kenswick clay (CH) | 1.76 | Predicted value/Adelaide, Australia |
| Arlington clay (CL-CH) | 1.35 | Predicted value/Arlington, Texas, US |
| Al-Ghat shale(CH) | 3.53 | Predicted value/Al-Ghat, Riyadh, Saudi Arabia |
| Zaoyang soil (CL-CH) | 1.03 | Predicted value/Zaoyang, Hubei, China |

## 3.9 Conclusion

In this research, a comprehensive characterization of Moreland clay is done. From the experiments, the PI (=51), EI (= 101), and $A_c$ (=1.37) values are measured. Using three different expansive soil identification procedures, it is found the Moreland clay has a high degree of expansion potential. Moreland clay is active in nature, and once again, Moreland clay has a high degree of expansion potential. Other than its expansion potential, Moreland clay's loading-unloading behavior and water susceptibility are also investigated. Finally, using the experimental results and heave prediction equations, heave in a sample from a 1-m depth layer of Moreland clay is predicted. From the predicted result, it was found that Moreland clay has an SP value of 7.22%, which was then compared with other expansive soils around the world. It was finally concluded that Moreland clay is one of the most expansive soils in the world.

# CHAPTER 4

# THE CONSTITUTIVE SURFACES FOR MORELAND CLAY

## 4.1 Introduction

The constitutive relation of soil correlates between deformation state variables and stress state variables. The mathematical equations relating the total volume and the water content state variables to the stress variables are called the volume-mass constitutive equations. When these equations are used to plot a 3-D surface, this surface is called the constitutive surface. This surface helps to visualize the behavior of unsaturated soil under the change of net mean stress and/or soil matric suction. Soil volume changes occur due to two reasons. The first one is the change in mechanical stress, and the second one is the change in matric suction. For unsaturated soil where multiple phases may be present (i.e., solid, water and air), this relation is very complicated. Generally, the saturated soil is considered as a special case of unsaturated soil. The constitutive surface can also be created by correlating moisture content change with the two-state change, once correlation between void ratio changes and the two-stress state change is known. As part of soil characterization, in this chapter, only the first type of the constitutive surface will be plotted for Moreland clay, following the six boundary conditions described by Zhang [271]. Sign convention of the stress state is very important and will be discussed before developing the constitutive surface.

## 4.2 Stress State Variables Sign Conventions

The compressibility form for the unsaturated soil structure constitutive equation is given in Eq. 4.1, and the water phase of the constitutive equation is shown in Eq. 4.2. $m_1^S$, $m_2^S$, $m_1^W$ and $m_2^W$ will be different according to various loading conditions.

$$d\varepsilon_V = m_1^S d\,(\sigma_{mean} - U_a) + m_2^S d\,(U_a - U_w) \tag{4.1}$$

$$\frac{dV_w}{V_0} = m_1^w d\,(\sigma_{mean} - U_a) + m_2^w d\,(U_a - U_w) \tag{4.2}$$

Where,

$m_1^S$= Coefficient of volume change with respect to net normal stress;

$m_2^S$= Coefficient of volume change with respect to matric suction;

$m_1^W$= Coefficient of water volume change with respect to net normal stress;

$m_2^W$= Coefficient of water volume change with respect to matric suction.

Consider a case where the load is applied, stress increases, volume decreases, stress increases and thereby strain decreases. According to classical soil mechanics where compression is taken as positive, young's modulus become negative. Equation 4.3 shows the expression.

$$\mathrm{E}(-) = \frac{\mathrm{d}\sigma(-)}{\mathrm{d}\varepsilon(+)} \tag{4.3}$$

However, according to Zhang [271], the confusion comes when the pore-water pressure is increased, which causes a decrease in effective stress and an increase in volume. This will cause a positive young's modulus, as shown in Eq. 4.4.

$$\mathrm{E}(+) = \frac{\mathrm{d}\sigma(-)}{\mathrm{d}\varepsilon(-)} \tag{4.4}$$

From Eq. 4.3 and Eq. 4.4, it can be seen the modulus of elasticity or Young's modulus for the soil structure has a reverse sign for an increase in net mechanical stress and an increase in pore-water pressure. The same confusion comes in the water phase modulus, too. To avoid this confusion, Zhang [271] suggested taking ($u_a$-$u_w$) as a whole to be the stress state variable for unsaturated soil when two stress state variables are used. Figure 4.1 will illustrate the stress state variables for the nonlinear curve for the soil [82].

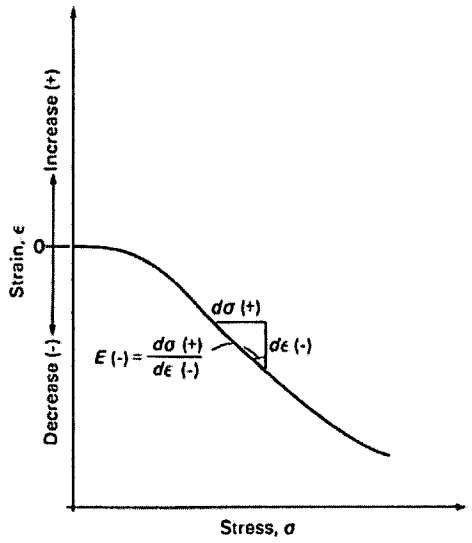


**Fig. 4.1 Definition of Variables for Nonlinear Stress-strain Curve for Soil [82]**

## 4.3 The Constitutive Surface for Unsaturated Soil

Matyas and Radhakrishna [279] showed how to find the constitutive surface of the soil experimentally using 80% flint powder and 20% kaolin, as shown in Fig. 4.2. This process was very lengthy and needed sophisticated experimental equipment. Below a simple mathematical process is described where, using some boundary conditions, a very close shape of the actual constitutive surface of any soil can be found. The effective stress of a soil exclusively defines its degree of compression. The effective stress is the difference between total stress and pore-water pressure. Equation 4.5 shows the relation

between void ratio and its stress state. Figure 4.3 shows the constitutive surface for the saturated soil while Fig. 4.4 shows the constitutive surface for the unsaturated soil. When the soil is saturated, the constitutive surface looks like AGFD, and when the soil becomes unsaturated, the surface becomes ABEDI. Axis OS shows the pore-water pressure, axis OI shows the matric suction, and axis OD shows the compressive stress. Curve AD represents the void ratio versus net normal stress when there is no suction and where curve AI represents the void ratio versus matric suction when there is no net normal stress. Curve AI was found by rotating the AD curve $90^0$ anticlockwise. It needs to be noted that for unsaturated soil the effective stress principle ($\sigma' = \sigma - u_w$) does not work. For this reason, instead of AP, AI represents the zero net normal stress curve. As mentioned before, using boundary conditions, the constitutive surface will be constructed, as shown by Fredlund *et al.* [82] and Zhang [271]. Figure 4.5 shows all six boundary curves needed for constructing the constitutive surface.

$$e = f(\sigma') = f(\sigma - u_w) = f(\sigma - u_a) + f(u_a - u_w) \qquad (4.5)$$

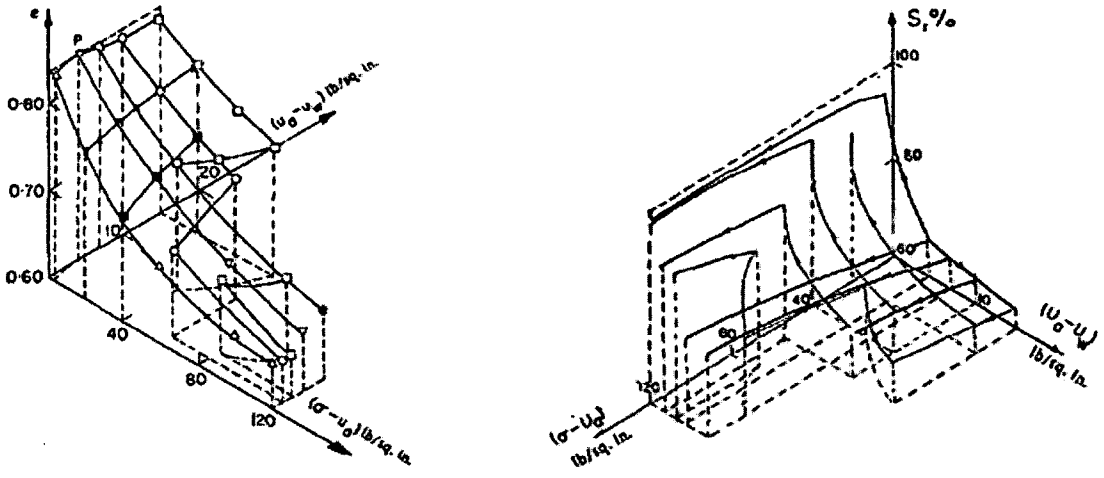


**Fig. 4.2 (a) Void Ratio Constitutive Surface and (b) Degree-of-saturation Constitutive Surface (Modified after Matyas and Radhakrishna [279])**

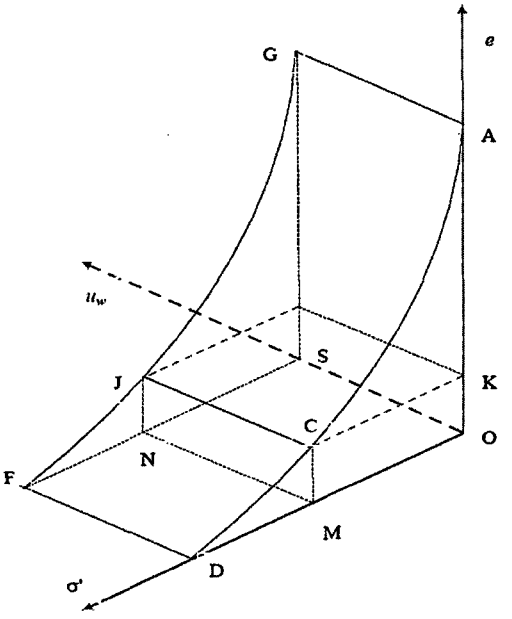


**Fig. 4.3 Void Ratio Constitutive Surface for a Saturated Soil (Zhang [271])**

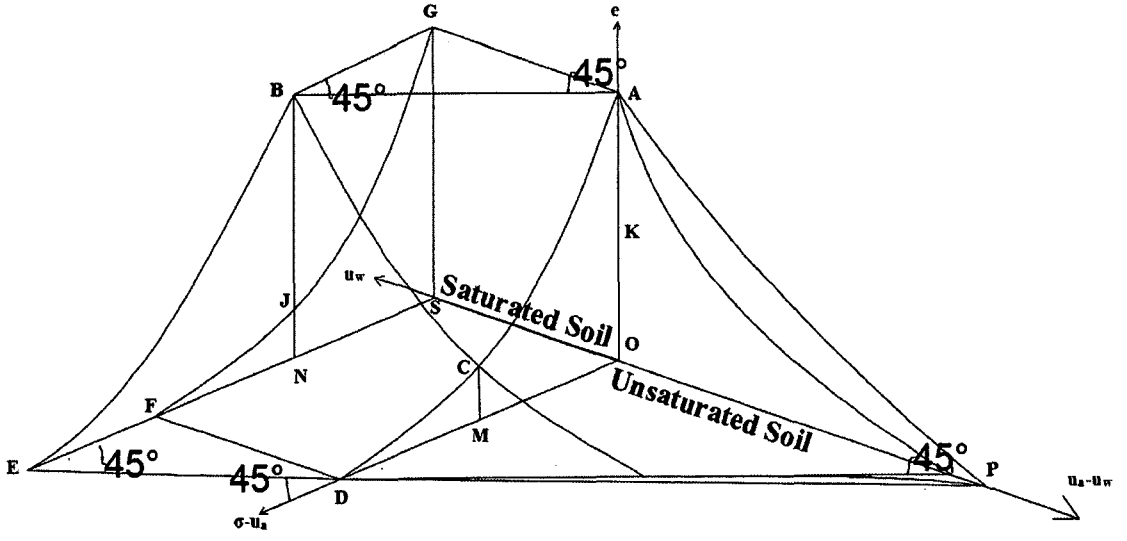


**Fig. 4.4 Void Ratio Constitutive Surface for a Saturated Soil (Modified after Zhang [271])**

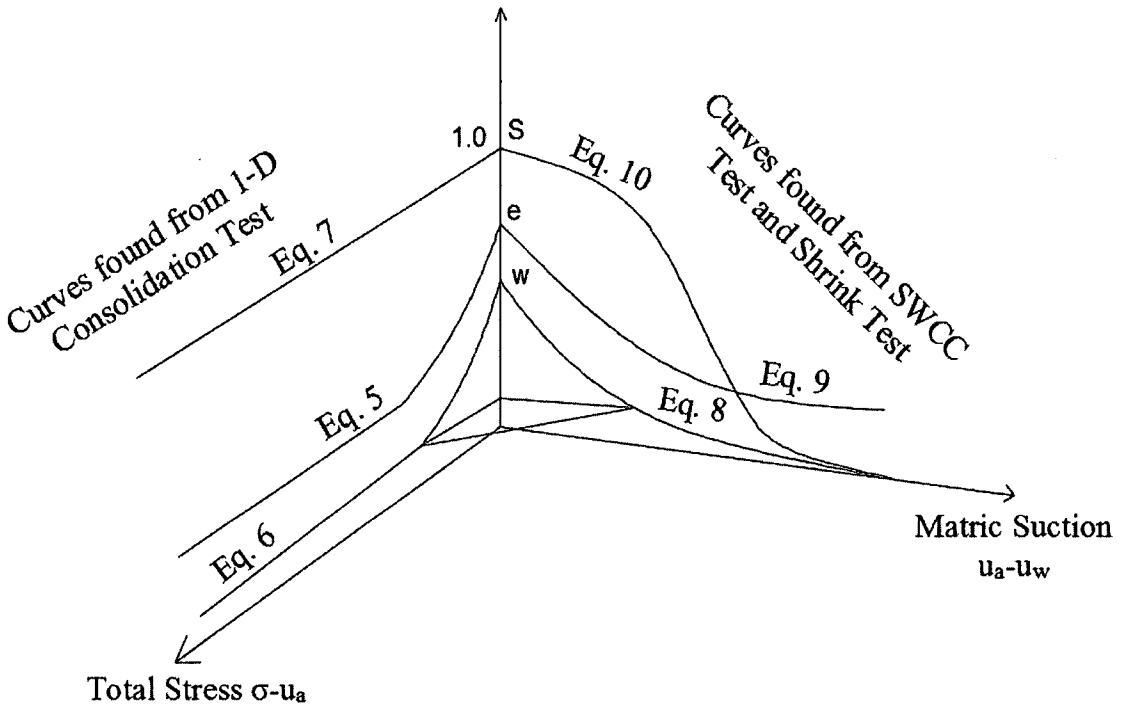


**Fig. 4.5 Curves Needed for Constructing the Constitutive Surfaces of an Unsaturated Soil (Modified after Zhang [271])**

Another assumption was made, which is that the constitutive surface is a plane for any particular void ratio. Using this assumption, by constructing a lot of planes at the various void ratios, the whole constitutive surface can be constructed. Figure 4.6 shows this method of constitutive surface construction. In Fig. 4.6, the straight lines $a_t$ and $a_m$ are small segments of void ratio versus net normal stress curve and void ratio versus matric suction curve, respectively. These two segments are assumed to be from the same void ratio range. Using the same procedure for different void ratio changes, other planes can be found. Once added together, they should provide the whole constitutive surface. At first glance, this method seemed to work. Then Zhang [271] described that, after a close investigation, it can be found in many cases this assumption is not satisfied. For example, in the case of unsaturated soil, the net normal stress and matric suction are

independent of each other, meaning the straight lines $a_t$ and $a_m$ may not be on the same plane.

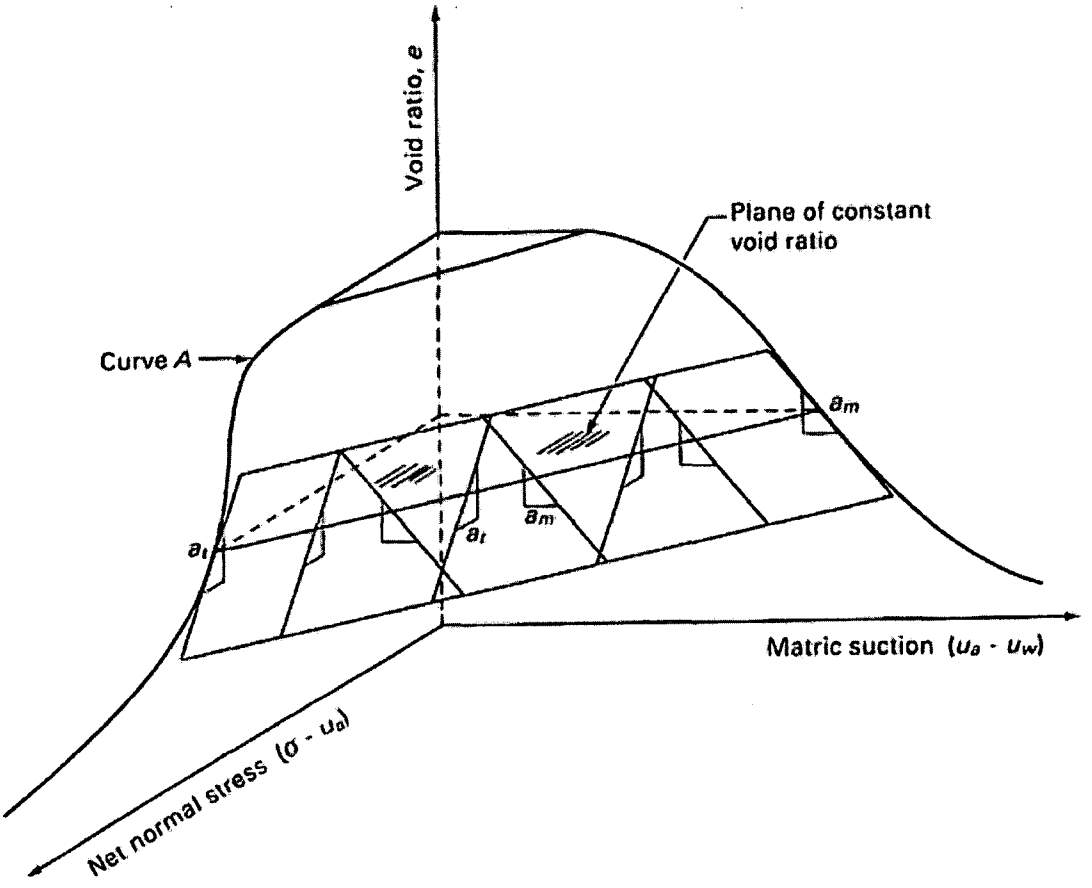


**Fig. 4.6 Proposed Assumption by Fredlund *et al.* [82]**

Zhang [271] proposed a simplified way to construct the constitutive surface. In this method, it is assumed that the constant void ratio curve is a straight line for any void ratio level. Figure 4.7 shows the constant void ratio of Madrid clay by Escario [280], and it matches the assumption.

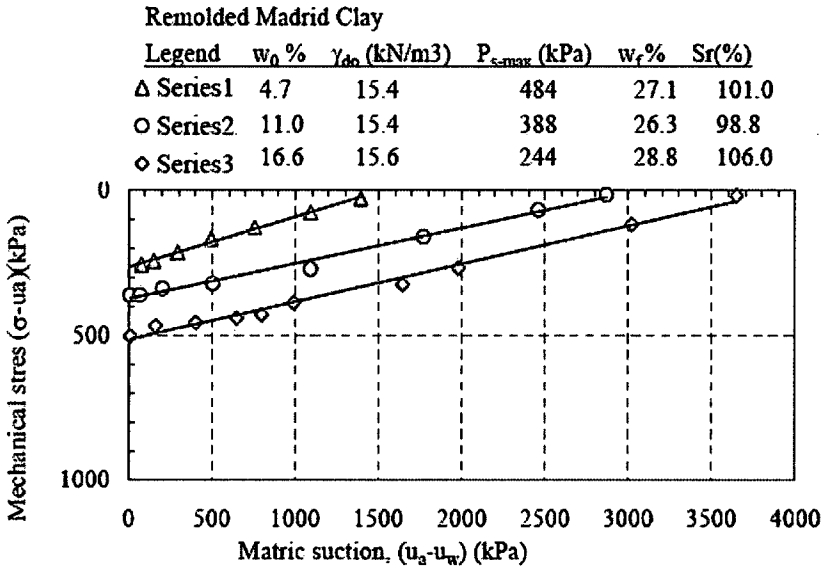


(a)

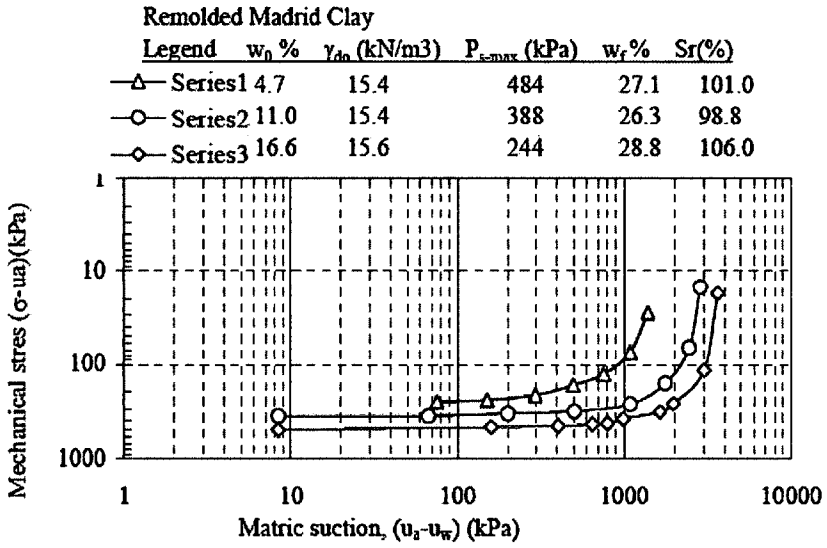


(b)

**Fig. 4.7 Constant Void Ratio Curves for Some Unsaturated Soil (a) Cartesian Coordinate and (b) Log-Log Coordinate by Zhang [271] and Escario [280]**

The proposed detailed procedure by Zhang [271], which will at the end give the same constitutive surface proposed by Fredlund *et al.* [82] is described here.

1. Find the corresponding two points for any void ratio from the void ratio versus net normal mechanical stress curve and the void ratio versus matric suction curve.
2. Connect the two points.
3. Repeat the procedure for all the void ratio levels; finally, a surface will be obtained.

A simplified mathematical expression to understand the procedure is given below. Assume the void ratio versus net normal mechanical stress curve and void ratio versus matric suction curve are given in Eq. 4.6 and Eq. 4.7, respectively.

$$e = a_1 \times \log_{10}(\sigma - u_a) + a_2 \tag{4.6}$$

$$e = a_3 \times \log_{10}(u_a - u_w) + a_4 \tag{4.7}$$

Here, $a_1$, $a_2$, $a_3$ and $a_4$ are best-fitted constants determined by laboratory test data.

Now, if the DP curve from Fig. 4.4 is assumed to be DP a straight line, the mathematical expression for DP can be found from Eq. 4.8, and for any particular void ratio ($e=e_0$), the value of OD and OP can be found from Eq. 4.9 and Eq. 4.10, respectively.

$$\frac{\sigma_m - u_a}{OD} + \frac{u_a - u_w}{OP} = 1 \tag{4.8}$$

$$OD_{e=e_0} = (\sigma_m - u_a)_{(u_a - u_w = 0, e = e_0)} = 10^{\left(\frac{e_0 - a_2}{a_1}\right)} \tag{4.9}$$

$$OP_{e=e_0} = (u_a - u_w)_{(\sigma_m - u_a = 0, e = e_0)} = 10^{\left(\frac{e_0 - a_4}{a_3}\right)} \tag{4.10}$$

By combining Eq. 4.9 and Eq. 4.10, a mathematical expression for the void ratio constitutive surface can be found, as shown in Eq. 4.11.

$$\frac{\sigma_m - u_a}{10^{\left(\frac{e_0 - a_2}{a_1}\right)}} + \frac{u_a - u_w}{10^{\left(\frac{e_0 - a_4}{a_3}\right)}} = 1 \tag{4.11}$$

Zhang [271] finally concluded the following:

1. The constant void ratio curve for the void ratio constitutive surface does not necessarily have to be a straight line. If only the constant void ratio curve is a function of both the net normal mechanical stress and matric suction, this method is applicable.
2. Furthermore, it can also be proven that the mathematical expressions for the void ratio versus net normal mechanical stress curve and the void ratio versus matric suction curve are continuous and have continuous first derivatives unlike the discontinuous first derivative of proposed method by Fredlund *et al.* [82].

After rearranging Eq. 3.15 and Eq. 3.22, Eq. 4.12 and 4.13 are found respectively. Equation 4.14 which is the combination of Eq. 4.12 and 4.13 will represent the constitutive surface of soil.

$$\log_{10}(\sigma_v) = 0.29184\left(\frac{0.50737}{(e-0.80761)} - 1\right) + 2.73049 \tag{4.12}$$

$$\log_{10}(u_a - u_w) = 0.682210\left(\frac{0.992809}{(e-0.347128)} - 1\right) + 2.66902 \tag{4.13}$$

$$\frac{\sigma_V - U_a}{10^{\left(0.29184\left(\frac{0.50737}{(e-0.80761)}-1\right)+2.73049\right)}} + \frac{U_a - U_w}{10^{\left(0.682210\left(\frac{0.992809}{(e-0.347128)}-1\right)+2.66902\right)}} = 1 \tag{4.14}$$

Using any net normal stress ($\sigma$-$u_a$) and matric suction ($u_a$-$u_w$), the void ratio can be found using the iterative method from Eq. 4.14. Sigmaplot [281] was used to plot the constitutive surface of the Louisiana expansive soil. Figure 4.8 shows the void ratio constitutive surface where the curve at the void ratio vs. suction axis represents the SWCC, and the curve at the void ratio vs. mechanical stress axis represents the consolidation test. Some published void ratio constitutive surfaces from different parts of the world are illustrated in Fig. 4.9, Fig. 4.10 and Fig. 4.11. From the figures, it is certain

the constitutive surfaces are unique for each soil, and a visual idea is given of how void ratio change affects the matric suction and mechanical stress of the soil.

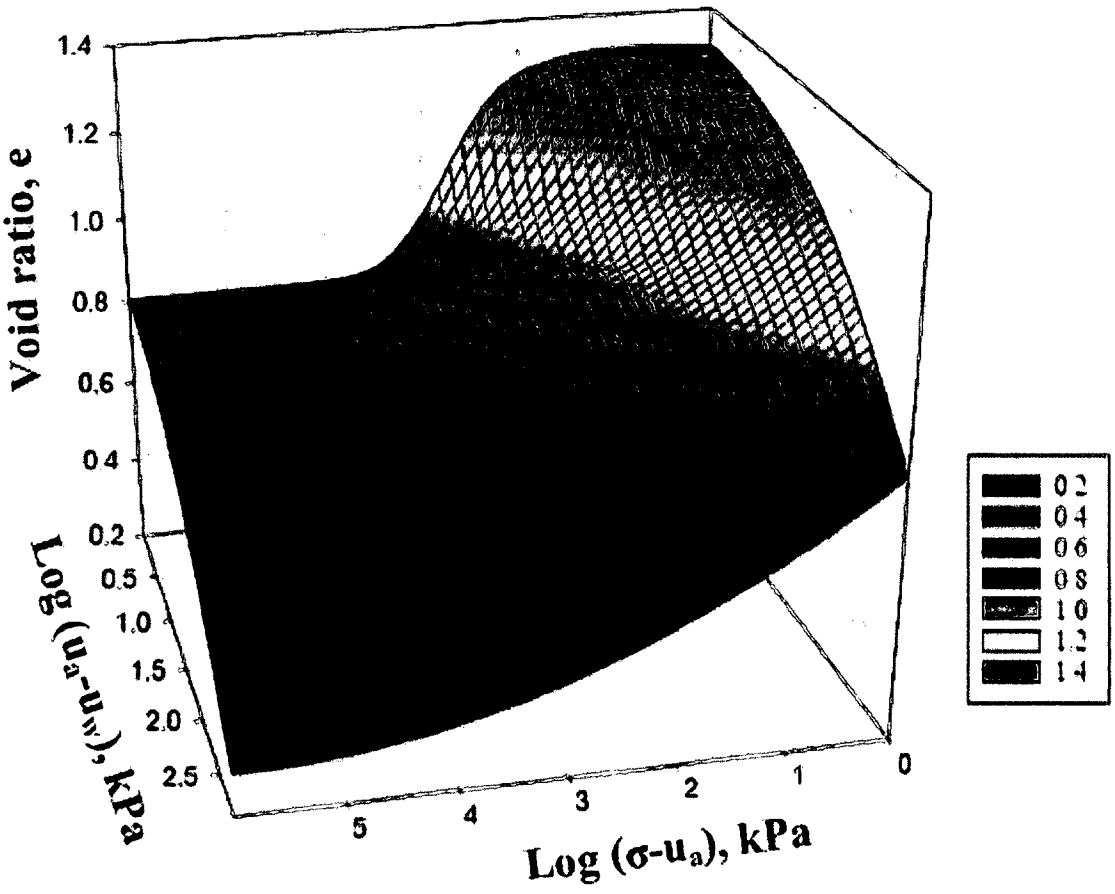


**Fig. 4.8 The Void Ratio Constitutive Surface of the Louisiana Expansive Soil**

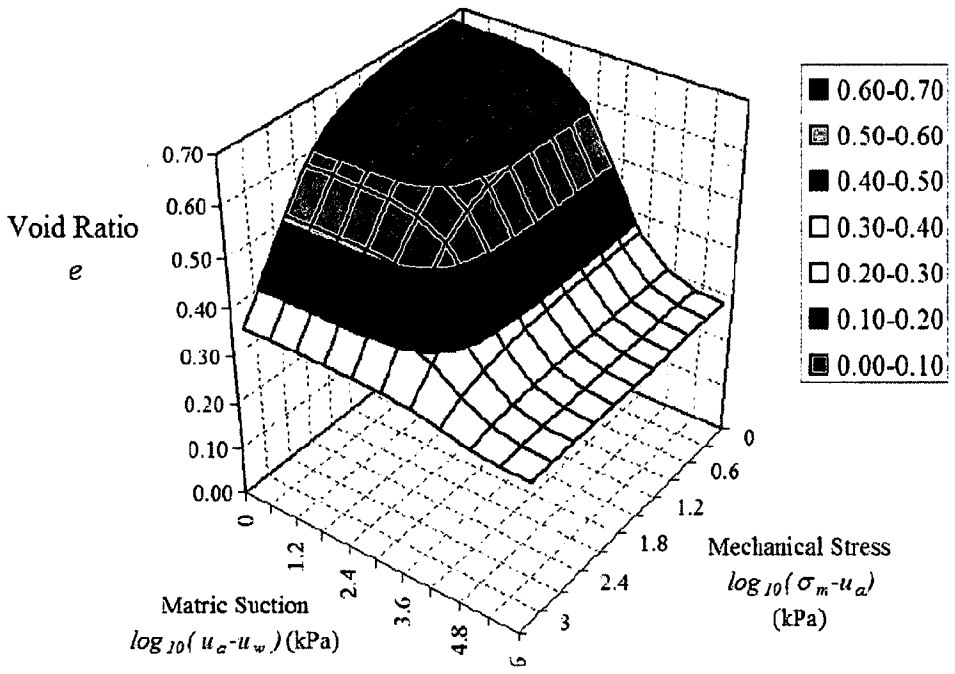


**Fig. 4.9 The Void Ratio Constitutive Surface of the Texas Expansive Soil (Zhang [271])**

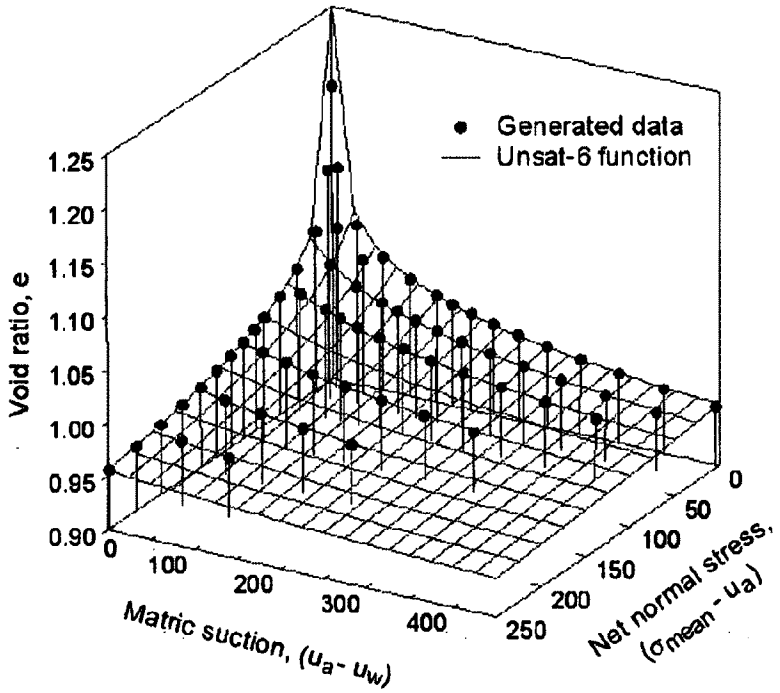


**Fig. 4.10 The Void Ratio Constitutive Surface of the Regina Soil (Hung [282])**

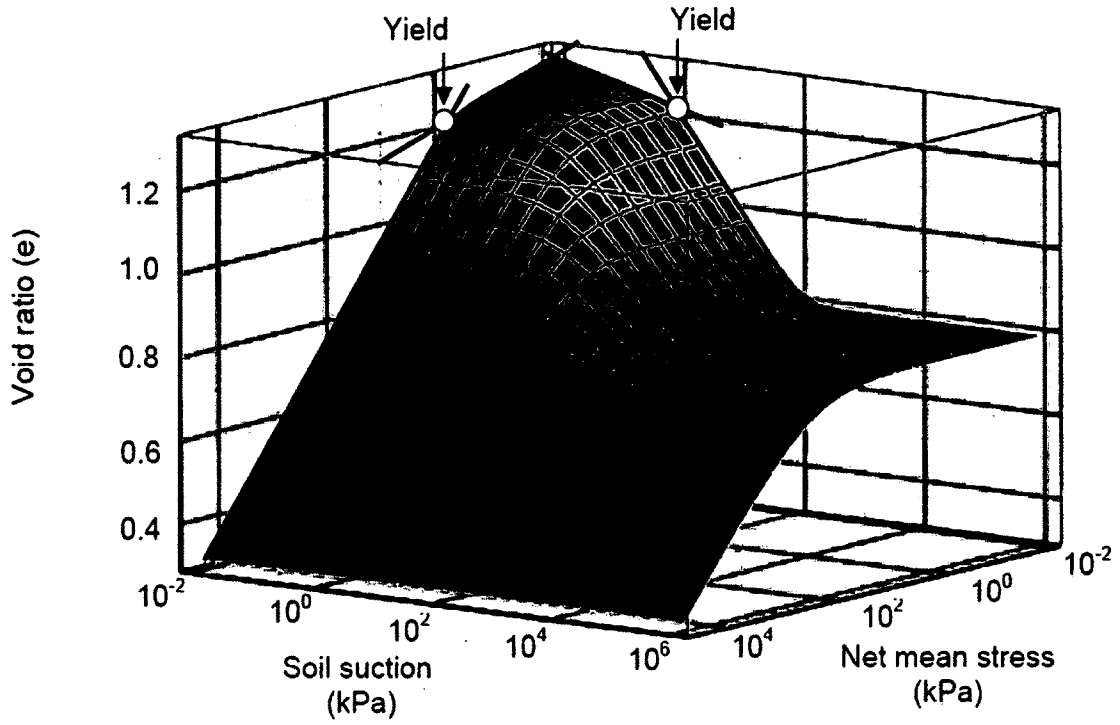


**Fig. 4.11 The Void Ratio Constitutive Surface of the Artificial Silt Soil (Pham [112])**

## 4.4 Conclusion

The constitutive surface would look like surface ABEDP from Fig. 4.4 if it is drawn in a Cartesian coordinate system. As the surface is plotted on a log-log scale (Fig. 4.8), the constructed constitutive surface looks as expected compared to other published constitutive surfaces. The constitutive surface is unique for each soil and gives a visual idea of how stress state affects the void ratio of a soil.

# CHAPTER 5

# DEVELOPMENT OF AN ANALYTIC METHOD TO CALCULATE EXPANSIVE-SOIL-INDUCED STRESSES IN PAVEMENT

## 5.1 Introduction

Expansive soil changes its volume due to changes in moisture content. Roads constructed over expansive soil will experience deflection due to the volume change of the subgrade soil. During the summer time, when the moisture content of the subgrade soil underneath decreases, pavement at the edge will experience downward deflection. On the other hand, in the rainy season due to moisture content increase in that same expansive soil, the pavement at the edge will experience upward deflection. Figure 5.1 shows some of the expansive-soil-induced longitudinal cracks on pavements.

**Fig. 5.1 Longitudinal Cracks on Pavement Due to Expansive Subgrade [283]**

If the pavement can be assumed as a beam, there are many methods available to analyze the beam on an elastic foundation due to the load imposed on it. The theory of Winkler foundation is a simple method to analyze beams on elastic foundation subject to load. So far, no mechanistic-based methodology is available to analyze a pavement using the Winkler foundation model due to the volume change of subgrade expansive soil. Since deflection of the pavement is caused by the heave/settlement of the expansive subgrade soil, instead of by any load, the model cannot be directly applied to solve the problem. In the dissertation research, one of the key achievements is to propose the concept of virtual load. The virtual load is applied to the pavement and yields pavement deflections, which are equivalent to the pavement deflections caused by the volume change of the expansive subgrade soils. In this chapter, a new analytic method based on the concept of virtual load is proposed for modeling granular fills/pavement/beam on expansive soil with or without surcharge load, using the Winkler foundation model. More details of the methodology will be described in section 5.4 of this chapter.

## 5.2 Description of the Winkler Foundation Model

To analyze structures on regular soil, knowledge of the properties of the structures as well as the properties of the soil is required. Generally, properties of the soil are difficult to obtain [284]. Different soils behave differently under the same applied load [285]. In 1867, Winkler first proposed modeling soil as an elastic medium. In the Winkler foundation model, soil is replaced with springs that behave the same under applied loads as real soil. Because of its simplicity, the Winkler model became the most popular soil model used by practicing engineers [284]. Many scientists like Hetenyi [286], Umansky [287] and others used the Winkler foundation as the base of their research. However,

some researchers tried to improve the soil model and recommended the use of new soil models. Some notable researchers include Pasternak [288], who proposed a soil model with two coefficients of subgrade reaction, and Reissner [289], who recommended a soil model that simplified analysis of foundations supported on elastic half-space.

The Winkler foundation model consists of infinite numbers of closely spaced unconnected linear-elastic springs whose behavior resembles that of a liquid base [290]. These springs are defined by subgrade modulus ($k_s$). Closed-form solutions for simple problems have been proposed by many researchers [286, 291-294]. The mechanism behind the model is the maximum displacement that will occur under the load. The Winkler foundation model has some assumptions as mentioned below:

1. The load applied to the soil surface produces settlements of the soil only under the applied load and does not produce any settlements and stresses outside of the loaded area.
2. The soil can resist compression as well as tension stresses.
3. The shape and size of the foundation do not affect the settlement of the soil.

These assumptions are not always true as described in the following paragraphs. The limitations of the Winkler model are given below:

1. When a load is applied to the soil, it produces settlement under the applied load and outside of the loaded area.
2. Soil does not resist any tension stresses, even a small amount.
3. Settlement of the soil is not only the function of applied load but also the shape and size of the foundation.

In spite of these limitations mentioned above, researchers such as Klepikov [295] proved that analysis based on the Winkler foundation produces realistic results that are practically close enough to results obtained from soil testing and observations of settlements of real structures.

For a beam of unit width and a length of L supported by the elastic foundation, as shown in Fig. 5.2, the relation between foundation reactions (R) at any point along the beam (Eq. 5.1) is directly proportional to the vertical displacement (w).

$$R = k_s * w \tag{5.1}$$

Here, $k_s$ is a constant of proportionality also known as subgrade modulus.

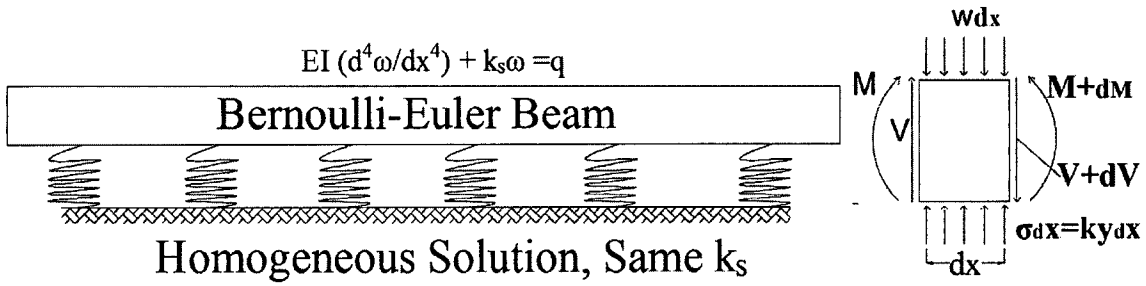


**Fig. 5.2 Bernoulli-Euler Beam Supported on Elastic Foundation**

Now, if a small piece of the beam is considered, x-distance from the left with a length dx as illustrated in Fig. 5.3, the shear force on that beam is considered V and the bending moment as M. From Fig. 5.3, Eq. 5.2 can be found using the equilibrium condition. Using solid mechanics relations (Eq. 5.3 to 5.7), Eq. 5.8 can be found.

$$V - (V + \delta V) + k_s w dx - q dx = 0 \tag{5.2}$$

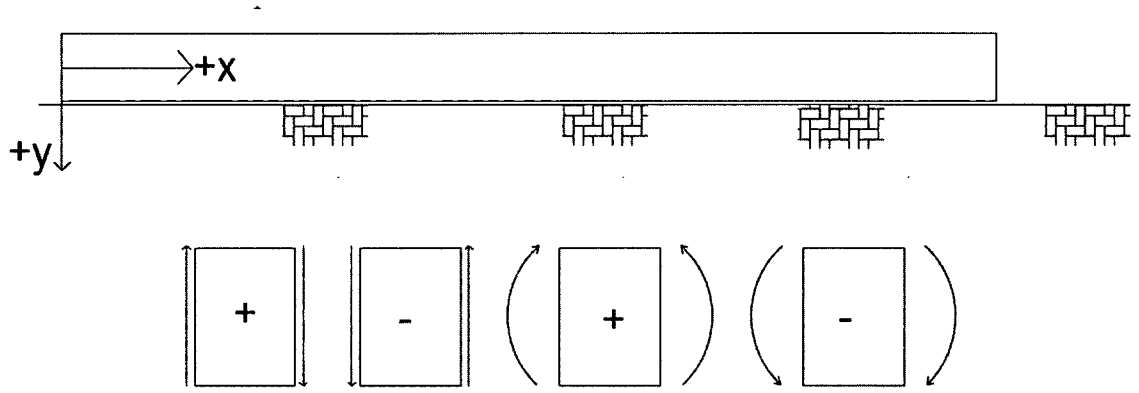


**Fig. 5.3 Sign Convention for Deflection, Shear Force and Bending Moment**

$$\frac{dV}{dx} = k_s w - q \tag{5.3}$$

$$\frac{dV}{dx} = k_s w - q \tag{5.4}$$

Using the relation between shear and moment

$$V = \frac{dM}{dx} \tag{5.5}$$

$$\frac{d^2M}{dx^2} = k_s w - q \tag{5.6}$$

Using the relation between moment and bending stiffness of the beam

$$EI\left(\frac{d^2w}{dx^2}\right) = -M \tag{5.7}$$

From Eq. 5.6 and Eq. 5.7,

$$\frac{d^2}{dx^2} EI\left(\frac{d^2w}{dx^2}\right) = k_s w - q \tag{5.8}$$

## 5.3 The Concept of Virtual Load

If a pavement represented as a beam is resting on a regular (unexpansive) soil, it will only deflect by the introduction of an external load. Figure 5.4 (a) and (b) shows the deflection of the beam on the regular soil. Beam deflection on a regular soil can be measured using the Winkler foundation model. Figure 5.4 (c) shows beam deflection due

to volume change of the subgrade expansive soil. This expansive-soil-induced beam deflection can be represented by the introduction of a virtual load on the beam with the subgrade considered as a regular soil. Figure 5.4 (d) shows the virtual load on a beam with a regular soil as a subgrade. The virtual load makes the beam deflected, which is equivalent to the real deflection induced by the volume change of the expansive soil subgrade. The advantage of this transformation is that this virtual load imposed beam-regular subgrade soil system can be analyzed using the Winkler foundation model.

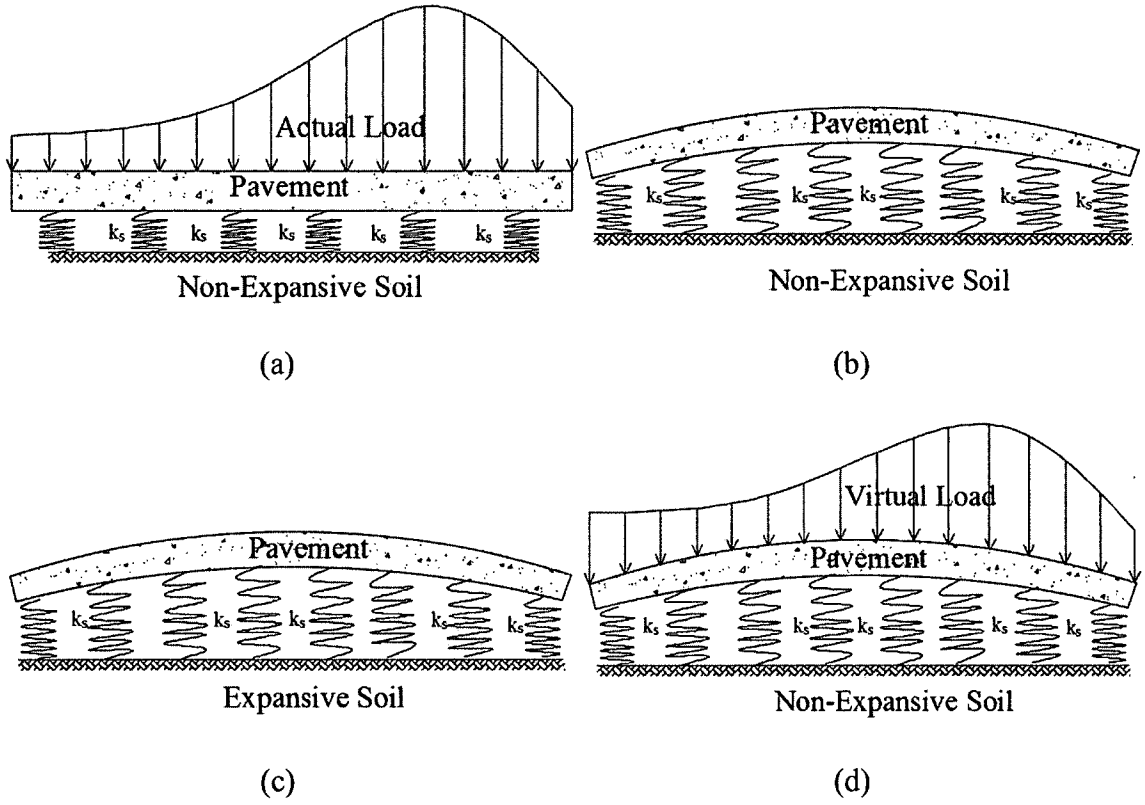


**Fig. 5.4 (a) Pavement on a Regular Soil, (b) Pavement Deflection Due to External, Load, (c) Pavement Deflection Due to Expansive Soil's Volume Change, and (d) Proposed Virtual Load Soil Model**

The virtual load distribution is not known; thus, it is expressed as a form of Fourier series. The model will be established in the following steps: 1) consider the virtual load as

a form of Fourier series in the combination of a few Fourier terms; 2) find the beam deflections at multiple points across the pavement from shoulder to shoulder, which are calculated from the heave or settlement prediction of the expansive subgrade soil; 3) find a closed-form solution of beam-like pavement deflection as a function of the only regression constants; 4) using regression analysis, find the Fourier constants, and the virtual load is thereby known; 5) once q (virtual load) is known, find the deflection, rotation, shear force and bending moment of the beam, using the closed-form solution of the Winkler foundation model; 6) again find the deflection, rotation, shear force and moment of the beam because of the self-weight and the external load (if any) by using the regular closed-form solution of the Winkler foundation, and 7) finally, using the super position theorem, find the combined deflection, rotation, shear force and moment of the beam.

## 5.4 Analytical Method to Find a Closed-Form Solution of a Beam Due to Any Known Load (q) Using the Winkler Foundation Theory

From Eq. 5.9 is the well-known differential equation of a beam,

$$EI\frac{d^4w}{dx^4} + k_s w = q. \tag{5.9}$$

Let us consider a finite beam (beam length L and bending stiffness EI) subjected to any form of pressure loading. The pressure q (i.e., self-weight, external load) can be expressed as a function of x, which is Eq. 5.10

$$q = f(x) \text{ for } 0 < x < L \tag{5.10}$$

Where, f(x) can be expressed in a Fourier cosine series (Eq. 5.11)

$$q = \sum A_n \cos\left(\frac{n\pi x}{L}\right). \tag{5.11}$$

Let's assume the particular integral is Eq. 5.12

$$w_{Particular} = a_n \cos\left(\frac{n\pi x}{L}\right). \tag{5.12}$$

Replacing the w and q value in Eq. 5.9, Eq. 5.13 is found

$$\left(\frac{n\pi}{L}\right)^4 a_n \cos\left(\frac{n\pi x}{L}\right) + \frac{k_s}{EI} a_n \cos\left(\frac{n\pi x}{L}\right) = \frac{A_n \cos\left(\frac{n\pi x}{L}\right)}{EI};$$

$$\left(\frac{n\pi}{L}\right)^4 a_n + \frac{k_s}{EI} a_{n\,n} = \frac{A_n}{EI};$$

$$a_n = \frac{A_n}{k_s + EI\left(\frac{n\pi}{L}\right)^4}. \tag{5.13}$$

To make the derivation simple but the solution precise enough, only four Fourier terms are taken (Eq. 5.14 and Eq. 5.15).

$$q(x) = \sum_{n=0}^{4} A_n \cos\left(\frac{n\pi x}{L}\right);$$

$$q(x) = A_0 + \sum_{n=1}^{4} A_n \cos\left(\frac{n\pi x}{L}\right) \tag{5.14}$$

Where,

$$A_0 = \frac{1}{L}\int_0^L f(x)dx \quad \text{and} \quad A_0 = \frac{2}{L}\int_0^L f(x)\cos\left(\frac{n\pi x}{L}\right)dx. \tag{5.15}$$

5.4.1 Beam Deflection $w_P(x)$ Equation Due to q Load

A homogeneous solution of the beam for any type of load (i.e., uniformly distributed load (UDL), point load, concentrated moment) is given in Eq. 5.16 and a particular solution, which is a function of load type, is given in Eq. 5.17.

$$w_H(x) = e^{\beta x}\{C_1 \cos(\beta x) + C_2 \sin s(\beta x)\} + e^{-\beta x}\{C_3 \cos(\beta x) + C_4 \sin(\beta x)\} \tag{5.16}$$

$$w_{PA}(x) = A_0 + \sum_{n=1}^{4} A_n \cos\left(\frac{n\pi x}{L}\right) \tag{5.17}$$

Here, $C_1$, $C_2$, $C_3$, and $C_4$ are four constants to be determined by four given boundary conditions.

The solution of equation (5.9) is the summation of the homogeneous solution and the particular solution. Equations 5.18 to 5.23 show the steps of beam deflection equation.

$$w_B(x) = w_H(x) + w_{PA}(x) \tag{5.18}$$

$$EI\frac{d^4w}{dx^4} + k_s w = A_0 + \sum_{n=1}^{4} A_n \cos\left(\frac{n\pi x}{L}\right) \tag{5.19}$$

$$w_B(x) = e^{\beta x}\{C_1 \cos(\beta x) + C_2 \sin s(\beta x)\} + e^{-\beta x}\{C_3 \cos(\beta x) + C_4 \sin(\beta x)\} + \frac{A_0}{k_s} + \sum_{n=1}^{4} a_n \cos\left(\frac{n\pi x}{L}\right) \tag{5.20}$$

Where,

$$a_n = \frac{A_n}{k_s + EI\left(\frac{n\pi}{L}\right)^4} \tag{5.21}$$

And

$$\beta = \sqrt[4]{\frac{k_s}{4EI}}. \tag{5. 22}$$

After rearranging Eq. 5.20,

$$[w_B(x)] = [e^{\beta x}\cos(\beta x) \quad e^{\beta x}\sin(\beta x) \quad e^{-\beta x}\cos(\beta x) \quad e^{-\beta x}\sin(\beta x)] * \begin{bmatrix} C_1 \\ C_2 \\ C_3 \\ C_4 \end{bmatrix} + \frac{A_0}{k_s} + \left[\cos\left(\frac{\pi x}{L}\right) \quad \cos\left(\frac{2\pi x}{L}\right) \quad \cos\left(\frac{3\pi x}{L}\right) \quad \cos\left(\frac{4\pi x}{L}\right)\right] * \begin{bmatrix} a_1 \\ a_2 \\ a_3 \\ a_4 \end{bmatrix}. \tag{5.23}$$

5.4.2 Beam Rotation $\phi(x)$ Equation Due to q Load

Equations 5.24 to 5.29 show the steps of beam rotation equation derivation.

$$\phi(x) = \frac{dw(x)}{dx} \tag{5.24}$$

$$\phi(x) = e^{\beta x}\{C_1\beta\cos(\beta x) + C_2\beta\sin(\beta x)\} + e^{\beta x}\{C_2\beta\cos(\beta x) - C_1\beta\sin(\beta x)\} - e^{-\beta x}\{C_3\beta\cos(\beta x) + C_4\beta\sin(\beta x)\} + e^{-\beta x}\{C_4\beta\beta\cos(\beta x) - C_3\beta\sin(\beta x)\} - \sum_{n=1}^{4}\left(\frac{n\pi}{L}\right)a_n\sin\left(\frac{n\pi x}{L}\right) \quad (5.25)$$

$$\phi(x) = e^{\beta x}\{(C_1\beta + C_2\beta)\cos(\beta x) + (-C_1\beta + C_2\beta)\sin(\beta x)\} + e^{-\beta x}\{(-C_3\beta + C_4\beta)\cos(\beta x) + (-C_3\beta - C_4\beta)\sin(\beta x)\} - \sum_{n=1}^{4}\left(\frac{n\pi}{L}\right)a_n\sin\left(\frac{n\pi x}{L}\right) \quad (5.26)$$

$$\phi(x) = e^{\beta x}\{C_5\cos(\beta x) + C_6\sin(\beta x)\} + e^{-\beta x}\{C_7\cos(\beta x) + C_8\sin(\beta x)\} - \sum_{n=1}^{4}\left(\frac{n\pi}{L}\right)a_n\sin\left(\frac{n\pi x}{L}\right) \quad (5.27)$$

Where,

$$C_5 = C_1\beta + C_2\beta;$$

$$C_6 = -C_1\beta + C_2\beta;$$

$$C_7 = -C_3\beta + C_4\beta;$$

$$C_8 = -C_3\beta - C_4\beta;$$

$$\begin{bmatrix} C_5 \\ C_6 \\ C_7 \\ C_8 \end{bmatrix} = \begin{bmatrix} \beta & \beta & 0 & 0 \\ -\beta & \beta & 0 & 0 \\ 0 & 0 & -\beta & \beta \\ 0 & 0 & -\beta & -\beta \end{bmatrix} * \begin{bmatrix} C_1 \\ C_2 \\ C_3 \\ C_4 \end{bmatrix}. \quad (5.28)$$

$$\phi(x) = [e^{\beta x}\cos(\beta x) \quad e^{\beta x}\sin(\beta x) \quad e^{-\beta x}\cos(\beta x) \quad e^{-\beta x}\sin(\beta x)] * \begin{bmatrix} \beta & \beta & 0 & 0 \\ -\beta & \beta & 0 & 0 \\ 0 & 0 & -\beta & \beta \\ 0 & 0 & -\beta & -\beta \end{bmatrix} * \begin{bmatrix} C_1 \\ C_2 \\ C_3 \\ C_4 \end{bmatrix} - \sum_{n=1}^{4}\left(\frac{n\pi}{L}\right)a_n\sin\left(\frac{n\pi x}{L}\right) \quad (5.29)$$

5.4.3 Beam Moment M(x) Equation Due to q Load

Equations 5.30 to 5.35 show the steps of beam moment equation derivation.

$$M(x) = -EI\frac{d\phi(x)}{dx} \quad (5.30)$$

$$\frac{d\phi(x)}{dx} = e^{\beta x}\{(C_1\beta^2 - C_1\beta^2 + 2C_2\beta^2)\cos(\beta x) + (C_2\beta^2 - C_2\beta^2 - 2C_1\beta^2)\sin(\beta x)\} +$$

$$e^{-\beta x}\{(C_3\beta^2 - C_3\beta^2 - 2C_4\beta^2)\cos(\beta x) + (C_4\beta^2 - C_4\beta^2 + 2C_3\beta^2)\sin(\beta x)\} -$$

$$\sum_{n=1}^{4}\left(\frac{n\pi}{L}\right)^2 a_n \cos\left(\frac{n\pi x}{L}\right) \tag{5.31}$$

$$\frac{d\phi(x)}{dx} = e^{\beta x}\{2C_2\beta^2\cos(\beta x) - 2C_1\beta^2\sin(\beta x)\} + e^{-\beta x}\{-2C_4\beta^2\cos(\beta x) +$$

$$2C_3\beta^2\sin(\beta x)\} - \sum_{n=1}^{4}\left(\frac{n\pi}{L}\right)^2 a_n \cos\left(\frac{n\pi x}{L}\right) \tag{5.32}$$

$$\frac{d\phi(x)}{dx} = e^{\beta x}\{C_9\cos(\beta x) + C_{10}\sin(\beta x)\} + e^{-\beta x}\{C_{11}\cos(\beta x) + C_{12}\sin(\beta x)\} -$$

$$\sum_{n=1}^{4}\left(\frac{n\pi}{L}\right)^2 a_n \cos\left(\frac{n\pi x}{L}\right) \tag{5.33}$$

Where,

$$C_9 = 2C_2\beta^2;$$

$$C_{10} = -2C_1\beta^2;$$

$$C_{11} = -2C_4\beta^2;$$

$$C_{12} = 2C_3\beta^2;$$

$$\begin{bmatrix} C_9 \\ C_{10} \\ C_{11} \\ C_{12} \end{bmatrix} = \begin{bmatrix} 0 & 2\beta^2 & 0 & 0 \\ -2\beta^2 & 0 & 0 & 0 \\ 0 & 0 & 0 & -2\beta^2 \\ 0 & 0 & 2\beta^2 & 0 \end{bmatrix} * \begin{bmatrix} C_1 \\ C_2 \\ C_3 \\ C_4 \end{bmatrix}. \tag{5.34}$$

$$M(x) = -EI * \left\{ [e^{\beta x}\cos(\beta x) \quad e^{\beta x}\sin(\beta x) \quad e^{-\beta x}\cos(\beta x) \quad e^{-\beta x}\sin(\beta x)] * \right.$$

$$\left. \begin{bmatrix} 0 & 2\beta^2 & 0 & 0 \\ -2\beta^2 & 0 & 0 & 0 \\ 0 & 0 & 0 & -2\beta^2 \\ 0 & 0 & 2\beta^2 & 0 \end{bmatrix} * \begin{bmatrix} C_1 \\ C_2 \\ C_3 \\ C_4 \end{bmatrix} - \sum_{n=1}^{4}\left(\frac{n\pi}{L}\right)^2 a_n \cos\left(\frac{n\pi x}{L}\right) \right\} \tag{5.35}$$

5.4.4 Beam Shear V(x) Equation Due to q Load

Equations 5.36 to 5.41 show the steps of beam shear equation derivation.

$$V(x) = \frac{dM(x)}{dx} \tag{5.36}$$

$$V(x) = EI\Big[e^{\beta x}\{(C_1\beta^3 - C_2\beta^3 + 3C_2\beta^3 - 3C_1\beta^3)\cos(\beta x) + (C_2\beta^3 + C_1\beta^3 - 3C_1\beta^3 - 3C_2\beta^3)\sin(\beta x)\} + e^{-\beta x}\{(-C_3\beta^3 - C_4\beta^3 + 3C_3\beta^3 + 3C_4\beta^3)\cos(\beta x) + (-C_4\beta^3 + C_3\beta^3 - 3C_3\beta^3 + 3C_4\beta^3)\sin(\beta x)\} - 2q_0\sum_{n=1}^{4}\left(\frac{n\pi}{L}\right)^3 a_n \sin\left(\frac{n\pi x}{L}\right)\Big] \tag{5.37}$$

$$V(x) = EI\Big[e^{\beta x}\{(2C_2\beta^3 - 2C_1\beta^3)\cos(\beta x) + (-2C_1\beta^3 - 2C_2\beta^3)\sin(\beta x)\} + e^{-\beta x}\{(2C_3\beta^3 + 2C_4\beta^3)\cos(\beta x) + (-2C_3\beta^3 + 2C_4\beta^3)\sin(\beta x)\} - 2q_0\sum_{n=1}^{4}\left(\frac{n\pi}{L}\right)^3 a_n \sin\left(\frac{n\pi x}{L}\right)\Big] \tag{5.38}$$

$$V(x) = EI\Big[e^{\beta x}\{C_{13}\cos(\beta x) + C_{14}\sin(\beta x)\} + e^{-\beta x}\{C_{15}\cos(\beta x) + C_{16}\sin(\beta x)\} - 2q_0\sum_{n=1}^{4}\left(\frac{n\pi}{L}\right)^3 a_n \sin\left(\frac{n\pi x}{L}\right)\Big] \tag{5.39}$$

Where,

$$C_{13} = -2C_1\beta^3 + 2C_2\beta^3;$$

$$C_{14} = -2C_1\beta^3 - 2C_2\beta^3;$$

$$C_{15} = 2C_3\beta^3 + 2C_4\beta^3;$$

$$C_{16} = -2C_3\beta^3 + 2C_4\beta^3;$$

$$\begin{bmatrix} C_{13} \\ C_{14} \\ C_{15} \\ C_{16} \end{bmatrix} = \begin{bmatrix} -2\beta^3 & 2\beta^3 & 0 & 0 \\ -2\beta^3 & -2\beta^3 & 0 & 0 \\ 0 & 0 & 2\beta^3 & 2\beta^3 \\ 0 & 0 & -2\beta^3 & 2\beta^3 \end{bmatrix} * \begin{bmatrix} C_1 \\ C_2 \\ C_3 \\ C_4 \end{bmatrix}. \tag{5.40}$$

$$V(x) = EI * \left[ [e^{\beta x}\cos(\beta x) \quad e^{\beta x}\sin(\beta x) \quad e^{-\beta x}\cos(\beta x) \quad e^{-\beta x}\sin(\beta x)] * \right.$$

$$\left. \begin{bmatrix} 2\beta^3 & -2\beta^3 & 0 & 0 \\ 2\beta^3 & 2\beta^3 & 0 & 0 \\ 0 & 0 & -2\beta^3 & -2\beta^3 \\ 0 & 0 & 2\beta^3 & -2\beta^3 \end{bmatrix} * \begin{bmatrix} C_1 \\ C_2 \\ C_3 \\ C_4 \end{bmatrix} - 2q_0 \sum_{n=1}^{4} \left(\frac{n\pi}{L}\right)^3 a_n \sin\left(\frac{n\pi x}{L}\right) \right] \quad (5.41)$$

5.4.5 Determination of Constants $C_1$ to $C_{16}$

Using boundary conditions x = 0, V = 0, M = 0, and x = L, V = 0, M = 0 in Eq. 5.35 and Eq. 5.41, matrix [M][C] = [R] can be found. This matrix is expressed in Eq. 5.42. M matrix is a function of basic parameters such as β, L, $k_s$, E and I, whereas R matrix is a function of parameter q load. Once all the parameters mentioned above are known, using the matrix $[C] = [M]^{-1}[R]$ (Eq. 5.43), constants $C_1$ to $C_4$ can be found. Once $C_1$ to $C_4$ are known, using Eq. 5.28, 5.34 and 5.40, constants $C_5$ to $C_{16}$ can be found. Equations 5.44 to 5.59 shows coefficients of M inverse matrix. Equations 5.60 to 5.67 are used to simplify the solution Equation 5.68 shows the final matrix solution of beam deflection. The same matrix can be developed for rotation, moment and shear.

$$[M][C] = [R]$$

$$\begin{bmatrix} 0 & 2\beta^2 & 0 & -2\beta^2 \\ 2*\beta^3 & -2*\beta^3 & -2*\beta^3 & -2*\beta^3 \\ -2\beta^2\, e^{\beta L}\sin(\beta L) & 2\beta^2 e^{\beta L}\cos(\beta L) & 2\beta^2\, e^{-\beta L}\sin(\beta L) & -2\beta^2 e^{-\beta L}\cos(\beta L) \\ 2\beta^3 * e^{\beta L}\{\cos(\beta L)+\sin(\beta L)\} & 2\beta^3 * e^{\beta L}\{\sin(\beta L)-\cos(\beta L)\} & -2\beta^3 * e^{-\beta L}\{\cos(\beta L)-\sin(\beta L)\} & -2\beta^3 * e^{-\beta L}\{\cos(\beta L)+\sin(\beta L)\} \end{bmatrix} \begin{bmatrix} C_1 \\ C_2 \\ C_3 \\ C_4 \end{bmatrix} =$$

$$\begin{bmatrix} \sum_{n=1}^{4}\left(\frac{n\pi}{L}\right)^2 a_n \\ 0 \\ \sum_{n=1}^{4}\left(\frac{n\pi}{L}\right)^2 a_n(-1)^n \\ 0 \end{bmatrix} \tag{5.42}$$

$$[C] = [M]^{-1}[R] = [D][R]$$

$$\begin{bmatrix} C_1 \\ C_2 \\ C_3 \\ C_4 \end{bmatrix} =$$

$$\begin{bmatrix} 0 & 2\beta^2 & 0 & -2\beta^2 \\ 2*\beta^3 & -2*\beta^3 & -2*\beta^3 & -2*\beta^3 \\ -2\beta^2\, e^{\beta L}\sin(\beta L) & 2\beta^2 e^{\beta L}\cos(\beta L) & 2\beta^2\, e^{-\beta L}\sin(\beta L) & -2\beta^2 e^{-\beta L}\cos(\beta L) \\ 2\beta^3 * e^{\beta L}\{\cos(\beta L)+\sin(\beta L)\} & 2\beta^3 * e^{\beta L}\{\sin(\beta L)-\cos(\beta L)\} & -2\beta^3 * e^{-\beta L}\{\cos(\beta L)-\sin(\beta L)\} & -2\beta^3 * e^{-\beta L}\{\cos(\beta L)+\sin(\beta L)\} \end{bmatrix}^{-1} \begin{bmatrix} \sum_{n=1}^{4}\left(\frac{n\pi}{L}\right)^2 a_n \\ 0 \\ \sum_{n=1}^{4}\left(\frac{n\pi}{L}\right)^2 a_n(-1)^n \\ 0 \end{bmatrix}$$

(5.43)

$$[D] = \begin{bmatrix} 0 & 2\beta^2 & 0 & -2\beta^2 \\ 2*\beta^3 & -2*\beta^3 & -2*\beta^3 & -2*\beta^3 \\ -2\beta^2 e^{\beta L}\sin(\beta L) & 2\beta^2 e^{\beta L}\cos(\beta L) & 2\beta^2 e^{-\beta L}\sin(\beta L) & -2\beta^2 e^{-\beta L}\cos(\beta L) \\ 2\beta^3 * e^{\beta L}\{\cos(\beta L)+\sin(\beta L)\} & 2\beta^3 * e^{\beta L}\{\sin(\beta L)-\cos(\beta L)\} & -2\beta^3 * e^{-\beta L}\{\cos(\beta L)-\sin(\beta L)\} & -2\beta^3 * e^{-\beta L}\{\cos(\beta L)+\sin(\beta L)\} \end{bmatrix}^{-1} =$$

$$\frac{1}{\text{Det of M}} \begin{bmatrix} b_{11} & b_{12} & b_{13} & b_{14} \\ b_{21} & b_{22} & b_{23} & b_{24} \\ b_{31} & b_{32} & b_{33} & b_{34} \\ b_{41} & b_{42} & b_{43} & b_{44} \end{bmatrix} \tag{5.44}$$

After performing the matrix operation, the co-efficients from $b_{11}$ to $b_{44}$ can be found as follows:

$$b_{11} = 8\beta^8 e^{-2\beta L}\{\sin^2(\beta L)+\cos^2(\beta L)\} + 8\beta^8\{-2*\sin(\beta L)*\cos(\beta L)-\cos^2(\beta L)+\sin^2(\beta L)\}; \tag{5.45}$$

$$b_{12} = -8\beta^7 e^{-2\beta L}\{-\cos^2(\beta L)-\sin^2(\beta L)\} - 8\beta^7 * \{\cos^2(\beta L)+\sin^2(\beta L)-2*\sin(\beta L)*\cos(\beta L)\}; \tag{5.46}$$

$$b_{13} = 8\beta^8 e^{-\beta L}\{3*\sin(\beta L)-\cos(\beta L)\}; \tag{5.47}$$

$$b_{14} = -8\beta^7 e^{-\beta L}\{2*\sin(\beta L)+\cos(\beta L)\} + 8\beta^7 e^{\beta L}\cos(\beta L); \tag{5.48}$$

$$b_{21} = 8\beta^8 e^{-2\beta L}\{\cos^2(\beta L)+\sin^2(\beta L)\} + 8\beta^8\{-\cos^2(\beta L)-3*\sin^2(\beta L)-2*\sin(\beta L)*\cos(\beta L)\}; \tag{5.49}$$

$$b_{22} = 16\beta^7\sin^2(\beta L); \tag{5.50}$$

$$b_{23} = 8\beta^8 e^{\beta L}\{\sin(\beta L)+\cos(\beta L)\} + 8\beta^8 e^{-\beta L}\{-\sin(\beta L)+\cos(\beta L)\}; \tag{5.51}$$

$$b_{24} = -8\beta^7 e^{-\beta L} * \sin(\beta L) + 8\beta^7 e^{\beta L} * \sin(\beta L); \tag{5.52}$$

$$b_{31} = -8\beta^8\{-2 * \sin(\beta L) + \cos(\beta L) + \cos^2(\beta L) - \sin^2(\beta L)\} + 8\beta^8 e^{2\beta L}\{\sin^2(\beta L) + \cos^2(\beta L)\}; \quad (5.53)$$

$$b_{32} = 8\beta^7\{\sin^2(\beta L) + \cos^2(\beta L) + 2 * \sin(\beta L) + \cos(\beta L)\} - 8\beta^7 e^{2\beta L}\{\cos^2(\beta L) + \sin^2(\beta L)\}; \quad (5.54)$$

$$b_{33} = -32\beta^8 e^{\beta L}\sin(\beta L) + 8\beta^8 e^{-\beta L}\{\sin(\beta L) + \cos(\beta L)\}; \quad (5.55)$$

$$b_{34} = -8\beta^7 e^{-\beta L}\cos(\beta L) - 8\beta^7 e^{\beta L}\{2\sin(\beta L) - \cos(\beta L)\}; \quad (5.56)$$

$$b_{41} = 8\beta^8\{3 * \sin^2(\beta L) - 2 * \sin(\beta L) * \cos(\beta L) + \cos^2(\beta L)\} - 8\beta^8 e^{2\beta L}\{\cos^2(\beta L) + \sin^2(\beta L)\}; \quad (5.57)$$

$$b_{42} = 16\beta^7\sin^2(\beta L); \quad (5.58)$$

$$b_{43} = -8\beta^8 e^{-\beta L}\{-\sin(\beta L) + \cos(\beta L)\} + 8\beta^8 e^{\beta L}\{\sin(\beta L) + \cos(\beta L)\}. \quad (5.59)$$

Let's assume,

$$[E] = [e^{\beta x}\cos(\beta x) \quad e^{\beta x}\sin(\beta x) \quad e^{-\beta x}\cos(\beta x) \quad e^{-\beta x}\sin(\beta x)]; \tag{5.60}$$

$$[F] = \begin{bmatrix} \left(\frac{\pi}{L}\right)^2 & \left(\frac{2\pi}{L}\right)^2 & \left(\frac{3\pi}{L}\right)^2 & \left(\frac{4\pi}{L}\right)^2 \\ 0 & 0 & 0 & 0 \\ -\left(\frac{\pi}{L}\right)^2 & \left(\frac{2\pi}{L}\right)^2 & -\left(\frac{3\pi}{L}\right)^2 & \left(\frac{4\pi}{L}\right)^2 \\ 0 & 0 & 0 & 0 \end{bmatrix}; \tag{5.61}$$

$$[G] = \left[\cos\left(\frac{\pi x}{L}\right) \quad \cos\left(\frac{2\pi x}{L}\right) \quad \cos\left(\frac{3\pi x}{L}\right) \quad \cos\left(\frac{4\pi x}{L}\right)\right]. \tag{5.62}$$

So,

$$\begin{bmatrix} C_1 \\ C_2 \\ C_3 \\ C_4 \end{bmatrix} = [D]\begin{bmatrix} \sum_{n=1}^{4}\left(\frac{n\pi}{L}\right)^2 a_n \\ 0 \\ \sum_{n=1}^{4}\left(\frac{n\pi}{L}\right)^2 a_n(-1)^n \\ 0 \end{bmatrix} = [D] * \begin{bmatrix} \left(\frac{\pi}{L}\right)^2 & 4\left(\frac{\pi}{L}\right)^2 & 9\left(\frac{\pi}{L}\right)^2 & 16\left(\frac{\pi}{L}\right)^2 \\ 0 & 0 & 0 & 0 \\ -\left(\frac{\pi}{L}\right)^2 & 4\left(\frac{\pi}{L}\right)^2 & -9\left(\frac{\pi}{L}\right)^2 & 16\left(\frac{\pi}{L}\right)^2 \\ 0 & 0 & 0 & 0 \end{bmatrix}\begin{bmatrix} a_1 \\ a_2 \\ a_3 \\ a_4 \end{bmatrix} \tag{5.63}$$

$$\begin{bmatrix} C_1 \\ C_2 \\ C_3 \\ C_4 \end{bmatrix} = [D][F]\begin{bmatrix} a_1 \\ a_2 \\ a_3 \\ a_4 \end{bmatrix} \tag{5.64}$$

$$[w_B(x)] = \left[[E] * [F] * [D]\right] * \begin{bmatrix} a_1 \\ a_2 \\ a_3 \\ a_4 \end{bmatrix} + \frac{A_0}{k_s} + [G] * \begin{bmatrix} a_1 \\ a_2 \\ a_3 \\ a_4 \end{bmatrix} \tag{5.65}$$

$$[w_B(x)] = \left[[E] * [F] * [D] + [G]\right] * \begin{bmatrix} a_1 \\ a_2 \\ a_3 \\ a_4 \end{bmatrix} + \frac{A_0}{k_s}. \tag{5.66}$$

Let's assume,

$$\left[[E] * [F] * [D] + [G]\right] = [H_1 \quad H_2 \quad H_3 \quad H_4] \tag{5.67}$$

$$[w_B(x)] = \left[\frac{1}{k_s} \quad H_1 \quad H_2 \quad H_3 \quad H_4\right]\begin{bmatrix} A_0 \\ a_1 \\ a_2 \\ a_3 \\ a_4 \end{bmatrix}. \tag{5.68}$$

Here are the steps of the solution in a systematic order for a known load:

1. Using the beam theory, a closed-form beam deflection, rotation, moment and shear equation was developed where the load q as a pressure load (i.e., self-weight, UDL) is expressed as a Fourier series.
2. Using the boundary conditions x = 0, V = 0, M = 0 and x = L, V = 0, M = 0, [M][C] = [R] matrix was developed.
3. Using [C] = [M]-1[R], matrix constants C1 to C4 can be found.
4. Using the values of C1 to C4, C5 to C16 can be measured.
5. Using Eq. 5.23, 5.29, 5.35 and 5.41 deflection, rotation, shear and moment can be found.

## 5.5 Expanding the Closed-Form Winkler Solution to Expansive Soil

In section 5.4, deflection, rotation, moment and shear force on a beam under a known q load has been derived. If the load is not known but the deflection of the beam due to an unknown load is known (i.e., deflection of the beam caused by the volume change of expansive soil below the beam), an analytical method has been proposed to find an equivalent virtual load q(x), which will create deflection of a beam resting on regular soil the same as the deflection of that beam resting on an expansive soil. If the structural property of the beam is known, then the only unknowns are $C_1$ through $C_4$, which is a function of constants $A_0$ and $a_1$ through $a_4$, where $A_0$ and $a_1$ through $a_4$ are Fourier constants of load q(x). So, basically in Eq. 5.68, the only unknowns are Fourier constants of load q(x). In a known deflection with an unknown load situation, these Fourier constants can be found using regression analysis with the predicted soil heave/shrinkage ($w_p$) of the

expansive soil. There are a numerber of empirical equations available to predict soil heave/shrinkage ($w_p$) as described in Chapter 3.

Here are the steps of the solution in a systematic order for a known soil heave/shrinkage:

1. Predict the heave/shrinkage at different points of the beam $w_p(x)$, using different soil volume change equations, as described in Chapter 3.
2. Using the closed-form Winkler solution, find the equation of deflection of the beam wB(x). The only unknown of the deflection equation (Eq. 5.68) will be the Fourier constants.
3. Using regression analysis between wP(x) and wB(x), find the Fourier constants. Now load q(x) is known as are the C1 to C4 constants since they are a function of Fourier constants.
4. Now follow steps 4-5 of the "Steps of the solution in a systematic order for a known load."

## 5.6 Calculating the Combined Solution Using Superposition Method

Using superposition theorem, the combined effect on the beam can be found. For example, in the case of soil heave, the combined beam deflection can be found from Eq. 5.69, and for soil shrinkage, the combined deflection can be found from Eq. 5.70.

$$w_C(x) = w_q(x) + w_w(x) + w_H(x), \tag{5.69}$$

and

$$w_C(x) = w_q(x) + w_w(x) + w_S(x) \tag{5.70}$$

Where,

$w_C(x)$ = Combined beam deflection;

$w_q(x)$ = Beam deflection due to external q load;

$w_w(x)$ = Beam deflection due to self-weight;

$w_H(x)$ = Beam deflection due to soil heave;

$w_S(x)$ = Beam deflection due to soil shrinkage.

In the same way, combined rotation, moment and shear can be found. Generally, beam self-weight is minimal, and its contribution to deflection, rotation, moment and shear can be ignored. Once moment and shear are known, bending stress and shear stress at every section can be found using Eq. 5.71 and Eq. 5.72.

$$\sigma(x) = \frac{M(x)y}{I} \tag{5.71}$$

$$\tau(x) = \frac{V(x)Q(x)}{It} \tag{5.72}$$

Here,

$\sigma$ = bending stress of a beam at a section x- distance from the side;

$\tau$ = shear stress of a beam at a section x- distance from the side;

M = total bending moment of a beam at a section x- distance from the side;

V = total shear force of a beam at a section x- distance from the side;

y = distance from the neutral axis to the top/bottom fiber of the beam at a section x- distance from the side;

I = the second moment of inertia of a beam at a section x- distance from the side;

Q = the first moment of area of the top/bottom portion of the cross-sectional area at a section x- distance from the side;

t = thickness of the section.

## 5.7 Parametric Study of the Proposed Method

Once the model is developed, a parametric study is carried out. In the parametric study, two extreme situations are considered: 1) extreme heave and 2) extreme shrinkage.

### 5.7.1 Defining Structural Properties of the Beam

A beam is considered resting on expansive soil, as shown in Fig. 5.5. The structural properties of the beam are defined in Table 5.1. Young's modulus $E_{Clay}$ for soft clay can be defined from its undrained shear strength $C_u$ from Eq. 5.73 [291]. In 1962, Korenev suggested $k_s$ values for different types of soil, as shown in Table 5.2 [296]. Here, Eq. 5.74 is used to find the subgrade modulus $k_s$ [297-299]. From Table 5.1, the $k_s$ value for analyzing soil heave/shrinkage (B=10) and beam self-weight (B=10) is found to be $2.67\times10^2$ kN/m$^3$, whereas for external load case (B=1), $k_s$ value is found to be $2.67\times10^3$ kN/m$^3$. For this parametric study, Young's modulus E is taken to be E = 50,000 kPa. Here, L is the width of the pavement, r is the distance from the edge of the pavement to the starting of the load, B is the width of the load, and finally, h is the height of the pavement. In the parametric study, soil heave and shrinkage-induced beam properties are calculated. Expansive-soil-induced virtual load is present for the whole cross-section. For that reason, while measuring the stress on pavement caused by expansive soil, the value of r is equal zero while the value of B is taken to be the same as L. Two extreme cases, soil extreme heave and soil extreme shrinakge, are taken into consideration in the study.

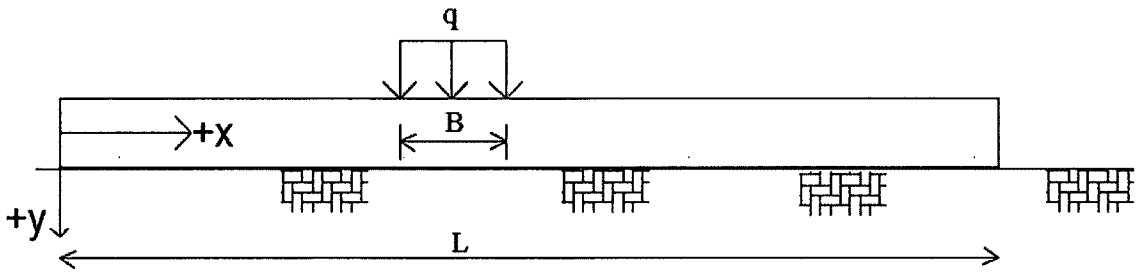


**Fig. 5.5 A Typically Loaded Beam**

$$E_{Clay} = (200 \sim 500) * C_u \tag{5.73}$$

$$k_s = \frac{E_{Clay}}{B(1-\upsilon^2)} \tag{5.74}$$

**Table 5.1 Structural Properties of the Beam**

| Parameters | Expansive Soil |
|---|---|
| r (m) | 0 |
| B (m) | 10 |
| L (m) | 10 |
| h (m) | 0.584 |
| $q_w$ (kPA) | -- |
| $k_s$ (kN/m$^3$) | $2.67\times10^2$ |
| E (kN/m$^3$) | 50000 |
| $\upsilon$ | 0.5 |
| $y_c$ (m) | 0.292 |
| EI (kN-m) | 830.756 |

**Table 5.2 Modulus of Subgrade Reaction $k_s$**

| General description of the soil | Type of Soil | $k_s$ (kg/cm$^3$) |
|---|---|---|
| Lower density soil | Quicksand; filled-up sand; wet, soft clay | 0.1-0.5 |
| Average density soil | Sandy ballast, loose gravel, wet clay | 0.5-5 |
| Compact solid soil | High-density sand, gravel, dry clay | 5-10 |
| Very solid compacted soil | Compacted sandy clay, stiff clay | 10-20 |
| Stiff soil | Soft, rocky soil; limestone; sandstone | 20-100 |
| Rocky soil | Rock | 100-1500 |
| Reinforced soil | Pile foundation | 5-15 |

5.7.2 Defining Soil Properties and Soil Heave Prediction

A road in Texas was constructed over expansive soils. TxDOT installed horizontal and vertical moisture content sensors underneath the pavement. A yearlong reading was taken by the TxDOT. Figure 5.7 shows the section of the Texas FM2 pavement. The Texas FM2 road is modeled using VADOSE/W program and heave distribution underneath the shoulder region is found [300]. Figure 5.6 shows the diagram of the model. After finishing the reading, moisture content distributions at different location were plotted for horizontal sensors and vertical sensors. Figure 5.7 shows the horizontal moisture distribution underneath the pavement where Fig. 5.8 shows the vertical moisture content distribution in the ditch.

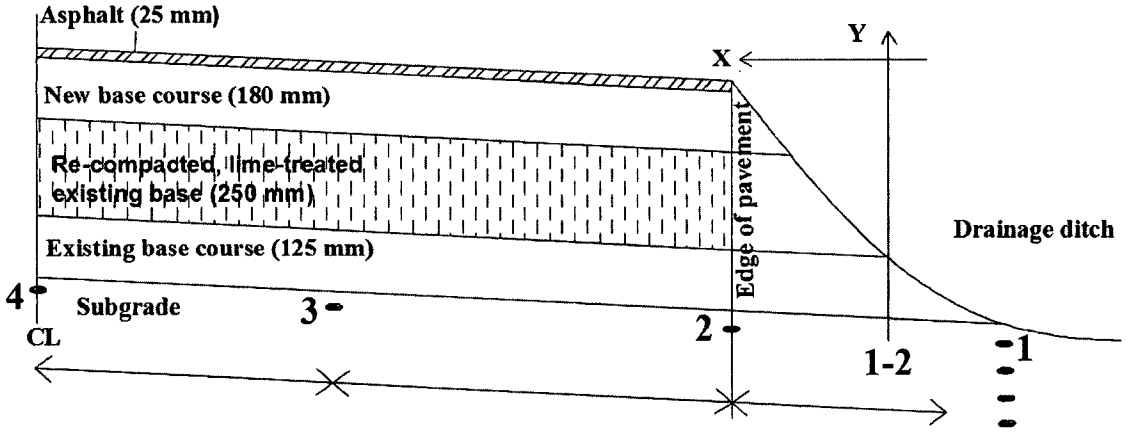


**Fig. 5.6 Placement of Horizontal and Vertical Moisture Sensors at FM 2 Site (Modified after Gupta [301])**

From the thirty year climate data of the pavement location the driest month was found July and the wettest month was found September as showed in the Fig. 5.9. Theoretically moisture distribution of the date close to July and September from Figs. 5.7 and 5.8 should be taken to replicate extreme shrinkage and replicate extreme heave condition.

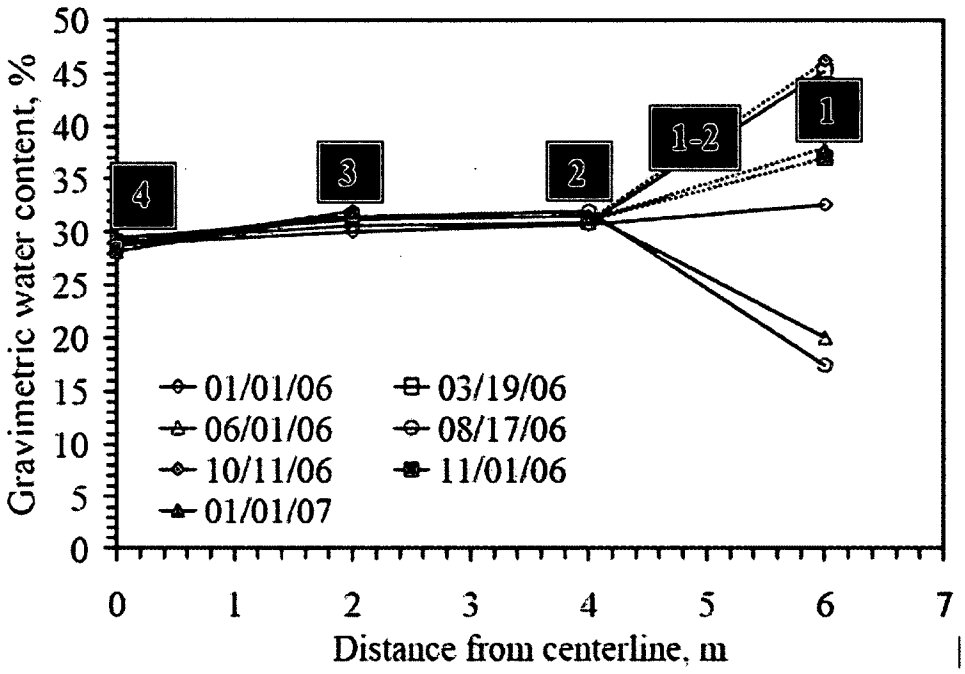


**Fig. 5.7 Horizontal Moisture Data from Four Sensors (Modified after Gupta [301])**

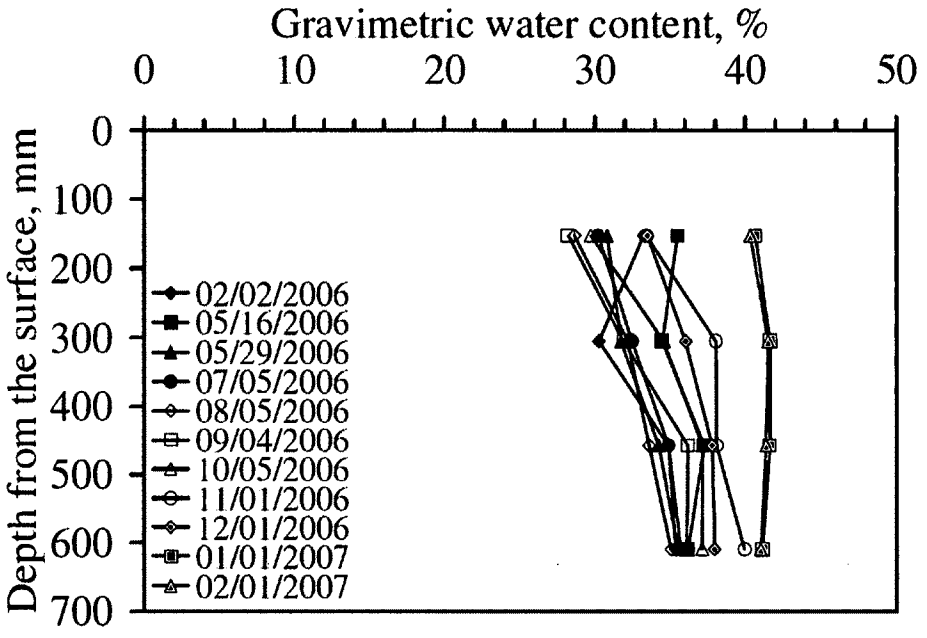


**Fig. 5.8 Vertical Moisture Data from Four Sensors [301]**

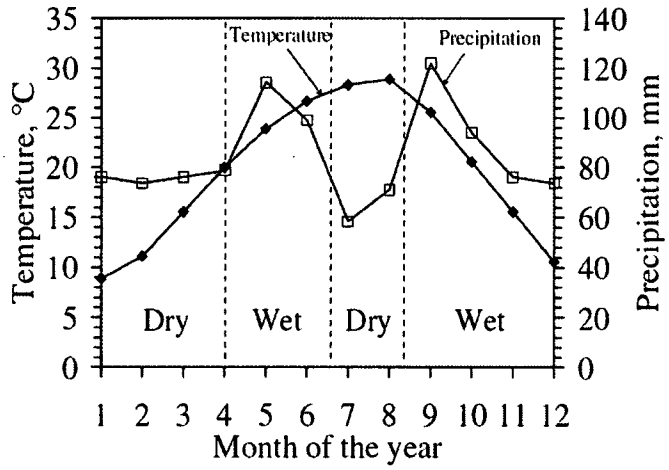


**Fig. 5.9 Wet and Dry Season at the Site Based on 30-year Average Climate Data [301]**

Ikra [300] used VADOSE/W to simulate the moisture distribution and calculate the heave underneath the Texas FM2 pavement. She used Daily weather data (from February 2, 2006 to February 1, 2007) from the station College Station, Bryan District of Texas was used to obtain the temperature, precipitation, relative humidity of FM 2 site. All those data showed the driest day was July 17$^{th}$ and the wettest day was January 20$^{th}$. Figure 5.10 shows the model which later she verified using the moisture distribution profile found from the model in the ditch at different dates with the moisture distribution found from Fig. 5.8 on those same dates.

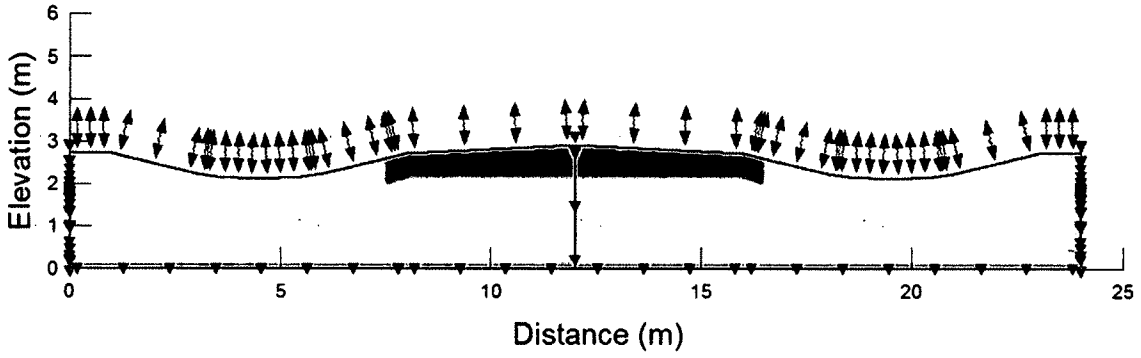


**Fig. 5.10 A Model Geometry used in VADOSE/W Simulation [300]**

Once the model is verified the extreme heave and shrinkage calculated from the VADOSE/W can be taken as a reference. In this analysis, the soil extreme heave and extreme shrinkage at the ditch (station 1) and the edge of the paved section (station 2) were taken from the VADOSE/W software. The soil heave and shrinkage at the edge of the shoulder (station 1-2) were calculated from the average heave and shrinkage of station 1 and station 2. At the pavement center there was no moisture content change and it is assumed no soil volume change at station 4. Finally, soil heave and shrinkage at stations in between station 2 and station 4 are linearly distributed as shown in Table 5.3.

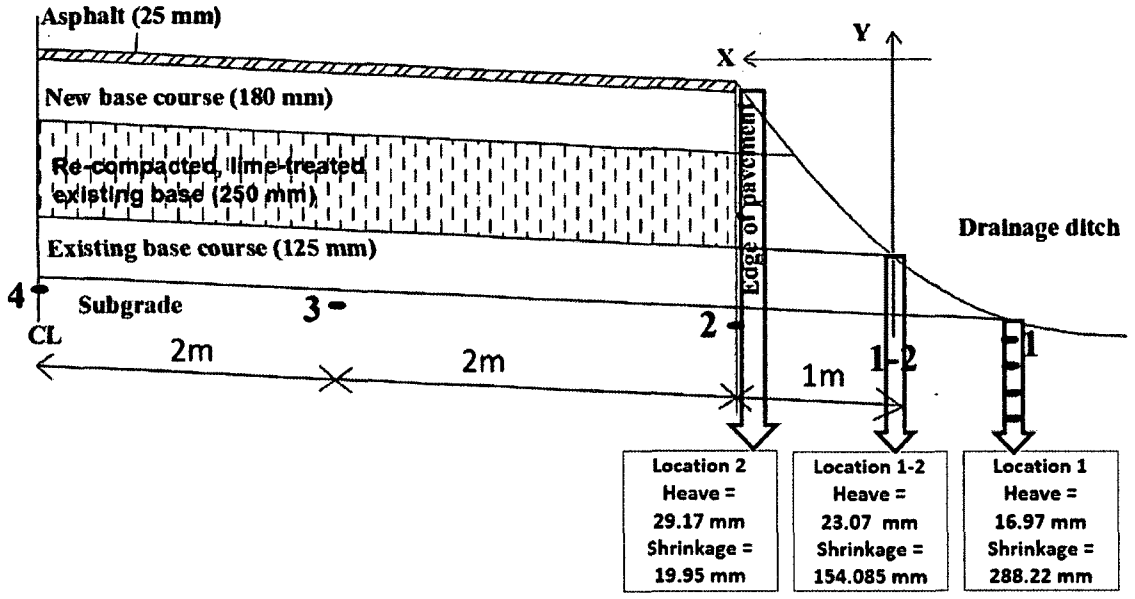


**Fig. 5.11 Soil extreme heave and shrinkage during one year found from the VADOSE/W Simulation**

**Table 5.3 Distribution of Moisture Content Change Induced Soil Deflection at the Cross-section of FM 2 Site**

| Moisture sensor station | Distance from the edge of the pavement | Extreme-heave condition | Extreme-shrinkage condition |
|---|---|---|---|
| | | Calculated heave (m) at different locations | Calculated shrinkage (m) at different locations |
| 1 | Ditch | 0.01697 | 0.2882 |
| 1-2 | 0.0 | 0.02307 | 0.1541 |
| | 0.3 | 0.02510 | 0.1094 |
| | 0.7 | 0.02714 | 0.0647 |
| 2 | 1.0 | 0.02917 | 0.0200 |
| | 1.3 | 0.02674 | 0.0168 |
| | 1.7 | 0.02431 | 0.0137 |
| | 2.0 | 0.02188 | 0.0106 |
| | 2.3 | 0.01945 | 0.0075 |
| | 2.7 | 0.01702 | 0.0043 |
| 3 | 3.0 | 0.01459 | 0.0012 |
| | 3.3 | 0.01215 | 0.0010 |
| | 3.7 | 0.00972 | 0.0008 |
| | 4.0 | 0.00729 | 0.0006 |
| | 4.3 | 0.00486 | 0.0004 |
| | 4.7 | 0.00243 | 0.0002 |
| 4 (Center) | 5.0 | 0.00000 | 0.0000 |

| Moisture sensor station | Distance from the edge of the pavement | Extreme-heave condition | Extreme-shrinkage condition |
|---|---|---|---|
| | | Calculated heave (m) at different locations | Calculated shrinkage (m) at different locations |
| | 5.3 | 0.00243 | 0.0002 |
| | 5.7 | 0.00486 | 0.0004 |
| | 6.0 | 0.00729 | 0.0006 |
| | 6.3 | 0.00972 | 0.0008 |
| | 6.7 | 0.01215 | 0.0010 |
| 3 | 7.0 | 0.01459 | 0.0012 |
| | 7.3 | 0.01702 | 0.0043 |
| | 7.7 | 0.01945 | 0.0075 |
| | 8.0 | 0.02188 | 0.0106 |
| | 8.3 | 0.02431 | 0.0137 |
| | 8.7 | 0.02674 | 0.0168 |
| 2 | 9.0 | 0.02917 | 0.0200 |
| | 9.3 | 0.02714 | 0.0647 |
| | 9.7 | 0.02510 | 0.1094 |
| 1-2 | 10.0 | 0.02307 | 0.1541 |
| 1 | Ditch | 0.01697 | 0.2882 |

### 5.7.3 Structural Analysis of Pavement Due to Extreme Soil Heave and Shrinkage

At first, the extreme soil heave/shrinkage is calculated from section 5.7.2. Once the heave/shrinkage values ($w_p$) is known then following the closed-form solution as described in section 5.4, the virtual load q(x) is found. Later the virtual load is used to find the deflection, rotation, bending moment, shear force, bending stress and shear stress of the pavement. Table 5.4 shows the extreme-heave condition and Table 5.5 shows the extreme-shrinkage condition deflection, rotation, bending moment, shear force, bending stress and shear stress at 31 locations of the 10-m pavement cross-section of the FM 2 road. A series of figures are plotted using the values of Tables 5.4 to 5.5. Figure 5.12 shows soil-heave-induced effects on the pavement, and Fig. 5.13 shows the shrinkage effect on the pavement. Table 5.6 shows the percent change of deflection, bending stress and shear stress between extreme heave and extreme-shrinkage conditions in the FM 2 road. From Table 5.6, it can be concluded that shrinkage has a more severe effect on the pavement than extreme-heave condition. Texas FM2 Pavement deflection increased by 369% and bending stress increased by 289%, but shear stress decreased by 422% in the extreme-shrinkage condition compared to extreme-heave condition. The maximum bending moment is found about 30 kPa during the extreme shrinkage condition. This peak value is found at 2.2-m from the shoulder edge. From the pictures of pavement, the longitudinal cracks occurs and propagates in between 1-m to 2.5-m. The location of the cracks found from the analytical solution would converge more with the field investigation if the whole cross-section including the shoulders of the pavement, is not taken as a paved section.

**Table 5.4 Pavement Structural Analysis Due to Virtual Load (Extreme Heave)**

| | Soil-heave-induced pavement properties | | | | | |
|---|---|---|---|---|---|---|
| x | $W_B(x)$, m | $\phi(x)$ | M(x), kN-m/m | V(x), kN/m | $\sigma$ (x), kPa | $\tau$ (x), kPa |
| 0.00 | -2.6E-02 | 1.2E-05 | 6.1E-16 | 2.9E-17 | 1.1E-14 | 7.4E-17 |
| 0.33 | -2.6E-02 | 4.6E-05 | -2.5E-01 | -3.0E+00 | -4.4E+00 | -7.6E+00 |
| 0.67 | -2.6E-02 | 2.8E-04 | -9.6E-01 | -5.3E+00 | -1.7E+01 | -1.4E+01 |
| 1.00 | -2.6E-02 | 8.5E-04 | -2.0E+00 | -6.5E+00 | -3.4E+01 | -1.7E+01 |
| 1.33 | -2.5E-02 | 1.9E-03 | -3.0E+00 | -6.1E+00 | -5.3E+01 | -1.6E+01 |
| 1.67 | -2.4E-02 | 3.3E-03 | -3.9E+00 | -4.2E+00 | -6.9E+01 | -1.1E+01 |
| 2.00 | -2.3E-02 | 4.9E-03 | -4.4E+00 | -1.1E+00 | -7.7E+01 | -2.8E+00 |
| 2.33 | -2.1E-02 | 6.7E-03 | -4.2E+00 | 2.9E+00 | -7.4E+01 | 7.3E+00 |
| 2.67 | -1.8E-02 | 8.2E-03 | -3.4E+00 | 6.9E+00 | -6.0E+01 | 1.8E+01 |
| 3.00 | -1.6E-02 | 9.3E-03 | -2.0E+00 | 1.0E+01 | -3.4E+01 | 2.7E+01 |
| 3.33 | -1.2E-02 | 9.7E-03 | 3.2E-03 | 1.3E+01 | 5.6E-02 | 3.3E+01 |
| 3.67 | -9.1E-03 | 9.3E-03 | 2.2E+00 | 1.3E+01 | 3.9E+01 | 3.4E+01 |
| 4.00 | -6.2E-03 | 8.0E-03 | 4.4E+00 | 1.2E+01 | 7.7E+01 | 3.1E+01 |
| 4.33 | -3.9E-03 | 5.8E-03 | 6.2E+00 | 9.3E+00 | 1.1E+02 | 2.4E+01 |
| 4.67 | -2.4E-03 | 3.1E-03 | 7.4E+00 | 5.0E+00 | 1.3E+02 | 1.3E+01 |
| 5.00 | -1.9E-03 | -9.3E-08 | 7.8E+00 | -2.0E-04 | 1.4E+02 | -5.0E-04 |
| 5.33 | -2.4E-03 | -3.1E-03 | 7.4E+00 | -5.0E+00 | 1.3E+02 | -1.3E+01 |
| 5.67 | -3.9E-03 | -5.8E-03 | 6.2E+00 | -9.3E+00 | 1.1E+02 | -2.4E+01 |
| 6.00 | -6.2E-03 | -8.0E-03 | 4.4E+00 | -1.2E+01 | 7.7E+01 | -3.1E+01 |
| 6.33 | -9.1E-03 | -9.3E-03 | 2.2E+00 | -1.3E+01 | 3.9E+01 | -3.4E+01 |
| 6.67 | -1.2E-02 | -9.7E-03 | 3.0E-03 | -1.3E+01 | 5.3E-02 | -3.3E+01 |
| 7.00 | -1.6E-02 | -9.3E-03 | -2.0E+00 | -1.0E+01 | -3.4E+01 | -2.7E+01 |
| 7.33 | -1.8E-02 | -8.2E-03 | -3.4E+00 | -6.9E+00 | -6.0E+01 | -1.8E+01 |
| 7.67 | -2.1E-02 | -6.7E-03 | -4.2E+00 | -2.9E+00 | -7.4E+01 | -7.3E+00 |
| 8.00 | -2.3E-02 | -4.9E-03 | -4.4E+00 | 1.1E+00 | -7.7E+01 | 2.8E+00 |
| 8.33 | -2.4E-02 | -3.3E-03 | -3.9E+00 | 4.2E+00 | -6.9E+01 | 1.1E+01 |
| 8.67 | -2.5E-02 | -1.9E-03 | -3.0E+00 | 6.1E+00 | -5.3E+01 | 1.6E+01 |
| 9.00 | -2.6E-02 | -8.5E-04 | -2.0E+00 | 6.5E+00 | -3.4E+01 | 1.7E+01 |
| 9.33 | -2.6E-02 | -2.8E-04 | -9.6E-01 | 5.3E+00 | -1.7E+01 | 1.4E+01 |
| 9.67 | -2.6E-02 | -4.6E-05 | -2.5E-01 | 3.0E+00 | -4.4E+00 | 7.6E+00 |
| 10.00 | -2.6E-02 | -1.2E-05 | -1.3E-09 | -2.2E-04 | -2.2E-08 | -5.6E-04 |
| ***Max*** | ***-1.9E-03*** | ***9.7E-03*** | ***7.8E+00*** | ***1.3E+01*** | ***1.4E+02*** | ***3.4E+01*** |
| ***Min*** | ***-2.6E-02*** | ***-9.7E-03*** | ***-4.4E+00*** | ***-1.3E+01*** | ***-7.7E+01*** | ***-3.4E+01*** |

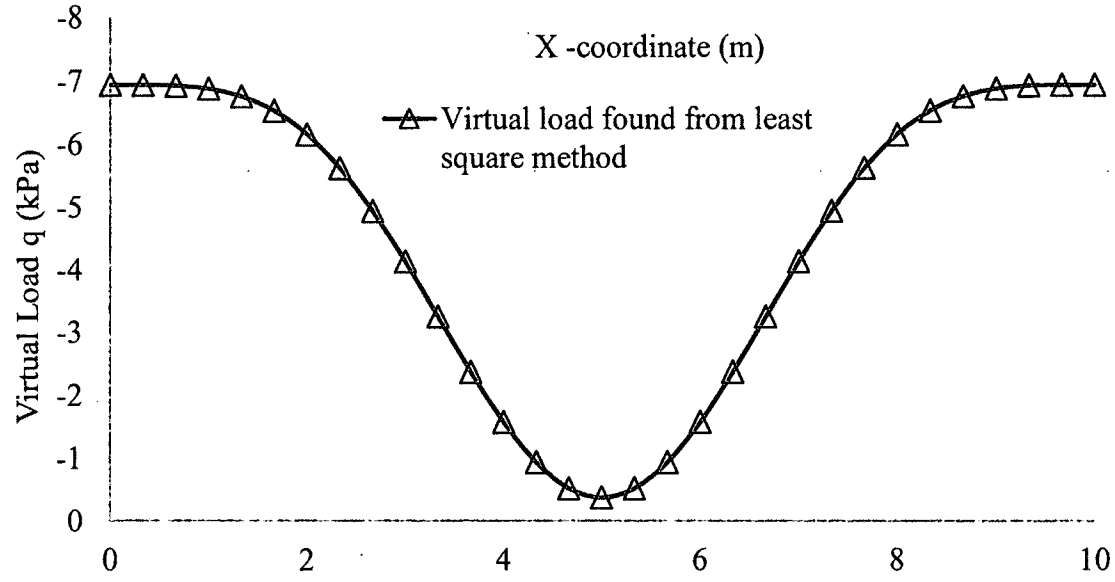


(a) Virtual Load

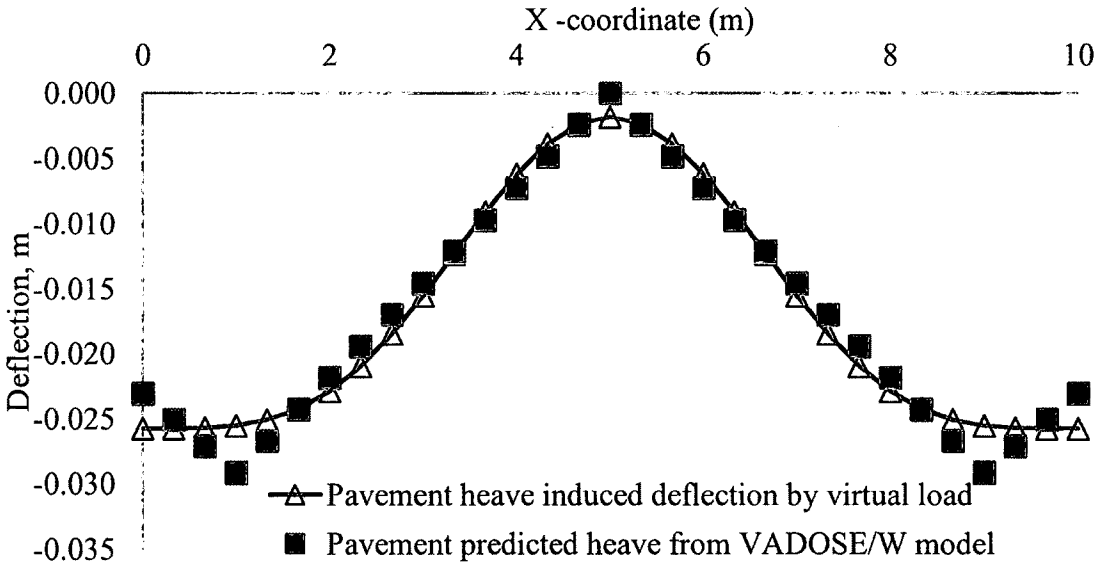


(b) Pavement Deflection

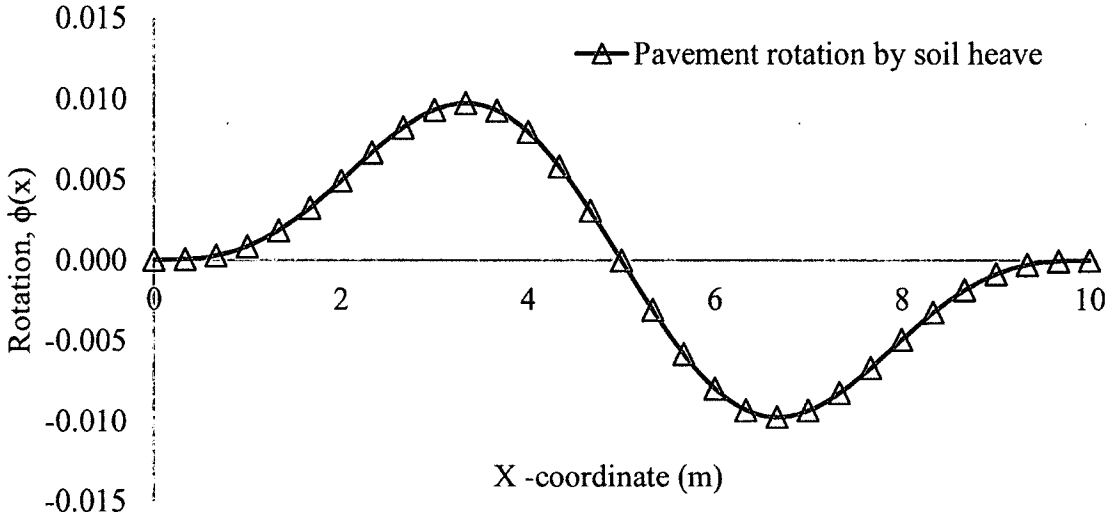


(c) Pavement Rotation

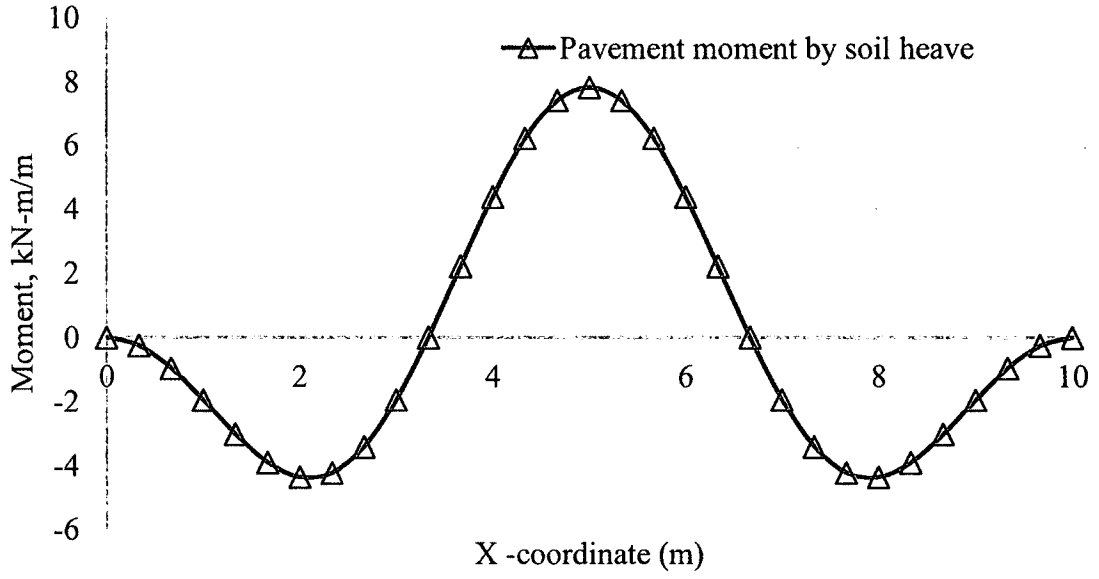


(d) Pavement Bending Moment

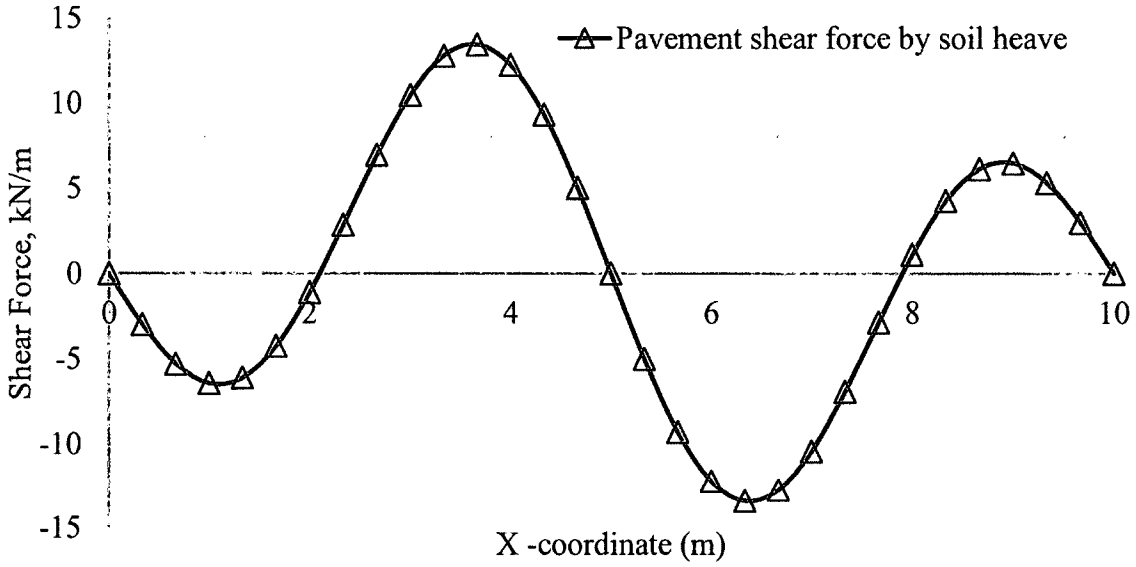


(e) Pavement Shear Force

**Fig. 5.12 Extreme-Heave Condition**

**Table 5.5 Pavement Structural Analysis Due to Virtual Load (Extreme Shrinkage)**

| | Soil-shrinkage-induced pavement properties | | | | | |
|---|---|---|---|---|---|---|
| x | $W_B(x)$, m | $\phi(x)$ | M(x), kN-m/m | V(x), kN/m | $\sigma$ (x), kPa | $\tau$ (x), kPa |
| 0.00 | 1.2E-01 | -6.3E-02 | 0.0E+00 | 2.1E-15 | 0.0E+00 | 5.3E-15 |
| 0.33 | 1.0E-01 | -6.3E-02 | -1.2E+00 | -2.8E+01 | -2.2E+01 | -7.3E+01 |
| 0.67 | 7.9E-02 | -6.2E-02 | -5.0E+00 | -5.1E+01 | -8.7E+01 | -1.3E+02 |
| 1.00 | 5.9E-02 | -5.9E-02 | -1.1E+01 | -6.6E+01 | -1.9E+02 | -1.7E+02 |
| 1.33 | 4.0E-02 | -5.3E-02 | -1.7E+01 | -7.0E+01 | -3.1E+02 | -1.8E+02 |
| 1.67 | 2.4E-02 | -4.5E-02 | -2.4E+01 | -6.4E+01 | -4.2E+02 | -1.6E+02 |
| 2.00 | 1.1E-02 | -3.4E-02 | -2.9E+01 | -4.9E+01 | -5.0E+02 | -1.3E+02 |
| 2.33 | 1.5E-03 | -2.2E-02 | -3.0E+01 | -2.7E+01 | -5.4E+02 | -7.0E+01 |
| 2.67 | -3.9E-03 | -1.0E-02 | -2.9E+01 | -3.4E+00 | -5.1E+02 | -8.6E+00 |
| 3.00 | -5.4E-03 | 7.2E-04 | -2.4E+01 | 1.9E+01 | -4.2E+02 | 4.9E+01 |
| 3.33 | -3.7E-03 | 9.0E-03 | -1.7E+01 | 3.6E+01 | -2.9E+02 | 9.3E+01 |
| 3.67 | 2.2E-04 | 1.4E-02 | -7.3E+00 | 4.5E+01 | -1.3E+02 | 1.2E+02 |
| 4.00 | 5.1E-03 | 1.5E-02 | 2.2E+00 | 4.5E+01 | 3.8E+01 | 1.2E+02 |
| 4.33 | 9.7E-03 | 1.2E-02 | 1.0E+01 | 3.6E+01 | 1.8E+02 | 9.2E+01 |
| 4.67 | 1.3E-02 | 6.9E-03 | 1.6E+01 | 2.0E+01 | 2.8E+02 | 5.1E+01 |
| 5.00 | 1.4E-02 | -1.6E-07 | 1.8E+01 | -6.8E-04 | 3.1E+02 | -1.7E-03 |
| 5.33 | 1.3E-02 | -6.9E-03 | 1.6E+01 | -2.0E+01 | 2.8E+02 | -5.1E+01 |
| 5.67 | 9.7E-03 | -1.2E-02 | 1.0E+01 | -3.6E+01 | 1.8E+02 | -9.2E+01 |
| 6.00 | 5.1E-03 | -1.5E-02 | 2.2E+00 | -4.5E+01 | 3.8E+01 | -1.2E+02 |
| 6.33 | 2.2E-04 | -1.4E-02 | -7.3E+00 | -4.5E+01 | -1.3E+02 | -1.2E+02 |
| 6.67 | -3.7E-03 | -9.0E-03 | -1.7E+01 | -3.6E+01 | -2.9E+02 | -9.3E+01 |
| 7.00 | -5.4E-03 | -7.2E-04 | -2.4E+01 | -1.9E+01 | -4.2E+02 | -4.9E+01 |
| 7.33 | -3.9E-03 | 1.0E-02 | -2.9E+01 | 3.4E+00 | -5.1E+02 | 8.6E+00 |
| 7.67 | 1.5E-03 | 2.2E-02 | -3.0E+01 | 2.7E+01 | -5.4E+02 | 7.0E+01 |
| 8.00 | 1.1E-02 | 3.4E-02 | -2.9E+01 | 4.9E+01 | -5.0E+02 | 1.3E+02 |
| 8.33 | 2.4E-02 | 4.5E-02 | -2.4E+01 | 6.4E+01 | -4.2E+02 | 1.6E+02 |
| 8.67 | 4.0E-02 | 5.3E-02 | -1.7E+01 | 7.0E+01 | -3.1E+02 | 1.8E+02 |
| 9.00 | 5.9E-02 | 5.9E-02 | -1.1E+01 | 6.6E+01 | -1.9E+02 | 1.7E+02 |
| 9.33 | 7.9E-02 | 6.2E-02 | -5.0E+00 | 5.1E+01 | -8.7E+01 | 1.3E+02 |
| 9.67 | 1.0E-01 | 6.3E-02 | -1.2E+00 | 2.8E+01 | -2.2E+01 | 7.3E+01 |
| 10.00 | 1.2E-01 | 6.3E-02 | -1.0E-08 | -1.7E-03 | -1.8E-07 | -4.4E-03 |
| ***Max*** | ***1.2E-01*** | ***6.3E-02*** | ***1.8E+01*** | ***7.0E+01*** | ***3.1E+02*** | ***1.8E+02*** |
| ***Min*** | ***-5.4E-03*** | ***-6.3E-02*** | ***-3.0E+01*** | ***-7.0E+01*** | ***-5.4E+02*** | ***-1.8E+02*** |

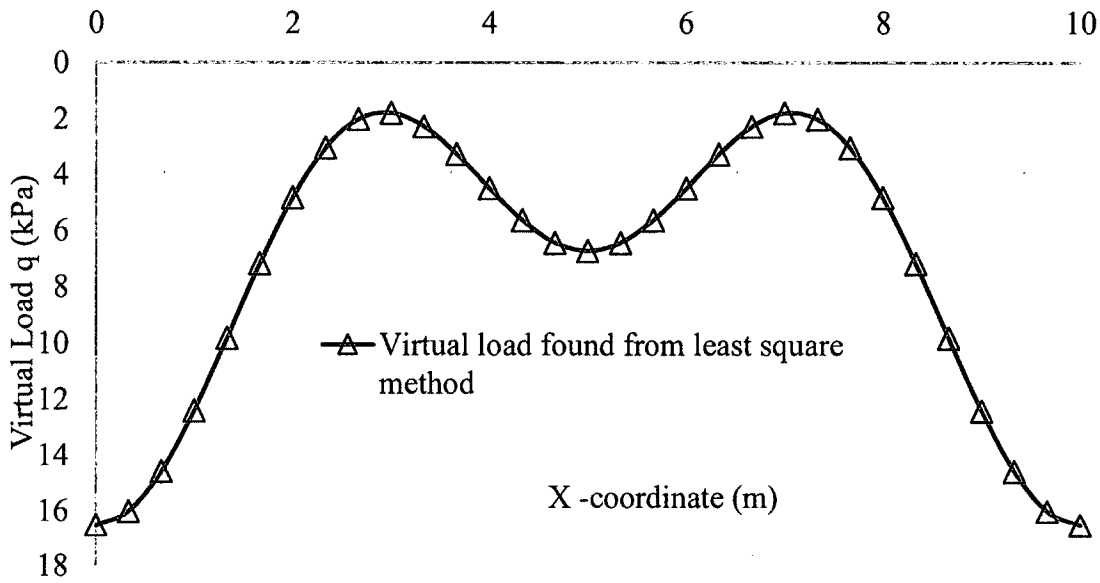


(a) Virtual Load

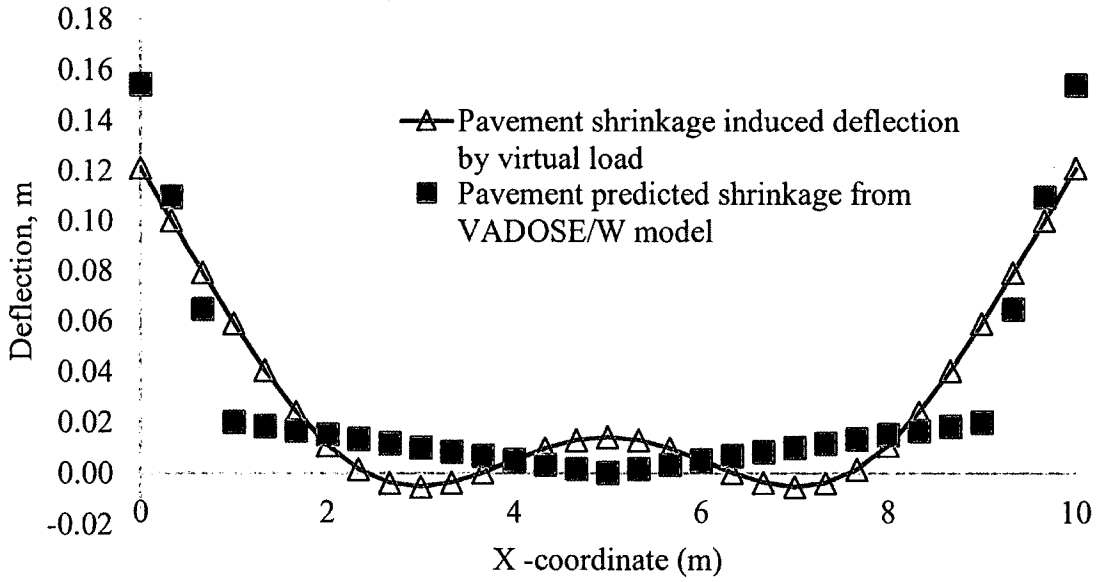


(b) Pavement Deflection

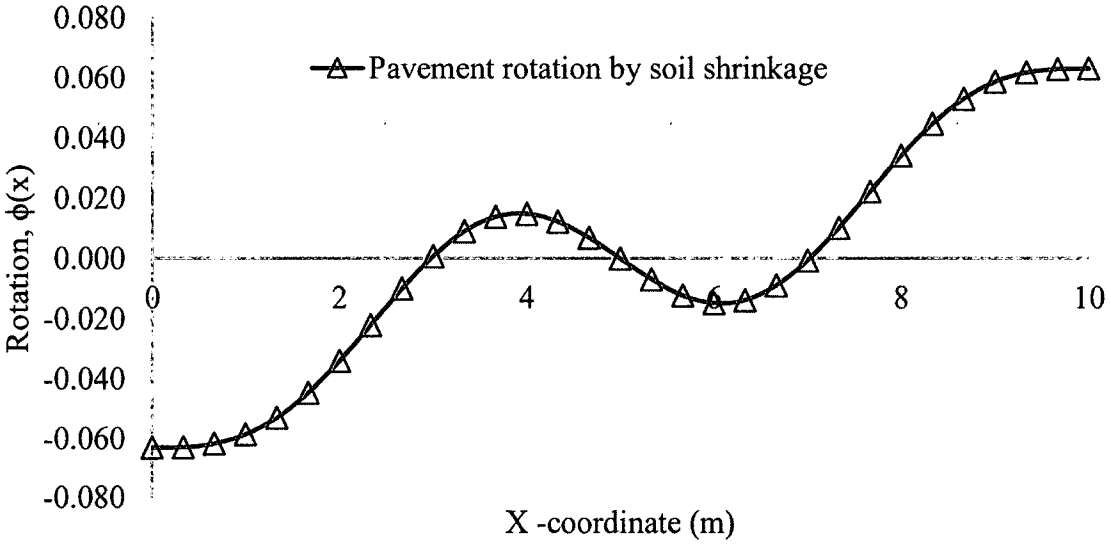


(c) Pavement Rotation

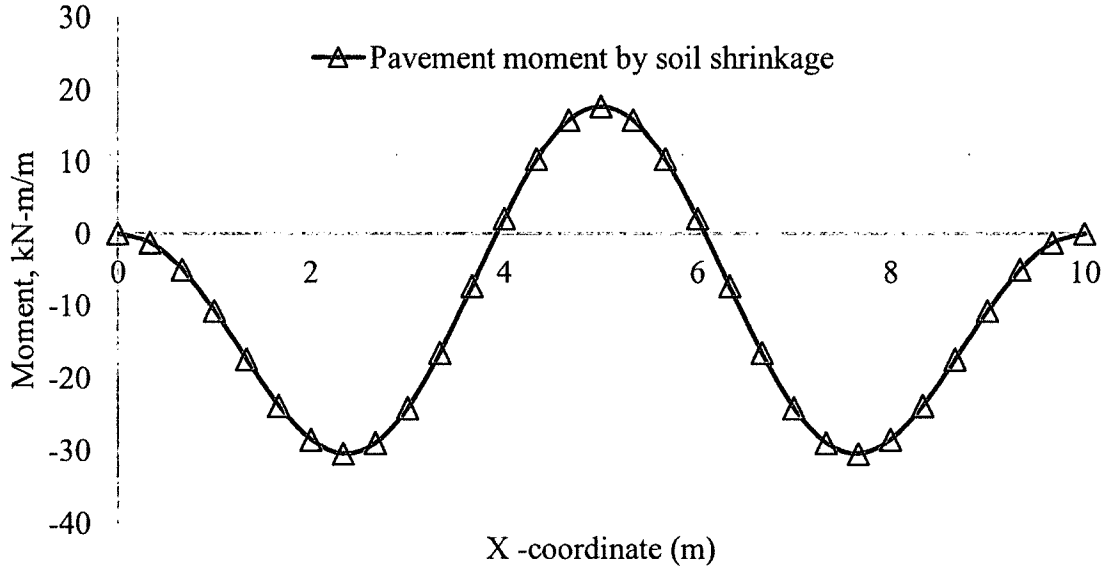


(d) Pavement Bending Moment

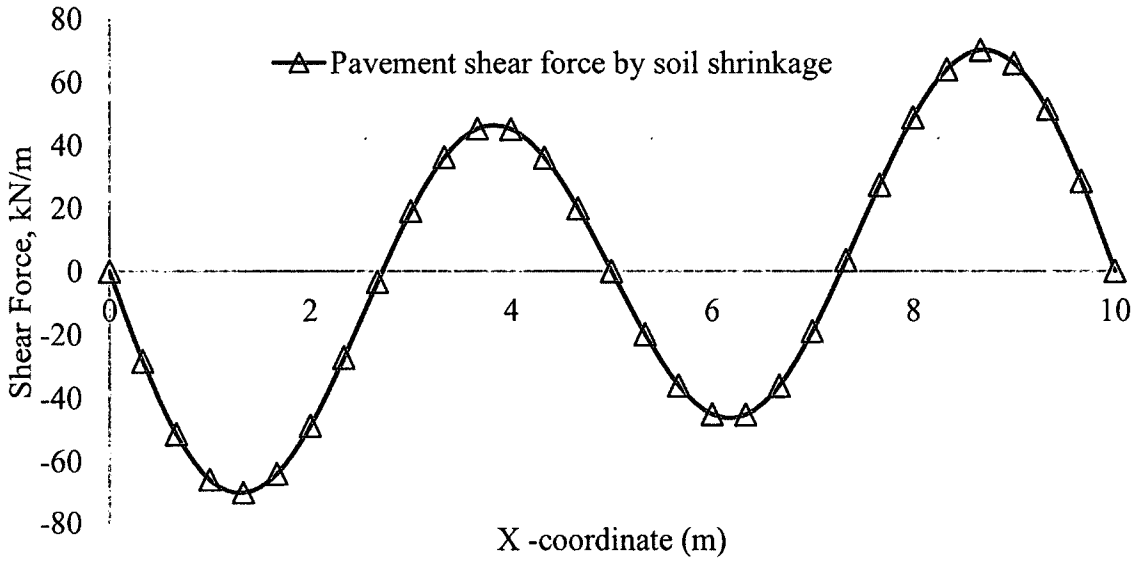


(e) Pavement Shear Force

**Fig. 5.13 Extreme-Shrinkage Condition**

**Table 5.6 Change of Pavement Structural Properties in Extreme Condition**

| | Maximum $W_B(x)$, (m) | | Maximum $\sigma$ (x), kPa | | Maximum $\tau$ (x), kPa | |
|---|---|---|---|---|---|---|
| | Extreme heave | Extreme shrinkage | Extreme heave | Extreme shrinkage | Extreme heave | Extreme shrinkage |
| By virtual load | 2.6E-02 | 1.2E-01 | 1.4E+02 | 5.4E+02 | 3.4E+01 | 1.8E+02 |
| % Change | 369 | | 289 | | 422 | |

## 5.8 Conclusion

From the moisture content sensor data, it was shown that the FM 2 pavement over expansive soil experiences more shrinkage than heave. As the soil volume change prediction is used to measure pavement deflection through regression, at shrinkage, the pavement experiences more bending moment than at the time of soil heave. This developed analytical method's performance is largely dependent on the accuracy of the

soil volume change prediction. In this research, soil volume change is calculated using VADOSE/W software. In the analytical method, using virtual load is a very simple but innovative idea, and from the plotted figures shows a good representation of how soil volume change affects pavement.

# CHAPTER 6

# SOIL STABILIZATION WITH GEOPOLYMER MATERIAL

## 6.1 Introduction

It is widely known that the production of Portland cement consumes considerable energy and at the same time contributes a large volume of $CO_2$ to the atmosphere. However, Portland cement is still the main binder in concrete construction prompting a search for more environmentally friendly materials. One possible alternative is the use of alkali-activated binder using industrial byproducts containing silicate materials. The most common industrial by-products used as binder materials are fly ash (FA) and ground granulated blast furnace slag (GGBS). GGBS has been widely used as a cement replacement material due to its latent hydraulic properties, while fly ash has been used as a pozzolanic material to enhance the physical, chemical and mechanical properties of cements and concretes. GGBS is a latent hydraulic material which can react directly with water, but requires an alkali activator. In concrete, this is the Ca(OH)2 released from the hydration of Portland cement. The term "geopolymeric" is used to characterize this type of reaction from the previous one, and accordingly, the name geopolymer has been adopted for this type of binder. The geopolymeric reaction differentiates geopolymer from other types of alkali activated materials (such as; alkali activated slag) since the product is a polymer rather than C-S-H gel.

In this chapter, soil stabilization using geopolymer will be evaluated. A series of soil samples were prepared with different concentrations of geopolymer and cement, and they were allowed to stabilize for 7, 14 and 30 days. Finally, experiments were conducted to evaluate their stabilization performance with concentration and time.

## 6.2 Geopolymer

Geopolymers are made up of aluminosilicate-based cementitious materials. It has properties similar to cement (i.e., high strength and strength gain rate, superior resistance to corrosion, heat and chemical attack, and low permeability) with a lesser carbon footprint than cement [302]. According to Davidovits [303], for every ton of Portland cement produced, one ton of carbon dioxide is released into the atmosphere, making it a serious concern to the global greenhouse gas effect. One of the impressive things about geopolymer is it can be produced either by naturally occurring raw materials (i.e., clay, mica, etc.) or by making use of industrial byproducts (i.e., fly ash and rice husk ash). One of the major problems is lack of awareness, and because Portland cement is used so widely, geopolymer is still perceived to be more of a laboratory product [304].

## 6.3 Geopolymer Chemistry

Geopolymer works like fly ash in the presence of an activator solution created of geopolymeric chains, which is referred to as geopolymerization. The empirical formula developed by Davidovits [303] for aluminosilicate can be written as $M_n\{-(SiO_2)_z-AlO_2)_n.wH_2O$ where M can be any number of cation (i.e., $Na^+$, $K^+$, $Ca^{++}$ , $Ba^{++}$, $NH_4^+$, $H_3O^+$), and n is the degree of polymerization. The letter z represents 1, 2, or 3,

determining the resulting geopolymer net. For the case of Z=1, the net will be of the polysialate type. If Z=2, the net will be a poly(sialate-siloxo), and if Z=3, the net will be a poly(sialate- disiloxo) [304]. Figure 6.1 presents the structural model proposed by Davidovits [302]. Scientists Van Deventer and Xu [305] described the three main steps of geopolymerization, which are described here. These four steps typically overlap each other under thermal curing and are hard to recognize in the reaction process [304].

1. Dissolution of silicon and aluminum species from the source material through the action of a highly alkaline solution.
2. Transportation of species and formation of monomers.
3. Polycondensation and growth of polymeric structures, resulting in the hardening of the material.

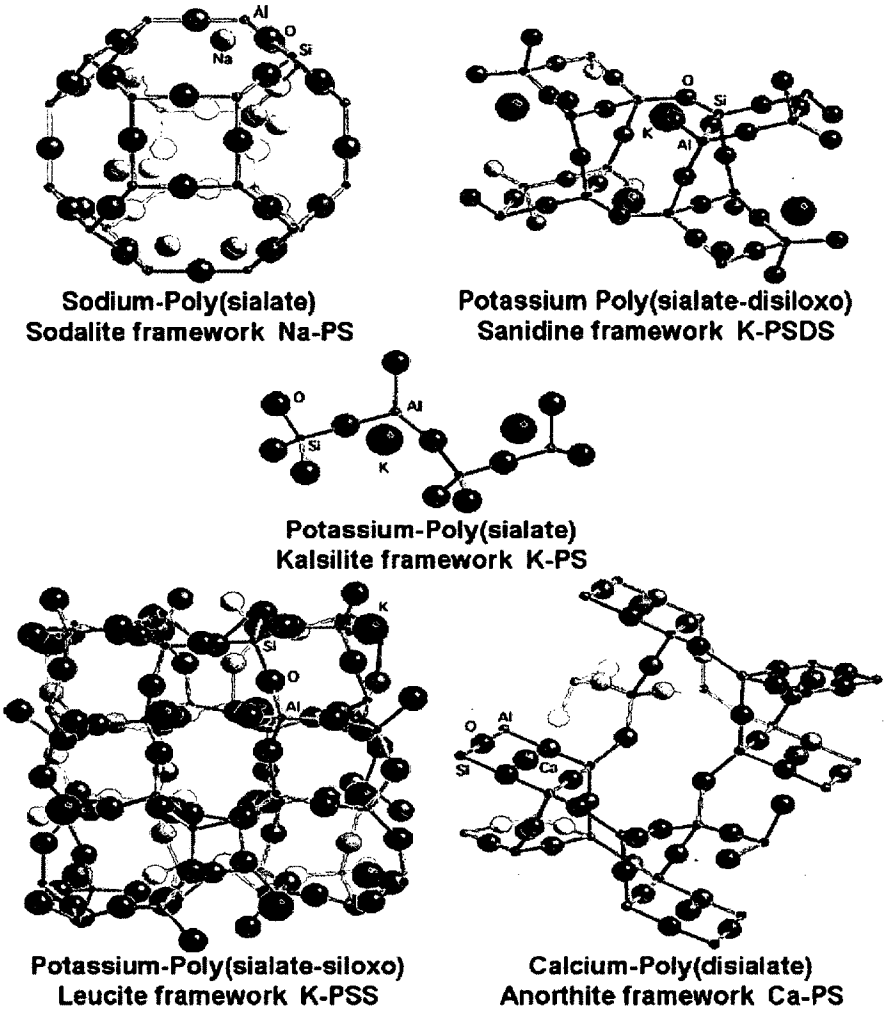


**Fig. 6.1 Structural Model of Geopolymer Proposed by J. Davidovits [302]**

## 6.4 Important Definition of Geopolymer

*Fly ash:* Fly ash is defined by the American Concrete Institute, ACI 116R, as "the finely divided residue that results from the combustion of ground or powdered coal and that is transported by flue gases from the combustion zone to the particle removal system" [306]. Fly ash, which is transported along with the flue gases and captured by pollution control devices, namely, electro precipitators or bughouses and occasionally by scrubber systems, is a very fine and powdery material made of spherical shaped particles that are in the range of a few microns to 100 μm [304]. Typically, a small portion of the

chemical composition is arranged in crystalline form, mainly quartz and mullite, and the rest are amorphous with no particular arrangement due to rapid cooling after leaving the boiler [226]. Fly ash is classified according to ASTM standard C618 into three different groups:

Class F fly ash is generally found as a byproduct of the burning of either lignite (or sub-bituminous) coal and anthracite (or bituminous) coal. The minimum requirement of summation of silicon, aluminum, and iron oxide is 70% with an Loss of Ignition (LOI) and calcium oxide maximum value of 6% and 10%, respectively [304].

Class C fly ash is generally found from lignite, sub-bituminous, anthracite and bituminous coal. This slightly cementitious fly ash allows a maximum summation of silicon, aluminum and iron oxide up to 50%, a maximum LOI of 6% and a minimum calcium oxide of 10% [304].

Class N fly ash is generally found from raw or calcine natural pozzolans such as opaline cherts, shales, volcanic ashes, pumicite and various materials. It has a requirement of a minimum summation of 70% of silicon, aluminum and iron oxide, as well as a maximum LOI of 10% [304].

*Add-water geopolymer:* Generally, geopolymer is used with its caustic activators, which may cause safety issues. For this reason, add-water geopolymer was developed in the construction industry, and it performs similarly to ordinary Portland cement (OPC). In this research, to produce add-water geopolymer, METSO® 2048 from PQ® was used.

## 6.5 Soil Stabilization Experiment Design

There is no standardized method for soil stabilization with geopolymer so far. In this research, an experiment was designed to evaluate soil stabilization with geopolymers.

For this process, four batches of soil samples were produced, and each batch of soil was mixed with either 5%, 10% or 20% geopolymer cement (GPC) and 10% cement by weight. Each batch consisted of three samples.

The procedure of producing GPC is described as follows:

1. 60 gm METSO® beats were mixed with 100 gm water to make a solution (Fig. 6.2a).
2. 100 gm fly ash were taken.
3. 100 gm fly ash were then mixed with 13 gm METSO® solution, creating 0.13 GPC (Fig. 6.2b).

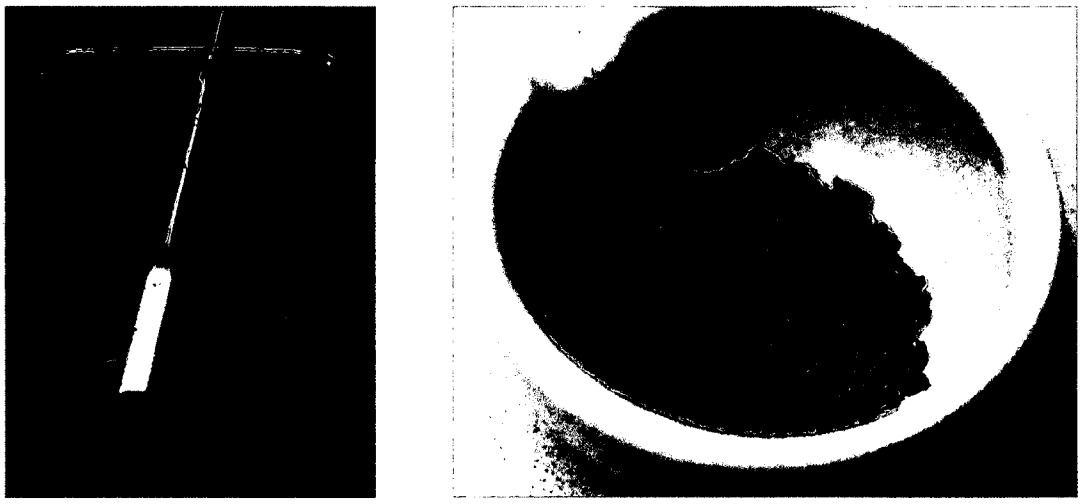

(a) (b)

**Fig. 6.2 (a) METSO® Solution and (b) 0.13 GPC**

The procedure for soil sample preparation is described as follows:

1. 500 gm expansive soil passed through 0.420 mm sieve were mixed with either 5%, 10% or 20% GPC, and 10% cement by weight.
2. To make a thorough mix, additional water was added. To find the minimum water to be added, water was added little by little to find the minimum moisture content

needed to make a thorough soil paste of soil and GPC. In every batch, the same moisture content was maintained so that the final results could be comparable with each other. The moisture content was found to be 27%, and a different amount of water was added in 5%, 10% or 20% GPC and 10% cement to make sure every batch had a 27% moisture content.

3. Once the soil batches were produced, they were placed in tube-like containers.
4. In containers soils were placed in three layers with 30 tamping in each layer.
5. After the tamping the samples were covered with a plastic covers to get air dried (Fig. 6.3).
6. The curing period was taken as 7 days, 14 days and 21 days.
7. After curing, the soil samples were taken out of the containers and again placed in the consolidation ring in three layers with 30 tamping in each layer.
8. Perform consolidation test of the nine samples, as illustrated in Fig. 6.4.

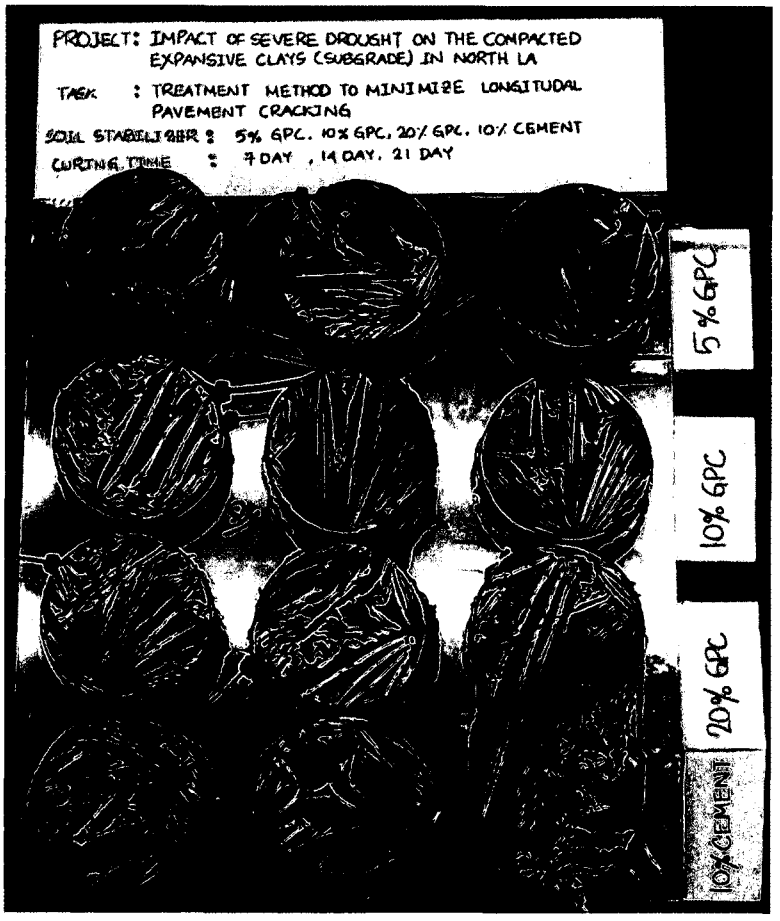


**Fig. 6.3 Stabilized Soil Samples under Curing Process**

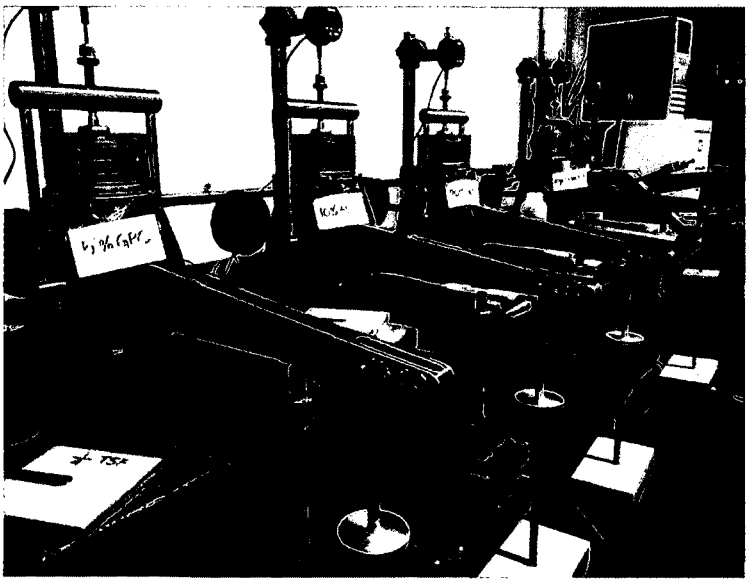

**Fig. 6.4 Consolidation Test of the Stabilized Soil**

6.5.1 Consolidation Test of the Stabilized Soil

Figs. 6.5 to 6.7 show the results of the consolidation test of all twelve soil samples. Finally, the relation between compression index ($C_c$) and swelling index ($C_s$) with curing time is shown in Figs. 6.8 and 6.9.

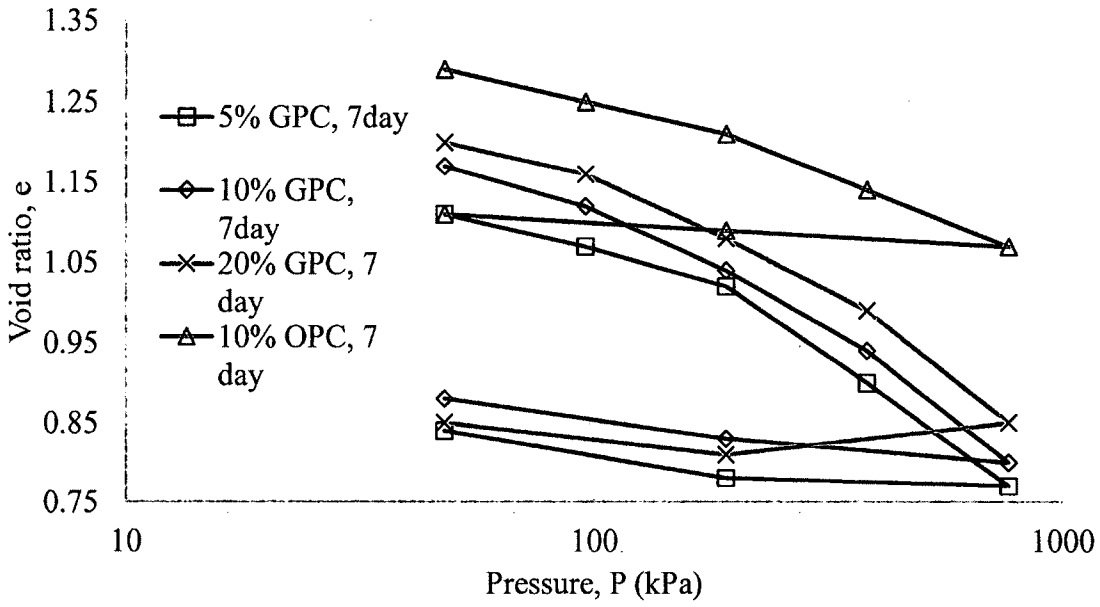


**Fig. 6.5 Seven-Day Soil Stabilization**

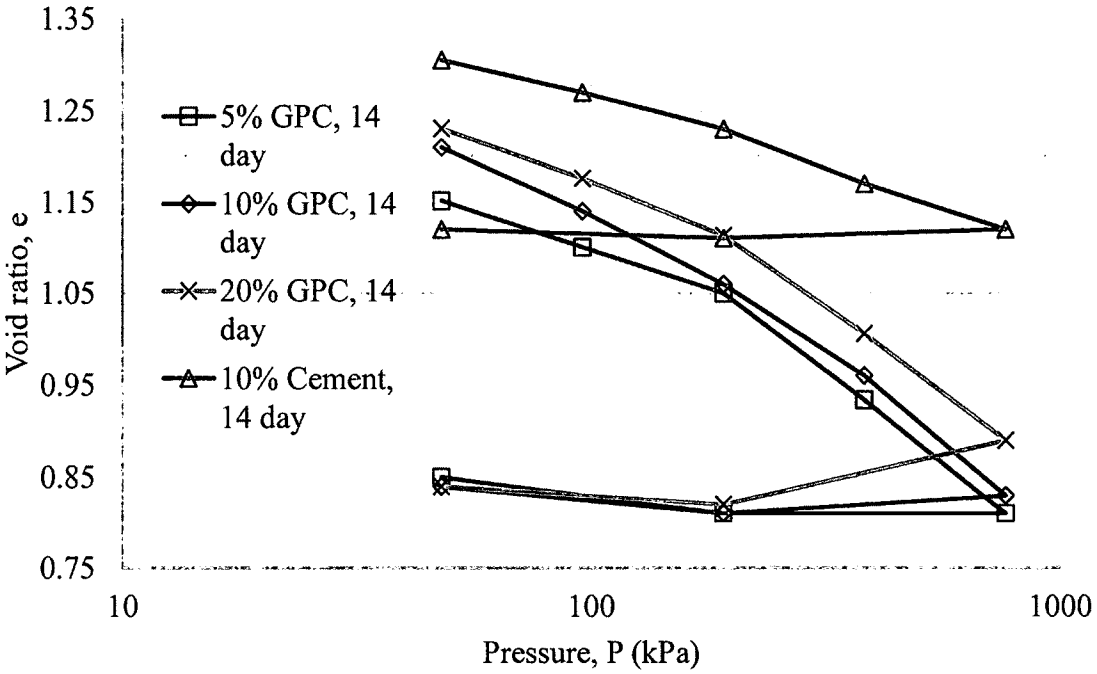


**Fig. 6.6 Fourteen-Day Soil Stabilization**

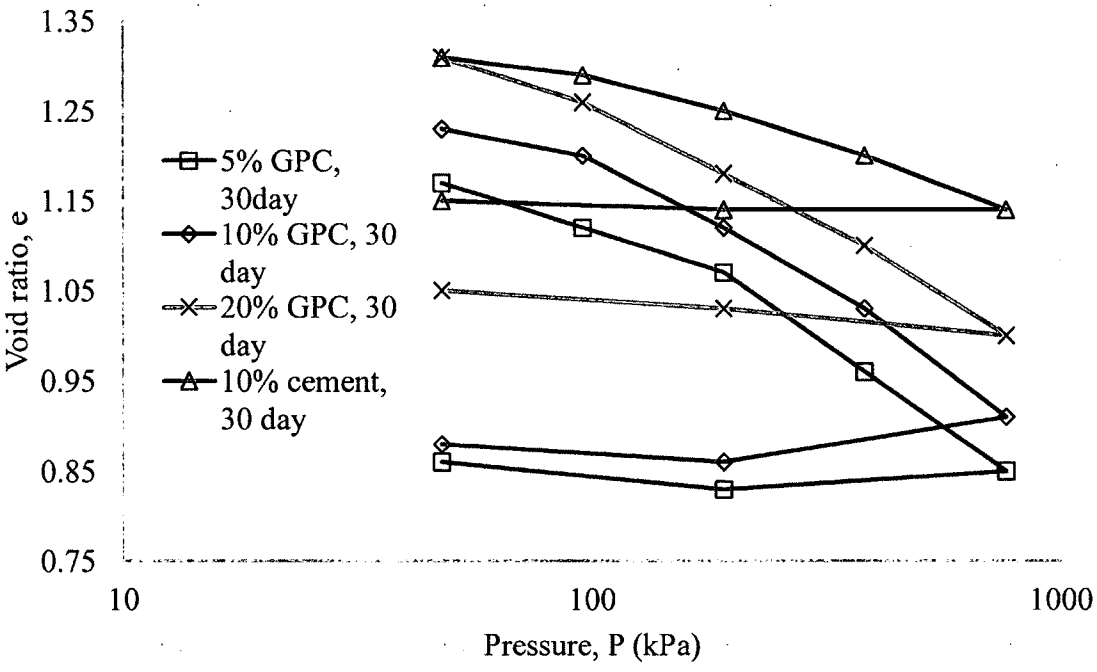


**Fig. 6.7 Thirty-Day Soil Stabilization**

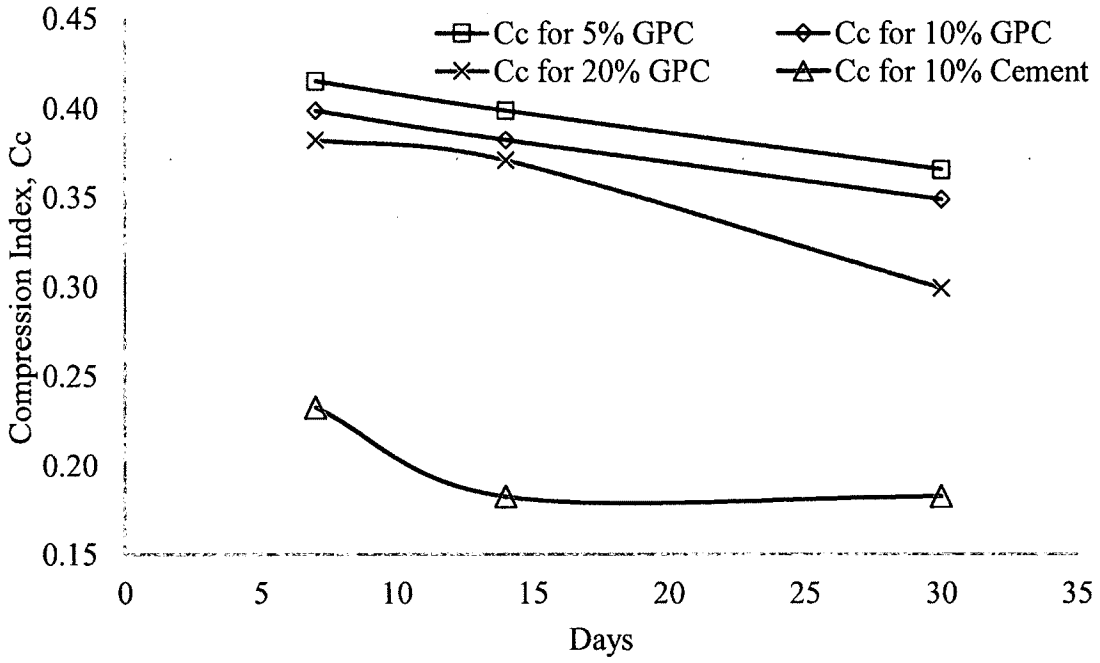


**Fig. 6.8 Relation Between Compression Index and Curing Time**

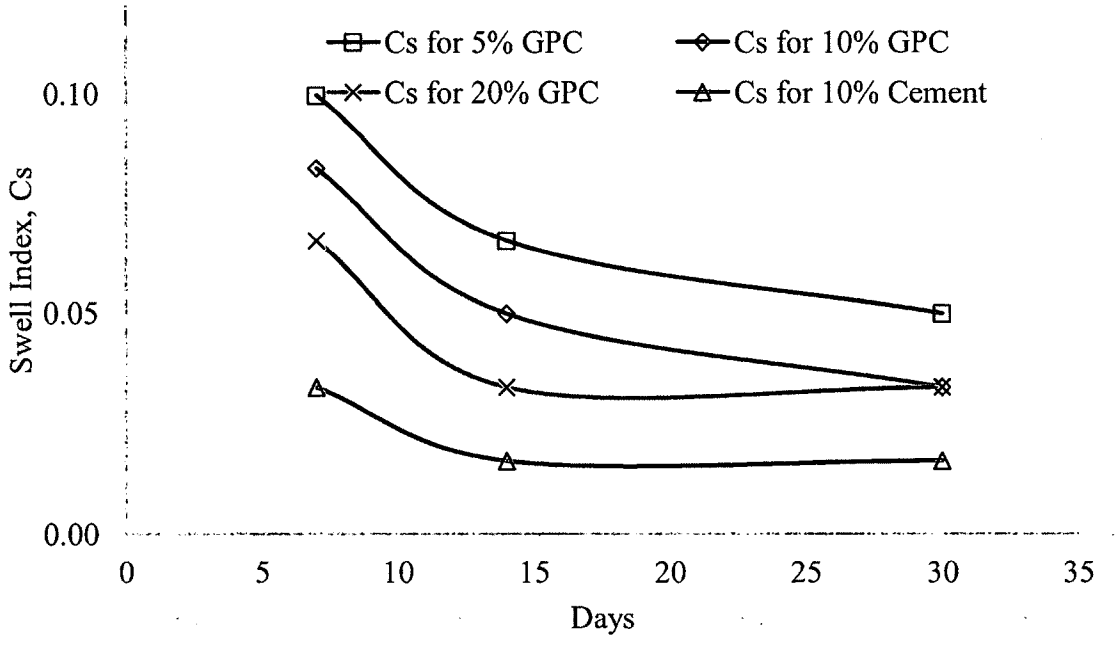


**Fig. 6.9 Relation Between Swelling Index and Curing Time**

## 6.6 Conclusion

The following conclusions can be made from this chapter:

1. As the GPC percentage is increased, the expansive soil becomes more stabilized with less void ratio change under the same pressure.
2. At any curing time, cement stabilizes soil better than GPC. Even 20% GPC, stabilizes soil under a specific load change more void than a 10% cement stabilized soil.
3. On average, 10% GPC stabilized soil has 90% more compression index than 20% GPC stabilized soil.
4. On average, 20% GPC stabilized soil has 77% more compression index than 10% cement stabilized soil.
5. On average, 10% GPC stabilized soil has 150% more swelling index than 20% GPC stabilized soil.
6. On average, 20% GPC stabilized soil has 100% more swelling index than 10% cement stabilized soil.

# CHAPTER 7

# EFFECT OF MOISTURE CONTENT ON GEOTHERMAL ENERGY

## 7.1 Introduction

Increased moisture content in soil can be used to harvest geothermal energy from the soil. This chapter describes the potential of heat-pump-based geothermal energy harvesting potential in Louisiana. Managing energy sources is one of the major challenges of the 21st century. Geothermal energy has far less carbon footprint than its hydrocarbon-based energy sources. Louisiana is still at an early stage in tapping its geothermal energy reserve. Most notable progress in this field is installing 10,000 ground source heat pumps in grout-filled boreholes at the Fort Polk Army base [251]. There are many types of heat-pump systems available. In this chapter, only the closed-loop, vertical heat exchanger system in Louisiana will be described. The closed-loop, vertical heat exchanger can be divided into two types: 1) borehole heat exchanger (Fig. 7.1), and 2) energy-pile heat exchanger (Fig. 7.2). In the borehole heat exchanger system, a vertical borehole will be constructed, and inside the borehole, U-tube will be placed. Finally, it will be filled with grout. However, in the energy-pile heat exchanger system, the building foundation pile will be used. During construction, U-tube will be placed inside the

concrete pile. Energy-pile heat exchanger systems are especially useful when there is a scarcity of free land around the building (i.e., apartments, offices in big cities, etc.). The fundamental method behind any kind of heat-pump system is that it uses the temperature difference between atmosphere and soil to heat and cool the building.

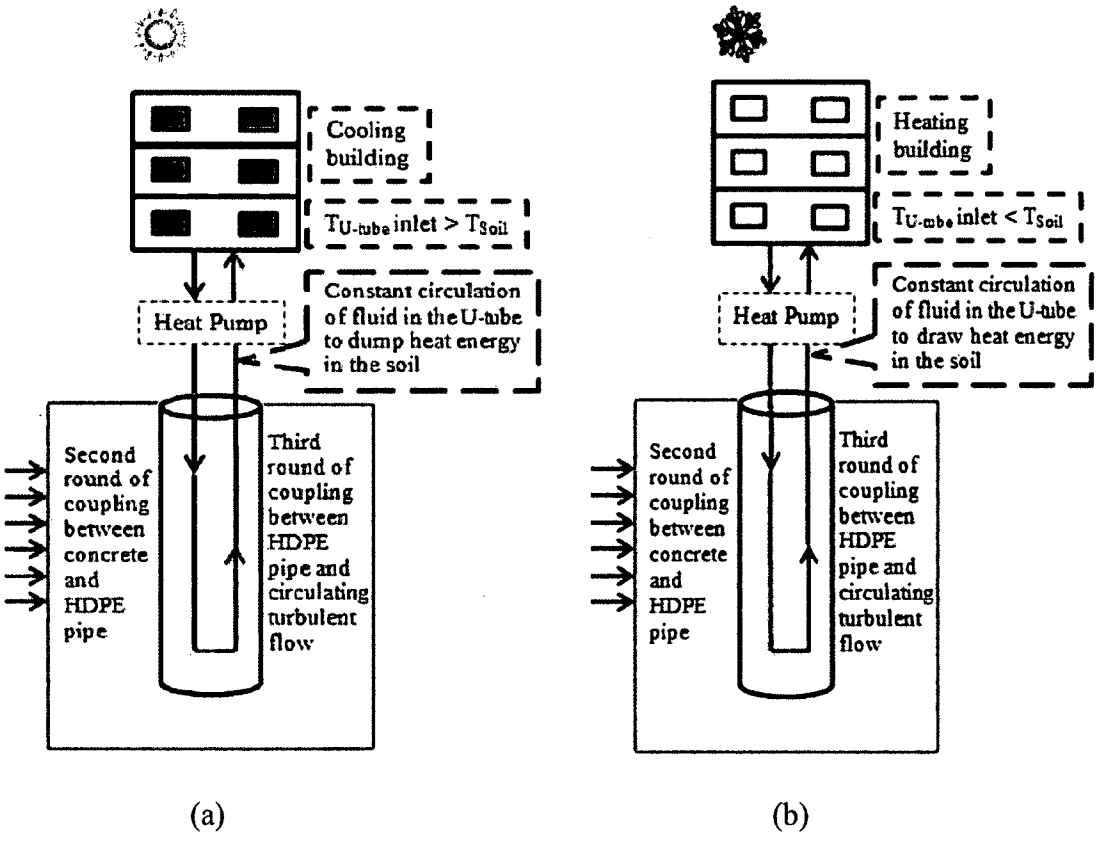


**Fig. 7.1 A Schematic Diagram of Energy-Pile Heat Exchanger in (a) Summer and (b) Winter [254]**

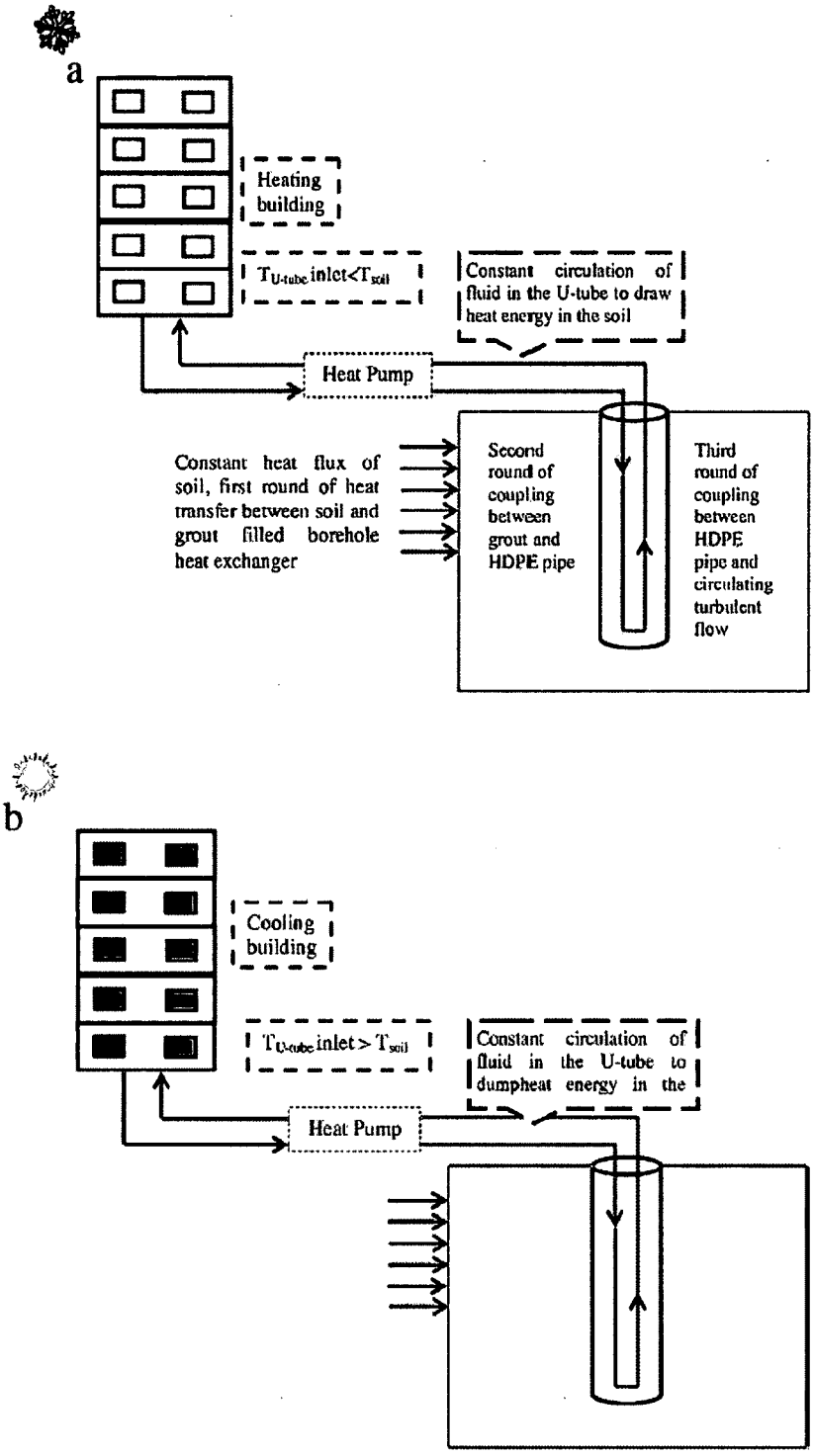


**Fig. 7.2 (a) A Schematic Diagram of a Borehole Heat Exchanger in Winter (b) A Schematic Diagram of a Borehole Heat Exchanger in Summer [253]**

## 7.2 Design Parameters of Heat-Pump Heat Exchanger System

*U-tube:* One of the most important design parameters of a heat-pump heat exchanger system is U-tube. In recent years, using high-density polyethylene (HDPE) pipe as a U-tube has become an industry standard. Generally, the pipe size is mentioned as "standard dimension ratio" or SDR. SDR can be placed inside a borehole or an energy pile as a single loop or as a double loop. Each loop type can be placed in three different orientations. Table 7.1 shows the relation between U-tube diameter and SDR, and Fig. 7.3 shows all three orientations for only single loop U-tube.

**Table 7.1 Equivalent Diameters and Thermal Resistances for Polyethylene U-Tube [307]**

| U-Tube Dia | SDR or Schedule | Pipe (Bore) Thermal Resistance (h•ft•F°/Btu) | | | |
|---|---|---|---|---|---|
| | | For Water Flows Above 2.0 US GPM | 20% Prop. Glycol Flow 3.0 US GPM | 20% Prop. Glycol Flow 5.0 US GPM | 20% Prop. Glycol Flow 10.0 US GPM |
| ¾ in. (0.15 ft) | SDR 11 | 0.09 | 0.12 | NR | NR |
| | SDR 9 | 0.11 | 0.15 | NR | NR |
| | SDR 40 | 0.10 | 0.14 | NR | NR |
| 1.0 in. (0.18 ft) | SDR 11 | 0.09 | 0.14 | 0.10 | NR |
| | SDR 9 | 0.11 | 0.16 | 0.12 | NR |
| | SDR 40 | 0.10 | 0.15 | 0.11 | NR |
| 1 ¼ in. (0.22 ft) | SDR 11 | 0.09 | 0.15 | 0.12 | 0.19 |
| | SDR 9 | 0.11 | 0.17 | 0.15 | 0.11 |
| | SDR 40 | 0.10 | 0.15 | 0.12 | 0.09 |
| 1 ½ in. (0.25 ft) | SDR 11 | 0.09 | 0.16 | 0.15 | 0.09 |
| | SDR 9 | 0.11 | 0.18 | 0.17 | 0.11 |
| | SDR 40 | 0.10 | 0.14 | 0.14 | 0.08 |

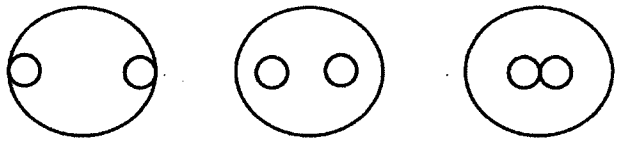

**Fig. 7.3 Possible U-tube Orientation in Borehole or Energy Pile**

*Fluid:* Inside the U-tube, there is a constant circulation of fluid. The fluid brings energy from the soil to the surface. The principle behind the heat transfer from the soil to the building is that the fluid, which has an atmospheric temperature, will be sent inside the soil from the surface. Once the fluid moves inside the soil, a heat transfer occurs between the soil and fluid because the soil temperature is not atmospheric, and, a heat transfer thereby occurs between the soil and fluid via the grout (borehole)/concrete (energy pile) and HDPE pipe. Thus, fluid is understood to be a critical part of the efficiency of this system. There are a few other elements that need to be remembered before selecting the type of fluid and the amount of fluid that will be circulated inside the U-tube. If the system is placed in the northern US, where the temperature at winter falls below the freezing point, antifreeze needs to be added to water. Methanol is a very common type of antifreeze used in the industry. In the southern US (i.e., Louisiana, etc.) direct water without any chemical can be used as the circulating fluid. Also, an important design parameter of the system is the discharge amount of the circulating fluid, which partly comes from the desired heat/cool energy. For example, a bigger building with an increased number of occupants needs more heating/cooling energy; therefore, more energy transfer may be needed, resulting in increased fluid discharge during circulation. Another important thing to be remembered is that there is a minimum flow rate needed inside the U-tube. Table 7.2 shows the minimum flow rate inside a U-tube. The reason behind maintaining the minimum flow rate is to make sure there is enough fluid velocity to keep the flow turbulent.

**Table 7.2 Minimum Flow Rate in Pipe [254]**

| Pipe size (m) | Minimum flow rate $\times 10^{-3}$ ($m^3/s$) | Pipe size (m) | Minimum flow rate $\times 10^{-3}$ ($m^3/s$) |
|---|---|---|---|
| 0.019 | 0.252 | 0.0381 | 0.757 |
| 0.0254 | 0.379 | 0.0508 | 1.136 |
| 0.0318 | 0.568 | 0.0762 | 2.254 |

*Soil temperature:* An energy pile operates with the assumption that soil temperature remains constant all year long at depths greater than 9.14 m [308]. During summertime, atmospheric temperature will be higher than the soil temperature, so heat transfer between the fluid and soil will take place. Again, in the winter time, the atmospheric temperature will go below the soil temperature, resulting in heat transfer between soil and fluid. Therefore, it is evident that the soil is the source of energy in this system. For this reason, in all the industrially available software location of the project is a design input. This location input will define the soil temperature in the simulation. This is because for a particular location the soil temperature at a certain depth may remain constant all through the year, but each location has its own constant soil temperature. Figure 7.4 shows the earth temperature at different locations in the US. For Louisiana, this temperature is 19.44$^0$C, as illustrated in Fig. 7.4.

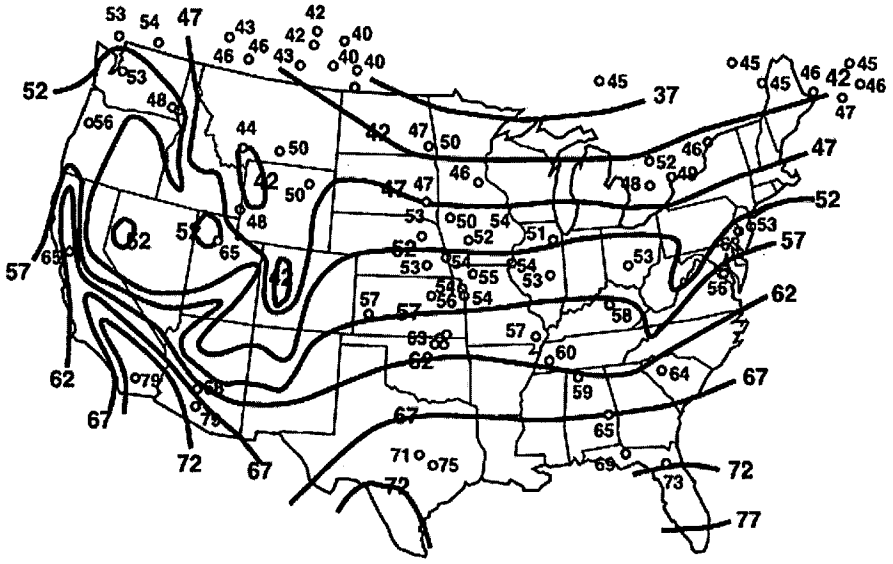

**Fig. 7.4 Mean Annual Earth Temperature in Fahrenheit Scale at Individual Stations, Superimposed on well-water Temperature Contours [254, 309, 310]**

*Borehole/energy-pile spacing:* Generally, boreholes/energy piles are constructed as a group. The reason behind this is, if one borehole/energy pile is used, then to have the design energy from the soil, the length of the borehole/energy pile must be huge to have the required surface area. The major cost in a borehole heat exchanger is the excavation cost. To make the heat exchanger system economical, the design is made in such a way that it requires the least amount of excavation work. Moreover, circulating the huge amount of fluid inside a very long borehole/energy pile will require a big energy-hungry circulating pump, which will at the end undermine the main objective of this system, which is to minimize the energy cost. Therefore, the spacing should not be so small that boreholes/energy piles interrupt each other's effective zone. Spacing should be varied within the allowable construction zone to find the most optimum distance.

*Inlet/outlet fluid temperature:* In general, the temperature gap between soil and atmosphere is very small. To increase the amount of heat transfer, an additional heat pump is used to increase the temperature difference. This will increase the overall efficiency of the system and is generally denoted as the coefficient of performance (COP). Figure 7.5 shows a typical system with a COP value of 4.

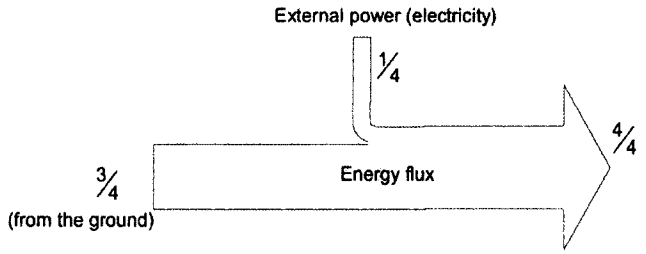


**Fig. 7.5 COP of a Heat-Pump System [311]**

*Circulation pump:* As mentioned before, to circulate the fluid inside the U-tube, a circulation pump is needed. Generally, commercial software has a data bank with all the industry available circulation pumps and can recommend the required strength pump from the list.

*Grout/concrete thermal conductivity (k):* The overall heat transfer process can be divided into three rounds, as shown in Figs. 7.1 and 7.2. The first round of coupling is done between ground soil and grout/concrete, the second round is done between grout/concrete and HDPE pipe, and finally, the third round is done between HDPE pipe and the circulating fluid. Therefore, the higher the grout/concrete heat transfer rate, the more energy can be transferred between ground soil and the U-tube carrying circulation fluid. From Table 7.3 it is seen that the thermal conductivity of the thermally enhanced concrete made from OPC can be as high as 2 W/m-$^0$C.

**Table 7.3 Thermal Conductivities of Typical Grouts and Backfills [254]**

| Grout and additives | k ($W/m^{*0}C$) | Thermal-enhanced grouts | k ($W/m^{*0}C$) |
|---|---|---|---|
| 20% Bentonite | 0.73 | 20% Bentonite – 40% Quartzite | 1.47 |
| 30% Bentonite | 0.74 | 30% Bentonite – 30% Quartzite | 1.21 – 1.30 |
| Cement mortar | 0.69-0.78 | 20% Bentonite – 40% Iron ore | 0.78 |
| Cement 2000/2500 $kg/m^3$ | 1.04-1.38 | 60% Quartzite – Flowable fill (Cement + fly ash + Sand) | 1.85 |
| Cement (50% quartz sand) | 1.9 – 2.94 | | |

*Borehole/energy-pile diameter:* The diameter of a borehole/energy pile is also an important parameter as it will define the surface area of heat transfer.

*Soil moisture content:* Soil moisture content is the most important factor that influences the extraction of geothermal energy. Clay soil retains more moisture than sandy soil; therefore, the presence of clay soil in the construction site will result in harvesting more geothermal energy from a shallow depth. For example, there is a high groundwater table in New Orleans, with the implication of high moisture content for ground soil. In the design, a value of 1.47 W/m-k was taken as the moist soil thermal conductivity [312]

A typical step-by-step design of a heat-pump geothermal energy system is shown in Fig. 7.6.

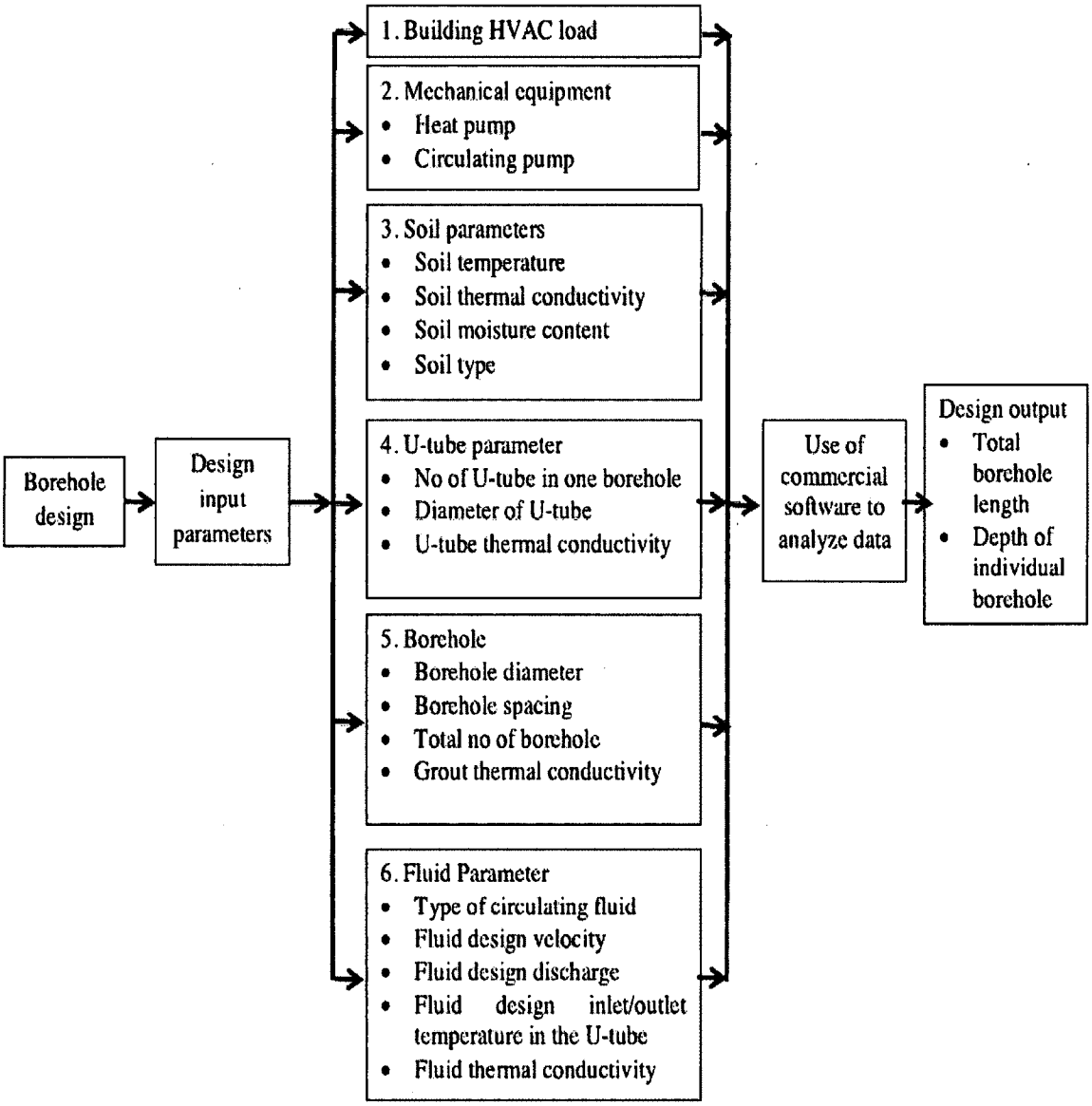


**Fig. 7.6 A Flowchart Demonstration of Typical Design Procedures of a Heat-Pump Geothermal Energy System [253]**

## 7.3 Design of an Energy Pile in South Louisiana

European countries like Austria and Switzerland are some of the first countries to pioneer using building foundation elements as a heat exchanger. At present, due to the ground-couple heat exchanger system's high efficiency and its environmental advantages, geothermal energy is becoming more popular day by day [311, 313, 314]. Concrete has a

high thermal conductivity and is, therefore, an ideal medium to exchange heat. Most commonly used energy foundations include piles and base slabs. Louisiana is still at an early stage in tapping its geothermal energy reserve. To investigate the potential use of geothermal energy through building foundations in South Louisiana, a building under construction in New Orleans was selected for analysis. The new 4-story office building with 2043.87 $m^2$ (22,000 $ft^2$) of footprint is situated on the same site of a previous building that was destroyed by Hurricane Katrina. This paper will estimate the amount of heating and cooling energy that can be extracted from underground using the existing, regular load-bearing pile foundation as an energy pile, as sketched in Fig. 7.7. The energy pile will use the temperature difference between atmosphere and soil to heat and cool the building. This energy will decrease the amount of cooling and heating of the building, which will finally result in less $CO_2$ emissions in the atmosphere.

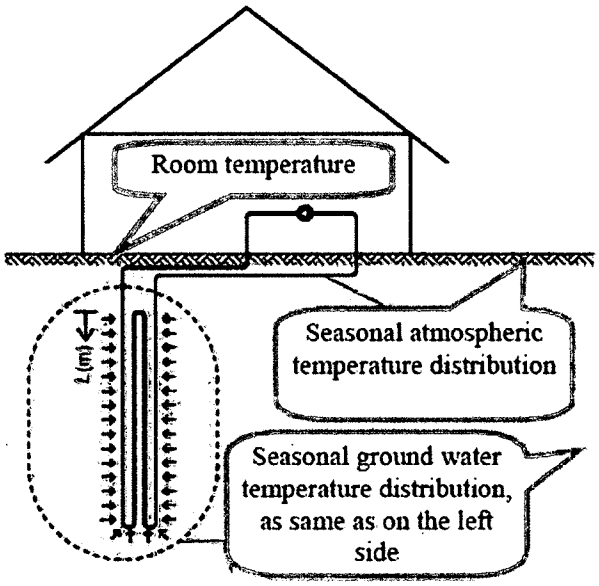


**Fig. 7.7 The First-Round Coupling: Atmosphere, Groundwater and Subsurface [310]**

### 7.3.1 Building Description

The structure is a four-story building. The first floor includes parking and an elevator lobby. Each of the upper floors provides 696.77 $m^2$ (7,500 $ft^2$) of office space. The building is supported by 0.33m- (12.75 in-) diameter open-ended steel H-piles with a wall thickness of 0.0064m (0.25 in). The design-compressive capacity of the pile foundation is 444.82 kN (50 tons), and the tensile capacity is 222.41 (25 tons). To handle these design loads, the largest pile group that is needed consists of nine piles, and the total number of piles under the building is 145. The footprint of the site is approximately 1048.70 $m^2$ (11,288 $ft^2$), and the building covers 723.99 $m^2$ (7,793 $ft^2$). The ground floor is used as a parking space with no heating/cooling unit installed, which means that a geothermal design will be done only for the $2^{nd}$, $3^{rd}$ and $4^{th}$ floors. According to the provided consultant geotechnical report, a pile depth of 24.38 m (80 feet) is used for compressive and tensile loads.

### 7.3.2 Heating, Venting, Air Conditioning (HVAC) Load of the Building

The pile foundation of the building was only designed by the construction company to carry the structural load. The design does not include any special features to use as an energy foundation. In this paper, the potential use of the existing pile foundation for geothermal energy extraction is studied. The four-story building is a cooling dominant structure, as expected of any building in South Louisiana. For any kind of geothermal design, the HVAC loading measurement is the most important part. As such, this value was used to measure the total pile length needed. Although the pile foundation of the building was designed only by considering the structural load, the

existing foundation was also used to evaluate how much energy could be extracted if the current pile spacing and pile length are used. The LEED Plus software provided by Gaia Geothermal Energy was employed to measure the energy demand of the building. In places like Louisiana, where the system should be designed as a more cooling-dominant system, there might be a few occasions where the system must run in its full capacity in cooling mode. For this reason, the percentage of running time in cooling mode is less than the percentage of running time in heating mode, as presented in Table 7.4.

**Table 7.4 HVAC Load of the Building using the LEED Plus Software [310]**

| Floor | Cooling Load (kW/hr) | % of run time in cooling mode | Heating Load (kW/hr) | % of run time in heating mode |
|---|---|---|---|---|
| $2^{nd}$ ,$3^{rd}$ , or $4^{th}$ | 147.27 | 21.9 | 39.54 | 57 |

Results found from the LEED Plus software were then used to produce Figs. 7.8 and 7.9. Figs. 7.8 and 7.9 show the annual energy consumption and corresponding expenses when using different types of energy to heat and cool this building. Finally, a comparison of $CO_2$ emissions according to energy source is given in Fig. 7.10. It is quite clear that geothermal energy is the greenest form of energy when compared to other types of energy sources. Furthermore, it will reduce the cost of HVAC significantly compared to other types of energy.

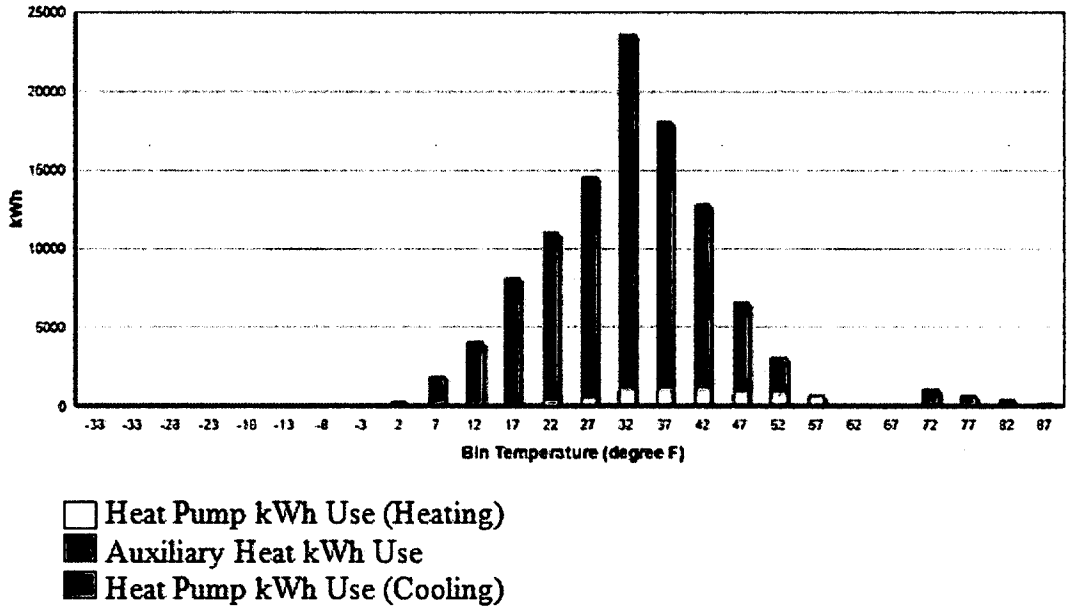


**Fig. 7.8 Annual Energy Consumption [310]**

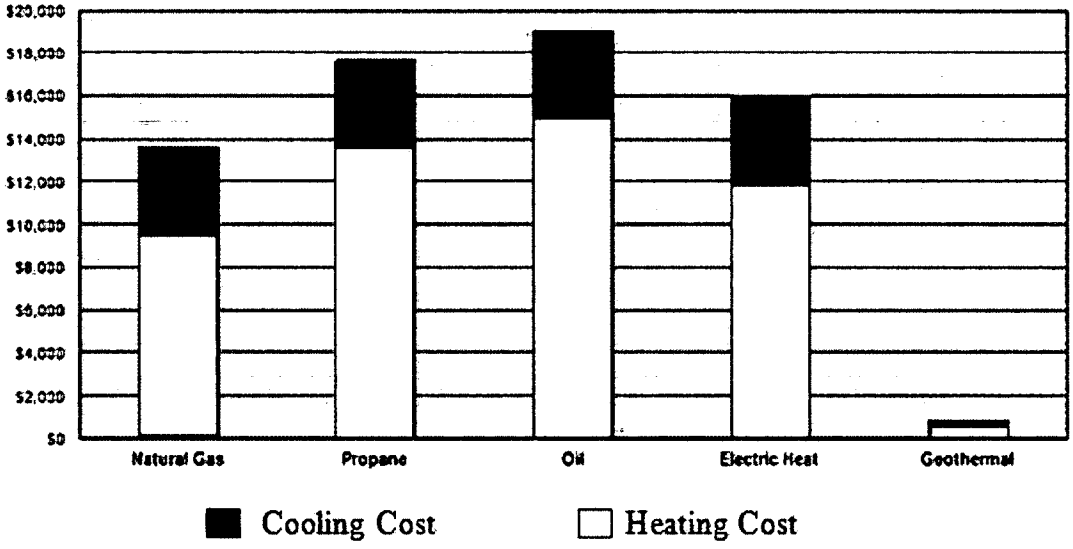


**Fig. 7.9 Annual Energy Cost Comparison [310]**

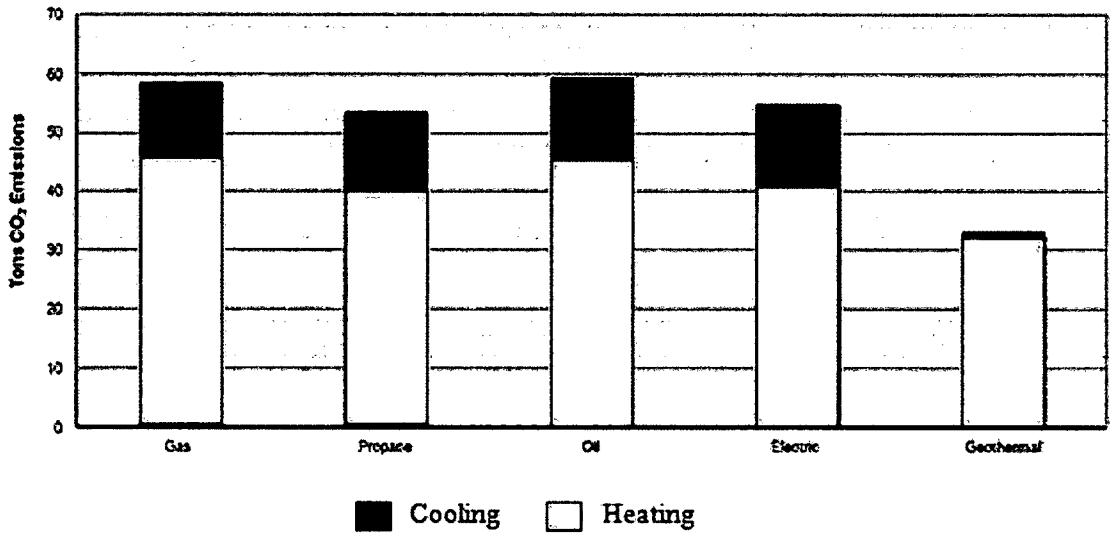


**Fig. 7.10 $CO_2$ Emission [310]**

7.3.3 Geothermal Design Parameters of Energy Foundation

There is a total of 145 piles installed in the foundation with several different pile groups and a maximum of 3×3 or 9 piles used in a single pile group. The spacing between any two piles in a group is around 1.22 m (4 feet), which also satisfies the minimum spacing requirement between piles for structural design. However, the 1.22 m (4 feet) spacing is very small for geothermal energy design. To make the design economical, a simple assumption is considered in the design. That is, there is a total of 145/9 ≈16 groups of piles in the building foundation, with one energy pile in every pile group used for energy extraction. The average spacing between pile groups are taken as the equivalent energy-pile spacing as given in Table 7.5. An average spacing is found to be 8.55 m (28.06 feet). The analysis was done by taking the distance of 8.53 m (28 feet) as the design spacing with a total 4×4 or 16 energy piles presented in the foundation. The result was found to be very satisfactory.

**Table 7.5 Spacing Between Major Pile Groups of the Building**

| Pile group | 1 | 2 | 3 | 4 | 5 | 6 | 7 | 8 | 9 |
|---|---|---|---|---|---|---|---|---|---|
| Spacing (m) | 6.91 | 13.24 | 6.22 | 9.79 | 9.50 | 9.50 | 9.50 | 5.47 | 8.23 |

To make the design more economical, a heating pump is considered in the design. The purpose of the heating pump is to heat and cool circulating fluid in the U-tubes to further increase the temperature gap between the fluid and ground soil. For cooling, a temperature gap in the range of 11.11$^0$C (20$^0$F) to 16.7$^0$C (30$^0$F) above the undisturbed ground water temperature is needed. For heating, a gap of 5.55$^0$C (10$^0$F) to 11.11$^0$C (20$^0$F) below the undisturbed groundwater temperature is needed [307]. The heat pump will ensure that the above-mentioned temperature gap is maintained throughout the year. In the design, the U-tube inlet fluid temperature is taken as 47.06$^0$C (116.7$^0$F), and the outlet fluid temperature is taken as 3$^0$C (37.4$^0$F). To circulate the fluid, a 1492 W (2 HP) circulation pump is adopted in the design. To minimize the energy cost of the heat pump and circulation pump, the system is designed in such a way that it will have variable fluid speed depending on the thermal load demand. Again, to ensure turbulent flow in the U-tube all the time, a minimum flow velocity of 0.61 m/s (2 fps) is used and the design velocity is taken as $0.757\times10^{-3}$ m$^3$/s (12 gpm), as shown in Table 7.2. In the design, no anti-freeze solution is considered because it is highly unlikely that water would be frozen in the U-tube in South Louisiana. Generally, in areas where temperature goes below the freezing point, one needs to use methanol with water in the U-tube.

For depths greater than 9.14 m (30 feet) below ground surface, the soil temperature is relatively constant, and it corresponds roughly to the water temperature

measured in groundwater wells, which are usually 9-15 m (30-50 feet) deep [309]. This is referred to as the "mean earth temperature." From Fig. 7.4, the soil temperature was taken at the building site as 19.44$^0$C (67$^0$F). From the geotechnical report, the groundwater table is 1.52 m (5 feet) below the surface. Although there is a seasonal change in the water table and the energy foundation design is done for 15 years, to be on the safe side, it was considered that the soil is not 100% saturated, since more moisture means more geothermal energy. In New Orleans, the groundwater table is high, which implies a higher thermal conductivity. After some literature review, the data provided by GLD 2012 software was adopted, and the thermal conductivity value was taken as 1.47 W/m-k (0.85 BTU/h*ft*$^0$F) [307, 311, 312].

In the actual building foundation, the structural engineer used steel H-piles. However, the GLD 2012 can only analyze concrete energy piles/grout-filled boreholes. For this reason, the building was designed as a concrete pile foundation with a pile dimension almost the same as the steel pile. Although the actual pile diameter in the foundation is 0.32 m (12.75 in), the GLD 2012 residential version only allows the use of a concrete pile with a diameter up to 0.25 m (10 in). Therefore, the energy pile was designed as a concrete pile with a diameter of 0.25 m (10 in). In the design, it was assumed that one SDR 11 type, 40mm U-tube is placed in one concrete pile. There are three types of possible pipe placements. They are illustrated in Fig. 7.3. In the design, only pipe placement of the middle one was taken into consideration.

7.3.4 Results and Discussion

The maximum energy demand of the building in New Orleans for cooling is 147.27 kW/hr, and heating is 39.54 kW/hr. Using the existing foundation layout, almost 20% of the cooling demand and 68% of the heating demand can be met, as listed in Table 7.6. This amount equals 1.83 kW/hr of heating energy and 1.68 kW/hr of cooling energy per pile as given in Table 7.7. Table 7.8 shows that natural gas and electricity are 13.6 and 16 times costlier than using geothermal energy, respectively. From Table 7.9 it is also clear that geothermal energy emits less $CO_2$ than other forms of energy.

**Table 7.6 Total Output of Energy Pile [310]**

| | | |
|---|---|---|
| Cooling load kW/hr | Max Demand | 147.27 |
| | Extraction from Energy Pile | 29.31 |
| | % | 19.9 |
| Heating load kW/hr | Max Demand | 39.54 |
| | Extraction from Energy Pile | 26.93 |
| | % | 68.12 |

**Table 7.7 Energy Output by Energy Piles [310]**

| Pile spacing (m) | Pile length (m) | Cooling load kW/hr | Heating load kW/hr |
|---|---|---|---|
| 8.26 | 390 (16 piles) | 29.31 | 26.93 |
| | 24.38 (1 pile) | 1.83 | 1.68 |

**Table 7.8 Comparison of Annual Energy Costs by Source of Energy [310]**

| Type of energy source | Annual cost (USD) | Comparison |
|---|---|---|
| Natural Gas | 13600 | 13.6 |
| Propane | 17600 | 17.6 |
| Oil | 19000 | 19.0 |
| electric heat | 16000 | 16.0 |
| Geothermal | 1000 | 1.0 |

**Table 7.9 Comparison of $CO_2$ Emissions by Source of Energy [310]**

| Type of energy source | Annual $CO_2$ emissions (tons) | Comparison |
|---|---|---|
| Natural Gas | 58.2 | 1.8 |
| Propane | 53 | 1.6 |
| Oil | 59.5 | 1.8 |
| Electric heat | 54.5 | 1.7 |
| Geothermal | 32.5 | 1.0 |

## 7.4 Sensitivity Analysis of Design Parameters in an Energy-Pile Design

As a design engineer, one may have some flexibility in combining the design parameters to get an equal amount of energy from ground soil, but the different combinations that may give the same geothermal energy can result in different construction costs. For example, using a longer pile length with a larger concrete surface area exposed to soil can extract the same amount of energy as a smaller length of energy pile with a more powerful heat pump to increase the temperature gap between soil and circulating fluid. In the sensitivity analyses, different design parameters were tested against energy-pile length needed for a certain amount of geothermal energy output. A designer of geothermal energy piles wants to extract the desired amount of geothermal energy with a minimum pile length because more pile length means more volume of concrete, which will mean more cost.

In the design of any geothermal energy system, a designer can vary input parameters, which are adjustable within a certain range, to achieve the desired energy output from the system with a minimum cost. In the energy-pile system, the biggest challenge is to reduce the total pile length. Therefore, it is vital to understand the impact of the input parameters on the energy output, which boils down to the effect on the total

energy-pile length. Some parameters might be more sensitive to the pile length than others. The sensitivity analysis was performed by varying the parameters individually, and their effects on a single energy-pile length for the building foundation in New Orleans were quantified, respectively. This sensitivity analysis can also be performed on the total combined length of the16 energy piles since the final graph will be plotted with each design parameter versus the increment percentile of each energy-pile length. Because the increment percentile of pile length is the same for every single pile or forthe total combined pile lengths, the graphs should be exactly the same. If the total HVAC load with 147.27 kW/hr of cooling and 39.54 kW/hr of heating is required from the energy-pile system, each of the sixteen energy piles must be at least 66 m as opposed to the pile length of 8.33 m needed for the structural purpose only. In this sensitivity analysis, the pile length of 66 m was taken as the base value. The percentile change in pile length was calculated by varying the design parameters, respectively, in an attempt to see the impacts of different design parameters on the pile length.

An important energy-pile design parameter is the ground-soil temperature. Based on the annual ground temperature distribution data presented in Fig. 7.4, the ground-soil temperature in South Louisiana was taken as $19.4^0$C. Figure 7.4 also shows that the ground-soil temperature all over the US varies within the range of $10^0$C to $23^0$C, which is used as the basis for the ground temperature sensitivity analysis. Figure 7.11 shows how the ground-soil temperature affects the required pile length. The analysis indicated that any ground-soil temperature higher than $19.4^0$C led to a narrower temperature gap between the ground soil and atmosphere; thus, a significant increase is required in energy-pile length. The ground-soil temperature versus pile-length relationship is nearly a

straight line displaying a monotonic increase in pile length with the ground-soil temperature increase. If the same energy-pile setup is taken from Louisiana to the northern US, and if the soil moisture is assumed to be the same in both places, due to lower ground-soil temperature in the northern US, for example in New Jersey, the required pile length will be almost 20% less than in Louisiana. On the other hand, if the same energy pile is installed further south, for example in Florida, the required pile length will increase by 10%.

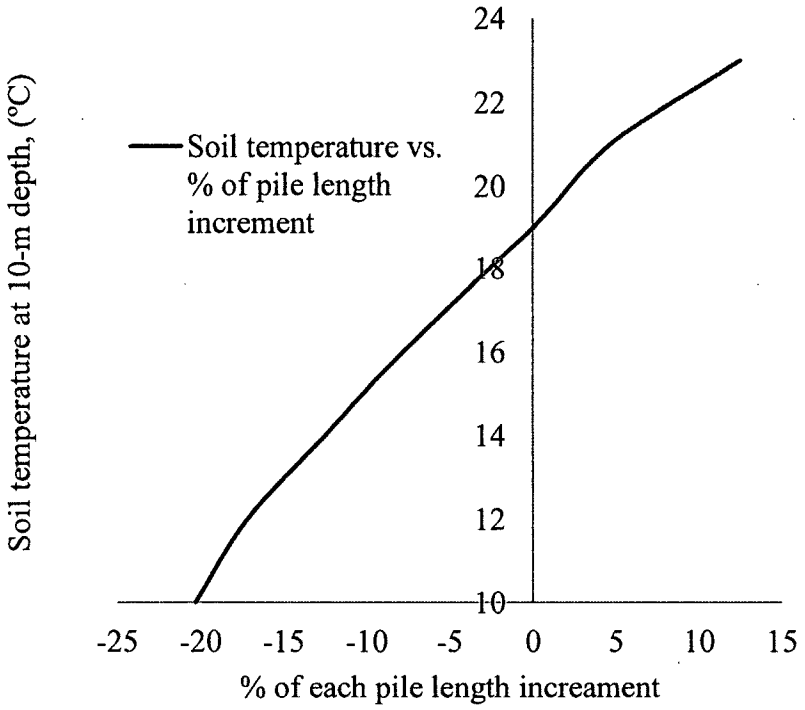


**Fig. 7.11 Effect of Ground Soil Temperature on the Required Pile Length**

Energy-pile designers might want to know how sensitive the soil moisture content is in energy-pile design. The pre-determined soil thermal conductivity (k) for the moist clayey ground soil in New Orleans was taken as 1.47 W/m-k. This k value was found from the supplementary data table relating soil type with a thermal conductivity, which

comes with the GLD 2012 software package. In Fig. 7.12, it can be clearly seen that a decrease in soil thermal conductivity monotonically increases the required pile length to achieve the required cooling energy of 147.27 kW/hr and heating energy of 39.54 kW/hr anticipated from the energy-pile system. Figure 7.12 shows that, if the soil thermal conductivity has a sharper increase, the required pile length will reduce more significantly.

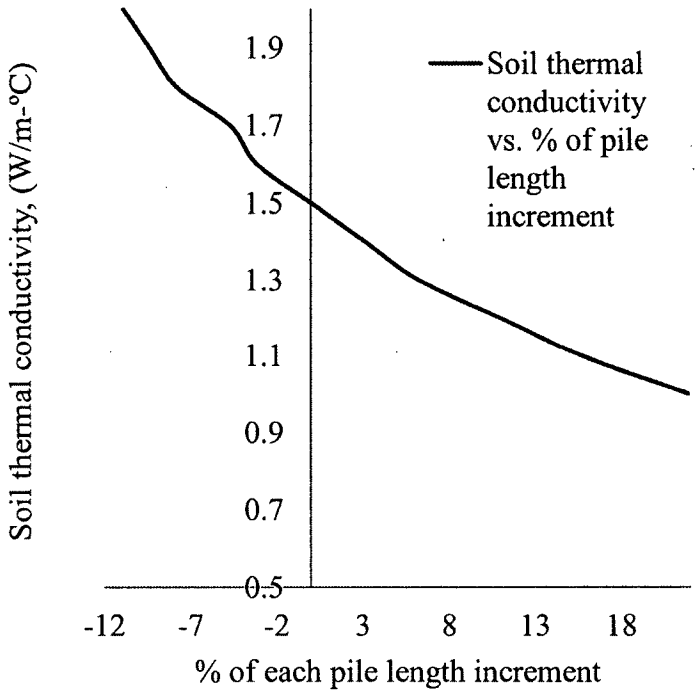


**Fig. 7.12 Effect of Soil Thermal Conductivity on Pile Length.**

As the third parameter, the concrete thermal conductivity was used for the sensitivity analysis. With results presented in Fig. 7.13, it is found that, if the thermal conductivity of concrete increases, the required pile length will decrease. The change is as significant as for the ground soil thermal conductivity. It is noted from Table 7.3 that the change from ordinary concrete (2000/2500 kg/m$^3$) to thermally enhanced concrete

(50% quartz) means an increase in the thermal conductivity by almost 2 W/m-0C. Therefore, the thermally enhanced concrete can dramatically decrease the overall pile length by 40% (Fig. 7.13).

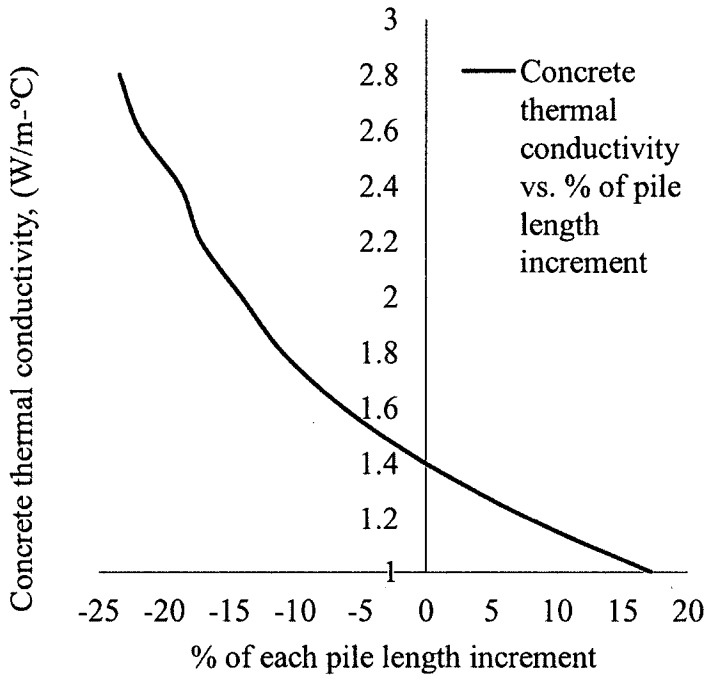


**Fig. 7.13 Effect of Concrete Thermal Conductivity on the Required Pile Length**

Another important parameter for the sensitivity analysis is the pile diameter. Any increase in pile diameter implies the increase in the surface area of the pile wall. It will provide more area for heat transfer. Thus, a shorter pile length is required for the desired HVAC energy. Figure 7.14 is consistent with the trend, and it quantitatively helps to understand the significance of varying pile diameter. It seems that the increase in pile diameter does not decrease the pile length drastically. By doubling the pile diameter, the pile length can only decrease by 9%.

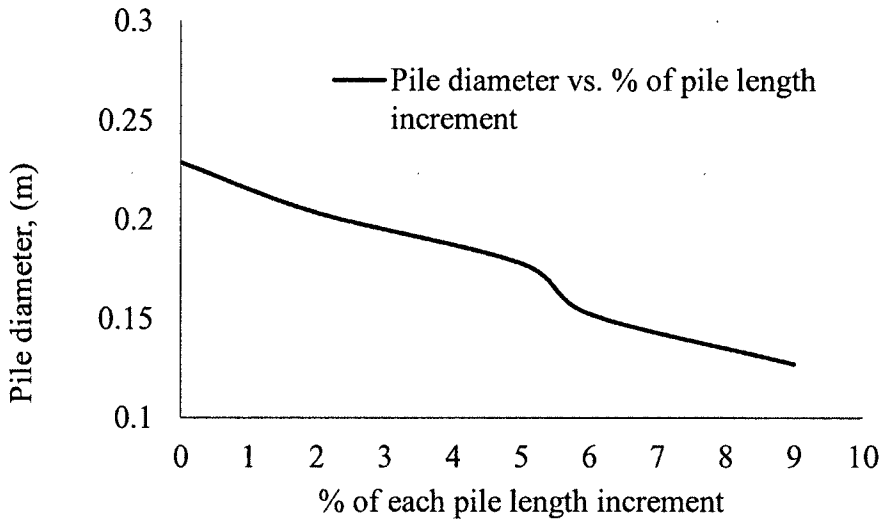


**Fig. 7.14 Effect of Pile Diameter on the Required Pile Length**

Flow rate is a very important design parameter in energy-pile design. Figure 7.15 shows that the smaller the flow in the U-tube, the shorter the length of the energy pile. However, the change in flow rate must meet desired needs within realistic constraints. The flow value should be enough to maintain the minimum fluid velocity. On the other hand, from the continuity equation, it is known that a higher flow rate in the U-tube leads to a greater velocity if the cross-sectional area of the U-tube remains constant. It turns out that more eddies in the U-bend will be created because the higher velocity makes the flow more turbulent and increases the Reynolds number. That is why Fig. 7.15 shows that there is no change in pile length with a further increase in flow rate after the flow rate reaches a critical value.

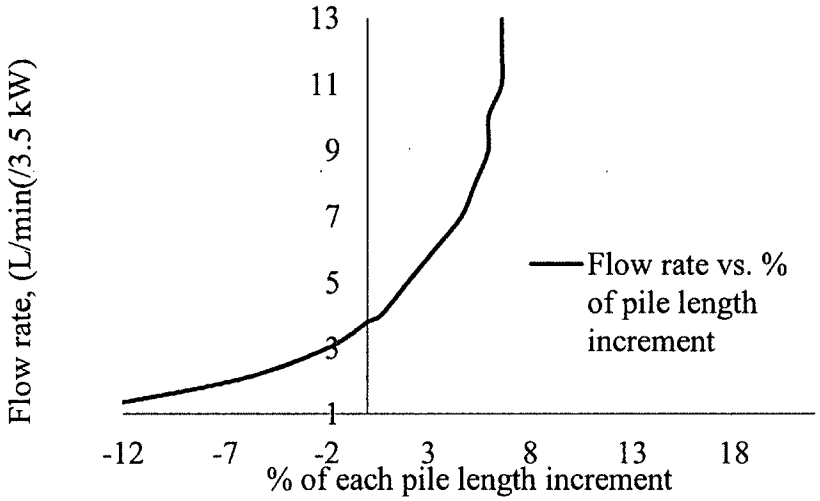


**Fig. 7.15 Effect of Flow Rate in U-tube on the Required Pile Length**

Figure 7.3 shows different types of U-tube orientations in an energy pile. Using the sensitivity analysis, it is found that, if the U-tubes are placed close together, as shown in the leftmost potential layout in Fig. 7.3, it will increase the pile length by 11% (Fig. 7.16). If the U-tube is placed along the outer wall as shown in the rightmost potential layout in Fig. 7.3, it will decrease pile length by 9%. It makes sense as the U-tube is placed closer to soil, which is the energy source, because more heat transfer will occur.

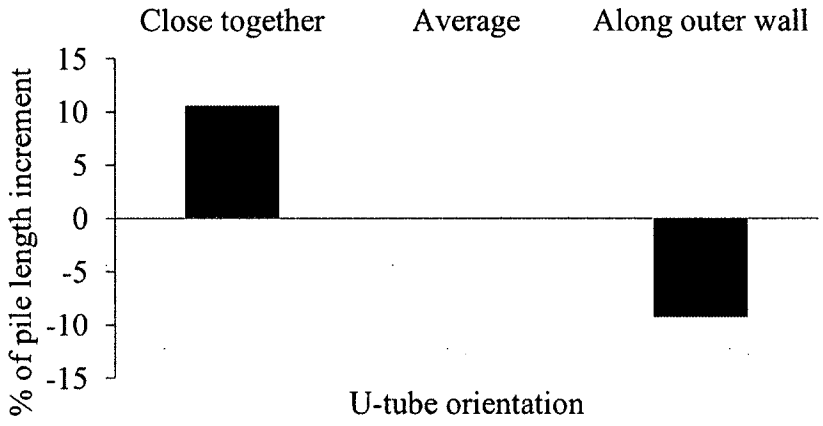


**Fig. 7.16 Effect of U-tube Orientation on the Required Pile Length**

The last parameter analyzed in the sensitivity analyses is the U-tube diameter. As shown in Fig. 7.17, an approximately linear relationship is achieved between the U-tube diameter and percentile pile length increment. A greater U-tube diameter results in a shorter pile length.

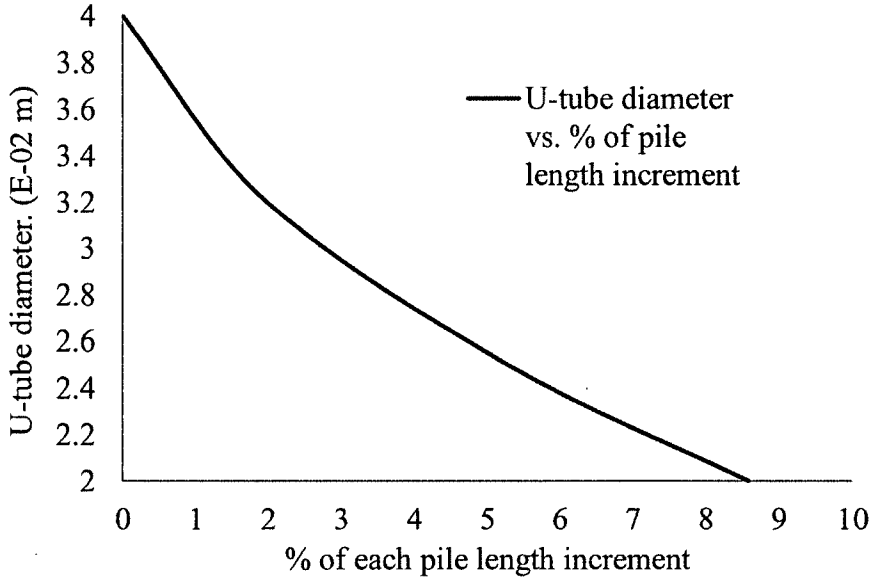


**Fig. 7.17 Effect of U-tube Diameter on the Required Pile Length**

## 7.5 Development of a Simple Graph Method for Borehole Design

In this section, the development of a simple graphical design method iss presented. All the charts were developed by running commercial software GLD 2012 and by varying the major parameters such as borehole length, the spacing between GHX boreholes, and thermal conductivities, etc. The goal was to make a simplified chart solution for the preliminary design of a GHX without running the software programs. At this stage, the designers may have little background information about the soil, fluid, U-tube and circulating pump parameters. However, with the graph method, the potential

geothermal energy, and the required borehole length could be effectively estimated. In the development of the charts, cooling/heating load ranges were selected such that they could meet the requirement of a small office building or a small apartment complex.

Heat exchangers change the ground temperature, especially when the cooling and heating loads are unbalanced. The process of ground temperature change may take several years before it moves to a steady state. With the ground-loop design, designers can change the modeling period (1 year, 5 years, 10 years, etc.) and then calculate the heat exchanger length corresponding to the period.

Several factors can have impacts on the duration of the ground temperature to stabilize, such as load balances/imbalances, water flow in the soil (fast-moving water can transfer heat quickly), and borehole depth. A large portion of a shallow borehole interacts with atmosphere/sunlight. Thus it has some of the characteristics that are typically associated with a horizontal system. Such systems tend to have a reduced or no soil temperature change since the soil can exchange heat with the atmosphere. Thus short modeling periods are oftentimes used. As the boreholes get deeper, a greater percentage of the borehole is not affected by sunlight/atmosphere, and long-term modeling periods become more common [312].

Currently, all the commercial software packages can do the simulation over a period of multiple years. Designing a borehole system over a 15-year period should consider all the variables [312]. Therefore, in the chart solution development (graph method), a matrix for a $6 \times 6$ rectangular, vertical borehole system was taken as a scenario for a prediction modeling period of 15 years, and a huge data bank was produced for different soil conditions, borehole spacing, and U-tube lengths.

In the 6 × 6 borehole matrix, a total of 36 boreholes (6 boreholes placed in one direction and 6 in another direction) were combined as a geothermal energy system. Of course, chart solutions for other combinations, such as the 2 × 2, 2 × 3, and 3 × 4 matrices, etc., should also be established for a complete chart-solution manual. The chart was developed using the design-day HVAC load method. In the design-day method, the design heating load was the HVAC demand of the building on the coolest day in winter and the design cooling load was the cooling load demand of the building on the warmest day in summer. These loads were referred to as the design peak heating and cooling loads, respectively. The heating and cooling systems were designed based on the assumption that, if the GHX system could provide adequate heating/cooling energy on the coolest/warmest day in a year, the system would work well for any other days of summer/winter. Peak heating/cooling load was found using the LEAD Plus software provided by Gaia Geothermal, LLC [315]. A maximum of 52,752 W (180 kBtu/h) cooling load can easily meet the HVAC requirement for a small office building or a two- or three-bedroom apartment complex in Louisiana. As for Louisiana, the cooling load is much greater than the heating load, the total borehole length needed for the cooling load would also meet the heating load requirement. A sample data set for the borehole spacing of 10.67 m (35′) was given in Table 7.10, in which peak cooling and heating loads were obtained by varying the thermal conductivity and the total borehole length.

**Table 7.10 Borehole Design Data Acquired for Northern Louisiana (spacing of 10.67 m)**

| Total borehole length (m) | k (W/m-K) | Cooling load (kW) | Heating load (kW) |
|---|---|---|---|
| 762 | 1.7 | 20.64 | 11.66 |
| | 1.6 | 19.91 | 11.25 |
| | 1.4 | 19.07 | 10.77 |
| | 1.2 | 18.07 | 10.21 |
| 914 | 1.7 | 25.16 | 14.21 |
| | 1.6 | 24.25 | 13.70 |
| | 1.4 | 23.21 | 13.11 |
| | 1.2 | 22.02 | 12.44 |
| | 1.0 | 20.59 | 11.64 |
| 1067 | 1.7 | 29.78 | 16.83 |
| | 1.6 | 28.72 | 16.23 |
| | 1.4 | 27.49 | 15.53 |
| | 1.2 | 26.05 | 14.72 |
| | 1.0 | 24.33 | 13.75 |
| 1219 | 1.7 | 34.40 | 19.44 |
| | 1.6 | 33.19 | 18.75 |
| | 1.4 | 31.78 | 17.96 |
| | 1.2 | 30.13 | 17.02 |
| | 1.0 | 28.16 | 15.91 |
| 1372 | 1.7 | 39.02 | 22.05 |
| | 1.6 | 37.66 | 21.28 |
| | 1.4 | 36.07 | 20.38 |
| | 1.2 | 34.21 | 19.33 |
| | 1.0 | 32.00 | 18.08 |
| 1524 | 1.7 | 43.65 | 24.66 |
| | 1.6 | 42.13 | 23.80 |
| | 1.4 | 40.37 | 22.81 |
| | 1.2 | 38.30 | 21.64 |
| | 1.0 | 35.83 | 20.24 |
| 1676 | 1.7 | 48.27 | 27.27 |
| | 1.6 | 46.60 | 26.33 |
| | 1.4 | 44.66 | 25.23 |
| | 1.2 | 42.38 | 23.94 |
| | 1.0 | 39.66 | 22.41 |

After plotting all those findings in a single graph, numerical relations among those variables were found. Two sets of graphs were produced for the two cases in which

the borehole spacing was 10.67 m (35′) and 12.19 m (40′), respectively. These graphs showed the relations of peak cooling/heating load with thermal conductivity and total borehole length. Total borehole length means the combined length for the 36 boreholes with one U-tube in each borehole. As an example, for a particular peak HVAC demand, if a total borehole length of 762 m (2500′) is found from the graph, it implies that the 36 boreholes with a depth of 762/36 = 21.17 m (69.45′) each could provide the equivalent HVAC energy. For every borehole spacing, a set of graphs can be developed relating the borehole length, thermal conductivity, and peak cooling/heating load. Figures 7.18 and 7.19 were plotted for the case of 10.67 m (35′) in borehole spacing, and Figs. 7.20 and 7.21 were for the case of 12.19 m (40 ft) in borehole spacing. From these figures, it is clearly seen that for any soil, if the total borehole length is made longer, more geothermal energy can be extracted from the ground since more surface area is available for heat transfer.

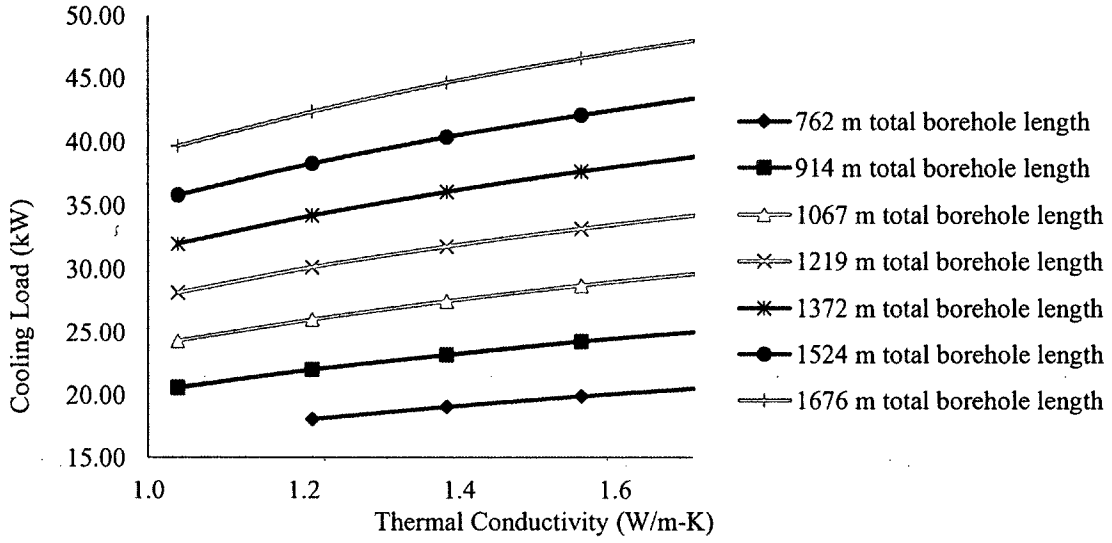


**Fig. 7.18 Cooling Load vs. Thermal Conductivity for the Borehole Spacing of 10.67m.**

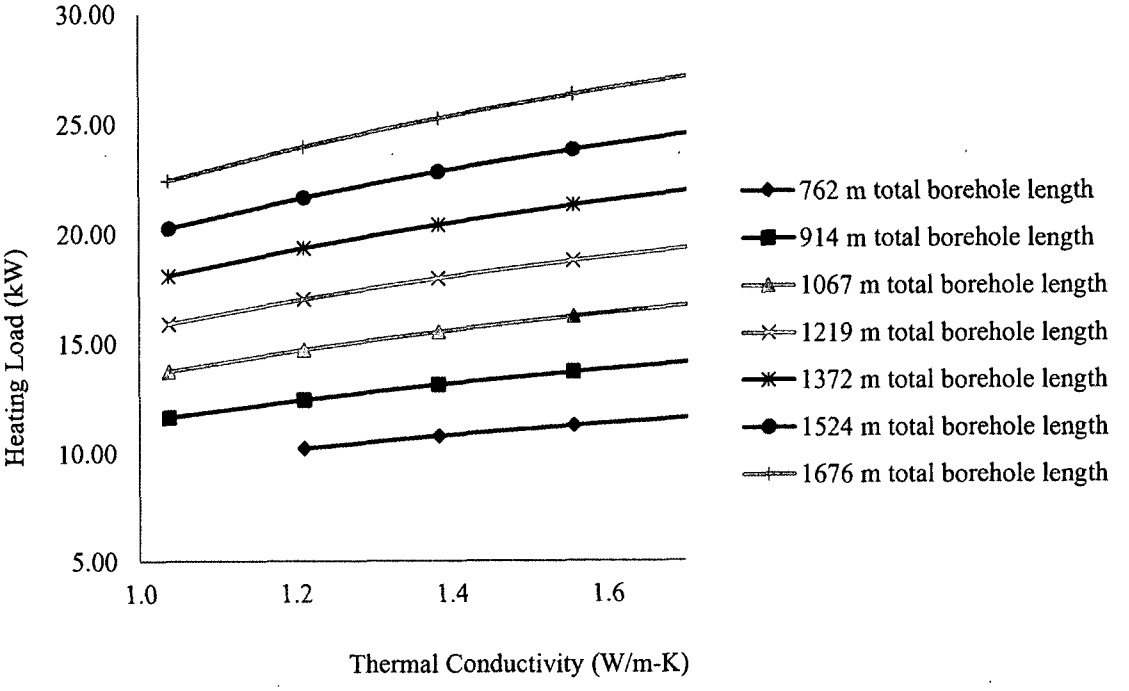


**Fig. 7.19 Heating Load vs. Thermal Conductivity for the Borehole Spacing of 10.67 m.**

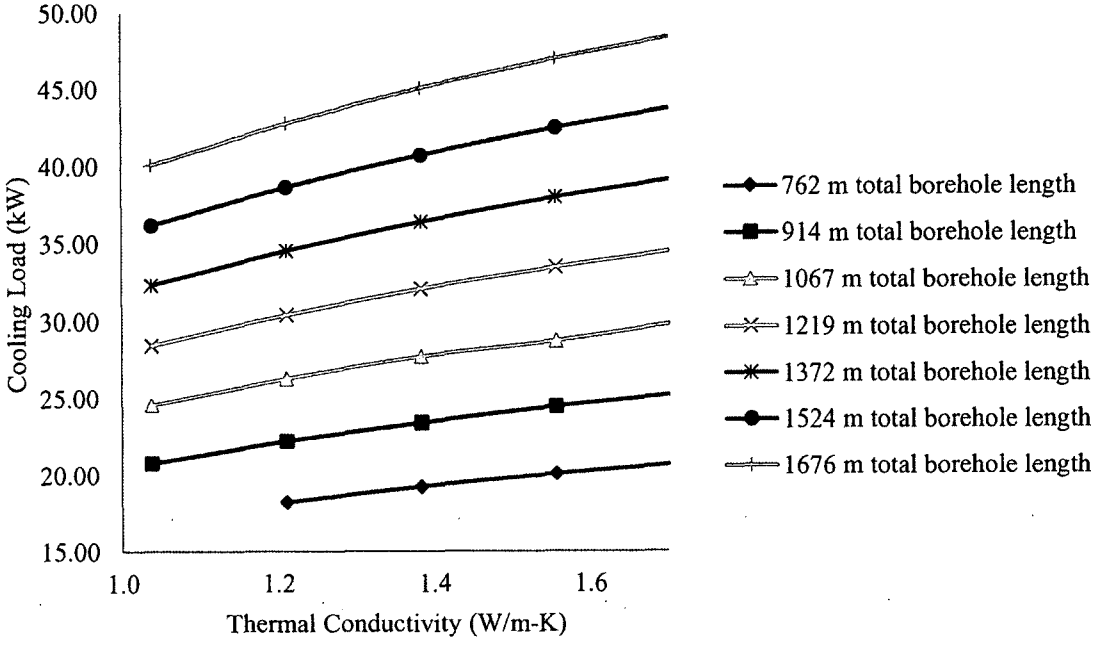


**Fig. 7.20 Cooling Load vs. Thermal Conductivity for the Borehole Spacing of 12.19 m.**

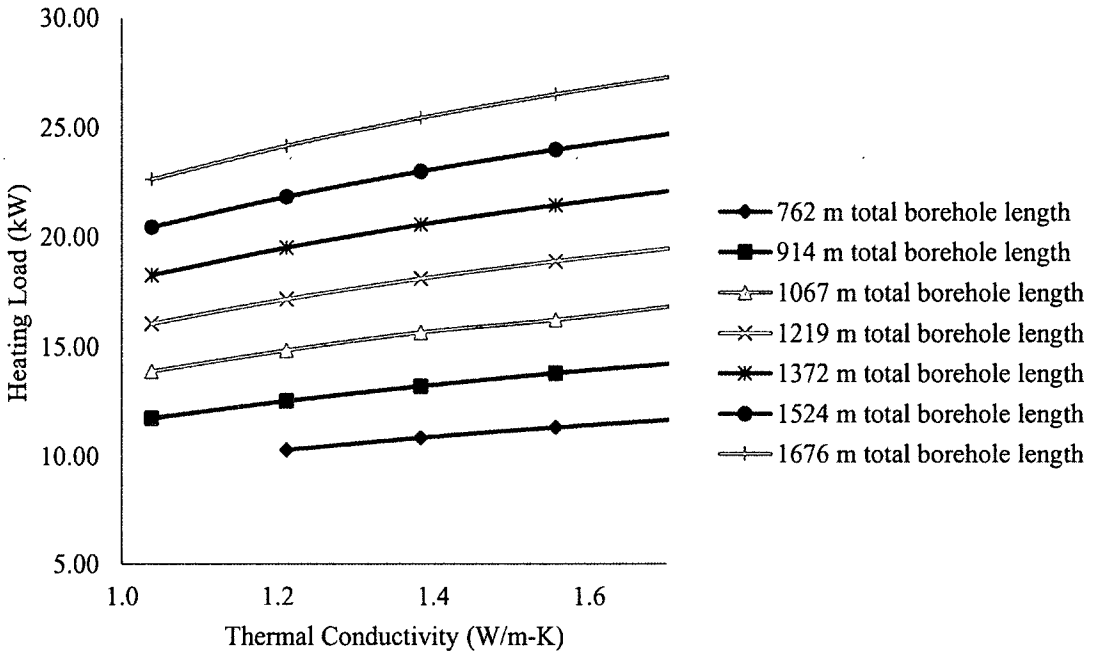


**Fig. 7.21 Heating Load vs. Thermal Conductivity for the Borehole Spacing of 12.19 m.**

For the required cooling demand of any building and the thermal conductivity of the ground soil around the building, a quick answer to the required borehole length could be found using either Fig. 7.18 or 7.20. The borehole length required for the cooling load would then be employed to determine the cooling energy that can be found from Fig. 7.19 or 7.21. The capacity of the extracting cooling energy of a GHX system using the graphs will always meet the heating load demand of a small residential/office building in Louisiana. Similar graphs can be generated for any other borehole spacing such as 6.10 m (20′) or 9.14 m (30′), if needed. These graphs are used in two ways. The first one is to evaluate the potential of geothermal energy for a certain borehole length, spacing, and thermal conductivity. The second one is that the required length and spacing of a borehole can be quickly found if a design HVAC load and soil thermal conductivity are

known. The HVAC load consists of heating and cooling loads. These graphs were prepared exclusively for northern Louisiana where the geothermal energy system is mainly designed to be cooling dominant. For example, if electricity and gas bills are collected for a two-bedroom apartment, the peak heating and cooling load can be determined for the apartment. Using Figs. 7.18-7.21 the total borehole length and spacing can be determined.

### 7.5.1 Example: A Quick Solution for the GHX Design of a Small House

The simplified graph method was developed using the industry-popular software package GLD 2012. Validation of the numerical results from GLD 2012 with field measurements has not been well documented. For this reason, another software package GLHEPRO that was popular in the green energy industry was selected and used to design the same GHX system. Numerical solutions from package GLHEPRO were compared to the solutions from package GLD 2012 to validate the reliability, effectiveness and accuracy of the package GLD 2012. In the research, numerical results from the simplified graph method were also compared with the outcomes from software programs GLD 2012 and GLHEPRO. The comparisons indicated that the simple graph method can provide a credible solution with an acceptable accuracy at the preliminary design stage.

The heating and cooling load requirement of a housing complex in Ruston, Louisiana, was selected as the example. It is a five-apartment house with all the apartments aligned side by side in a line. The annual heating and cooling load requirement for one of the five apartments was collected, and it was assumed that the HVAC requirement for all the five apartments is just five times the heating and cooling

requirement of a single apartment. On the average, all the two-bedroom apartments were 9.57 m (31.4') long and 7.32 m (24') wide with two outside doors and six windows. Annual HVAC requirements for the single apartment and all five apartments were given in Table 7.11, respectively. Walton [315] suggested that an effective starting point could be selected such that 1% of total HVAC load demand is taken as the peak load/h, and thus the peak cooling load was 34,558 W (117.92 kBtu/h) and peak heating load was 996 W (3.4 kBtu/h).

**Table 7.11 The HVAC Load for the Five-Apartment Building**

| Billing cycle | The single apartment | | The five-apartment building | |
|---|---|---|---|---|
| | Heating kW/month | Cooling kW/month | Heating kW/month | Cooling kW/month |
| 17-Jan-2013 | 19.64 | 0 | 98.18 | 0 |
| 14-Feb-2013 | 14.36 | 0 | 71.80 | 0 |
| 15-Mar-2013 | 14.95 | 0 | 74.73 | 0 |
| 17-Apr-2013 | 0 | 201.63 | 0 | 1007.87 |
| 17-May-2013 | 0 | 190.50 | 0 | 951.90 |
| 14-Jun-2013 | 0 | 512 | 0 | 2559.98 |
| 18-Jul-2013 | 0 | 613.69 | 0 | 3067.87 |
| 19-Aug-2013 | 0 | 691.06 | 0 | 3455.90 |
| 16-Sep-2013 | 0 | 592 | 0 | 2960.02 |
| 15-Oct-2013 | 0 | 276.66 | 0 | 1383.88 |
| 14-Nov-2012 | 0 | 271.97 | 0 | 1359.85 |
| 14-Dec-2012 | 12.31 | 0 | 61.55 | 0 |

It was assumed that six boreholes with a diameter of 0.25 m (10") and a spacing of 10.67 m (35') were set to meet the load requirements. The soil thermal conductivity was assumed to be 1.3 W/m K (0.75 Btu/h $ft^0F$), as shown in Table 7.3. Then, the required borehole length was determined quickly from Fig. 7.18. The borehole length was also compared with outcomes from GLD 2012 and GLHEPRO, respectively. For the

same parameters and the HVAC load, the total borehole length with the 6 × 6 borehole option was determined using the graph method and the two software packages, respectively. The borehole length with other borehole options was also determined using GLD 2012 and GLHEPRO, respectively, in an effort to check if the solutions the software packages provided were consistent with each other. All the results were summarized in Table 7.12 and Fig. 7.22.

**Table 7.12 Required Borehole Lengths with Different Borehole Options**

| Thermal conductivity (watt/m-k) | Borehole options | No. of borehole(s) | Total borehole length (m) | | |
|---|---|---|---|---|---|
| | | | Graph Method | GLD 2012 | GLHEPRO |
| 1.3 | 6X6 | 36 | 1311 | 1442.00 | 1425.00 |
| | 2X2 | 4 | N/A | 1425.66 | 1230.00 |
| | 2X3 | 6 | | 1426.89 | 1252.50 |
| | 2X4 | 8 | | 1427.52 | 1286.52 |
| | 3X3 | 9 | | 1428.54 | 1294.62 |
| | 3X5 | 15 | | 1429.86 | 1316.10 |
| | 4X4 | 16 | | 1430.31 | 1320.00 |
| | 4X5 | 20 | | 1430.85 | 1380.00 |
| | 4X6 | 24 | | 1431.24 | 1403.40 |

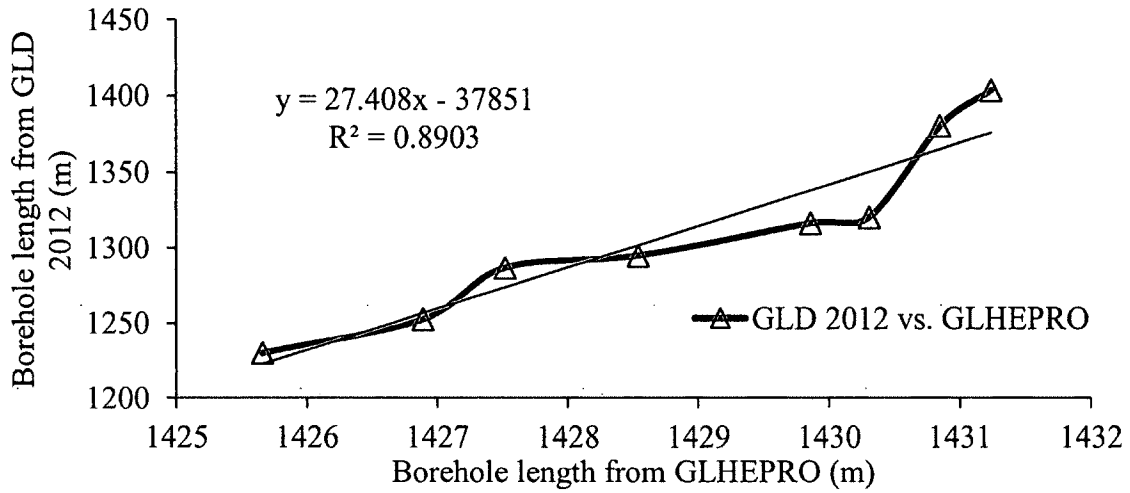


**Fig. 7.22 Comparison of Results from GLD 2012 and GLHEPRO**

Table 7.12 and Fig. 7.22 presented the required total borehole lengths from the software packages GLD 2012 and GLHEPRO, respectively, for the five-apartment house. They indicated that the solutions from the two independent software packages were reasonably close from an engineering perspective, and thus results from any of the software programs are consistently effective. It indicated that the numerical solutions from the software package GLD 2012, which was used to develop the graph method, were reliable and credible. For the borehole option 6 × 6, the required total borehole lengths presented in Table 7.12 were 1311 m, 1442 m and 1425 m from the graph method, GLD 2012 and GLHEPRO, respectively. The graph method provided a borehole length that was 9% lower than that from package GLD 2012, and 8% lower than that from package GLHEPRO. The design results using the graph method showed that total borehole length needed for the peak HVAC load had a reasonable agreement with the results from the two software packages GLD 2012 and GLHEPRO. Using regression analysis, it was found that the results from two software packages came up with a coefficient of determination ($R^2$) of 90%. It implied that discrepancies among the results given by the graph method and the commercial software packages were within the acceptable range for industry use from an engineering perspective. The simple graph method is promising and feasible, and it can provide a quick, reliable and accurate solution for the GHX design of a small apartment house, especially in the early design stage. As a supplementary achievement using GLHEPRO, the research results demonstrated that, for the five-apartment building, the vertical borehole GHX thermally interacted with surrounding soil following complicated, three-dimensional transient heat conduction. It led to a non-uniform geothermal energy distribution for the 6 × 6 borehole

area. In this example, to understand the effects of variable heat pulse on the ground response, the thermal response factors calculated from the G-function [316, 317] were plotted in Fig. 7.23 as the G-map for the 36 boreholes. From Fig. 7.23, it was seen that the thermal response factor was the highest at the center of the borehole, which indicated that the thermal energy use reached its maximum value.

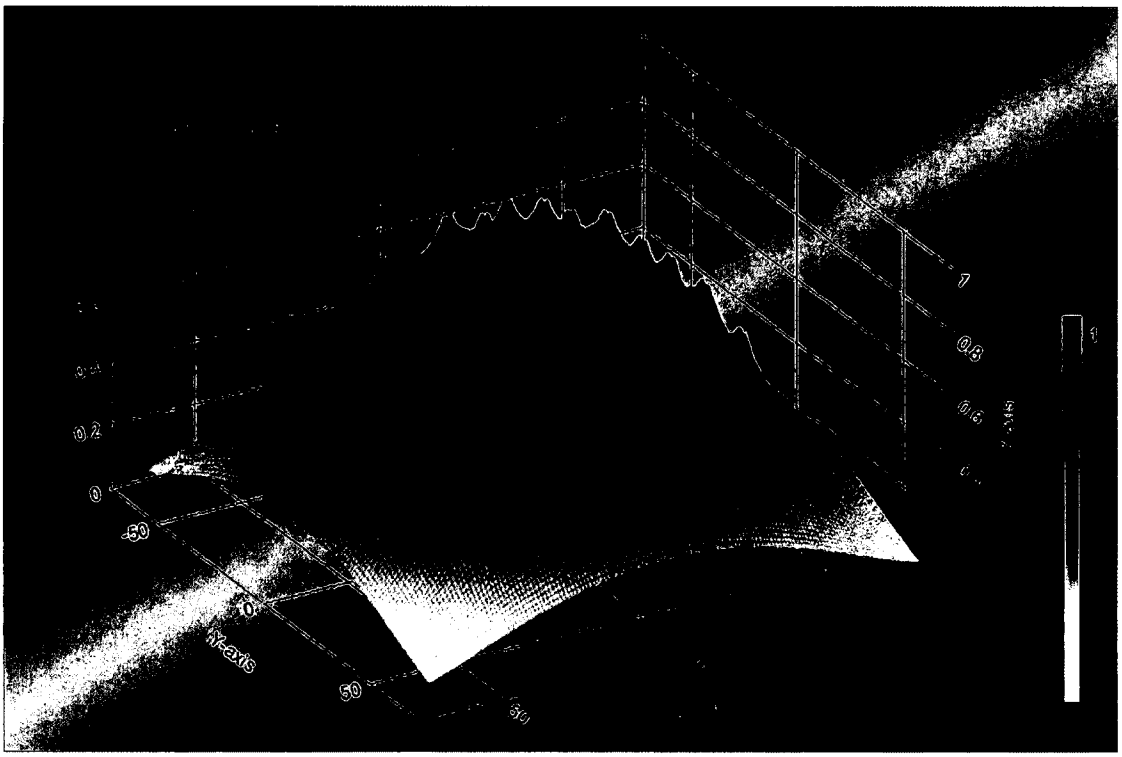


(1 ft = 0.30 m; 1 in = 0.025 m)

**Fig. 7.23 A G-map of the 6 × 6 Borehole Option.**

# CHAPTER 8

# CONCLUSIONS AND RECOMMENDATIONS

In this dissertation, a complete understanding of the swell-shrink behavior of Moreland clay, stress on a pavement resting on expansive soil and potential harvesting of geothermal energy from Louisiana's soil has been studied.

The principal conclusions that can be drawn from this study are summarized in section 8.1, and recommendations for future research are discussed in section 8.2.

## 8.1 Conclusions

The following conclusions can be drawn:

1. A major type of North Louisiana's expansive soil is Moreland clay. While volume changes can cause structural failure and pavement cracks, wven pavement consisting of geosynthetics resting on non-stabilized Moreland clay can experience longitudinal cracks. After measuring the swelling percent, it has one of the highest magnitudes of volume change in the world. Using a USDA mapping tool, a map of Moreland clay was produced showing Moreland clay is only present in Louisiana, Arkansas and Oklahoma. Among these three states, it is present mostly in North Louisiana.

2. After a consolidation test and shrinkage test, it may be concluded that the macrostructure of the soil is mainly influenced by the mechanical stress state while the suction stress state influences both the macrostructure and microstructure.
3. After field observations, it can be concluded that the actual volume change of the soil in the field is much smaller than the predicted one. It may be because a) most of the predicted method uses 1-D soil experiment results while, in reality, the volume change happens three-dimensionally and b) soil at different depths cannot reach its maximum or minimum possible moisture content at the same time.
4. An empirical equation was proposed for the unsaturated shear strength of the Moreland clay.
5. A map to show the distribution of expansive soils and their degrees of severity over Louisiana, based on the calculated swelling potential, was plotted using ArcGIS software. A conclusion may be drawn from the map that the southern Louisiana soil has more swelling potential compared to the soil in northern Louisiana. It must be noted that the map is not to give a real measurement of soil heave, but to offer a general idea regarding the distribution of expansive soil based on swelling degrees across Louisiana.
6. A new analytical method for the calculation of the stress of pavement resting on expansive soil is proposed. To the author's knowledge, it is for the first time the deflection, rotation, shear force and bending moment of a pavement due to the volume change of subgrade expansive soil can be calculated without any use of complicated finite element analysis. It makes incorporating the expansive-soil-induced bending stress in pavement design easily possible.

7. From the data of expansive soil in Texas, it may be concluded that the volume change of expansive soil during shrinkage is more critical than the volume change during heave.
8. The accuracy of the analytical model results largely depends on the accuracy of the measurements of moisture content change in subgrade soil throughout the year.
9. In a very detailed and systematic way, twelve Moreland clay soil samples stabilized with GPC and cement were tested. From the experiment results, it may be concluded that cement is a far better stabilizer than GPC.
10. North Louisiana is better suited for borehole geothermal systems, and energy-pile systems are more suitable for South Louisiana. This is because in southern Louisiana, pile foundation is more common than in northern Louisiana.
11. One test case from North and one from South Louisiana show that for a small building/office using geothermal energy is one of best alternatives compared to fossil fuels.
12. A simplified graphical method to design a geothermal energy system has been developed for small buildings and offices of Louisiana.

## 8.2 Future Research Recommendations

Recommendations for future research are summarized as follows:

1. More data points should be included in the SP map of Louisiana, including more boundary conditions (i.e., rivers, geological formations, etc.).
2. A larger data set for Moreland clay should be developed so that statistical evaluation of accuracy and reliability of swell-shrink properties can be conducted.

3. A consolidation test with a suction control device should be used experimentally to find shear strength at different combinations of mechanical stress and matric suction. Using this dataset, the empirically found shear strength equation would need to be evaluated.
4. Results found from the analytically developed model of pavement resting on expansive soil should be tested against an experimentally found dataset. This can be done by installing strain-gauge and moisture-content sensors on a pavement and recording data for an entire year. Finite element analysis can also be done to verify the result.
5. In the analytical solution, the soil is considered elastic although the soil is actually elastoplastic. Soil also experiences creep under constant load. More research should be done to address these two critical conditions.
6. In the analytical solution, the soil is modeled as simple Winkler foundation. There are other more advanced soil models available. Those models should be incorporated and compared with the solution found by Winkler foundation.
7. Pavement with geosynthetic inside can be analyzed by incorporating a shear stiffness parameter using this analytical solution.
8. Using simple lab experiment results, the constitutive surface of Moreland clay has been developed. The constitutive surface of a soil can be measured directly but needs sophisticated equipment, and the process is very time-consuming. More research should be done to find a simpler way to obtain this high-quality data experimentally.

9. Initial results found from the GPC-stabilized soil look promising. As more and more states are allowing GPC-stabilized subgrade, it is high time to find a specification of GPC stabilization in Louisiana.
10. The two case studies described in this dissertation show using boreholes/energy piles in Louisiana can be an excellent option compared to fossil fuel. More case studies should be done to encourage people considering geothermal energy to heat/cool buildings.
11. Repeated circulation of heated and cold water inside an energy pile causes thermal stress on the concrete. The understanding of how this thermal stress is affecting the bearing capacity and structural integrity of the pile is not well documented. An experimental study or development of a thermo-hydro-mechanical coupling model could solve many of these concerns.
12. The proposed graphical model for small offices/houses should be extended to large-scale buildings.

# REFERENCES


[1] D. E. Jones Jr and W. G. Holtz, "Expansive Soil-The Hidden Disaster," Civil Engineering, American Society of Civil Engineers, pp. 87-89, 1973.

[2] J. P. Krohn and J. E. Slosson, "Assessment of Expansive Soils in The United States," in Proc. 4th International Conference on Expansive Soils, Denver, CO, vol. 1, pp. 596-608, 1980.

[3] D. R. Snethen, "Expansive Soils: Where Are We?," National Research Council Communication on Ground Failure Hazards and National Research Council, Washington, D.C., 1986.

[4] D. G. Fredlund, "Appropriate Concepts and Technology for Unsaturated Soils," *Canadian Geotechnical Journal*, vol. 16, no. 1, pp. 121-139, 1979. doi.10.1139/t79-011

[5] G. W. Donaldson, "The Occurrence of Problems of Heave and the Factors Affecting Its Nature," in Proc. 2nd International Research and Engineering Conference on Expansive Clay Soils, Texas A&M University, College Station, Texas, pp. 25-36, 1969.

[6] H. A. Tourtelot, "Geologic Origin and Distribution of Swelling Clays," in Proc. Workshop on Expansive Clay and Shale in Highway Design and Construction, vol. 1, 1973.

[7] H. Tu, "Prediction of the Variation of Swelling Pressure and 1-D Heave of Expansive Soils with Respect to Suction," M.Sc. Thesis, University of Ottawa, Ottawa, Canada, 2015.

[8] D. D. Eberl, "Clay Mineral Formation and Transportation in Rocks and Soils," Philosophical Transactions of the Royal Society of London, 1984.

[9] J. K. Mitchell and K. Soga, "Fundamentals of Soil Behavior," 3rd ed., John Wiley and Sons, Hoboken, N.J., 2005.

[10] R. E. Grim, "Physico-Chemical Properties of Soils," *Journal of the Soil Mechanics and Foundations Division*, vol. 85, no. 2, pp. 1-70, 1959.

[11] J. D. Nelson, K. C. Chao, D. D. Overton, and E. J. Nelson, "Foundation Engineering for Expansive Soils," John Wiley & Sons, 2015.

[12] J. Krenz, B. Lee, and P. Owens. (2006, 28th September), "Swelling Clays and Septic Systems," Available: https://www.extension.purdue.edu/extmedia/RW/RW-3-W.pdf

[13] G. Huang, "Evaluation of Ground Heave Prediction Methods," Ph.D. Dissertation, Department of Civil Engineering, Oklahoma State University, 1992.

[14] R. E. Grim, "Clay Mineralogy," McGraw-Hill, New York, 1968.

[15] D. Hillel, "Fundamentals of Soil Physics," San Diego: Academic Press, San Diego, 1980.

[16] R. N. Yong and B. P. Warkentin, "Introduction to Soil Behavior," Macmillan, New York, 1966.

[17] T. W. Lambe, "The Structure of Inorganic Soil," in Proc. ASCE, vol. 79, no. 1, pp. 1-49, 1953.

[18] A. Casagrande, "Classification and Identification of Soils," *Transactions of the American Society of Civil Engineers*, ASCE, vol. 113, no. 1, pp. 901-930, 1948.

[19] R. D. Holtz and W. D. Kovacs, "An Introduction to Geotechnical Engineering," Prentice-Hall, Englewood Cliffs, N. J., 1981.

[20] R. E. Grim, "Applied Clay Mineralogy," McGraw-Hill, New York, 1962.

[21] J. H. Shamburger, D. M. Patrick, and R. J. Lutten, "Survey of Problem Areas and Current Practices," U.S. Department of Transportation, FHWA-RD-75-61, 1975, vol. 1.

[22] D. R. Snethen, F. C. Towsend, l. D. Johnson, D. M. Patrick, and P. J. Vedros, "A Review of Engineering Experiences with Expansive Soils in Highway Subgrades," Army Engineer Waterways Experiment Station, Vicksburg, Mississippi, FHWA-RD-75-48, 1975.

[23] T. W. Lambe, "The Structure of Compacted Clay," *Journal of the Soil Mechanics and Foundations Division*, ASCE, vol. 84, no. SM2, pp. 1-34, 1958.

[24] R. T. Martin, "Adsorbed Water on Clay: a Review," in Proc. 9th National Conference on Clays and Clay Minerals, vol. 9, no. 1, pp. 28-70, 1960.

[25] D. J. Hamberg, "A Simplified Method for Predicting Heave in Expansive Soils," M.Sc. Thesis, Colorado State University, Fort Collins, CO., 1985.

[26] G. H. Bolt, "Physico-Chemical Analysis of the Compressibility of Pure Clays," *Géotechnique*, vol. 6, no. 2, pp. 86-93, 1956. doi.10.1680/geot.1956.6.2.86

[27] J. E. Gillott, "Clay in Engineering Geology," Elsevier, London, 2012.

[28] F. H. Chen, "Foundations on Expansive Soils," vol. 12, Elsevier Scientific Pub. Co., Amsterdam, Netherlands, 1975.

[29] R. K. Taylor and T. J. Smith, "The Engineering Geology of Clay Minerals; Swelling, Shrinking and Mudrock Breakdown," *Clay Minerals*, vol. 21, no. 3, pp. 235-260, 1986.

[30] W. M. Schafer and M. J. Singer, "Influence of Physical and Mineralogical Properties on Swelling of Soils in Yolo County, California," *Soil Science Society of America Journal*, vol. 40, no. 4, pp. 557-562, 1976.

[31] J. D. Nelson and D. J. Miller, "Expansive Soils: Problems and Practice in Foundation and Pavement Engineering," John Wiley and Sons, Inc., New York, 1992.

[32] E. I. Stavridakis, "A Solution to the Problem of Predicting the Suitability of Silty–Clayey Materials for Cement-Stabilization," *Geotechnical & Geological Engineering*, vol. 24, no. 2, pp. 379-398, 2006. doi.10.1007/s10706-004-7934-6

[33] W. J. Likos, "Measurement of Crystalline Swelling in Expansive Clay," *Geotechnical Testing Journal*, vol. 27, no. 6, pp. 540-546, 2004. doi.10.1520/GTJ11857

[34] A. C. D. Newman, "Chemistry of Clays and Clay Minerals," Longman Scientific and Technical, Essex, England,, 1987.

[35] H. V. Olphen, "An Introduction to Clay Colloid Chemistry, for Clay Technologists, Geologists, and Soil Scientists," Krieger, Malaba, Florida, 1991.

[36] J. A. Greathouse, S. E. Feller, and D. A. McQuarrie, "The Modified Gouy-Chapman Theory: Comparisons between Electrical Double Layer Models of Clay Swelling," *Langmuir*, vol. 10, no. 7, pp. 2125-2130, 1994. doi.10.1021/la00019a018

[37] G. H. Bolt and R. D. Miller, "Compression Studies of Illite Suspensions," *Soil Science Society of America Journal*, vol. 19, no. 3, pp. 285-288, 1955. doi.10.2136/sssaj1955.03615995001900030010x

[38] B. P. W. G. H. Bolt and R. D. Miller, "Swelling Pressure of Montmorillonite," *Soil Science Society of America Journal*, vol. 21, no. 5, pp. 495-497, 1957. doi.10.2136/sssaj1957.03615995002100050009x

[39] J. K. Mitchell, "The Application of Colloidal Theory to Compressibility of Clays," in Proc. Seminar on Interparticle Forces in Clay–Water–Electrolyte Systems, Commonwealth Scientific and Industrial Research Organisation, Melbourne, Australia, vol. 2, pp. 92-97, 1960.

[40] G. Mesri and R. E. Olsen, "Consolidation Characteristics of Montmorillonite," *Géotechnique*, vol. 21, no. 4, pp. 341-352, 1971.

[41] A. Sridharan and M. S. Jayadeva, "Double Layer Theory and Compressibility of Clays," *Géotechnique*, vol. 32, no. 2, pp. 133-144, 1982. doi.10.1680/geot.1982.32.2.133

[42] S. Tripathy, A. Sridharan, and T. Schanz, "Swelling Pressures of Compacted Bentonites From Diffuse Double Layer Theory," *Canadian Geotechnical Journal*, vol. 41, no. 3, pp. 437-450, 2004. doi.10.1139/t03-096

[43] T. K. Mitchell and L. Raad, "Control of Volume Changes in Expansive Earth Materials," University of Wyoming, Laramie, 1973, vol. 2.

[44] D. R. Snethen, "An Evaluation of Expedient Methodology for Identification of Potentially Expansive Soils," U.S. Army Waterways Experiment Station, Vicksburg, MS, Interim Report FHWA-RD-77- 94 1977, vol. 2.

[45] J. K. Mitchell, "Fundamentals of Soil Behavior," John Wiley, New York, 1976.

[46] D. R. Snethen, "Characterization of Expansive Soils using Soil Suction Data," in Proc. 4th International Conference on Expansive Soils, ASCE, Denver, Colorado, pp. 54-75, 1980.

[47] D. G. Fredlund and N. R. Morgenstern, "Stress State Variables for Unsaturated Soils," *Journal of Geotechnical and Geoenvironmental Engineering*, ASCE, vol. 103, no. GT5, pp. 447-466, 1977.

[48] L. D. Johnson, "Influence of Suction on Heave of Expansive Soils," DTIC Document, Vicksburg, MS, S-73-17, 1973.

[49] R. E. Olson and L. J. Langfelder, "Pore Water Pressures in Unsaturated Soils," *Journal of Soil Mechanics & Foundations Division*, ASCE, vol. 97, no. SM1, pp. 127-150, 1965.

[50] G. D. Aitchison, "Discussion," in Proc. 6th International Conference on Soil Mechanics and Foundation Engineering, Montreal, QC, pp. 318-321, 1965.

[51] L. D. Johnson and D. R. Snethen, "Prediction of Potential Heave of Swelling Soil," *ASTM Geotechnical Testing Journal*, vol. 1, no. 3, pp. 117-124, 1978.

[52] H. B. Seed, J. K. Mitchell, and C. K. Chan, "Studies of Swell and Swell Pressure Characteristics of Compacted Clays," Highway Research Board Bulletin, no. 313, pp. 12-39, 1962.

[53] F. H. Chen, "The Basic Physical Property of Expansive Soils," in Proc. 3rd International Conference Expansive Soils, Haifa, Israel, pp. 17-25, 1973.

[54] L. D. Johnson, "Review of Literature on Expansive Clay Soils," U.S. Army Engineer Waterways Experiment Station, Vicksburg, MS, S-73-17, 1969.

[55] J. E. Holland and C. E. Lawrence, "Seasonal Heave of Australia Clay Soils," in Proc. 4th International Confernece on Expansive Soils, ASCE, New York, pp. 302-321, 1980.

[56] L. M. Krazynski, "Expansive Soils in Highway Construction-Some Problems and Solutions," in Proc. 4th International Road Fed. African Highways Conference, Nairobi, Kenya, 1980.

[57] G. Donaldson, "A Study of Level Observations on Buildings as Indications of Moisture Movements in the Underlying Soil," National Building Research Institute, Butterworths, Australia, 1965.

[58] E. L. Buckley, "Loss and Damage on Residential Slab-on-Ground Foundations," Construction Research Center, University of Texas at Arlington, Arlington, TX, TR-2-74, 1974.

[59] J. R. Wise and W. R. Hudson, "An Esamination of Expansive Clay Problems in Texas," Center for Highway Research, University of Texas at Austin, Austin, TX, 118-5, 1971.

[60] C. M. A. De Bruijin, "Some Observations on Soil Moisture Conditions Beneath and Adjacent to Tarred Roads and Other Surface Treatments in South Africa," Butterworths, Australia, 1965.

[61] L. D. Johnson and W. R. Stroman, "Analysis of Behavior of Expansive Soil Foundations," U.S. Army Engineer Waterways Experiment Station, Vicksburg, MS, Technical Reporty S-76-8, 1976.

[62] J. J. Hamilton, "Effects of Environment on the Performance of Shallow Foundations," *Canadian Geotechnical Journal*, vol. 6, no. 1, pp. 65-80, 1969. doi.10.1139/t69-008

[63] G. Kassiff and R. Baker, "Aging Effects on Swell Potential of Compacted Clays," *Journal of Soil Mechanics & Foundations Division*, ASCE, vol. SM 3, no. 1, pp. 529-540, 1971.

[64] W. G. Holtz, "Expansive Clays- Properties and Problems," vol. 54, Quarterly Colorado School Mines, 1959.

[65] E. Buckingham, "Studies of the Movement of Soil Moisture," United States Department of Agriculture, Bulletin no 38, 1907.

[66] W. Gardner and J. A. Widtsoe, "The Movement of Soil Moisture," Soil Science, vol. 11, no. 3, pp. 215–232, 1921.

[67] L. A. Richards, "The Usefulness of Capillary Potential to Soil Moisture and Plant Investigators," *Journal of Agricultural Research*, vol. 37, no. 12, pp. 719-742, 1928.

[68] N. E. Edlefsen and A. B. C. Anderson, "Thermodynamics of Soil Moisture," University of California, Oakland, California, U.S., 1943.

[69] R. G. McKeen and D. J. Hamberg, "Characterization of Expansive Soils," Transportation Research Board, no. 790, pp. 73-78, 1981.

[70] D. R. Snethen, L. D. Johnson, and D. M. Patrick, "An Evaluation of Expedient Methodology for Identification of Potentially Expansive Soils," 1977.

[71] B. G. Richards, "Measurement of the Free Energy of Soil Moisture by the Psychrometric Technique Using Thermistors," Butterworths, Sydney, 1965.

[72] J. Krahn and D. G. Fredlund, "On Total Matric and Osmotic Suction," *Soil Science*, vol. 114, no. 5, pp. 339-348, 1972.

[73] Y. H. Wang and D. G. Fredlund, "Towards a Better Understanding of the Role of the Contractile Skin," in Proc. 2nd Asian Conference on Unsaturated Soils, April, Osaka, Japan, pp. 15-17, 2003.

[74] J. D. Nelson, "Design Parameters for Slab-On-Grade Foundations," in Proc. Unsaturated Soils 2006, ASCE, Carefree, Arizona, United States, pp. 2110-2120, 2006. doi.10.1061/40802(189)178

[75] M. T. Van Genuchten, "A Closed-Form Equation for Predicting the Hydraulic Conductivity of Unsaturated Soils," *Soil science society of America journal*, vol. 44, no. 5, pp. 892-898, 1980. doi.10.2136/sssaj1980.03615995004400050002x

[76] E. E. Alonso, A. Gens, and A. Josa, "A Constitutive Model for Partially Saturated Soils," *Géotechnique*, vol. 40, no. 3, pp. 405-430, 1990. doi.10.1680/geot.1990.40.3.405

[77] S. K. Vanapalli, D. G. Fredlund, D. E. Pufahl, and A. W. Clifton, "Model for the Prediction of Shear Strength with Respect to Soil Suction," Canadian *Geotechnical Journal*, vol. 33, no. 3, pp. 379-392, 1996. doi.10.1139/t96-060

[78] D. W. Rassam and D. J. Williams, "A Relationship Describing the Shear Strength of Unsaturated Soils," *Canadian Geotechnical Journal*, vol. 36, no. 2, pp. 363-368, 1999. doi.10.1139/t98-102

[79] C. Rampino, C. Mancuso, and F. Vinale, "Experimental Behaviour and Modelling of an Unsaturated Compacted Soil," *Canadian Geotechnical Journal*, vol. 37, no. 4, pp. 748-763, 2000. doi.10.1139/t00-004

[80] S. K. Vanapalli and W. T. Oh, "A Model for Predicting the Modulus of Elasticity of Unsaturated Soils Using the Soil-Water Characteristic Curve," *International Journal of Geotechnical Engineering*, vol. 4, no. 4, pp. 425-433, 2010. doi.10.3328/IJGE.2010.04.04.425-433

[81] D. G. Fredlund, H. Rahardjo, E. C. Leong, and C. W. W. Ng, "Suggestions and Recommendations for the Interpretation of Soil-water Characteristic Curves," presented at the 14th Southeast Asian Geotechnical Conference, Hong Kong, China, pp. 503-508, 2001.

[82] D. G. Fredlund, H. Rahardjo, and M. D. Fredlund, "Unsaturated Soil Mechanics in Engineering Practice," John Wiley & Sons, 2012.

[83] S. K. Vanapalli, D. G. Fredlund, and D. E. Pufahl, "The Influence of Soil Structure and Stress History on the Soil–Water Characteristics of a Compacted Till," *Géotechnique*, vol. 49, no. 2, pp. 143-159, 1999. doi.10.1680/geot.1999.49.2.143

[84] D. G. Fredlund and H. Rahardjo, "Soil Mechanics for Unsaturated Soils," John Wiley & Sons, New York, 1993.

[85] D. B. McWhorter and D. K. Sunada, "Ground-Water Hydrology and Hydraulics," Water Resources Publication, Highlands Ranch, Colorado,, 1977.

[86] A. T. Corey, "Mechanics of Immiscible Fluids in Porous Media," Water Resources Publication, Highlands Ranch, Colorado, 1994.

[87] D. G. Fredlund and A. Xing, "Equations for the Soil-water Characteristic Curve," *Canadian Geotechnical Journal*, vol. 31, no. 4, pp. 521-532, 1994. doi.10.1139/t94-061

[88] J. Bear, "Hydraulic of Groundwater," McGraw-Hill, New York, 1979.

[89] W. R. Gardner, "Some Steady-State Solutions of the Unsaturated Moisture Flow Equation with Application to Evaporation from a Water Table," *Soil Science*, vol. 85, no. 4, pp. 228-232, 1958.

[90] R. H. Brooks and A. T. Corey, "Hydraulic Properties of Porous Media," Colorado State University, Fort Collins, Colorado, 1964.

[91] Y. Mualem, "A New Model for Predicting the Hydraulic Conductivity of Unsaturated Porous Media," *Water Resources Research*, vol. 12, no. 3, pp. 513-522, 1976. doi.10.1029/WR012i003p00513

[92] E. C. Leong and H. Rahardjo, "Review of Soil-Water Characteristic Curve Equations," *Journal of Geotechnical and Geoenvironmental Engineering*, vol. 123, no. 12, pp. 1106-1117, 1997. doi.10.1061/(ASCE)1090-0241(1997)123:12(1106)

[93] A. J. Puppala, K. Punthutaecha, and S. K. Vanapalli, "Soil-Water Characteristic Curves of Stabilized Expansive Soils," *Journal of Geotechnical and Geoenvironmental Engineering*, vol. 132, no. 6, pp. 736-751, 2006. doi.doi:10.1061/(ASCE)1090-0241(2006)132:6(736)

[94] S. C. Gupta and W. E. Larson, "Estimating Soil Water Retention Characteristics from Particle Size Distribution, Organic Matter Percent, and Bulk Density," *Water Resources Research*, vol. 15, no. 6, pp. 1633-1635, 1979. doi.10.1029/WR015i006p01633

[95] M. D. Fredlund, D. G. Fredlund, and G. W. Wilson, "Prediction of the Soil-Water Characteristic Curve from Grain-Size Distribution and Volume-Mass Properties," in Proc. 3rd Brazilian Symposium on Unsaturated Soils, NSAT '97, Rio de Janeiro, Brazil, vol. 1, pp. 13-23, 1997.

[96] L. Zhang and Q. Chen, "Predicting Bimodal Soil–Water Characteristic Curves," *Journal of Geotechnical and Geoenvironmental Engineering,* vol. 131, no. 5, pp. 666-670, 2005. doi.10.1061/(ASCE)1090-0241(2005)131:5(666)

[97] K. R. J. Smettem and C. Kirkby, "Measuring the Hydraulic Properties of a Stable Aggregated Soil," *Journal of Hydrology*, vol. 117, no. 1, pp. 1-13, 1990. doi.10.1016/0022-1694(90)90084-B

[98] G. V. Wilson, P. M. Jardine, and J. P. Gwo, "Modeling the Hydraulic Properties of a Multiregion Soil," *Soil Science Society of America Journal*, vol. 56, no. 6, pp. 1731-1737, 1992. doi.10.2136/sssaj1992.03615995005600060012x

[99] W. Durner, "Hydraulic Conductivity Estimation for Soils with Heterogeneous Pore Structure," *Water Resources Research*, vol. 30, no. 2, pp. 211-223, 1994. doi.10.1029/93WR02676

[100] D. Mallants, P.-H. Tseng, N. Toride, A. Tinunerman, and J. Feyen, "Evaluation of Multimodal Hydraulic Functions in Characterizing a Heterogeneous Field Soil," *Journal of Hydrology*, vol. 195, no. 1, pp. 172-199, 1997. doi.10.1016/S0022-1694(96)03251-9

[101] M. M. Abbaszadeh, S. Houston, C. Zapata, W. Houston, B. Welfert, and K. Walsh, "Laboratory Determination of Soil-Water Characteristic Curves for Cracked Soil," in Proc. 5th International Conference on Unsaturated Soils, Spain, Barcelona, pp. 409-415, 6–9 September 2010, 2010.

[102] T. Y. Elkady, A. M. Al-Mahbashi, and T. O. Al-Refeai, "Stress-Dependent Soil-Water Characteristic Curves of Lime-Treated Expansive Clay," *Journal of Materials in Civil Engineering*, vol. 27, no. 3, p. 04014127, 2015. doi.10.1061/(ASCE)MT.1943-5533.0000995

[103] S. C. Qi and S. K. Vanapalli, "Numerical study on expansive soil slope stability considering the cracks and coupling effects," in Unsaturated Soil Mechanics - from Theory to Practice, ed CRC Press, 2015, pp. 621-627.

[104] W. Brutsaert, "Some Methods of Calculating Unsaturated Permeability," *Transactions of the ASABE*, vol. 10, no. 3, pp. 400-404, 1967.

[105] G. E. Laliberte, "A Mathematical Function for Describing Capillary Pressure-Desaturation Data," International Association of Scientific Hydrology Bulletin, vol. 14, no. 2, pp. 131-149, 1969. doi.10.1080/02626666909493724

[106] G. S. CAMPBELL, "A Simple Method for Determining Unsaturated Conductivity from Moisture Retention Data," *Soil Science*, vol. 117, no. 6, pp. 311-314, 1974.

[107] N. T. Burdine, "Relative Permeability Calculations From Pore Size Distribution Data," *Transactions of the Metallurgical Society of AIME*, vol. 198, pp. 71-78, 1953. doi.10.2118/225-G

[108] C. R. McKee and A. C. Bumb, "The Importance of Unsaturated Flow Parameters in Designing a Hazardous Waste Site," in Proc. Hazardous Waste and Environmental Emergencies, Hazardous Materials Control Research Institute National Conference, Houston, Texas, pp. 50-58, 1984.

[109] J. H. F. Pereira and D. G. Fredlund, "Volume Change Behavior of Collapsible Compacted Gneiss Soil," *Journal of Geotechnical and Geoenvironmental Engineering*, vol. 126, no. 10, pp. 907-916, 2000. doi.10.1061/(ASCE)1090-0241(2000)126:10(907)

[110] C. A. Burger and C. D. Shackelford, "Soil-Water Characteristic Curves and Dual Porosity of Sand–Diatomaceous Earth Mixtures," *Journal of Geotechnical and Geoenvironmental Engineering*, vol. 127, no. 9, pp. 790-800, 2001. doi.10.1061/(ASCE)1090-0241(2001)127:9(790)

[111] J. Gilson de F. N. Gitirana and D. G. Fredlund, "Soil-Water Characteristic Curve Equation with Independent Properties," *Journal of Geotechnical and Geoenvironmental Engineering*, vol. 130, no. 2, pp. 209-212, 2004. doi.10.1061/(ASCE)1090-0241(2004)130:2(209)

[112] H. Q. Pham, "A Volume-Mass Constitutive Model for Unsaturated Soils," Ph.D. Dissertation, Department of Civil and Geological Engineering, University of Saskatchewan, Saskatchewan, Canada, 2005.

[113] A. Satyanaga, H. Rahardjo, E.-C. Leong, and J.-Y. Wang, "Water Characteristic Curve of Soil with Bimodal Grain-Size Distribution," *Computers and Geotechnics*, vol. 48, pp. 51-61, 2013. doi.10.1016/j.compgeo.2012.09.008

[114] X. Li, J. H. Li, and L. M. Zhang, "Predicting Bimodal Soil–Water Characteristic Curves and Permeability Functions Using Physically Based Parameters," *Computers and Geotechnics*, vol. 57, pp. 85-96, 2014. doi.10.1016/j.compgeo.2014.01.004

[115] R. B. Peck, W. E. Hanson, and T. H. Thornburn, "Foundation Engineering," vol. 10, Wiley New York, 1974.

[116] A. W. Skempton, "The Colloidal Activity of Clays," Selected Papers on Soil Mechanics, pp. 106-118, 1953.

[117] C. Zapata, S. Houston, W. Houston, and H. Dye, "Expansion Index and Its Relationship with Other Index Properties," in Proc. 4th International Conference on Unsaturated Soils, ASCE, Carefree, AZ, pp. 2133-2137, 2006. doi.10.1061/40802(189)180

[118] "ICBO: Uniform Building Code (1997)," International Conference of Building Officials, Whittier, CA, 1997.

[119] "Standard Test Methods for Expansion Index of Soil," ASTM D4829-11, Annual book of ASTM standards,ASTM, West Conshohocken, PA, 2011. doi.10.1520/D4829-11

[120] J. D. Nelson, D. D. Overton, and D. B. Durkee, "Depth of Wetting and the Active Zone," in Proc. Expansive clay soils and vegetative influence on shallow foundations, ASCE, Houston, Texas, United States, pp. 95-109, 2001. doi.10.1061/9780784405925

[121] M. W. O'Neill, "Adaptive Model for Drilled Shafts in Expansive Clay," *Geotechnical Special Publication*, ASCE, vol. 16, pp. 1-20, 1988.

[122] B. Rajani and N. R. Morgenstern, "Behaviour of a Semi-Infinite Beam in a Creeping Medium," *Canadian Geotechnical Journal*, vol. 29, no. 5, pp. 779-788, 1992/10/01, 1992. doi:10.1139/t92-085

[123] B. B. Rajani and N. R. Morgenstern, "Uplift of Model Steel Pipelines Embedded in Polycrystalline Ice," *Canadian Geotechnical Journal*, vol. 30, no. 3, pp. 441-454, 1993. doi.10.1139/t93-038

[124] B. B. Rajani and N. R. Morgenstern, "Comparison of Predicted and Observed Responses of Pipeline to Differential Frost Heave," *Canadian Geotechnical Journal*, vol. 31, no. 6, pp. 803-816, 1994. doi.10.1139/t94-098

[125] C. Ferregut and M. Picornell, "Calibration of Safety Factors for the Design of Piers in Expansive Soils," in Proc. Risk and Reliability in Ground Engineering, Institution of Civil Engineers, London, pp. 277-290, 1994. doi.10.1680/rarige.19867.0023

[126] K. Venkataramana, "Building on Expansive Clays with Special Reference to Trinidad," *West Indian Journal of Engineering*, vol. 25, no. 2, pp. 43-53, 2003.

[127] L. Miao, F. Wang, and Y. Cui, "Improvement and Controlling Deformation of the Expansive Soil Ground," in Proc. 5th International Conference on Unsaturated Soils, Barcelona, Spain, pp. 1321-1324, 2010.

[128] M. A. Ismail and M. A. Shahin, "Finite Element Modeling of Innovative Shallow Foundation System for Reactive Soils," *International Journal of Geomate*, vol. 1, no. 1, pp. 78-82, 2011.

[129] H. G. Poulos, "Program PIES-Axial Response of Piles in Expansive Soils-User's Guide," Centre for Geotechnical Research, University of Sydney, Australia, 1989.

[130] D. E. L. Ong, "Pile Behaviour Subject to Excavation-Induced Soil Movement in Clay," Ph.D. Dissertation, National University of Singapore, Singapore, 2004.

[131] D. E. L. Ong, C. E. Leung, and Y. K. Chow, "Pile Behavior Due to ExcavationInduced Soil Movement in Clay. I: Stable Wall," *Journal of Geotechnical and Geoenvironmental Engineering*, ASCE, vol. 132, no. 1, pp. 36-44, 2006. doi.10.1061/(ASCE)1090-0241(2006)132:1(36)

[132] S.-T. Wang, L. Vasquez, and L. C. Reese, "Study of the Behavior of Pile Groups in Liquefied Soils," in Proc. The 14th World Conference on Earthquake Engineering, Beijing, China., 2008.

[133] K. S. Ti, B. B. K. Huat, J. Noorzaei, M. S. Jaafar, and G. S. Sew, "Modeling of Passive Piles–An Overview," *Electronic Journal of Geotechnical Engineering*, vol. 14, 2009.

[134] ISRM, "International Society for Rock Mechanics Commission on Swelling Rock and Working Group on Swelling Rock of the Commission on Testing Methods," *International Journal of Rock Mechanics and Mining Sciences & Geomechanics* Abstracts, vol. 26, no. 5, pp. 415-426, 1989. doi.10.1016/0148-9062(89)90937-6

[135] "Standard Test Methods for One-Dimensional Swell or Collapse of Soils," ASTM D4546-14, Annual book of ASTM standards,ASTM, West Conshohocken, PA, 2014. doi.10.1520/D4546-14

[136] K.-C. Chao, "Design Principles for Foundations on Expansive Soils," Ph.D. Dissertation, Department of Civil and Environmental Engineering, Colorado State University, Fort Collins, Colorado, 2007.

[137] D. W. Taylor, "Fundamentals of Soil Mechanics," John Wiley & Sons, Inc., New York, 1948.

[138] J. E. B. Jennings and K. Knight, "The Prediction of Total Heave from the Double Oedometer Test," in Proc. Symposium on Expansive Clays, South African Institution of Civil Engineers, Johannesburg, vol. 7, no. 9, pp. 13-19, 1957.

[139] J. A. J. Salas and J. M. Serratosa, "Foundations on Swelling Clays," in Proc. 4th International Conference on Soil Mechanics and Foundation Engineering, London, England, vol. 1, pp. 424-428, 1957.

[140] R. M. Palit, "Determination of Swelling Pressure of Black Cotton Soil," in Proc. 3rd International Conference on Soil Mechanics and Foundation Engineering, Switzerland, 1953.

[141] G. D. Aitchison and R. Martin, "A Membrane Oedometer for Complex Stress–Strain Studies in Expansive Clays," in Proc. 3rd International Conference on Expansive Soils, Haifa, Israel, vol. 2, pp. 83-88, 1973.

[142] D. G. Fredlund, J. U. Hasan, and H. L. Filson, "The Prediction of Total Heave," in Proc. 4th International Conference on Expansive Soils, Denver, CO, USA, vol. 1, pp. 1-17, 1980.

[143] L. Lu, "A Simple Technique for Estimating the 1-D Heave of Natural Expansive Soils," M.Sc. Thesis, Department of Civil Engineering, University of Ottawa, Ottawa, Canada, 2010.

[144] L. Lu and S. K. Vanapalli, "A State-of-the art Review of 1-D Heave Prediction Methods for Expansive Soils," *International Journal of Geotechnical Engineering*, vol. 6, no. 1, pp. 15-41, 2012. doi.10.3328/ijge.2012.06.01.15-41

[145] A. S. Rao, B. R. Phanikumar, and R. S. Sharma, "Prediction of Swelling Characteristics of Remoulded and Compacted Expansive Soils Using Free Swell Index," *Quarterly Journal of Engineering Geology and Hydrogeology*, vol. 37, no. 3, pp. 217-226, 2004. doi.10.1144/1470-9236/03-052

[146] Ö. Çimen, S. N. Keskin, and H. Yıldırım, "Prediction of Swelling Potential and Pressure in Compacted Clay," *Arabian Journal for Science and Engineering*, vol. 37, no. 6, pp. 1535-1546, 2012. doi.10.1007/s13369-012-0268-4

[147] Hana H. Adem and Sai K. Vanapalli, "Review of Methods for Predicting in Situ Volume Change Movement of Expansive Soil over Time," *Journal of Rock Mechanics and Geotechnical Engineering*, vol. 7, no. 1, pp. 73-86, 2015. doi.10.1016/j.jrmge.2014.11.002

[148] H. B. Seed, R. J. Woodward Jr, and R. Lundgren, "Prediction of Swelling Potential for Compacted Clays," *Journal of the soil mechanics and foundations division*, vol. 88, no. 3, pp. 53-88, 1962.

[149] D. H. Van der Merwe, "The Prediction of Heave from the Plasticity Index and the Percentage Clay Fraction of Soils," vol. 6, South African Council for Scientific and Industrial Research, 1964.

[150] B. V. Ranganatham and B. Satyanarayana, "A Rational Method of Predicting Swelling Potential for Compacted Expansive Clays," in Proc. 6th Inter. Conf. Soil Mechanics Foundation Eng, International Society for Soil Mechanics and Geotechnical Engineering, London, vol. 1, pp. 92-96, 1965.

[151] N. V. Nayak and R. W. Christensen, "Swelling Characteristics of Compacted Expansive Soils," *Clays and Clay Minerals*, vol. 19, no. 4, pp. 251-261, 1971.

[152] V. N. Vijayvergiya and O. I. Ghazzaly, "Prediction of Swelling Potential of Natural Clays," in Proc. 3rd International Conference on Expansive Clays, Academic Press, Haifa, Israel, vol. 1, pp. 227-236, 30 July – 1 August 1973, 1973.

[153] G. L. Schneider and A. R. Poor, "The Prediction of Soil Heave and Swell Pressures Developed by an Expansive Clay," Construction Research Center, University of Texas, Austin, TX, TR-9-74, 1974.

[154] D. J. Weston, "Expansive Roadbed Treatment for Southern Africa," in Proc. 4th International Conference on Expansive Soils, vol. 1, pp. 339-360, 1980.

[155] M. Picornell and R. L. Lytton, "Modelling the Heave of a Heavily Loaded Foundation," in Proc. 5th International Conference on Expansive Soils, Institution of Engineers, Adelaide, Australia, pp. 104-108, 1984.

[156] A. W. Dhowian, "Field Performance of Expansive Shale Formation," *Journal of King Abdulaziz University*, vol. 2, pp. 165-82, 1990. doi.10.4197/eng.2-1.11

[157] D. E. McCormack and L. P. Wilding, "Soil Properties Influencing Swelling in Canfield and Geeburg Soils," *Soil Science Society of America Journal*, vol. 39, no. 3, pp. 496-502, 1975. doi.10.2136/sssaj1975.03615995003900030034x

[158] P. Pells, A. Robertson, and I. J. A. Brackley, "A Model of Unsaturated Clay Structure and its Application to Swell Behaviour," in Proc. 6th Regional Conference for Africa on Soil Mechanics and Foundation Engineering, Durban, South Africa, pp. C26–C34, 1975.

[159] M. W. O'Neill and O. I. Ghazzaly, "Swell Potential Related to Building Performance," *Journal of the Geotechnical Engineering Division*, ASCE, vol. 103, no. 12, pp. 1363-1379, 1977.

[160] L. D. Johnson, "Predicting Potential Heave and Heave With Time in Swelling Foundation Soils," U.S. Army Engineer Waterways Experiment Station, Vicksburg, Mississippi, S-78-7, 1978.

[161] S. S. Bandyopadhyay, "Prediction of Swelling Potential for Natural Soils," *Journal of Geotechnical and Geoenvironmental Engineering*, vol. 107, no. 5, pp. 658-691, 1981.

[162] A. A. Basma, "Prediction of Expansion Degree for Natural Compacted Clays," *Geotechnical Testing Journal*, vol. 16, no. 6, pp. 542-549, 1993. doi.10.1520/GTJ10294J

[163] E. ÇOKÇA, "Relationship Between Methylene Blue Value, Initial Soil Suction and Swell Percent of Expansive Soils," *Turkish Journal of Engineering and Environmental Sciences*, vol. 26, no. 6, pp. 521-530, 2002.

[164] Z. Abiddin Erguler and R. Ulusay, "A Simple Test and Predictive Models for Assessing Swell Potential of Ankara (Turkey) Clay," *Engineering Geology*, vol. 67, no. 3-4, pp. 331-352, 2003. doi.10.1016/S0013-7952(02)00205-3

[165] Y. Erzin and O. Erol, "Swell Pressure Prediction by Suction Methods," *Engineering Geology*, vol. 92, no. 3, pp. 133-145, 2007. doi.10.1016/j.enggeo.2007.04.002

[166] A. A. Sabtan, "Geotechnical Properties of Expansive Clay Shale in Tabuk, Saudi Arabia," *Journal of Asian Earth Sciences*, vol. 25, no. 5, pp. 747-757, 2005. doi.10.1016/j.jseaes.2004.07.003

[167] S. Azam, "Study on the Swelling Behaviour of Blended Clay–Sand Soils," *Geotechnical and Geological Engineering*, vol. 25, no. 3, pp. 369-381, 2007. doi.10.1007/s10706-006-9116-1

[168] I. Yilmaz, "Swell Potential and Shear Strength Estimation of Clays," *Applied Clay Science*, vol. 46, no. 4, pp. 376-384, 12//, 2009. doi.10.1016/j.clay.2009.09.011

[169] M. Türköz and H. Tosun, "The Use of Methylene Blue Test for Predicting Swell Parameters of Natural Clay Soils," *Scientific Research and Essays*, vol. 6, no. 8, pp. 1780-1792, 2011. doi.10.5897/SRE10.629

[170] M. Zumrawi, "Swelling Potential of Compacted Expansive Soils," *International Journal of Engineering Research and Technology*, vol. 2, no. 3, pp. 1-6, 2013.

[171] S. K. Vanapalli, L. Lu, and W. T. Oh, "Estimation of Swelling Pressure and 1-D Heave in Expansive Soils," in Proc. 5th International Conference on Unsaturated Soils, CRC Press, Barcelona, Spain, vol. 2, pp. 1201-1207, 2010.

[172] J. B. Burland, "The Estimation of Field Effective Stresses and the Prediction of Total Heave Using a Revised Method of Analyzing the Double Oedometer Test," The Civil Engineer in South Africa. Transactions of South African Institute of Civil Engineering, 1962.

[173] D. G. Fredlund, "Prediction of Ground Movement in Swelling Clays," presented at the 31st Annual Soil Mechanics and Foundation Engineering Conference, Minneapolis, Minnesota, 1983.

[174] J. D. Nelson, D. B. Durkee, and J. P. Bonner, "Prediction of Free Field Heave Using Oedometer Test Data," presented at the 46th Annual Geotechnical Engineering Conference, University of Minnesota, St. Paul, Minnesota, 1998.

[175] J. P. Bonner, "Comparison of Predicted Heave Using Oedometer Test Data to Actual Heave," M.Sc. Thesis, Colorado State University, Fort Collins, Colorado, 1998.

[176] J. D. Nelson, D. K. Reichler, and J. M. Cumbers, "Parameters for Heave Prediction by Oedometer Tests," in Proc. Unsaturated Soils 2006, ASCE, pp. 951-961, 2006.

[177] C. M. A. DeBruijn, "Swelling Characteristics of a Transported Soil Profile at Leeuhof, Vereeniging (Transvaal)," in Proc. 5th International Conference Soil Mechanics Foundation Engineering, Paris, vol. 1, pp. 43-49, 1961.

[178] E. Sampson Jr, R. L. Schuster, and W. D. Budge, "A Method of Determining Swell Potential of an Expansive Clay," in Proc. 1st International Conference of Expansive Soils, Texas A & M University Press, College Station, TX, pp. 255-275, 1965.

[179] C. A. Noble, "Swelling Measurements and Prediction of Heave for a Lacustrine Clay," *Canadian Geotechnical Journal*, vol. 3, no. 1, pp. 32-41, 1966. doi.10.1139/t66-003

[180] R. A. Sullivan and B. McClelland, "Predicting Heave of Buildings on Unsaturated Clay," in Proc. 2nd International Research and Engineering Conference on Expansive Clay soils, Texas A&M University Press, College Station, TX, pp. 404-420, 1969.

[181] A. Komornik, Y. Ben-Yaacob, and G. Wiseman, "Studies of In-Situ Moisture and Swelling Potential Profiles," in Proc. 2nd International Engineering Conference of Expansive Soils, Texas, pp. 348-361, 1969.

[182] NAVFAC, "Soil Mechanics, Foundation and Earth Structures - Design Manual," Naval Facilities Engineering Command, Department of the Navy, Bureau of yards and Docks, Washington, D.C., NAVFACDM-7, 1971.

[183] H. Y. Wong and R. M. Yong, "A Study of Swelling and Swelling Force During Unsaturated Flow in Expansive Soils," in Proc. 3rd International Conference of Expansive Soils, Haifa, Israel, pp. 143-151, 1973.

[184] H. J. Gibbs, "Use of a Consolidometer for Measuring Expansion Potential of Soils," in Proc. Workshop on Expansive Clays and Shales in Highway Design and Construction, University of Wyoming, Laramie, vol. 1, no. Workshop Proceedings, pp. 206-213, 1973.

[185] A. W. Smith, "Method for Determining the Potential Vertical Rise (PVR)," in Proc. Workshop on Expansive Clays and Shales in Highway Design and Construction, University of Wyoming, Laramie, vol. 1, pp. 189-205, 1973.

[186] J. E. B. Jennings, R. A. Firth, T. K. Ralph, and N. Nagar, "An Improved Method for Predicting Heave Using the Oedometer Test," in Proc. 3rd International Conference on Expansive Soils, Haifa, Israel, pp. 149-154, 1973.

[187] T. C. P. Teng, R. M. Mattox, and M. B. Clisby, "A Study of Active Clays as Related to Highway Design," Mississippi State Highway Department, Jackson, 1972.

[188] T. C. P. Teng, R. M. Mattoy, and M. B. Clisby, "Mississippi Experimental Work on Active Clays," in Proc. Workshop on Expansive Clays and Shales in Highway Design and Construction, pp. 1-27, 1973.

[189] T. C. P. Teng and M. B. Clisby, "Experimental Work for Active Clays in Mississippi," *Journal of Transportation Engineering*, ASCE, vol. ASCE 101, no. TE 1, pp. 77-95, 1975.

[190] A. A. Porter and J. D. Nelson, "Strain Controlled Testing of Expansive Soils," in Proc. 4th International Conference of Expansive Soils, ASCE, Denver, Colorado, pp. 34-44, 1980.

[191] A. Sridharan, A. Rao, and P. Sivapullaiah, "Swelling Pressure of Clays," *Geotechnical Testing Journal*, ASTM, vol. 9, no. 1, pp. 24-31, 1986. doi.10.1520/GTJ10608J

[192] A. O. Erol, A. Dhowian, and A. Youssef, "Assessment of Oedometer Methods for Heave Prediction," in Proc. 6th International Conference on Expansive Soils, New Delhi, India, pp. 99-103, 1987.

[193] N. B. Shanker, M. V. Ratman, and A. S. Rao, "Multi-Dimensional Swell Behavior of Expansive Clays," in Proc. 6th International Conference of Expansive Soils,, New Delhi, India., pp. 143-147, 1987.

[194] M. A. Al-Shamrani and A. I. Al-Mhaidib, "Prediction of Potential Vertical Swell of Expansive Soils Using a Triaxial Stress Path Cell," *Quarterly Journal of Engineering Geology and Hydrogeology*, vol. 32, no. 1, pp. 45-54, 1999. doi.10.1144/GSL.QJEG.1999.032.P1.03

[195] A. A. Basma, A. S. Al-Homoud, A. I. Husein Malkawi, and M. A. Al-Bashabsheh, "Swelling-shrinkage Behavior of Natural Expansive Clays," *Applied Clay Science*, vol. 11, no. 2, pp. 211-227, 1996. doi.10.1016/S0169-1317(96)00009-9

[196] K. S. Subba Rao and S. Tripathy, "Effect of Aging on Swelling and Swell-Shrink Behavior of a Compacted Expansive Soil," *ASTM Geotechnical Testing Journal*, vol. 26, no. 1, pp. 36-46, 2003. doi.10.1520/GTJ11100J

[197] USA Department of the Army (DA), "Technical Manual TM 5-818-7, Foundations in Expansive Soils," Washington, D.C., 1983.

[198] D. J. Miller and J. D. Nelson, "Osmotic Suction in Unsaturated Soil Mechanics," Unsaturated Soils 2006, ASCE, pp. 1382-1393, 2006. doi.10.1061/40802(189)114

[199] A. Casagrande, "The Determination of the Pre-Consolidation Load and Its Practical Significance," in Proc. 1st International Conference on Soil Mechanics and Foundation Engineering, Harvard University Cambridge, vol. 3, pp. 60-64, 1936.

[200] S. G. Fityus, D. A. Cameron, and P. F. Walsh, "The Shrink Swell Test," *Geotechnical Testing Journal*, vol. 28, no. 1, pp. 92-101, 2005. doi.10.1520/GTJ12327. ISSN 0149-6115

[201] M. B. Jaksa, R. L. Cavagnaro, and D. A. Cameron, "Uncertainties Associated with the Visual-Tactile Method for Quantifying the Reactivity of Expansive Soils," *Australian Geomechanics*, vol. 31, pp. 84-91, 1997.

[202] G. D. Aitchison, "A Statement of the Problems the Engineer Faces with Expansive Soils," presented at the Proceedings of the 2nd International Research and Engineering Conference on Expansive Clay Soils, Texas A & M University, College Station, pp. 33-51, 1970.

[203] R. L. Lytton and J. A. Woodburn, "Design and Performance of Mat Foundation on Expansive Clay," in Proc. 3rd Int. Conf. Expansive Soils, Haifa, Isreal, vol. 1, pp. 301-308, 1973.

[204] Standards Australia, "Residential Slabs and Footings Construction," Committee BD-025, Australia, 06/05/1996.

[205] "Moisture Flow and Equilibria in Unsaturated Soils for Shallow Foundations," STP417, Permeability and Capillarity of Soils, American Society For Testing And Materials, 1967. doi.10.1520/STP47257S

[206] R. L. Lytton, "Foundations in Expansive Soils," in Numerical Methods in Geotechnical Engineering, C. S. Desai and J. T. Christian, Eds., ed New York McGraw-Hill, 1977, pp. 427-457.

[207] R. G. McKeen, "A Model for Predicting Expansive Soil Behavior," presented at the Proceedings of the 7th International Conference on Expansive Soils, ASCE, Dallas, Texas, vol. 1, pp. 1-6, 1992.

[208] P. W. Mitchell and D. L. Avalle, "A Technique to Predict Expansive Soil Movements," in Proc. Fifth International Conference on Expansive Soils, Adelaide, South Australia, pp. 124-130, 21-23 May, 1984.

[209] D. J. Hamberg and J. D. Nelson, "Prediction of Floor Slab Heave," presented at the Proceedings of the 5th International Conference on Expansive Soils, Australian Geomechanics Society (South Australian Group) and the Institution of Engineers, Adelaide, South Australia, pp. 137-140, 21-23 May, 1984.

[210] W. K. Wray, "The Principle of Soil Suction and its Geotechnical Engineering Applications," presented at the 5th International Conference on Expansive Soils, National Conference Publication, Adelaide, South Australia, pp. 114-118, 1984.

[211] R. L. Lytton, "Prediction of Movement in Expansive Clay," in Proc. In Vertical and Horizontal Deformations of Foundations and Embankment, Geotechnical Special Publication ,ASCE, New York, pp. 1827–1845, 1994.

[212] S. Fityus and D. W. Smith, "A Simple Model for the Prediction of Free Surface Movements in Swelling Clay Profiles," presented at the Proceedings of the 2nd International Conference on Unsaturated Soils, Beijing, China, pp. 473-478, 1998.

[213] A. P. Covar and R. L. Lytton, "Estimating Soil Swelling Behavior Using Soil Classification Properties," in Expansive Clay Soils and Vegetative Influence on Shallow Foundations, ed ASCE, 2001, pp. 44-63.

[214] J. L. Briaud, X. Zhang, and S. Moon, "Shrink Test-Water Content Method for Shrink and Swell Predictions," *Journal of Geotechnical and Geoenvironmental Engineering*, vol. 129, no. 7, pp. 590-600, 2003. doi.10.1061/(ASCE)1090-0241(2003)

[215] R. Lytton, C. Aubeny, and R. Bulut, "Design Procedure for Pavements on Expansive Soils: Volume 1," Texas Department of Transportation, Austin,Texas, FHWA/TX-05/0-4518-1, 2005, vol. 1.

[216] P. W. Mitchell, "Site Investigation Processes," Linn Education and Training Services, 1989.

[217] B. R. Brasher, D. P. Franzmeier, V. Valassis, and S. E. Davidson, "Use of Saran Resin to Coat Natural Soil Clods for Bulk Density and Water Retention Measurements," *Soil Science*, vol. 101, no. 2, p. 108, 1966. doi.10.1097/00010694-196602000-00006

[218] R. G. McKeen, "Design of Airport Pavements for Expansive Soils," DTIC Document, DOT/FAA/RD/81/25, 1981.

[219] R. G. McKeen, "Field Studies of Airport Pavements on Expansive Clay," presented at the Proceedings of the 4th International Conference on Expansive Soils, ASCE, Denver, Colorado, pp. 242-261, 1980.

[220] R. G. McKeen, "Validation of Procedures for Pavement Design on Expansive Soils," DTIC Document, DOT/FAA/PM-85/15, 1985.

[221] R. G. McKeen and L. D. Johnson, "Climate-Controlled Soil Design Parameters for Mat Foundations," *Journal of Geotechnical Engineering*, vol. 116, no. 7, pp. 1073-1094, 1990. doi.10.1061/(ASCE)0733-9410(1990)116:7(1073)

[222] H. W. Olsen, L. Krosley, K. Nelson, S. Chabrillat, A. F. H. Goetz, and D. C. Noe, "Mineralogy-Swelling Potential Relationships for Expansive Shales," in Advances in Unsaturated Geotechnics, ed Denver ASCE, 2000, pp. 361-378.

[223] F. Fan, "Mechanical And Thermal Properties Of Fly Ash-Based Geopolymer Cement," M.Sc. Thesis, Civil and Environmental Engineering, Louisiana State University, Baton Rouge, Louisiana, 2015.

[224] J. Davidovits and C. James, "Why the Pharaohs Built the Pyramids with Fake Stones," Geopolymer Institute, Saint-Quentin, France, 2009.

[225] American Coal Ash Association. (2014, 28th September). 2014 Coal Combustion Product (CCP) Production & Use Survey Report. Available: https://www.acaa-usa.org/Portals/9/Files/PDFs/2014ReportFinal.pdf

[226] E. I. Diaz and E. N. Allouche, "Recycling of Fly Ash into Geopolymer Concrete: Creation of a Database," in Proc. 2010 IEEE Green Technologies Conference, pp. 1-7, 15-16 April 2010, 2010. doi.10.1109/GREEN.2010.5453790

[227] "Treatment," 305.04.1.2, Subgrade Layer, Louisiana Department of Transportation and Development, Baton Rouge, 2016. Available: http://wwwsp.dotd.la.gov/Inside_LaDOTD/Divisions/Engineering/Standard_Specifications/Standard%20Specifications/2016%20Standard%20Specifications%20for%20Roads%20and%20Bridges%20Manual/07%20-%202016%20-%20Part%20III%20-%20Base%20Courses.pdf

[228] "Treatment," 305.04, Subgrade Layer,LADOTD, Louisiana Department of Transportation and Development, 2006. Available: http://wwwsp.dotd.la.gov/Inside_LaDOTD/Divisions/Engineering/Standard_Specifications/Standard%20Specifications/2016%20Standard%20Specifications%20for%20Roads%20and%20Bridges%20Manual/01%20-%202016%20-%20Cover.pdf

[229] "Additive Selection Criteria, "Subgrade Treatment,Texas Department of Transportation, Austin, Texas, 2005. Available: ftp://ftp.dot.state.tx.us/pub/txdot-info/cd/tech/stabilization.pdf

[230] "Additive Selection Criteria, "Base Material treatment,Texas Department of Transportation, Austin, Texas, 2005. Available: ftp://ftp.dot.state.tx.us/pub/txdot-info/cmd/tech/stabilization.pdf

[231] "Material," NMOT 306.2, Portland Cement or Lime Treated Subgrade,NMDOT, Santa Fe, New Mexico, 2014. Available: http://dot.state.nm.us/content/dam/nmdot/Plans_Specs_Estimates/2014_Specs_For_Highway_And_Bridge_Construction.pdf

[232] "Soil Stabilization Table," OHD L-50, Soil Stabilization Mix Design Procedure,Oklahoma Department of Transportation, Department Test Methods (OHDL), Oklahoma D.O.T, 2009. Available: http://www.odot.org/materials/pdfs-ohdl/ohdl50.pdf

[233] "Composition," 307.02, Cement Treated Base Course,Arkansas D.O.T, Little Rock, Arkansas, 2014. Available: http://www.arkansashighways.com/standard_spec/2014/Division%20300.pdf

[234] "Criteria for Chemical Selection," INDOT 3.01, Design Procedures for Soil Modification or Stabilization,INDOT, Indiana Department of Transportation, 2008. Available: http://www.in.gov/indot/files/smod.pdf

[235] "Subgrade Treatment," Guidelines for Modification and Stabilization of Soils and Base for Use in Pavement Structures,TxDOT, Texas, 2005. Available: ftp://ftp.dot.state.tx.us/pub/txdot-info/cmd/tech/stabilization.pdf

[236] J. Prusinski and S. Bhattacharja, "Effectiveness of Portland cement and lime in stabilizing clay soils", *Transportation Research Record: Journal of the Transportation Research Board*, no. 1652, pp. 215-227, 1999. doi.10.3141/1652-28

[237] J. Mallela, H. V. Quintus, and K. L. Smith, "Consideration of Lime-stabilized Layers in Mechanistic-empirical Pavement Design," ERES Consultants, Arlington, Virginia, 2004.

[238] S. K. Dhakal, "Stabilization of Very Weak Subgrade Soil with Cementitious Stabilizers," M.Sc. Thesis, Civil and Environmental Engineering, Louisiana State University, Baton Rouge, 2009.

[239] Missouri Department of Natural Resources. (28th September), "Education - Energy For Missouri: Today and Tomorrow," Available: https://energy.mo.gov/docs/default-source/energy_division/GeothermalPower.pdf

[240] J. W. Lund and T. L. Boyd, "Direct Utilization of Geothermal Energy 2015 Worldwide Review," *Geothermics*, vol. 60, pp. 66-93, 2016. doi.10.1016/j.geothermics.2015.11.004

[241] GEA. (2016, 28th September), "2016 Annual U.S. & Global Geothermal Power Production Report," Available: http://geo-energy.org/reports/2016/2016%20Annual%20US%20Global%20Geothermal%20Power%20Production.pdf

[242] DSIRE. (1995, 28th September), "Database of State Incentives for Renewables & Efficiency," Available: http://programs.dsireusa.org/system/program?state=LA

[243] LSU AgCenter. (2010, 28th September), "Federal & Louisiana Energy Tax Credits for 2009 and 2010," Available: http://www.lsuagcenter.com/nr/rdonlyres/aaa8184c-50e6-4ee7-ad72-4e00e182b625/67680/ac_29572010.pdf

[244] B. J. Roberts. (2009, 28th September), "Leading Clean Energy Innovation," Available: http://www.nrel.gov/gis/images/geothermal_resource2009-final.jpg

[245] B. J. Roberts. (2015, 28th September), "Leading Clean Energy Innovation" Available: http://www.nrel.gov/gis/images/2015-04-17_Geothermal_Capacity.jpg

[246] U.S. Energy Information Administration. (2015, 28th September), "Geothermal Explained," Available: http://www.eia.gov/energyexplained/index.cfm?page=geothermal_power_plants#tab1

[247] C. J. John, "Geology of the Gladys McCall Geopressured-Geothermal Prospect, Cameron Parish, Louisiana," *Journal of Energy Resources Technology*, vol. 110, no. 4, pp. 255-261, 1988.

[248] Louisiana Tank INC., "Final Technical Report," The Department of Energy, January 13, 2012 2012.

[249] S. M. Jordan and J. Phillip A. Gayle, "Louisiana Geothermal," Geothermal Technologies Program 2010 Peer Review, 2010.

[250] ClimateMaster. (2005, 28th September), "Commercial Case Study," Available: http://www.climatemaster.com/downloads/lc308-climatemaster-commercial-fort-polk-geothermal-heating-and-cooling-systems-case-study.pdf

[251] Oak Ridge National Laboratory. (1997, 28th September), "Big Savings from the World's Largest Installation of Geothermal Heat Pumps at Fort Polk, Louisiana," Available: http://www.ornl.gov/sci/femp/pdfs/fortpolk.pdf

[252] J. Egg. (2013, 28th September), "Ten Myths About Geothermal Heating and Cooling," Available: http://energyblog.nationalgeographic.com/2013/09/17/10-myths-about-geothermal-heating-and-cooling/

[253] M. A. Khan and J. X. Wang, "Development of a Graph Method for Preliminary Design of Borehole Ground-coupled Heat Exchanger in North Louisiana," *Energy and Buildings*, vol. 92, no. 1, pp. 389-397, 2015. doi.10.1061/9780784413272.368

[254] M. A. Khan and J. X. Wang, "Evaluation of low temperature ground coupled vertical heat exchanger in South Louisiana," presented at the 2015 7th Annual IEEE Green Technologies Conference, IEEE, New Orleans, pp. 183-190, 2015. doi.10.1109/GREENTECH.2015.12

[255] "Standard Test Methods for Soil Exploration and Sampling by Auger Borings," ASTM D1452-09, Annual book of ASTM standards,ASTM, West Conshohocken, PA, 2009. doi.10.1520/D1452-09

[256] "Standard Practice for Thin-Walled Tube Sampling of Fine-Grained Soils for Geotechnical Purposes," ASTM D1587/D1587M-15, Annual book of ASTM standards,ASTM, West Conshohocken, PA, 2015. doi.10.1520/D1587_D1587M-15

[257] "Standard Test Methods for Liquid Limit, Plastic Limit, and Plasticity Index of Soils," ASTM D4318-10e1, Annual book of ASTM standards,ASTM, West Conshohocken, PA, 2010. doi.0.1520/D4318-10E01

[258] United States Department of Agriculture. (2013, 28th September), "Web Soil Survey," Available: http://websoilsurvey.sc.egov.usda.gov/App/HomePage.htm

[259] United States Department of Agriculture. (2013, 28th September), "Web Soil Survey," Available: http://apps.cei.psu.edu/soiltool/

[260] "Standard Test Methods for Specific Gravity of Soil Solids by Water Pycnometer," ASTM D854-14, Annual book of ASTM standards, ASTM, West Conshohocken, PA, 2014. doi.10.1520/D0854-14

[261] "Standard Test Methods for Particle-Size Analysis of Soils," ASTM D422-63 (Reapproved 2007)e2, Annual book of ASTM standards,ASTM, West Conshohocken, PA, 2007. doi.10.1520/D0422-63R07E02

[262] "Standard Test Methods for Classification of Soils for Engineering Purposes (Unified Soil Classification System)," ASTM D2487-11, Annual book of ASTM standards,ASTM, West Conshohocken, PA, 2011. doi.10.1520/D2487-11

[263] "Standard Test Methods for Laboratory Compaction Characteristics of Soil Using Standard Effort (12400 ft-lbf/ft$^3$ (600 kN-m/m$^3$))," ASTM D698-12e1, Annual book of ASTM standards,ASTM, West Conshohocken, PA, 2012. doi.10.1520/D0698-12E01

[264] "Standard Test Method for Laboratory Determination of Water (Moisture) Content of Soil and Rock by Mass," ASTM D2216-10, Annual book of ASTM standards,ASTM, West Conshohocken, PA, 2010. doi.10.1520/D2216-10

[265] F. A. M. Marinho and O. M. Oliveira, "Unconfined Shear Strength of Compacted Unsaturated Plastic Soils," Proceedings of the Institution of Civil Engineers - Geotechnical Engineering, vol. 165, no. 2, pp. 97-106, 2012. doi.10.1680/geng10.00027

[266] D. G. Fredlund, "Consolidometer Test Procedural Factors Affecting Swell Properties," in Proc. 2nd International Conference on Expansive Clay Soils, Texas A & M Press, College Station, TX, pp. 435-456, 1969.

[267] B. M. Das, "Principles of Foundation Engineering," 7th ed., Cengage learning, Stamford, CT, 2016.

[268] J. H. Dane and J. W. Hopmans, "Pressure Plate Extractor," in Methods of Soil Analysis: Part 4 Physical Methods, J. H. Dane and C. G. Topp, Eds., ed Madison, WI Soil Science Society of America, 2002, pp. 688-690.

[269] R. B. Grossman and T. G. Reinsch, "Bulk Density and Linear Extensibility," in Methods of Soil Analysis: Part 4 Physical Methods, J. H. Dane and C. G. Topp, Eds., ed Madison, WI Soil Science Society of America, 2002, pp. 201-228.

[270] B. R. Scanlon, B. J. Andraski, and J. Bilskie, "Bulk Density and Linear Extensibility," in Methods of Soil Analysis: Part 4 Physical Methods, J. H. Dane and C. G. Topp, Eds., ed Madison, WI Soil Science Society of America, 2002, pp. 643-670.

[271] X. Zhang, "Consolidation Theories for Saturated-unsaturated Soils and Numerical Simulation of Residential Buildings on Expansive Soils," Ph.D. Dissertation, Department of Civil Engineering, Texas A&M University, College Station, TX, 2004.

[272] K. Terzaghi, R. B. Peck, and G. Mesri, "Soil Mechanics in Engineering Practice," John Wiley & Sons, New York, USA, 1996.

[273] D. G. Fredlund, N. R. Morgenstern, and R. A. Widger, "The Shear Strength of Unsaturated Soils," *Canadian Geotechnical Journal*, vol. 15, no. 3, pp. 313-321, 1978. doi.10.1139/t78-029

[274] E. A. Garven and S. K. Vanapalli, "Evaluation of Empirical Procedures for Predicting the Shear Strength of Unsaturated Soils," in Unsaturated Soils 2006, ed, 2006, pp. 2570-2592.

[275] M. R. H. Chowdhury, "Shear Strength Properties of Compacted Expansive Soils," Master of Applied Science in Environmental Systems Engineering, Department of Civil Engineering, University of Regina, Regina, 2013.

[276] Systat Software Inc., "SigmaPlot for Windows, version 13.0," ed: Systat Software, Inc San Jose, California, 2016.

[277] A. J. Puppala, A. Pedarla, L. R. Hoyos, C. Zapata, and T. V. Bheemasetti, "A Semi-Empirical Swell Prediction Model Formulated from 'Clay Mineralogy and Unsaturated Soil's Properties," *Engineering Geology*, vol. 200, pp. 114-121, 2016. doi.10.1016/j.enggeo.2015.12.007

[278] S. Azam and R. H. Chowdhury, "Swell-Shrink-Consolidation Behavior of Compacted Expansive Clays," *International Journal of Geotechnical Engineering*, vol. 7, no. 4, pp. 424-430, 2013. doi.10.1179/1939787913Y.0000000005

[279] E. L. Matyas and H. S. Radhakrishna, "Volume Change Characteristics of Partially Saturated Soils," *Géotechnique*, vol. 18, no. 4, pp. 432-448, 1968. doi.10.1680/geot.1968.18.4.432

[280] V. Escario, "Swelling of Soils in Contact with Water at a Negative Pressure," presented at the Proceedings of the 2nd international conference expansive clay soils,, Texas A&M University, College Station, pp. 207-217, 1969.

[281] Systat Software Inc., "SigmaPlot 13," 13 ed. San Jose, California, 2016.

[282] V. Q. Hung, "Uncoupled and Coupled Solutions of Volume Change Problems in Expansive Soils," Ph.D. Dissertation, Department of Civil Engineering, University of Saskatchewan, Saskatoon, 2002.

[283] Asphalt Institute. (27th October). Asphalt Pavement Distress Summary. Available: http://www.asphaltinstitute.org/asphalt-pavement-distress-summary/

[284] E. Tsudik, "Analysis of Structures on Elastic Foundations," J. Ross Publishing, 2012.

[285] E. Winkler, "Die Lehre von der Elustizitat und Festigkeit," Dominicus, Prague, 1867.

[286] M. Hetényi, "Beams on Elastic Foundation;: Theory with Applications in the Fields of Civil and Mechanical Engineering," University of Michigan press, Ann Arbor, 1946.

[287] A. A. Umansky, "Analysis of Beams on Elastic Foundation," Central Research Institute of Auto-Transportation, Leningrad, Russia, 1933.

[288] P. L. Pasternak, "On a New Method of Analysis of an Elastic Foundation by Means of Two Foundation Constants (in Russian) Gosudarstvennoe Izdatelstvo Literaturi po Stroitelstvu i Arkhitekture," Moscow, 1954.

[289] E. Reissner, "A Note on Deflections of Plates on a Viscoelastic Foundation," *Journal of Applied Mechanics*, vol. 25, no. 1, pp. 144-145, 1958.

[290] E. S. Melerski, "Design Analysis of Beams, Circular Plates and Cylindrical Tanks on Elastic Foundations," Taylor and Francis, 2006.

[291] J.-H. Yin, "Closed-Form Solution for Reinforced Timoshenko Beam on Elastic Foundation," *Journal of Engineering Mechanics*, vol. 126, no. 8, pp. 868-874, 2000. doi.10.1061/(ASCE)0733-9399(2000)126:8(868)

[292] A. Dodge, "Influence Functions for Beams on Elastic Foundations," *Journal of the Structural Division*, vol. 90, pp. 63-101, 1964.

[293] C. Miranda and K. Nair, "Finite Beams on Elastic Foundation," *Journal of the Structural Division*, ASCE, vol. 92, pp. 131-142, 1966.

[294] B.-Y. Ting, "Finite Beams on Elastic Foundation with Restraints," *Journal of the Structural Division*, vol. 108, no. 3, pp. 611-621, 1982.

[295] S. N. Klepikov, "Analysis of Structures on Elastic Foundation," Budivelnik, Kiev, Ukraine, 1967.

[296] B. G. Korenev, "Analysis of Plates on Elastic Foundation," Gosstroiizdat, Moscow, Russia, 1962.

[297] A. S. Vesic, "Beams on Elastic Subgrade and the Winkler's Hypothesis," in Proc. 5th International Conference on Soil Mechanics and Foundation Engineering, Paris, France, vol. 1, pp. 845-850, 1961.

[298] A. P. S. Selvadurai, "Elastic Analysis of Soil-Foundation Interaction: Development of Geotechnical Engineering," Elsevier Scientific Publishing Company, New York, 2013.

[299] J. E. Bowles, "Foundation Analysis and Design," McGraw-Hill, New York, 1996.

[300] B. A. Ikra, "Prediction of Moisture Content Changes and Heave Analysis of Expansive Soils Under Extreme Weather," M.Sc., Civil Engineering, Louisiana Tech University, Ruston, LA, 2017.

[301] R. Gupta, "A Study of Geosynthetic Reinforced Flexible Pavement System," Ph.D. Dissertation, Department of Civil Engineering, The University of Texas at Austin, Austin, TX, 2009.

[302] J. Davidovits, "Carbon-dioxide green-house Warming: What future for Portland cement, in: Emerging Technologies," presented at the Symposium on Cement and Concretes in the Global Environment, Portland Cement Association, Chicago, p. 21, 1993.

[303] J. Davidovits, "Geopolymers," *Journal of thermal analysis*, vol. 37, no. 8, pp. 1633-1656, 1991. doi.10.1007/bf01912193

[304] M. R. Islam, "Creation and Analysis of a Fly Ash Database for Facilitating the Standardization of Geopolymer Concrete," M.Sc. Thesis, Civil Engineering, Louisiana Tech University, Ruston, Louisiana, 2013.

[305] Hua Xu and J. S. J. V. Deventer, "The Geopolymerisation of Alumino-silicate Minerals," *International Journal of Mineral Processing*, vol. 59, no. 3, pp. 247-266, 6//, 2000. doi.10.1016/S0301-7516(99)00074-5

[306] J.-B. Edouard, "Experimental Evaluation Of The Durability Of Fly Ash-Based Geopolymer Concrete In The Marine Environment," M.Sc. Thesis, The College of Engineering and Computer Science, Florida Atlantic University, Boca Raton, Florida, 2011.

[307] McQuay International, "Geothermal Heat Pump Design Manual," McQuay International, 2002.

[308] Virginia Department of Mines Minerals and Energy. (2012, January 22), "Earth Temperature and Site Geology," Available: http://www.geo4va.vt.edu/indexGeo4VA.htm

[309] Virginia Department of Mines Minerals and Energy. (2012, 28th September), "Earth Temperature and Site Geology," Available: http://www.geo4va.vt.edu/indexGeo4VA.htm

[310] M. A. Khan and J. X. Wang, "Study on Energy Foundation Design in South Louisiana," presented at the Geo-Congress 2014, American Society of Civil Engineers, Atlanta, Georgia, vol. 234, pp. 23-26, 2014. doi.10.1061/9780784413272.368

[311] H. Brandl, "Energy foundations and other thermo-active ground structures," *Géotechnique*, vol. 56, no. 2, pp. 81-122, 2006. doi.10.1680/geot.2006.56.2.81

[312] Thermal Dynamics Inc, "Ground Loop Design 2012," Residential ed, 2012.

[313] F. Dupray, L. Laloui, and A. Kazangba, "Numerical analysis of seasonal heat storage in an energy pile foundation," *Computers and Geotechnics*, vol. 55, pp. 67-77, 2014. doi.10.1016/j.compgeo.2013.08.004

[314] A. Zarrella, M. De Carli, and A. Galgaro, "Thermal performance of two types of energy foundation pile: Helical pipe and triple U-tube," *Applied Thermal Engineering*, vol. 61, no. 2, pp. 301-310, 11/3/, 2013. doi.10.1016/j.applthermaleng.2013.08.011

[315] J. Walton, Telephone conversation, Training & Support Services, Gaia Geothermal, LLC ed, 2014.

[316] M. He, S. Rees, and L. Shao, "Simulation of a Domestic Ground Source Heat Pump System Using a Transient Numerical Borehole Heat Exchanger Model," in Proc. Eleventh International IBPSA Conference, pp. 607-614, 2009.

[317] P. Eskilson, "Thermal Analysis of Heat Extraction Boreholes," Ph.D. Dissertation, Department of Mathematical Physics, University of Lund, Sweden, 1987.